Bio-based Production of Succinate from Renewable Resources

Elucidation of *Basfia succiniciproducens* metabolism
by ^{13}C metabolic flux analysis
for knowledge-based strain engineering

Dissertation

zur Erlangung des Grades des
Doktors der Ingenieurwissenschaften (Dr.-Ing.)

an der Naturwissenschaftlich-Technischen Fakultät III
Chemie, Pharmazie, Bio- und Werkstoffwissenschaften
der Universität des Saarlandes

von Anna Lange

aus Leverkusen

Saarbrücken

2016

Publications

Partial results of this work have been published in advance. This was authorized by the Institute of Systems Biotechnology represented by Prof. Dr. Christoph Wittmann.

Peer-reviewed articles

Becker, J., Reinefeld, J., Stellmacher, R., Schäfer, R., **Lange, A.**, Meyer, H., Lalk, M., Zelder, O., von Abendroth, G., Schröder, H., Haefner, S., Wittmann, C. (2013). Systems-wide analysis and engineering of metabolic pathway fluxes in bio-succinate producing *Basfia succiniciproducens*. Biotechnol. Bioeng. 110, 3013-23.

Becker, J., **Lange, A.**, Fabarius, J., Wittmann, C. (2015). Top value platform chemicals: bio-based production of organic acids. Curr. Opin. Biotechnol. 36, 168-175.

Conference contributions

Lange, A., Becker, J., Haefner, S., Schröder, H., Wittmann, C.: Systems metabolic engineering of *Basfia succiniciproducens* for improved succinate production based on ^{13}C metabolic flux analysis. European Symposium on Biochemical Engineering Sciences (ESBES) 2016, September 11-14, 2016, Dublin, Ireland.

Patents

Krawczyk, J. M., Haefner, S., Schröder, H., Dantas Costa, E., Zelder, O., Von Abendroth, G., Wittmann, C., Stellmacher, R., Becker, J., **Lange, A.**, Lyons, B. J., Lyons, T. J., De Crecy, E., Hughes, E. (2015). Improved microorganisms for succinic acid production. Application No./Patent No. PCT/EP2015/052048

Danksagung

Contents

Summary

Succinic acid is a highly versatile chemical with the potential of replacing the maleic acid platform currently derived from petroleum. Among the microorganisms suitable for succinic acid production, *Basfia succiniciproducens* stands out as one of the most efficient commercial producers. In the present work, succinic acid production by *B. succiniciproducens* from sucrose, fructose, and xylose was analyzed at a systems level by means of ^{13}C metabolic flux analysis. Qualitative ^{13}C tracer studies and *in vitro* enzymatic assays shed light on so far unknown key properties of the *B. succiniciproducens* metabolism. Strategies for systems metabolic engineering of *B. succiniciproducens* were inferred from these results and successfully applied.

Compared to other sugars, succinate yields on sucrose and fructose were reduced. This effect could be traced back to the PTS systems responsible for substrate uptake. The beneficial effect of fructokinase, a key enzyme of the *B. succiniciproducens* sucrose catabolism newly discovered in this work, was exploited to engineer a mutant strain with a tremendously increased succinate yield. Towards utilizing hemicellulose as a raw material, xylose was identified as a promising substrate for succinate production, with formate dehydrogenase possibly involved in superior redox recycling, leading to high succinate yields coupled to reduced by-product formation.

Zusammenfassung

Bernsteinsäure ist eine vielfältig einsetzbare Chemikalie mit dem Potential, die aus Rohöl gewonnene Plattformchemikalie Maleinsäure zu ersetzen. Unter den verschiedenen Bernsteinsäure-produzierenden Mikroorganismen sticht *Basfia succiniciproducens* als effizienter kommerzieller Produzent hervor. Im Rahmen dieser Arbeit wurde die Bernsteinsäurebildung durch *B. succiniciproducens* auf Saccharose, Fructose und Xylose mithilfe von ^{13}C-metabolischer Flussanalyse auf Systemebene untersucht. Qualitative ^{13}C Markierungsstudien und Enzymaktivitätsmessungen trugen zur Aufklärung bisher unbekannter Eigenschaften des Metabolismus von *B. succiniciproducens* bei. Aus den Ergebnissen wurden Strategien zur Stammverbesserung mittels Systems Metabolic Engineering abgeleitet und erfolgreich umgesetzt.

Die Produktausbeuten auf Saccharose und Fructose waren vergleichsweise gering. Dies konnte auf die für die Aufnahme der Zucker verantwortlichen PTS Systeme zurückgeführt werden. Der vorteilhafte Effekt der Fruktokinase, eines wichtigen Enzyms im Saccharosekatabolismus von *B. succiniciproducens*, das in dieser Arbeit erstmals nachgewiesen wurde, konnte zur Konstruktion eines Produzenten mit deutlich erhöhter Bernsteinsäureausbeute genutzt werden. In Hinblick auf die Verwendung von Hemicellulose als Rohstoff wurde Xylose als vielversprechendes Substrat identifiziert. Dabei war das Enzym Formiatdehydrogenase in einen vorteilhaften Redoxstoffwechsel involviert, der zu hohen Produktausbeuten führte.

Abbreviations and Symbols

Abbreviations

ABC transporter	ATP-binding cassette transporter
ABU	α-amino butyric acid
Acteyl-CoA	Acetyl coenzyme A
Ala	alanine
approx.	approximately
Arg	arginine
Asp	aspartic acid
BDO	1,4-butanediol
BHI	brain heart infusion
Bis-Tris	2,2-Bis(hydroxymethyl)-2,2',2"nitrilotriethanol
bp	base pair
DMF	dimethylfomamide
ED pathway	Entner-Doudoroff pathway
EMP pathway	Embden-Meyerhof-Parnas pathway
G6PDH	glucose 6-phosphate dehydrogenase
GC/MS	gas chromatography-mass spectrometry
Glu	glutamic acid
Gly	glycine
HPLC	High performance liquid chromatography
Ile	isoleucine
Leu	leucine
Lys	lysine
MBDSTFA	N-methyl-N-tert-butyldimethylsilyl-trifluoroacetamide
ME	molecular enrichment
MFA	metabolic flux analysis
MID	mass isotopomer distribution
MOPS	3-(N-morpholino)propanesulfonic acid
MQ-H_2O	Milli-Q $^{\circledR}$ ultrapure water
MSD	mass selective detector
NADH	nicotinamide adenine dinucleotide, reduced
NADPH	nicotinamide adenine dinucleotide phosphate, reduced
NAD$^+$	nicotinamide adenine dinucleotide, oxidized
NADP$^+$	nicotinamide adenine dinucleotide phosphate, oxidized
OAA	oxaloacetic acid
2-OG	2-oxoglutaric acid
OPA	O-phthaldialdehyde
ORF	Open reading frame
P5P	pentose 5-phosphate
PCR	polymerase chain reaction

PEP	phosphoenol pyruvate	
PEPCK	PEP carboxykinase	
PEPCX	PEP carboxylase	
Phe	phenylalanine	
Pro	proline	
Pyr	pyruvate	
PP pathway	Pentose phosphate pathway	
PTS	phosphotransferase system	
Ser	serine	
SFL	summed fractional labeling	
SIM	selective ion monitoring	
TBDMS	*tert*-butyl-dimethylsilyl	
TCA cycle	tricarboxylic acid cycle	
Thr	threonine	
TMS	trimethylsilyl	
Tyr	tyrosine	
UK	United Kingdom	
US	United States	
UV	ultraviolet (light)	
Val	valine	

Symbols and units

—	Molar concentration	$[M] = [mol \cdot L^{-1}]$
—	Rotational speed	[rpm] (revolutions per minute)
—	Enzymatic activity	$[U] = [\mu mol \cdot min^{-1}]$ (unit)
μ	Specific growth rate	$[h^{-1}]$
m/z	Mass-to-charge ratio	[-]
OD_{600}	Optical density at 600 nm	[-]
q_S	Specific substrate uptake rate	$[mmol \cdot (g\ CDW)^{-1} \cdot h^{-1}]$
vvm	gas volume flow per unit of liquid volume per minute	$[L \cdot L^{-1} \cdot min^{-1}]$
$Y_{P/S}$	Product yield	$[mol \cdot mol^{-1}]$
$Y_{X/S}$	Biomass yield	$[g \cdot mol^{-1}]$

1

Introduction and Objectives

The industrialized world we live in thrives on energy and materials derived from petroleum. Mankind, however, must shift its focus away from fossil resources, which will eventually be depleted, to renewable resources. The increasing public awareness on the dangers of carbon dioxide-enhanced climate change and the public demand for environmentally acceptable production of chemicals and materials drive industry to explore alternatives.

The search for building block chemicals led to identification of the best suited candidates towards a bio-based economy, one of which is succinic acid (Bozell and Petersen, 2010; Werpy and Petersen, 2004). This important platform chemical has a broad range of applications, for example as detergent, as ion-chelator, as food additive or as building block for biopolymers (Beauprez *et al.*, 2010; Cheng *et al.*, 2012; Lin *et al.*, 2012). Until recently, most of the demand for succinic acid was covered by petrochemical production. In this process, n-butane from crude oil is converted into maleic anhydride and finally into succinic acid (Lin *et al.*, 2011). A biotechnological approach for succinic acid production is a promising alternative, since succinic acid is an intermediate of the core metabolism of most organisms. Because of its versatility and the straightforward approach for its biotechnological production, succinic acid has received much attention from the chemical and biotechnological industries. Four global companies have recently started to produce biosuccinic acid on a large scale with a current annual production capacity of approximately 65,000 tons (Becker *et al.*, 2015; Hartmann, 2015). Additional production plants, which will nearly quadruple the annual production volume, are currently under construction or in planning. All four companies use proprietary microorganisms, including yeast and *Escherichia coli* strains.

Succinity, a joint venture of BASF SE and Corbion Purac, employ *Basfia succiniciproducens*, a natural succinic acid producer that was recently isolated and sequenced (Becker *et al.*, 2015; Kuhnert *et al.*, 2010; Scholten and Dägele, 2008). Thriving on a broad array of substrates, including glycerol and various carbohydrates, *B. succiniciproducens* fixes CO_2 in order to produce succinic acid, its main metabolic product. The natural succinic acid production capacity of the wild type strain DD1 is already fairly high. In addition to

succinic acid, however, *B. succiniciproducens* accumulates a variety of by-products during fermentation – a rather undesirable behavior that leads to an effective loss of substrate and impedes downstream processing. This provides an opportunity to improve *B. succiniciproducens* towards more efficient succinic acid production by systems metabolic engineering. This approach aims at understanding the organism at a systems level so that it can be modified in a targeted manner using a global engineering strategy that tailors the whole metabolism towards the desired phenotype. The first part of this optimization process can involve various "omics" techniques, such as genomics and transcriptomics, which are applied to elucidate the metabolism of the organism. In case of *B. succiniciproducens*, this is especially important, since its metabolism is rather unexplored. An especially useful tool for target prediction is ^{13}C fluxomics, also called ^{13}C metabolic flux analysis, since the fluxome directly represents the cellular phenotype. In the second part, engineering targets derived from the analysis are implemented, thus generating a superior producer.

The objective of this work was to analyze the metabolism of the wild type *B. succiniciproducens* strain DD1 at a systems wide level by unraveling its *in vivo* fluxes. Based on these results, strategies for rational design of superior mutants were developed and successfully applied. State-of-the-art ^{13}C metabolic flux analysis requires accurate information about extracellular rates and the combination of multiple ^{13}C-labeling data sets derived from parallel experiments with different ^{13}C tracers. Therefore, a small-scale setup was developed that allowed for highly reproducible cultivation of *B. succiniciproducens* on a number of relevant carbon sources, i.e., sucrose, fructose, and xylose. Based on qualitative ^{13}C tracer experiments and enzymatic assays, the metabolic network model of *B. succiniciproducens* was expanded and refined. Next, parallel cultivations on different isotopic tracer substrates were carried out. Mass isotopomer distributions (MIDs) of biomass components and extracellular metabolites were determined using gas chromatography-mass spectrometry (GC/MS). Integrating the extensive labeling data and additional experimental network constraints, high-resolution metabolic flux maps were calculated and subsequently analyzed carefully with regards to possible targets for metabolic engineering. Based on these findings, superior producers were constructed by the BASF SE, which revealed improved characteristics and high production capacity in batch and fed-batch production processes.

2

Theoretical Background

2.1 Succinic Acid: A Highly Versatile Platform Chemical

The global demand for energy, chemicals, and materials is nowadays saturated to a large degree by production and subsequent processing of petroleum and natural gas. As the world population grows, these fossil resources will inevitably be depleted. Besides this, the negative environmental impact of the petroleum industry and the possible enhancement of global warming by excessive release of previously-bound CO_2 into the atmosphere are arguably two of the greatest challenges facing mankind. This is why alternatives for petroleum-derived products have become the focus of extensive research (Burk and Dien, 2016). Several countries, including Canada, the US, and Germany, have commissioned governmentally-funded projects with the explicit aim of promoting industrial biotechnology (Archambault *et al.*, 2004; Hüsing *et al.*, 2003; Werpy and Petersen, 2004). The European Union expects the market share of bio-based products to rise to more than 20% by 2020, with a predicted annual growth rate of close to 20% (European Commission, 2016). In 2013, a commission of experts was set up to support the development of a sustainable bio-based economy in the European Union. In the United States, a "Biomass Program" aiming at the promotion of biorefineries was launched in 2002. As one result of this program, a list of chemicals most suited to provide a basis for a bio-economy was published in 2004. The platform chemicals, or building blocks, identified in this pioneering report shared several important characteristics, such as their suitability for integrated biorefineries, their ability to be converted into multiple other useful compounds, and the fact that they could replace bulk chemicals currently produced by petrochemistry. Succinic acid was listed among the top 12 most promising biotechnological products (Werpy and Petersen, 2004), and is still on the revised list from 2010 (Bozell and Petersen, 2010).

Succinic acid (Figure 2.1), i.e., butanedioic acid by systematic nomenclature, is a saturated four-carbon dicarboxylic acid, which is best known by its biochemical role as
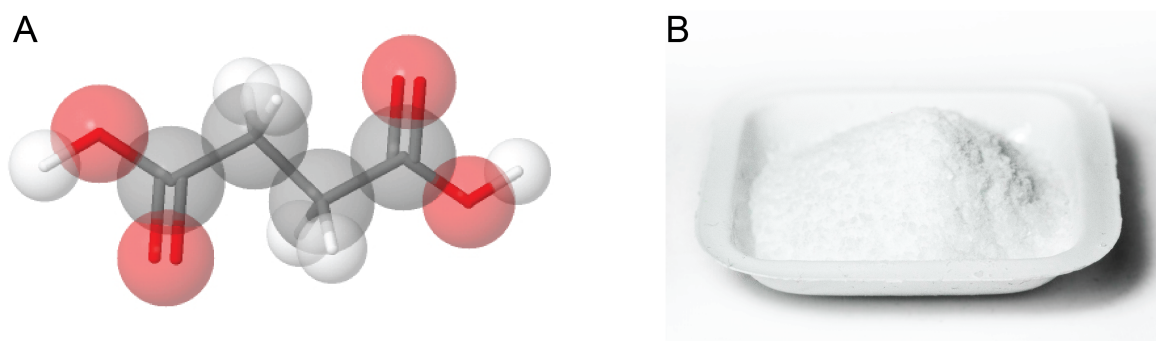
Figure 2.1: Succinic acid. (A) Chemical structure of succinic acid, i. e., 1,4-butanedioic acid. Black: carbon, red: oxygen, white: hydrogen. (B) Pure succinic acid is a colorless, odorless, and opaque powder.

intermediate of the tricarboxylic acid (TCA) cycle, which is ubiquitous in living organisms. Discovered by the German humanist Gregorius Agricola in the 16th century through dry distillation of amber (latin: *succinium*, from *succus*, juice), it was originally described as a sour-tasting, colorless crystalline substance (Agricola, 2004) and only identified as an acid 300 years later (Matuszewska, 2016). Interestingly, the mechanisms which led to deposition of up to 8% succinic acid in Baltic amber (Moreno *et al.*, 2000) are not yet fully understood but the absence of succinic acid in other types of amber suggests that it is actually a degradation product of organic acids typically present in resin (Rottländer, 1970).

While initially used mainly for medical purposes (Matuszewska, 2016), succinic acid has by now been recognized as a most versatile chemical. As such, succinic acid and its derivatives have become highly important and are used in many areas of everyday life, in the fields of agriculture, food and feed, pharma, health and cosmetics, as well as in the chemical and the textile industry (Figure 2.2). It has the potential to replace the petrochemical platform chemicals maleic acid and maleic anhydride, which currently have an annual market size of US-\$ 2.30 billion or 225,000 tons (GrandViewResearch, 2016). Due to its acidic properties, succinic acid and its sodium salt are used as flavoring agents and preservatives in food and feed (Broz *et al.*, 2010; Ernst *et al.*, 1979; Igoe, 2011; Nicholas J. Russell, 2012) but also in toothpaste and hair care products (Salvador and Chisvert, 2011). Succinic acid also has numerous applications in the chemical and textile industry, e. g., as an accelerator in electroplating baths (Bunce *et al.*, 2006; Davis, 2000), as a substance used for anodizing aluminum (Economy, 1966), or as substance involved in shrinkproofing
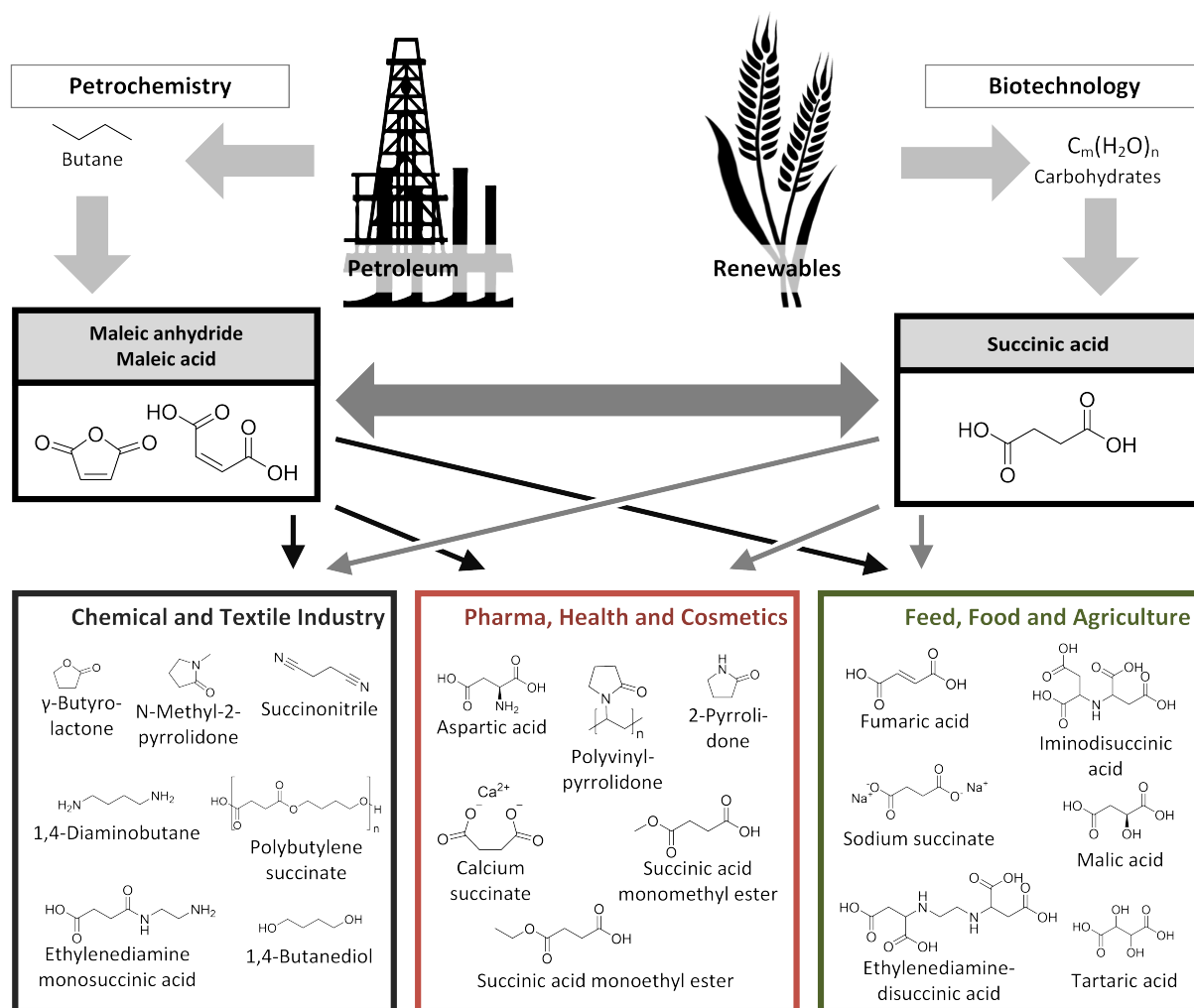
Figure 2.2: The succinic acid/maleic acid platform. Biotechnology-derived succinic acid has the potential to replace petrochemical maleic acid/maleic anhydride. The two chemicals can be inter-converted and are precursors to a variety of other chemicals used in the fields of pharma, health and cosmetics, food and feed, agriculture, and in the chemical and textile industries. The list of compounds is just an excerpt of the possible applications.

wool (Maurice, 1947). Calcium succinate has anti-carcinogenic properties (Harzevili and Chen, 2014), and sodium succinate can be used as antidote (Collicchio-Zuanaze *et al.*, 2006). The total market for succinic acid has been estimated at 58,500 tons, worth US-$ 157.2 million in 2015 by one report (MarketsandMarkets, 2016), and 100,000 tons, worth US-$ 400 million in 2014 by another (Zion Research, 2015). It is projected to reach US-$ 1,000 million by 2020, largely due to the high potential of succinic acid derived polymers and the many succinic acid derivatives, including the platform chemicals maleic acid and maleic anhydride. By reduction or oxidation, several other dicarboxylic acids, i.e., fumaric acid, malic acid and tartaric acid, can be produced from succinic acid, all of which are acidulants, i.e., acids used as food additives (Igoe, 2011). Fumaric acid acid is also used as reducing agent during bread production (Hui, 2006). Succinonitrile, produced by reacting ammonia with aqueous succinic acid (Jacquot and Marion, 2009), is used to im-

prove characteristics of lithium batteries (Abouimrane and Davidson, 2007). Polyamino monosuccinic acid is a bleaching agent used in photography (Strickland *et al.*, 1996). Chelating agents based on succinic acid, such as iminodisuccinic acid and ethylendiamine disuccinic acid, are used in agriculture for soil treatment (Pinto *et al.*, 2014). Succinic acid esters have been suggested to be used as insulinotropic agents (Malaisse, 1995; Saravanan and Pari, 2007). Derivatisation of vitamin A with succinic acid yields retinoids, which are used in cosmetics and pharmaceuticals to prevent cancer (Maugard and Legoy, 2000), and derivatisation of erythrodiol yields compounds with anti-inflammatory properties (Vanstone, 1976). 2-Pyrrolidone, generated by direct reaction of succinic acid with hydrogen and ammonia (Matson, 1990), is a precursor for a number of pharmaceuticals such as Cotinine and Doxapram. Especially important derivatives of succinic acid are N-methyl-2-pyrrolidone, γ-butyrolactame and γ-butyrolactone, all of which are widely used organic solvents and have several other applications in the chemical industry. The fabrication of biodegradable plastics and bio-based polymers, mostly from succinic acid, 1,4-diaminobutane, and 1,4-butanediol (BDO) is a large field of application. This covers polymers such as polyvinylpyrrolidon, which is mainly used in the pharmaceutical industry, and polybutylene succinate (PBS). More than one third of all succinic acid is used for production of BDO, which is a precursor for pulyurethanes with numerous applications, e. g., in the automotive industry (GrandViewResearch, 2014).

Recently, four companies have started to commercialize the production of biosuccinic acid (Table 2.1). Myriant, a US company from Quincy, Massatchusetts, has been producing succinic acid at a large scale in cooperation with ThyssenKrupp Uhde since 2010. BioAmber, another North American company headquartered in Montreal, Canada, was founded in 2008. Reverdia, a Royal DSM and Roquette Frères joint venture located in Geleen, Netherlands, started production of Biosuccinium™ in 2012. Succinity, a BASF/Corbion Purac joint venture headquartered in Düsseldorf, Germany, is the youngest of the four companies, having been founded in 2013. Taken together, these companies produce more than 60,000 tons per year of succinic acid. The largest plant with a capacity of 30,000 tons per year was opened in August, 2015 by BioAmber (Hartmann, 2015). All four companies are planning to construct new, larger plants with an overall additional capacity of more than 180,000 tons per year. Clearly, the industry has just begun to tap the biosuccinic acid market, since the market potential for succinic acid and its derivatives (up to 245,000 tons per year) and for succinic acid derived polymers (possibly 2,000,000 tons per year) is exceptionally high (Bozell and Petersen, 2010).

Table 2.1: Companies producing succinic acid from biomass feedstock. The four companies that have commercialized biosuccinic acid production, their respective plant sizes, the used microorganisms and feedstocks are listed. Information on all four companies has been gathered from recent review by (Jansen and Gulik, 2014).

Company	Current production capacity (plant site) [t/a]	Expected production capacity (plant site) [t/a]	Organism	Feedstock	Source
Succinity[a]	10,000 (Spain)	50,000	*Basfia succiniciproducens*	Glycerol, sugars	(BASF and CSM, 2012; Succinity, 2016a,b)
Myriant[b]	13,600 (USA) / 1,400 (Germany)	63,500 (North America)	*Escherichia coli*	Sorghum and other cellulosic feedstock	(Myriant, 2016, 2013)
BioAmber[c]	30,000 (Canada)	70,000 (North America), by late 2018	*Escherichia coli* (demonstration plant), yeast (possibly *Candida krusei*)	Corn; sugar from cane, beets, sorghum, wheat, tapioca; future: agricultural, forestry and industrial waste	(BioAmber, 2008; Chemicals-Technology.com, 2016; Hartmann, 2015)
Reverdia[d]	10,000 (Italy)	"Site selection and feasibility studies for large-scale commercial plants are ongoing and are being carried out with partners on all major continents"	Low pH yeast (*Saccharomyces cerevisiae*)	Starch	(Reverdia, 2016b)

[a] Joint venture between BASF SE and Corbion (previously CSM, Purac, and Caravan)
[b] Cooperation with ThyssenKrupp Uhde
[c] Joint venture between DNP Green Technology, ARD, and Mitsui & Co
[d] Joint venture between Royal DSM N.V. and Roquette Frères.

2.1.1 Chemical and biotechnological production routes

Despite its many uses, succinic acid has, for a long time, been considered a niche product of the chemical industry, mainly because of its high price, which was directly linked to the current oil price (Taylor, 2010). Two decades ago, succinic acid was solely produced petrochemically. Several companies started investing in biotechnological succinic acid production, so that by 2010, the amount of biotechnologically produced succinic acid equaled that of petrochemically produced succinic acid. By now, the annual bio-succinate production has by far surpassed production from crude oil (Pinazo *et al.*, 2015). Nevertheless, maleic anhydride and maleic acid remain important platform chemicals that have not yet been completely replaced by biotechnological succinic acid, although biotechnological succinic acid production is economically just as feasible (Beauprez *et al.*, 2010).

The petrochemical production route to succinic acid starts with the extraction of benzene or n-butane from natural gas or petroleum. By oxidation of these substances, maleic anhydride is formed, which can then be hydrolyzed to maleic acid (Lohbeck *et al.*, 2000). Maleic anhydride is hydrogenated at temperatures ranging from 120 to 180 °C and at pressures between 0.5 and 4.0 MPa, often employing Nickel or Palladium based toxic redox catalysts (Pinazo *et al.*, 2015). The formed succinic anhydride can easily be hydrolyzed to form succinic acid.

The biotechnological production of succinic acid only requires renewables as raw material and is carried out under environmentally friendly, moderate conditions. It is an obvious alternative to petrochemical production from butane since succinic acid is a metabolic intermediate of the TCA cycle. Several metabolic routes exist, which allow microorganisms to convert a number of substrates into succinic acid (Figure 2.3). Carbohydrates from biomass, e. g., glucose from starch, are converted into the three-carbon metabolites phosphoenolpyruvate (PEP) or pyruvate via the Embden–Meyerhof–Parnas (EMP) pathway, the pentose phosphate (PP) pathway, or the Entner-Doudoroff (ED) pathway. Conversion of these three-carbon metabolites into succinic acid can occur via one of three possible pathways (Cheng *et al.*, 2013). The most direct route, which allows for the highest theoretical succinate yield, is the reductive branch of the TCA cycle (Figure 2.3A). Pyruvate or phosphoenolpyruvate is carboxylated to form malate or oxaloacetate, which is then reduced in order to generate succinic acid. This pathway is employed by natural succinic acid producers such as *Actinobacillus succinogenes* and *B. succiniciproducens* (Becker *et al.*, 2013; McKinlay *et al.*, 2007). The two other possible pathways are used by aerobically growing yeasts (Raab *et al.*, 2010; Rezaei *et al.*, 2015), and are overall less advantageous due to their lower possible theoretical carbon yields. The glyoxylate shunt (Figure 2.3B) and the oxidative branch of the TCA cycle (Figure 2.3C) share the

first reaction steps, which comprise conversion of acetyl coenzyme A (acetyl-CoA) and oxaloacetate into isocitrate. Isocitrate can then be cleaved into succinate and glyoxylate by the isocitrate lyase, an enzyme of the glyoxylate shunt, or it can be decarboxylated twice to form succinate, following the oxidative branch of the TCA cycle. While the reductive pathway requires CO_2 fixation, the two other pathways result in the release of CO_2. Indeed, the oxidative TCA cycle branch can only be kept running, when oxaloacetate is supplied via anaplerotic, carboxylating reactions. It must be noted, however, that additional reducing power must be provided, if all carbon from carbohydrates is to be converted to succinic acid via the reductive branch of the TCA cycle. This can for example be achieved by providing H_2, or by choosing a more reduced substrate, such as glycerol. Using the oxidative branch of the TCA cycle in organisms with a respiratory chain allows for generation of ATP through oxidative phosphorylation and for regeneration of NAD^+ by reduction of O_2. Combination of both the glyoxylate shunt and the reductive pathway allows for a closed redox balance at an optimal carbon yield for succinic acid (Raab and Lang, 2011).

The actual industrial production process towards succinic acid can be divided into three stages, i.e., upstream processing, the fermentation, and downstream processing. Upstream processing comprises preparatory steps such as preparation of the substrate, isolation and engineering of the microorganism, cleaning and sterilization of the fermenter, and pre-cultivations in seed tanks in increasing size (Pandey *et al.*, 2015). The fermentation of the substrate to succinic acid, a relatively cheap bulk chemical, is carried out in large-scale bioreactors. In industrial amino acid production, which might be comparable, vessels with a volume up to $500 \, \text{m}^2$ are commonly used (Wendisch, 2007). For optimal process efficiency, fed-batch strategies are applied, since they allow for much higher titers and yields than simple batch processes and do not carry the contamination risks inherent to continuous processes. Finally, downstream processing describes all steps necessary for recovery of succinic acid from the cultivation broth. Methods that have been suggested for succinic acid recovery include direct crystallization, only suitable for low pH fermentations, precipitation with $(NH_4)_2SO_4$, electrodialysis, membrane separation, *in situ* separation, and chromatography (Cheng *et al.*, 2012; Cok *et al.*, 2014). Recently, an extraction method was patented which describes a six-step process: (1) removal of microorganisms by centrifugation or filtration, (2) acidification of the supernatant with sulfuric acid or another strong acid, (3) extraction of succinic acid with a water insoluble nitrile, (4) re-extraction of succinic acid with hot water, (5) crystallization of succinic acid from the cooling water, and finally (6) recovery of the crystals by means of filtration or centrifugation (Kiefer, 2014).
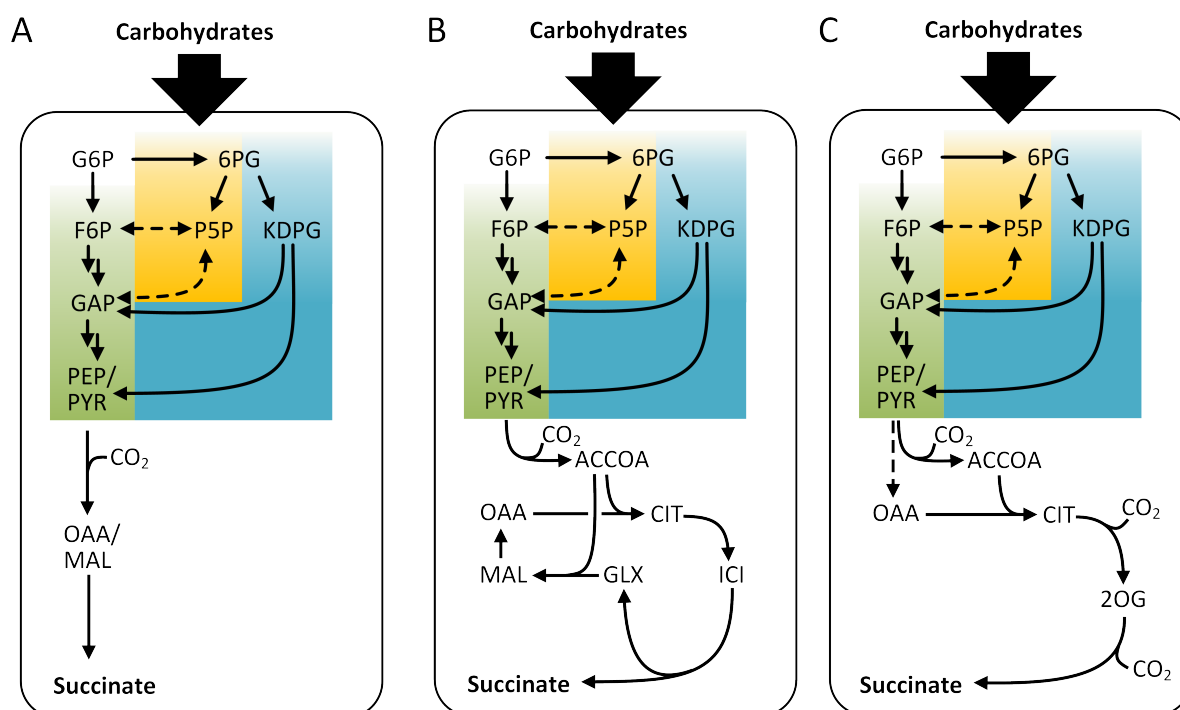
Figure 2.3: Metabolic pathways for succinic acid production. Carbohydrates are usually metabolized via the Embden-Meyerhof-Parnas pathway (green), the pentose phosphate pathway (yellow), or the Entner-Doudoroff pathway (blue), leading to formation of pyruvate (PYR) or phosphoenolpyruvate (PEP). Conversion to succinic acid occurs via three possible routes: (A) following the reductive branch of the TCA cycle, PYR/PEP is carboxylated to oxaloacetate (OAA) or malate (MAL), and subsequently reduced to succinate. (B) The glyoxylate shunt comprises the conversion of acetyl-CoA (ACCOA), generated by oxidative decarboxylation of pyruvate, and oxaloacetate to citrate. This is followed by isomerization to isocitrate, which is then split into succinate and glyoxylate (GLX). By adding glyoxylate to another acetyl-CoA, malate is formed, which can then be converted to oxaloacetate. (C) The oxidative branch of the TCA cycle describes the synthesis of citrate from oxaloacetate and acetyl-CoA, which is then twice decarboxylated and yields succinate via 2-oxoglutarate. Oxaloacetate has to be supplied by carboxylation reactions, as indicated by a dashed arrow.

2.1.2 Renewables as industrial raw materials

Using renewable feedstock has several advantages for the chemical industry, including sustainability, the recycling of carbon dioxide, the use of eco-friendly technology and independence from petroleum-supplying countries (Hari *et al.*, 2015). To make biotechnological production of a bulk chemical such as succinic acid feasible, however, the raw material must fulfill key criteria, such as being cheap and readily available in large quantities. Also, the succinic acid yield that can be achieved on the substrate must be high.

A number of different raw materials have been used in this regard. They can be divided into five main classes (Willke and Vorlop, 2004): oil plants, starch plants, sucrose plants, and wood and waste materials. In addition to this, plants that do not compete with food crops for different reasons receive increasing attention. This applies to algae, which do

not require use of land and grow exceptionally fast, as well as a number of land plants such as halophytes, *Camelina* and *Jatropha* (Hari *et al.*, 2015).

Sugar beet and sugar cane, both of which are sucrose plants, are mainly grown for the production of sucrose (retail sugar), a heterodisaccharide consisting of glucose and fructose, connected by an α-1,2 glycosidic bond. Approximately 40 % of the sucrose crops' dry weight is, indeed, sucrose (Giaquinta, 1979; Muchow *et al.*, 1996). Starch crops, including grains, such as corn, wheat, and rice and tubers, such as potatoes and cassava, are typically used as staple food or animal fodder. The main nutrient components of these plants are carbohydrates, which make up up to 80 % of the dry weight. Most of these carbohydrates is starch, a glucose polysaccharide, or monomeric glucose (US Department of Agriculture, 2016). Industrial production of biosuccinic acid is currently mostly based on such feedstock (Table 2.1): the company Reverdia uses starch as feedstock; the BioAmber process is mostly based on corn, although sugar from cane, beets, sorghum (another important starch crop (Anglani, 1998)), wheat, and tapioca (cassava starch) is also suitable for the process (BioAmber, 2008); Myriant has specialized on utilizing grain sorghum; and the Succinity process also requires sugars.

The main components of oil plants, such as rape, are fat, glycerol and celluloses (Willke and Vorlop, 2004). This feedstock is of special interest for biodiesel production but has already been used for succinate production with yeasts (Kamzolova *et al.*, 2014).

The utilization of waste materials for biotechnological processes is without question the most advantageous. Not only is waste material usually cheap, but its recycling will reduce pollution (Goel, 1994). Glycerol is a by-product of biodiesel production from animal fats and vegetable oils (Silva *et al.*, 2009). Because of its reduced state, glycerol is an interesting carbon source for succinic acid production and is used in the Succinity process in combination with sugars (Succinity, 2016a). One of the most interesting agro-industrial waste products is molasses, a concentrated syrup that is a by-product of sucrose production, and contains high amounts of sucrose, glucose and fructose (Banat *et al.*, 2014). Corn steep liquor is a nitrogen-rich waste product of corn wet-milling (Liggett and Koffler, 1948), and has been used for succinic acid production in combination with molasses as a carbon source (Shen *et al.*, 2015). Other agricultural waste, such as wheat, corn or rice straw, or bagasse of sugarcane, is available in significantly larger quantities, but cannot be as easily used as a substrate since vigorous pretreatment is required to hydrolyze the lignocellulosic plant material (Grimaldi *et al.*, 2015; Lynd *et al.*, 2005). The same is true for forestry waste materials. Lignocellulose consist of cellulose, a glucose polymer, hemicellulose, and lignin (Pérez *et al.*, 2002). Hemicellulose consists of a variety of sugars, including D-xylose, D-mannose, D-glucose and L-arabinose. This is challenging for biotechnology since many organisms cannot utilize all of these sugars. Lignin, finally,

is a cross-linked aromatic polymer consisting of phenolic subunits. Although it is the most abundant of the three fractions, it is also most difficult to access, although researchers are putting much effort into making lignin accessible for biotechnology (Beckham *et al.*, 2016). For *B. succiniciproducens*, digested cellulose and hemicellulose are part of the natural substrate spectrum since they are abundantly available in its native environment, the cattle rumen.

2.1.3 Industrial succinic acid producers

Although succinic acid is an intermediate of the central metabolism of most organisms, there is only a small number of natural succinic acid producers. Metabolic engineering, however, has been used to construct other succinic acid-producing microorganisms. A broad array of different bacteria and fungi has been analyzed regarding their succinic acid production capacity and performance, as reviewed recently in great detail (Ahn *et al.*, 2016).

Of the four companies that have commercialized succinic acid production, only one has focused its attention on a natural producer: Succinity employs the bacterium *B. succiniciproducens* for production of succinic acid. Myriant and BioAmber are using engineered (non-GMO) *Escherichia coli* (Hartmann, 2015; Myriant, 2016, 2013), although BioAmber has decided to switch to a yeast producer (possibly *Candida krusei*, also called *Pichia orientalis* or *Issatchenkia orientalis*) for their large scale production plants (Ahn *et al.*, 2016; Dewulf *et al.*, 2016; Jansen and Gulik, 2014). Reverdia relies on a low pH yeast (engineered *Saccharomyces cerevisiae*) (Reverdia, 2016a). Although not much is known about the specific strains used in the production processes, many publications show the potential and capabilities of these organisms very clearly. Neglecting biomass formation costs, *E. coli* AFP111-pyc reached a titer of $99\,\text{g·L}^{-1}$ with a yield of $1.1\,\text{g·L}^{-1}$ in a dual phase fed-batch process (Vemuri *et al.*, 2002). An even higher titer of $127\,\text{g·L}^{-1}$ was achieved with strain NZN111 (Chen *et al.*, 2014). Different techniques were used for strain engineering, including rational engineering, as for the strains NZN111 and AFP111-pyc, and evolutive adaptation approaches (Jiang *et al.*, 2014; Kwon *et al.*, 2011; Li *et al.*, 2013). *S. cerevisiae* Suc-297, an engineered yeast strain patented by Royal DSM, showed only a rather low yield of $0.45\,\text{g·g}^{-1}$ and a titer of $43\,\text{g·L}^{-1}$ in an aerobic fed-batch process (Cheng *et al.*, 2013; Verwaal *et al.*, 2009). However, yeast cultivations for succinate production have been carried out at pH values of 3.8 with *S. cerevisiae* strain PMCFfg (Yan *et al.*, 2014) and even below pH 3.5 employing *Yarrowia lipolytica* (Kamzolova *et al.*, 2014; Yuzbashev *et al.*, 2010). Despite relatively low yields and titers, such process conditions are potentially advantageous because they allow to recover succinic acid instead of succinic

acid salts. Another advantage of *Candida krusei* is its high tolerance towards succinic acid, revealing its potential to reach high succinic acid titers during cultivations (Ahn *et al.*, 2016). Succinic acid production with engineered *B. succiniciproducens* strains was recently patented. High titers of more than $60\,\text{g·L}^{-1}$ at yields of $1.04\,\text{g·g}^{-1}$($1.10\,\text{C-mol·C-mol}^{-1}$) were achieved when cultivating strain DD1 $\Delta ldhA$ $\Delta pflA$ $pykA2$ on a mixture of maltose and glycerol (Krawczyk *et al.*, 2015).

2.2 *Basfia succiniciproducens*: a Promising Succinic Acid Producer

2.2.1 The physiology of *Basfia succiniciproducens*

The first *Basfia succiniciproducens* strain, DD1, was isolated from bovine rumen while screening for microorganisms with a naturaly capability to produce succinic acid (Scholten and Dägele, 2008). The cells of the Gram-negative bacterium are non-motile, coccoid to rod shaped, and usually arranged in chains or clusters (Fig 2.4A). All seven described *B. succiniciproducens* strains are closely related and belong to the family *Pasteurellaceae*, gammaproteobacteria that are usually parasites or commensals of vertebrates, mostly farm animals (Kuhnert and Christensen, 2008). An overview over the evolutional relationship between *B. succiniciproducens* and other succinic acid producing bacteria is shown in Figure 2.4B.
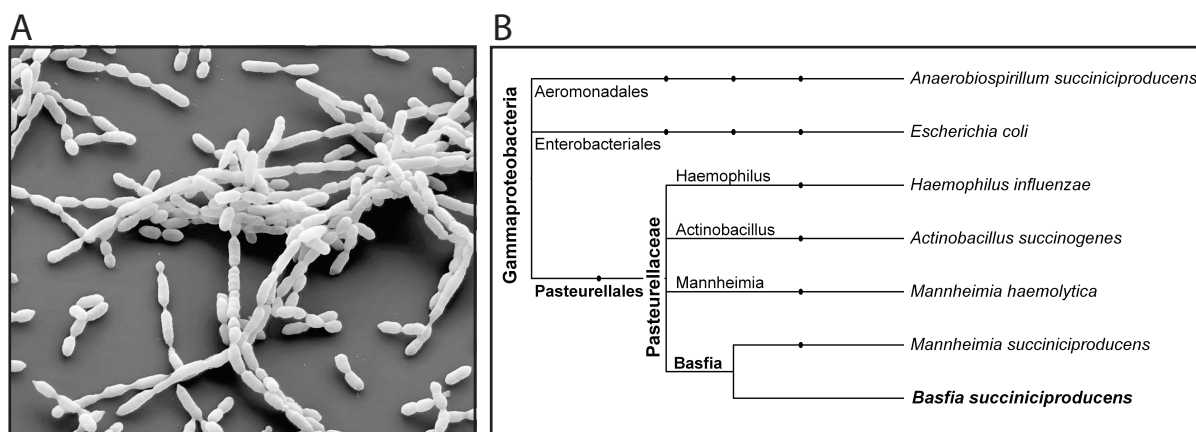
Figure 2.4: The industrial succinic acid producer *B. succiniciproducens*. (A) Scanning electron microscope image of *B. succiniciproducens* DD1, showing the typical chains and clusters formed by the bacterium. (B) Cladogram of important natural succinic acid producers, including *B. succiniciproducens*, other *Pasteurellaceae*, and Gram-negative model organism *E. coli*. The tree was generated using iTOL v. 3.2.3. Nodes represent branching points of the phylogenetic tree. Similar figures can also be found elsewhere (Ahn *et al.*, 2016; Kuhnert *et al.*, 2010).

In contrast to other *Pasteurellaceae*, *B. succiniciproducens* is neither toxic nor pathogenic, and only harbors auxotrophies for a small number of vitamins, rendering it an ideal candidate for industrial production. Although *B. succiniciproducens* is facultative anaerobic, it shows better growth under anaerobic conditions (Stellmacher *et al.*, 2010) and requires complex media to grow aerobically. It is capnophilic, i. e., it thrives in a CO_2-atmosphere. The reason for this specific life style is that in its natural environment, the bovine rumen, CO_2 is highly abundant, comprising $65.5 \, mol\%$ of the atmosphere (Hong *et al.*, 2004). *B. succiniciproducens* uses this to its advantage, even gaining energy through ATP-generation while assimilating CO_2. Its main metabolic product is succinic acid, which is in turn used as a substrate by propioni bacteria. Propionic acid generated through this symbiosis is finally assimilated by the cattle host (Guettler *et al.*, 1999). In the bovine rumen, various carbohydrates are readily available as potential carbon sources for *B. succiniciproducens*, explaining why *B. succiniciproducens* has the ability to metabolize a broad array of substrates, including D-glucose, D-fructose, D-galactose, D-mannitol, D-mannose, sucrose, trehalose, D-xylose, and glycerol (Kuhnert *et al.*, 2010; Scholten *et al.*, 2009). Besides succinic acid, other organic acids, mainly formic acid, acetic acid and lactic acid, as well as ethanol are produced during fermentation.

2.2.2 The central carbon metabolism of *Basfia succiniciproducens*

The genome of *B. succiniciproducens* was sequenced and annotated when the *Basfia* genus was first described (Kuhnert *et al.*, 2010). It showed significant similarity to the genome sequence of patent strain *Mannheimia succiniciproducens* MBEL55E, described a few years earlier (Kuhnert *et al.*, 2010; Lee *et al.*, 2002b) and now re-classified as *Basfia*. Nearly 2400 open reading frames (ORFs) were identified in the 2 340,000 base pair (bp) genome, 85% of which were homologous to ORFs from *M. succiniciproducens* MBEL55E, whereas 145 annotated genes were unique to strain DD1. The central carbon metabolism of *B. succiniciproducens* (Figure 2.5) comprises the EMP pathway, gluconeogenesis and the PP pathway, but no evidence of the ED pathway was found. *B. succiniciproducens* encodes a number of genes with putative activity at the pyruvate node: phosphoenolpyruvate carboxykinase (PEPCK, encoded by *pckA*), phosphoenolpyruvate carboxylase (PEPCX, encoded by *ppc*), oxaloacetate decarboxylase (OADC, encoded by *oadA*, *oadB*, and *oadG*), and malic enzyme (MAE, encoded by *maeB*, originally termed *sfcA*) are all capable of catalyzing interconversions between the linked C4 and C3 metabolite pools. Knockout studies in *M. succiniciproducens* LPK ($\Delta ldhA$, $\Delta pflD$) revealed that MAE is not relevant for growth and succinic acid production (Lee *et al.*, 2006b). While knocking out *ppc*, on the one hand, led to an increased growth rate but also increased

accumulation of pyruvate, this deletion did not influence succinate production significantly. Knocking out *pckA*, on the other hand, resulted in a strain with strongly retarded growth which was, however, still able to produce succinic acid. From theses results, it can be concluded that carboxylation of PEP by both PEPCX and PEPCK is essential for succinate production in *Mannheimia succiniciproducens*. Carboxylation of PEP by PEPCK yields ATP, which is probably the reason why the lack of this enzyme hamperes growth profoundly. Malate and oxaloacetate are converted along the reductive TCA cycle branch, through malate dehydrogenase (encoded by *mdh*), fumarase (encoded by *fumC*), and fumarate reductase (encoded by *frdA*, *frdB*, *frdC*, and *frdD*). The fumarate reductase complex catalyzes the reduction of fumarate to succinate using menaquinol (reduced menaquinone) as an electron donor. The complex is closely related but not identical, to Complex II of the respiratory chain (succinate dehydrogenase), which catalyzes the reverse reaction (Weingarten *et al.*, 2009).

To produce biomass precursors, malate and oxaloacetate are in part converted via the oxidative branch of the TCA cycle, starting with the formation of citrate from oxaloacetate and acetyl-CoA by citrate synthase (encoded by *gltA*). Acetyl-CoA is supplied by either pyruvate dehydrogenase (encoded by *aceE*, *aceF*, and *lpd*) which additionally yields CO_2 and NADH, or by the anaerobic enzyme pyruvate formate lyase (encoded by *pflD*), which catalyzes the cleavage of pyruvate into formate and acetyl-CoA (Figure 2.5).

Several reactions required for production of the metabolic end products acetate, ethanol and lactate were annotated as well. *B. succiniciproducens* has a number of different substrate uptake systems, including PTS systems and ABC transporters, the most relevant of which are also displayed in Figure 2.5.

A first study of the *B. succiniciproducens* fluxome (Becker *et al.*, 2013) recently revealed that the main metabolic route of carbon is through the EMP pathway and the reductive C_4-reactions of the TCA cycle. The PP pathway and the oxidative TCA cycle reactions showed only low activity, mostly to supply anabolic precursors. The results also suggested that a transhydrogenase might actively transfer electrons from NADH to NADPH since *B. succiniciproducens* does not directly produce sufficient NADPH for biomass production.
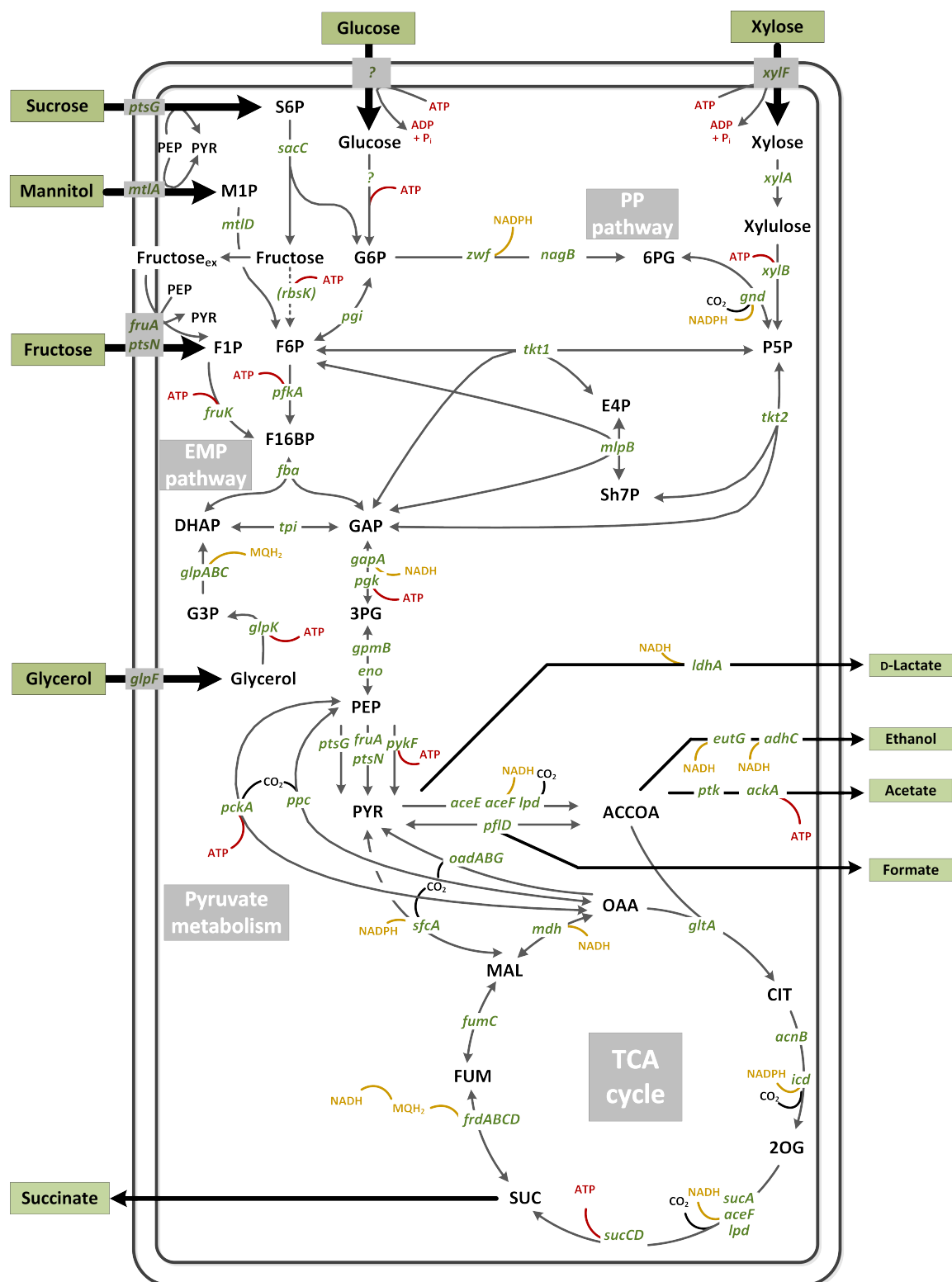
Figure 2.5: Central carbon metabolism of *B. succiniciproducens*. The core metabolism of *B. succiniciproducens* comprises the pentose phosphate (PP) pathway, the Embden-Meyerhof-Parnas (EMP) pathway, various reactions at the pyruvate node, and the tricarboxylic acid cycle (TCA cycle) which can be operated both in the oxidative and in the reductive direction. The interconversions are catalyzed by enzymes encoded by the indicated genes. Question marks (?) denote unidentified enzymes. Dotted arrows and enzymes in parentheses denote putatively inactive but annotated enzymes. S6P: sucrose 6-phosphate; M1P: mannitol 6-phosphate; G6P: glucose 6-phosphate; 6PG: 6-phosphogluconate; F1P: fructose 1-phosphate; F6P: fructose 6-phosphate; P5P: pentose 5-phosphate (mixed pool of ribulose 5-phosphate, ribose 5-phosphate, and xylulose 5-phosphate); F16BP: fructose 1,6-bisphosphate; E4P: erythrose 4-phosphate; Sh7P: sedoheptulose 7-phosphate; DHAP: dihydroxyacetone phosphate; GAP: glyceraldehyde 3-phosphate; G3P: glycerol 3-phosphate; 3PG: 3-phospho glycerate; PEP: phosphoenolpyruvate; PYR: pyruvate; ACCOA: acetyl coenzyme A; OAA: oxaloacetate; MAL: malate; CIT: citrate; FUM: fumarate; 2OG: 2-oxoglutarate; SUC: succinate; ATP: adenosine triphosphate; NADH: nicotinamide adenine dinucleotide, reduced; NADPH nicotinamide adenine dinucleotide phosphate, reduced; MQH$_2$: menaquinol.

2.3 Tailor-made Production Hosts by Metabolic Engineering

The biotechnological industry regards microorganisms as cell factories that are supposed to convert substrates into specific products (Lee *et al.*, 2012). The "industrial objective" to achieve optimal productivity and product yield, however, clearly differs from the "microbial objective" which is usually to optimize cellular growth and form biomass (Smolke, 2009). Therefore, measures must be taken to force a production host into the desired unnatural production behavior.

The so-called classical approach, by which until recently most industrial production strains were constructed, involves random mutagenesis and selection of improved strains. Such classical strains, however, often suffer from detrimental side effects of the various unnecessary mutations they carry, e. g., slow growth, formation of by-products, weak stress tolerance, and a resistance towards further improvement (Wittmann, 2010). Therefore, research started to focuses on rational, targeted improvement of production strains. This approach is called metabolic engineering and can be defined as the purposeful manipulation of the whole cellular metabolism by modification, knock-out, or introduction of specific biochemical reactions with the means of recombinant DNA technology (Bailey, 1991; Stephanopoulos *et al.*, 1998). More recently, systems metabolic engineering emerged as most superior strain engineering technique. While classical metabolic engineering is limited to engineer an organism using local modifications, systems metabolic engineering allows improvement towards an optimal production host on a true systems level.

2.3.1 Quantification of the physiological state by ^{13}C metabolic flux analysis

The cellular metabolism can only be specifically adjusted and finetuned for tailor-made production once the metabolic and regulatory networks are understood on a systems-wide level (Kohlstedt *et al.*, 2010). Therefore, tools of systems biology are a straightforward choice for analyzing the prospective production hosts. A number of "omics"-techniques provide the basis for understanding the organism. Among these, fluxomics has the highest impact on systems metabolic engineering. By describing the metabolite fluxes in an organism, it provides the closest available description of the actual cellular phenotype which is the sum of all transcripts, proteins, and metabolites in a cell (Sauer, 2006). Once a flux map has been identified for a certain organism, it is possible to identify key

routes and bottlenecks and infer targets for optimization of the fluxes (Kohlstedt *et al.*, 2010). The application of fluxomics, however, requires genomics, since the analysis of the cellular metabolism relies on a complete and annotated genome sequence. Other relevant techniques are transcriptomics, the analysis of RNA, proteomics, which deals with cellular proteins, and metabolomics, the analysis of all small molecule intermediates in a cell. Integrative analysis of several functional layers of the microbial system is already a well recognized tool for strain improvement (Chen and Nielsen, 2013; Park *et al.*, 2005).

Metabolic fluxes, the *in vivo* rates of the various enzymatic reactions taking place in a cell, describe the conversion of metabolites into one another. These reactions cannot be measured directly. To determine absolute fluxes of the relevant metabolites through the core metabolism, MFA therefore combines genome-based computer models and experimental data. Depending on the system in question and the desired information, different types of MFA can be conducted (Antoniewicz, 2015). There are two criteria by which the different approaches are distinguished, namely the metabolic state of the system, which can be either instationary or in equilibrium (metabolic steady state), and whether or not isotopic tracer substances are used. Fluxes of cells in a metabolic steady state, i. e., in which fluxes between the metabolite pools are constant, can be resolved at a high resolution by ^{13}C metabolic flux analysis (Figure 2.6). This is usually the case during the exponential growth phase of bacteria.

First, a stoichiometric metabolic model of the organism of interest has to be developed which contains all relevant reactions. Usually, MFA focuses on the 50 to 100 most important reactions of the core metabolism (Kohlstedt *et al.*, 2010). Next, experimental data have to be gathered to constrain the metabolic network. Such information includes the composition of the biomass, the substrate-uptake rate and the product-secretion rates. To gain additional information, ^{13}C-tracer studies are performed: cells are grown on a carbon source which contains ^{13}C atoms at certain, known positions in the molecule. The isotopically labeled substrate is taken up by the cell, metabolized, and finally converted into biomass and products. Since the exact mechanisms of the relevant enzymatic reactions are well known, it can be predicted how a certain amino acid, which is part of the biomass, will be labeled depending on the pathways that are used for its biosynthesis. Therefore, the resulting ^{13}C-labeling pattern of the amino acids in the biomass can be used to quantify metabolic fluxes if the cells fulfill two important conditions when harvested: they must be in metabolic steady state, i. e., intracellular metabolite concentrations and fluxes must be constant, and in isotopic steady state, i. e., the ^{13}C-labeling patterns in all metabolites must be constant (Wittmann, 2007). In the most routine approach, cellular protein from harvested cells is hydrolyzed. After derivatization of the proteinogenic amino acids to

make them more volatile, they are analyzed by gas chromatography-mass spectrometry (GC/MS). Finally, an analysis software, such as the open source software OpenFLUX (Quek *et al.*, 2009), is used to integrate the experimental data and the *in silico* model in order to calculate the metabolic fluxes. As shown in Figure 2.6, labeling distributions are iteratively calculated for presumed flux distributions (based on free fluxes that can be varied), until the difference between simulated and experimental labeling data becomes sufficiently small. Once parameter estimation has yielded an optimal set of fluxes, the result should be statistically evaluated, e. g., by determining 90 % confidence intervals of the fluxes using a Monte Carlo approach.

In comparison to approaches without use of isotopic tracers, such as flux balance analysis, ^{13}C metabolic flux analysis allows resolving the metabolic fluxes with higher fidelity and can even determine reaction reversibilities, rendering it the current "gold standard" of metabolic flux analysis techniques (Sims *et al.*, 2013). The only drawbacks are higher costs and a rather high experimental effort.
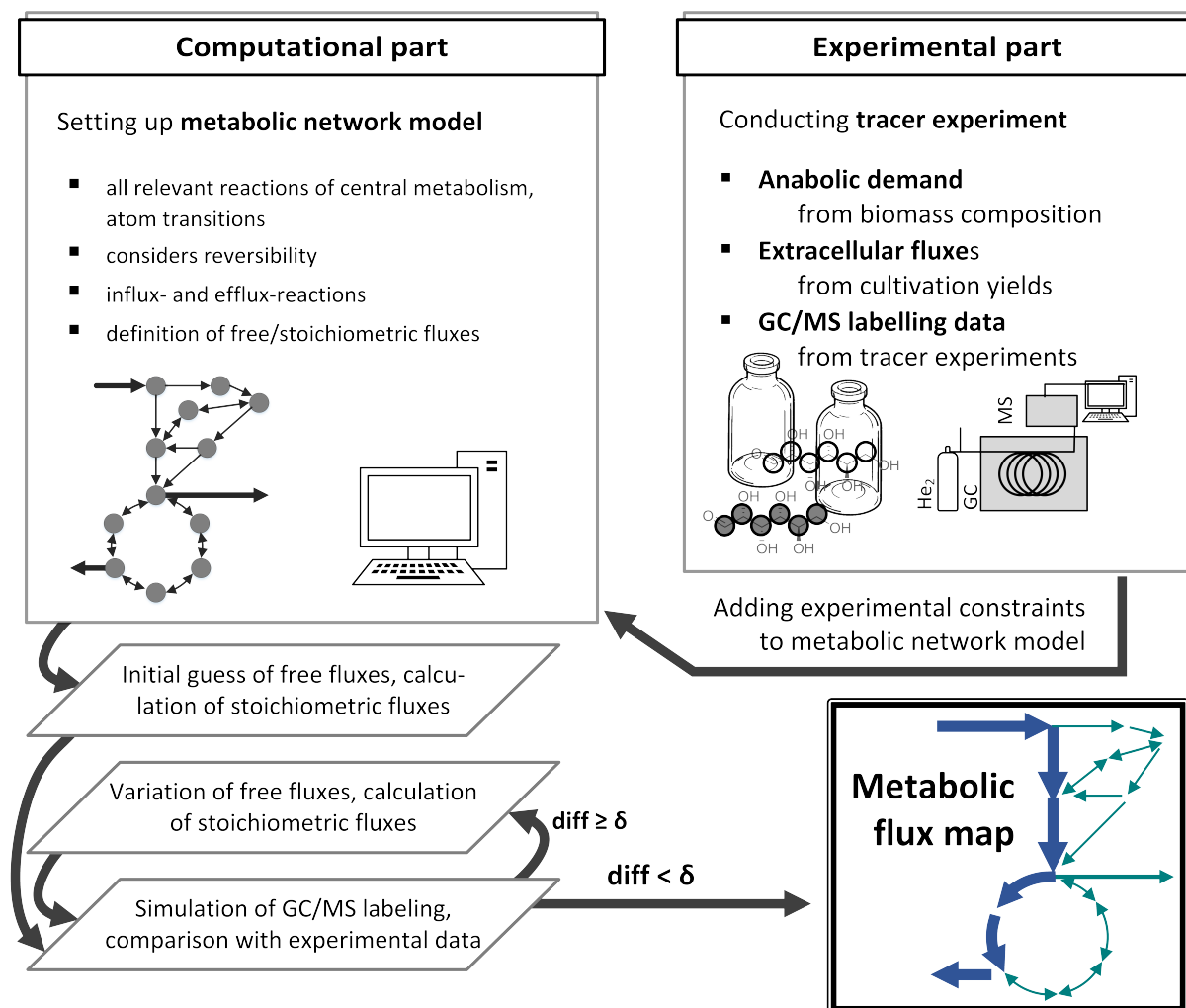
Figure 2.6: Principle of ^{13}**C metabolic flux analysis.** The experimental part comprises the determination of the anabolic precursor demand, the measurement of the extracellular fluxes (substrate uptake and product yields), and cultivation experiments with tracers to determine the labeling patterns, which are a fingerprint of the metabolic fluxes. The computational part comprises setting up an *in silico* metabolic network model. The experimental data are used to constrain the model. Then, the software (e. g., OpenFLUX) guesses an initial set of free fluxes. By comparing the derived *in silico* mass isotopomer distributions to the experimental data and interative variation of the free fluxes, a set of free fluxes is identified which represents the actual *in vivo* fluxes.

2.3.2 Metabolic engineering of succinic acid producers

The techniques of systems biotechnology, especially ^{13}C metabolic flux analysis, are powerful tools for metabolic engineering. One prominent example is the construction of a superior *Corynebacterium glutamicum* strain with the ability to overproduce the amino acid lysine through iterative cycles of ^{13}C metabolic flux analysis and implementation of metabolic engineering targets (Becker *et al.*, 2007, 2005, 2011). There are several other examples of successful application of ^{13}C metabolic flux analysis to improve production hosts in a targeted manner, e. g., during L-valine production and during enzyme production by *C. glutamicum* (Bartek *et al.*, 2011; Umakoshi *et al.*, 2011).

In the field of succinic acid production, both rational and non-rational engineering approaches have been applied to generate superior producers from different organisms. Although several natural succinic acid producers have been described, none of these organisms show homofermentative succinic acid production. Therefore, eliminating by-products is certainly an important task of metabolic engineering. Additional goals are to optimize the succinic acid productivity, yield, and the substrate-utilization efficiency (Ahn *et al.*, 2016).

Other organisms have been engineered to produce succinic acid in the first place. A selective excerpt of metabolically engineered microorganisms for succinic acid production is given in Table 2.2. Due to the sheer number of publications in this field, the table does not provide a complete list, but rather a comprehensive overview over the most important strains that demonstrate different approaches (rational and non-rational), strategies and relevant analysis techniques used in strain engineering for succinic acid production. More strains have been described elsewhere (Ahn *et al.*, 2016; Beauprez *et al.*, 2010; Cheng *et al.*, 2013; Choi *et al.*, 2015).

2.3.2.1 Analysis and optimization of natural producers

So far, only three of the known strains of natural succinic acid producers have been modified with the aim of improving their characteristics. The reason for this is most likely the lack of genetic engineering tools for the other organisms.

A mutant of *Actinobacillus succinogenes* 130Z, called FZ-6, showing increased succinic acid production and reduced formation of formic acid and acetic acid was generated by random mutagenesis with monofluoroacetate and subsequent selection (Guettler *et al.*, 1996). Strain FZ-6 lacked pyruvate formate lyase activity and formate dehydrogenase activity (Park *et al.*, 1999). Apparently, metabolic flux analysis revealed significant changes at the pyruvate node (Liu *et al.*, 2008b). Other studies focused on unraveling the

A. succinogenes metabolism by ^{13}C metabolic flux analysis but no improved strains were constructed (McKinlay *et al.*, 2007; McKinlay and Vieille, 2008).

Succinic acid production of *B. succiniciproducens* from glucose was analyzed by ^{13}C metabolic flux analysis and improved in two iterative cycles of flux analysis and genetic engineering to reduce by-product formation (Becker *et al.*, 2013). After eliminating the main by-product formic acid by deleting *pflD*, the gene encoding pyruvate formate lyase, lactic acid emerged as a new by-product, possibly due to a backlog of pyruvate at the pyruvate node: the flux through pyruvate dehydrogenase increased only marginally. In the next step, lactate dehydrogenase was eliminated. This led to a significant improvement of the succinate production, a slightly increased flux through the pyruvate dehydrogenase, and an increased flux towards other pyruvate-based products. The remaining backbone of the flux map, i. e., the flux through the PP pathway and the oxidative branch of the TCA cycle, remained largely unaffected.

Two years after the isolation of *M. succiniciproducens* and the description of its *pckA* gene (Lee and Chang, 2002; Lee *et al.*, 2002a), the complete genome sequence was published (Hong *et al.*, 2004). Based on the annotated genome and a first metabolic flux analysis, an improved strain LPK7 was constructed by disrupting three by-product forming pathways (deletion of *ldhA*, *pflB*, *pta* and *ackA*) (Lee *et al.*, 2006b). Also, a minimal medium for *M. succiniciproducens*, taking into account all its auxotrophies, was developed through *in silico* analysis (Song *et al.*, 2008). A genome-scale model, allowing constraint-based metabolic flux analysis, was constructed (Kim *et al.*, 2007). Using this model, the effect of H_2 and CO_2 on the *M. succiniciproducens* metabolism was analyzed (Kim, 2009). Only recently, new strains were constructed based on predictions from this model: PALK, PALFK, and PALKG all showed improved succinate production (Ahn *et al.*, 2016). It was found that deletion of the *pfl* gene was not necessary to prevent formate production, so that PALK actually harbored less mutations than the previously described strain LPK7 (Lee *et al.*, 2015). In strain PALFK, the fructose PTS system had additionally been disrupted, in order to deregulate the metabolism and allow for simultaneous consumption of glycerol and sucrose (Lee *et al.*, 2014). Strain PALKG carried an additional *E. coli* glycerol kinase to improve glycerol consumption. Other studies focused on different aspects of the *M. succiniciproducens* metabolism, e. g., its proteome (Lee and Lee, 2010; Lee *et al.*, 2006a), its specific signal-transduction systems (Jung *et al.*, 2008), and its sucrose-utilization mechanism (Lee *et al.*, 2010a). The latter was analyzed by means of enzymatic assays and knockout studies.

2.3.2.2 Metabolic engineering of other microorganisms

Other microorganisms with little or no natural ability to secrete succinic acid have successfully been engineered for succinic acid production (Ahn *et al.*, 2016; Becker and Wittmann, 2015). *E. coli*, *S. cerevisiae* and *C. glutamicum* are model microorganisms with a long tradition as industrial production hosts (Li and Borodina, 2015; Wendisch *et al.*, 2006). Therefore, numerous studies describe engineering of these hosts for succinic acid production (Ahn *et al.*, 2016; Becker *et al.*, 2015; Cheng *et al.*, 2013; Jantama *et al.*, 2008; Thakker *et al.*, 2015). Other yeast strains have been chosen because of their characteristics.

The strategies for metabolic engineering towards succinic acid production in these organisms can be divided into approaches for aerobic succinate production (using the oxidative TCA cycle and the glyoxylate shunt) and anaerobic succinate production (via the reductive TCA cycle), as discussed in Chap. 2.1.1.

A variety of *S. cerevisiae* strains have been described in literature. The only strain, however, which has been reported to produce a significant amount of succinic acid at a final titer of $43 \, g \cdot L^{-1}$ is the patent strain SUC-297 (Van De Graaf *et al.*, 2015). It harbors twelve modifications and combines different metabolic engineering approaches for improved succinate production, as listed in Table 2.2. By comparison, the best succinate production performances from scientific literature report titers of $13 \, g \cdot L^{-1}$ (Yan *et al.*, 2014) and approx. $4 \, g \cdot L^{-1}$ (Raab *et al.*, 2010). Nevertheless, interesting metabolic engineering strategies have been described, such as channeling carbon through the glyoxylate pathway by disrupting the oxidative TCA cycle branch (Raab *et al.*, 2010) or linking succinate production to cell growth combined with evolution to improve cell growth (Otero *et al.*, 2013). The latter approach required a genome-scale metabolic simulation to predict suitable targets. In another study, flux balance analysis was applied to identify a mitochondrial dicarboxylic acid transporter as target (Agren *et al.*, 2013). Production via the reductive TCA cycle has until now proven most successful (Van De Graaf *et al.*, 2015; Yan *et al.*, 2014).

Other related microorganisms have been engineered as well. A succinate tolerant *Pichia kudriavzevii* strain was selected and further improved through directed evolution and metabolic engineering, resulting in the patent strain 13723 (Rush and Fosmer, 2013). A titer of nearly $50 \, g \cdot L^{-1}$ at a yield of $0.7 \, mol \cdot mol^{-1}$ glucose was achieved, which is exceptionally high for a yeast-based strain. The strain produces succinic acid via the reductive TCA cycle at a low pH value.

The highest succinate titers described in literature have been achieved with *E. coli* and *C. glutamicum* strains in dual phase fed-batch fermentations: cells were first grown aer-

obically to high cell densities, and then an anaerobic production phase was initiated. Among the *E. coli* strains, a number of which are listed elsewhere (Cheng *et al.*, 2013), the highest titer, 127 g·L^{-1} has been reported for strain NZN111 (Chen *et al.*, 2014). NZN111 is actually a very simple strain, in which only *pfl* and *ldhA* have been deleted, and which is unable to grow anaerobically. Further improvement of NZN111 through metabolic engineering (Wang *et al.*, 2009), directed evolution (Chatterjee *et al.*, 2001), or a combination of both (Vemuri *et al.*, 2002) yielded strains with restored ability to grow fermentatively. NZN111 with heterologous malic enzyme from *E. coli* was analyzed by MFA (Hong and Lee, 2001). The study revealed a high intracellular accumulation of pyruvate and succinate, rendering this undesired accumulation a possible target for future strain engineering.

In another approach, pathways leading to production of lactate, formate, acetate, and ethanol were disrupted, resulting in a strain with an apparent acetate-auxotrophy. This could be overcome by directed evolution (Jantama *et al.*, 2008).

Another mentionable strain is *E. coli* SBS550MG, in which—in addition to blocking by-product synthesis—the glyoxylate shunt was enhanced by deleting its transcriptional repressor, encoded by *iclR*. Further modifications included a heterologous expression of a pyruvate carboxylase and a formate dehydrogenase, to provide additional reducing equivalent when formate is fed as co-substrate to glucose (Balzer *et al.*, 2013). Only recently, metabolic flux analysis has been applied to construct and analyze a new succinate producer (Zhao *et al.*, 2016). The analysis of the intracellular fluxes revealed that, although the glyoxylate shunt had theoretically been enhanced by deleting *iclR*, it was not used *in vivo*. Fine tunig of *pykF* expression using small RNAs, however, reduced the flux from PEP to pyruvate and thus increased the succinate yield. The Myriant patent strain MH28 is, by comparison, modified more profoundly: it harbours 12 rational modifications and a number of additional mutations generated by directed evolution. Nevertheless, the metabolic engineering strategies are mostly similar to those described before. In addition, the strain was especially engineered for glycerol consumption, since a point mutation in glycerol kinase inactivates feedback-inhibition.

The succinic acid titers achieved with *C. glutamicum* are exceptionally high: strain ΔldhA-pCRA717 produced 146 g·L^{-1} (Okino *et al.*, 2008), and strain BOL-3/pAN6-gap 134 g·L^{-1} (Litsanov *et al.*, 2012). It should, however, be mentioned that such titers were only reached in dual-phase fermentations which require an initial, aerobic phase for cell growth before the actual anaerobic production phase. This clearly limits industrial application. Similar to NZN111, ldhA-pCRA717 is rather simple since only *ldhA* was deleted and a *pyc* gene was overexpressed. No further studies of the metabolic properties of this strain are available. Strain BOL-3/pAN6-gap overexpresses a heterologous *fdh* gene, so

that it can use formate as source of additional reduction equivalent. Glycolysis was enhanced by overexpression of *gapA*. Overall, an exceptionally high yield of $1.67\,\text{mol·mol}^{-1}$ glucose was achieved with this strain. Finally, a study by Zhu *et al.* (2014) should be mentioned because it is a good example of how "omics" techniques can be applied to iteratively improve a strain by metabolic engineering. Here, *real time* qPCR for transcriptome analysis as well as enzyme assays and MFA led to the identification of several targets, so that finally, without additional reducing agents such as formate, 84 % of the maximal yield was achieved. In this strain, the glyoxylate shunt was successfully activated by overexpression of its genes.

Table 2.2: Metabolically engineered succinic acid producers. Summary of modifications, techniques, and improved production parameters, as reported in selected publications. The metabolic engineering strategies applied in these studies are: [1]deletion of competing by-product pathways; [2] increase of PEP/pyruvate carboxylation; [3] introduction/enhancement of glyoxylate shunt; [4] increase of NADH availability; [5] improvement of substrate uptake; [6] improvement of succinate secretion; [7] disruption of succinate-, oxaloacetate- or fumarate-withdrawing reactions (succinate dehydrogenase [a; aerobic], malate dehydrogenase [b; anaerobic], fumarase [c; aerobic]), malic enzyme [d]; [8] enhancement of reductive TCA cycle (specific for anaerobic production); [9] directed evolution or selection. N/A: no information available; GE studies: genetic engineering studies

Strain	Analysis, strategies	Modifications	Performance	Source
		Saccharomyces cerevisiae		
SUC-297[a]	M/A [1, 2, 6, 7b, 8]	$\Delta adh1$ $\Delta adh2$ $\Delta gpd1$ $+pckA^1+gsh1^2_+ +cys3^2_+$ $+glr1^2_+ +mdh3^2_+ +pyc2p^2_+$ $+fumR^5_+ +frdm1^5_+ +mae1^3$	$43.0\,\text{g·L}^{-1}$, $0.45\,\text{g·(L\,h)}^{-1}$	Van De Graaf *et al.* (2015)
S149sdh12/ pNV11-mae1	Metabolite profiling, [1, 6, 7a]	disruption of *adh1-5*, *sdh1-2*, + mae1[4]	$0.036\,\text{mol·mol}^{-1}$, $<500\,\text{mg·L}^{-1}$	Ito *et al.* (2014)
AH22ura3-4Δ	GE studies, metabolite measurement[1, (3), 7a]	$\Delta sdh1\text{-}2$, $\Delta idh1$, $\Delta idp1$	$3.62\,\text{g·L}^{-1}$, $0.11\,\text{mol·mol}^{-1}$	Raab *et al.* (2010)
PMCFf	GE studies, enzyme assays, [1, 2, 7c, 8]	$\Delta fum1$, $\Delta gpd1$,$\Delta pdc1$, $\Delta pdc5\text{-}6$, $+pyc2^2_+$ $+mdh3r^2_+ +fumC^4_+ +frds1^2$	$12.97\,\text{g·L}^{-1}$, $0.14\,\text{g·g}^{-1}$, $0.11\,\text{g·(L\,h)}^{-1}$	Yan *et al.* (2014)
		Pichia kudriavzevii		
13723[a]	N/A, [1, 2, 6, 8, 9]	Δpdc, $+pyc1^5_+ +fum^5_+$ $+frd^5_+ +mdh^5_+ +mae^3$	$48.2\,\text{g·L}^{-1}$, $0.69\,\text{mol·mol}^{-1}$	Rush and Fosmer (2013)
		Escherichia coli		
NZN111	$\Delta ldhA$, Δpfl	[1]	$127\,\text{g·L}^{-1}$, $0.86\,\text{g·g}^{-1}$[b], $3.23\,\text{g·(L\,h)}^{-1}$[b]	Chen *et al.* (2014)

Table 2.2: Metabolically engineered succinic acid producers (continued)

Strain	Analysis, strategies	Modifications	Performance	Source
AFP111-pyc	GE studies, enzyme assays, [1, 2, 9]	$\Delta ldhA$, Δpfl, $ptsG*$, $+pyc^5$	99.2 g·L⁻¹, 1.1 g·g⁻¹[b], 1.31 g·(L h)⁻¹[b]	Vemuri *et al.* (2002)
SBS550MG-Cms243 (pHL413KF1)	Consideration, [1, 2, 3, 4]	$\Delta adhE$ $\Delta ldhA$ $\Delta iclR$ Δack-pta $+pycA$,[5] $+fdh1$[5]	1.64 mol·mol⁻¹[b]	Balzer *et al.* (2013)
MH28[a]	N/A, [1, 5, 7d, 9]	$\Delta aspC$, $\Delta citF$, $\Delta tdcDE$, $\Delta sfcA$, $\Delta focA$-$pflB$, $\Delta ldhA$, $\Delta adhE$, $\Delta mgsA$, $\Delta ackA$, $\Delta poxB$, $glpK*$, disruption of $glpR$, directed evolution	84.3 g·L⁻¹, 1.0 g·g⁻¹[b]	Yocum *et al.* (2011)

Corynebacterium glutamicum

Strain	Analysis, strategies	Modifications	Performance	Source
ΔldhA-pCRA717	Consideration,[1, 2]	$\Delta ldhA$, $+pyc$	146 g·L⁻¹, 0.92 g·g⁻¹[b], 3.17 g·(L h)⁻¹[b]	Okino *et al.* (2008)
BOL-3/pAN6-gap	GE studies, enzyme activities, [1, 2, 4, (5)]	Δcat, Δpqo, Δpta-$ackA$, $\Delta ldhA$, $+pyc^{P458S}$, $+fdh$,[5] $+gapA$	134 g·L⁻¹, 1.09 g·g⁻¹[b], 2.53 g·(L h)⁻¹[b]	Litsanov *et al.* (2012)
SA5	MFA, enzyme assays, RT-qPCR, metabolite measurement, [1,2,3, (5), 6]	$\Delta ldhA$, Δpqo, Δcat, $\Delta ackA$, $+pyc$, $+ppc$, $+aceA$, $+aceB$, $+gltA$, $+sucE$	109 g·L⁻¹, 1.32 mol·mol⁻¹[b]	Zhu *et al.* (2014)

Mannhemia succiniciproducens

Strain	Analysis, strategies	Modifications	Performance	Source
PALFK[a]	*In silico* genome-scale metabolic simulation, [1, 5]	$\Delta ldhA$, Δpta-$ackA$, $\Delta fruA$	78.41 g·L⁻¹, 1.07 g·g⁻¹	Lee *et al.* (2014)

Basfia succiniciproducens

Strain	Analysis, strategies	Modifications	Performance	Source
DD3	¹³C metabolic flux analysis, [1]	$\Delta pflD$, $\Delta ldhA$	35 g·L⁻¹, 0.71 g·g⁻¹	Becker *et al.* (2013)
DD1 [a]	¹³C metabolic flux analysis, [1]	$\Delta pflA$, $\Delta ldhA$, + pykA*	66.04 g·L⁻¹, 1.1 C-mol·C-mol⁻¹	(Krawczyk *et al.*, 2015)

Actinobacillus succinogenes

Strain	Analysis, strategies	Modifications	Performance	Source
FZ-6	[9]	Random mutagenesis	106 g·L⁻¹, 0.8 g·g⁻¹, 1.34 g·(L h)⁻¹	Guettler *et al.* (1996)

[1] from *M. succiniciproducens*
[2] from *S. cerevisiae*
[3] from *Schizosaccharomyces pombe*
[4] from *E. coli*
[5] from other microorganisms
[a] patent strain, possibly industrial producer
[b] performance in dual-phase fermentation; higher apparent yields and productivities since costs for biomass growth are neglected.

Although many succinic acid producers were constructed by exploiting experimental or *in silico* analyses of the metabolism to predict targets, only a smaller number of studies dealt with the specifics of utilizing substrates other than glucose, such as sucrose or glycerol. It is, however, clear that the substrate has a significant influence on succinic acid production (Andersson *et al.*, 2007). The number of studies analyzing *B. succiniciproducens* is especially low, despite the exceptional status of this bacterium among the different microorganisms that have been employed for succinic acid production: besides its highly advantageous innate characteristics, such as being non-pathogenic, not harboring any amino acid auxotrophies, showing fast growth under anaerobic conditions, being able to utilize a broad substrate spectrum, and possessing a high natural succinic acid production capacity, *B. succiniciproducens* can also be optimized using standard genetic engineering and adaptive evolution techniques. Taken together, a closer inspection of *B. succiniciproducens* is a highly promising approach towards improved succinic acid production from renewable carbon sources.

The aim of this thesis was to analyze the metabolism of *B. succiniciproducens* by ^{13}C metabolic flux analysis on industrially relevant substrates, in order to provide the basis for successful metabolic engineering and, possibly, to enable their large-scale application.

3

Material and Methods

3.1 Chemicals and Media

3.1.1 Chemicals

Chemicals were derived from Sigma Aldrich (Taufkirchen, Germany), Roth (Karlsruhe, Germany) and Becton Dickinson (Franklin Lakes, NJ, US), if not noted otherwise. Stable isotopic tracer substances were used for qualitative labeling experiments and for ^{13}C metabolic flux analysis, as listed in Table 3.1.

3.1.2 Media for genetic engineering

For genetic engineering of *B. succiniciproducens*, brain heart infusion (BHI) medium (Becton Dickinson, Franklin Lakes, NJ, US) was used (37 g·L^{-1}). BHI agar plates for solid cultures additionally contained 18 g·L^{-1} agar (Becton Dickinson) and were buffered with 9.38 g·L^{-1} (*N*-morpholino)propanesulfonic acid (MOPS), 1.25 g·L^{-1} Mg(OH)$_2$, 5.8 g·L^{-1} 2,2-*Bis*(hydroxymethyl)-2,2',2"nitrilotriethanol (Bis-Tris) and 1.8 g·L^{-1} NaHCO$_3$. For selection of cells with chloramphenicol resistance, chloramphenicol (10 µg·mL^{-1}) was added to the medium formulation.

3.1.3 Media for serum bottle cultivations

Media for routine cultivations in serum bottles were freshly prepared from sterile filtered stock solutions (Filtropur S 0.2 syringe filter, Sarstedt, Nümbrecht, Germany; Table 3.2), and demineralized water sterilized by autoclaving. The vitamin stock solution was freshly prepared and stored at 4 ℃ for up to two weeks. For first precultures, a complex medium containing yeast extract and bacto peptone was used (Table 3.3), whereas second precultures and main cultures were carried out in minimal medium (Table 3.4).

Table 3.1: Isotopic tracers used in this work. Stable isotopic tracer substances, including carbohydrates and organic acids, were used for qualitative tracer experiments and ^{13}C metabolic flux analysis. Glc: glucose subunit of of sucrose; Frc: fructose subunit of sucrose

Tracer	Supplyer	Labeling Purity [%]	Reference
[^{13}C$_2$] Acetic acid	Sigma Aldrich[a]	99	Chapter 4.1
[1-^{13}C^{Frc}] Sucrose	Omicron Biochemicals[b]	99	Chapter 4.2
[1-^{13}C^{Glc}] Sucrose	Omicron Biochemicals[b]	99	Chapter 4.2
[^{13}C$_6$^{Frc}] Sucrose	Omicron Biochemicals[b]	99	Chapter 4.2
Mg^{13}CO$_3$	Sigma Aldrich [a]	99	Chapter 4.2
^{13}CO$_2$	Sigma Aldrich[a]	98	Chapter 4.2
[1-^{13}C] Fructose	Omicron Biochemicals[b]	99	Chapter 4.2
[^{13}C$_6$] Fructose	Omicron Biochemicals[b]	99	Chapter 4.2
[1-^{13}C] Xylose	Omicron Biochemicals[b]	99	Chapter 4.3.2
[^{13}C$_5$] Xylose	Omicron Biochemicals[b]	99	Chapter 4.3.2

[a] Taufkirchen, Germany
[b] South Bend, Indiana, US

The precultivation for fed-batch production in bioreactors was conducted in serum bottles using complex medium (Table 3.5).

3.1.4 Media and solutions for cultivation in lab-scale bioreactors

The starting medium for fed-batch processes was freshly prepared as described in Table 3.7. Base-FB solution (containing Mg(OH)$_2$ and NH$_3$(aq)) was used for pH maintenance. As feed, concentrated fructose or sucrose solutions were used (Table 3.6). Bioreactor cultivations to supply cells for enzyme assays were carried out in standard minimal medium without MgCO$_3$ (Table 3.4), using Base-B solution (1 M Na$_2$CO$_3$) for pH regulation (Table 3.6).

Table 3.2: Stock solutions for preparation of media. All compounds were dissolved in demineralized water to the final volume indicated, and subsequently sterilized by filtration into sterile tubes using sterile syringe filters (0.2 µm pore size; Filtropur S 0.2 syringe filter, Sarstedt, Nümbrecht, Germany). For preparation of vitamin stock 1, nicotinic acid, riboflavine and biotin were first resuspended individually in demineralized water and then dissolved by addition of approx. 150 µL 6 M NaOH. Subsequently, all dissolved vitamins were pooled, and the pH of the mixture was adjusted to pH 7.5 with 1 M NaOH. Finally, the solution was sterilized by filtration. Vitamin stock 2 and the trace element stock were prepared at BASF.

Stock	Substances	Amount [g]	Volume [mL]
Glucose, 50 %	Glucose $\cdot$ H$_2$O	55	100
Sucrose, 50 %	Sucrose	50	100
Fructose, 50%	Fructose	50	100
Xylose, 25%	Xylose	25	100
Yeast extract, 10%	Yeast extract	10	100
Bacto peptone, 10 %	Bacto peptone	10	100
Phosphate, 50 %	K$_2$HPO$_4$	50	100
Ammonium sulfate, 50 %	(NH$_4$)$_2$SO$_4$	50	100
Salt stock, 14 %	CaCl$_2 \cdot$ 2 H$_2$O	2	
	MgCl$_2 \cdot$ 6 H$_2$O	2	
	NaCl	10	100

		Amount [mg]	Volume [mL]
Vitamin stock 1, 100x	Thiamine $\cdot$ HCl	300	
pH 7.5	Riboflavine	60	
	Nicotinic acid	300	
	Calcium pantothenate	1000	
	Pyridoxal $\cdot$ HCl	100	
	Biotin	50	
	Cyanocobalamine	5	100
Vitamin stock 2, 100x	Thiamine $\cdot$ HCl	100	
(for fed-batch cultivation)	Riboflavine	100	
	Nicotinic acid	100	
	Calcium pantothenate	100	
	Pyridoxal $\cdot$ HCl	100	
	Biotin	5	
	Cyanocobalamine	5	
	Lipoic acid	0.5	
	Betaine	23 430	100
Trace element stock, 500x	Fe(II)SO$_4 \cdot$ 7 H$_2$O	816	
	MnCl$_2 \cdot$ 4 H$_2$O	120	
	ZnSO$_4 \cdot$ 7 H$_2$O	185	
	Na$_2$MoO$_4 \cdot$ 2 H$_2$O	3.8	
	CoCl$_2 \cdot$ 6 H$_2$O	10.1	
	NiCl$_2 \cdot$ 6 H$_2$O	3.2	
	Na$_2$SeO$_3$	1	
	Citric acid	1344	100

Table 3.3: Complex medium for first precultures in serum bottles. The medium was freshly prepared from stock solutions. The specific carbohydrate stock solution required for a certain experiment was added to the medium. Solid $MgCO_3$ was required as a buffer and as a source of HCO_3^-. The amount required to achieve a final concentration of $30\,g{\cdot}L^{-1}$, after addition of the medium, was autoclaved in serum bottles.

Stock	Volume [mL]	Concentration [g·L^{-1}]
Yeast extract, 10 %	5.0	5.0
Bacto peptone, 10 %	5.0	5.0
Salt stock, 14 %	1.0	1.4
Phosphate, 50 %	0.6	3.0
Ammonium sulfate, 50 %	0.2	1
Glucose, 50 %	10	50
or Sucrose, 50 %	10	50
or Fructose, 50 %	10	50
or Xylose, 25 %	20	50
H$_2$O, demineralized	ad 100 mL	

Table 3.4: Minimal medium for second precultures and main cultures. The medium was freshly prepared from stock solutions. The specific carbohydrate stock solution required for a certain experiment was added to the medium. Solid $MgCO_3$ was required as a buffer and as a source of HCO_3^-. The amount required to achieve a final concentration of $50\,g{\cdot}L^{-1}$, after addition of the medium, was autoclaved in serum bottles.

Stock	Volume [mL]	Concentration [g·L^{-1}]
Salt stock, 14 %	1.0	
Phosphate, 50 %	0.6	3
Ammonium sulfate, 50 %	1	1
Vitamin stock, 100x	1	
Glucose, 50 %	10	50
or Sucrose, 50 %	10	50
or Fructose, 50 %	10	50
or Xylose, 25 %	20	50
H$_2$O, demineralized	ad 100 mL	

Table 3.5: Complex medium for serum bottle precultures of fed-batch production in bioreactors. The medium was freshly prepared from stock solutions. The carbohydrate stock solution required for a certain experiment was added to the medium. Solid $MgCO_3$ was required as a buffer and as a source of HCO_3^-. The amount required to achieve a final concentration of $50\,g\cdot L^{-1}$, after addition of the medium, was autoclaved in serum bottles.

Stock	Volume [mL]	Concentration [g·L⁻¹]
Yeast extract, 50 %	5.0	5.0
Bacto peptone, 10 %	5.0	5.0
Salt stock, 14 %	1.0	1.4
Phosphate, 50 %	0.6	3.0
Ammonium sulfate, 50 %	0.2	1
Vitamin stock 2, 100 x	0.2	1
Sucrose, 50 %	10	50
or Fructose, 50 %	10	50
H_2O, demineralized	ad 100 mL	

Table 3.6: Minimal medium for second precultivation and main cultivation. The medium was freshly prepared from stock solutions. Only the carbohydrate stock solution required for the current experiment was added to the medium. Solid $MgCO_3$ was autoclaved in serum bottles and added to the medium to a final concentration of $50\,g\cdot L^{-1}$.

Cultivation	Solution	Substance	Amount [g]	Concentration [%]	[g·L⁻¹]	[mol·L⁻¹]
Batch	Base-B	Na_2CO_3	96.7	9.7	106	1.0
		H_2O, demineralized	903.3			
Fed-Batch	Base-FB	$Mg(OH)_2$	250	25		
		NH_3	7	0.7		
		H_2O, demineralized	743			
	Sucrose-Feed	Sucrose	630	63	813	2.4
		H_2O, demineralized	370			
	Fructose-Feed	Fructose	600	60	767	4.3
		H_2O, demineralized	400			

Table 3.7: Minimal medium for the batch-phase of bioreactor cultivations. The medium for bioreactor cultivations was freshly prepared and autoclaved. The vitamin stock and the trace element stock were added after autoclaving.

Substance	Amount [g]	Concentration [g·L^{-1}]
Sucrose	15	25
Fructose	15	25
$(NH_4)_2SO_4$	2.1	3.5
KH_2PO_4	0.9	1.5
$(NH_4)_2HPO_4$	2.1	3.5
Stock	**Volume [mL]**	
Vitamin stock 2, 100x	6.0	
Trace elements stock, 500x	1.2	
H_2O, demineralized	ad 600 mL	

3.2 Strains and Genetic Engineering

3.2.1 Strains and plasmids

All strains and plasmids used and constructed in this thesis, including corresponding references, where appropriate, are listed in Table 3.8 and in Table 3.9.

3.2.2 Transformation by electroporation

Prior to transformation, *B. succiniciproducens* was grown aerobically in shake flasks. First, a BHI-based pre-culture was inoculated from a cryo-stock and incubated over night (37 ℃, 180 rpm). The main cultivation in BHI medium was inoculated to an initial OD_{600} of 0.1 and harvested at different cell concentrations (OD_{600} 0.4, 0.6, and 0.8) by centrifugation (10 000 x g, 4 ℃ , 5 min). TAfter a washing step with sterile, ice-cold 10 % glycerol, the pellet was resuspended in the same solution. Electroporation was then conducted with a MicroPulser electroporator (BioRad Laboratories, Hercules, CA, USA) at 2 kV, 400 Ω and 25 µF after mixing of 200 µL cell suspension with 2 µg plasmid in an electroporation cuvette. After the pulse, 1 mL of pre-warmed BHI medium was added to the mixture and cells were regenerated for 2 h (37 ℃ , 600 rpm, Thermomixer comfort, Eppendorf, Hamburg, Germany). Afterwards, the cells were plated on buffered BHI agar plates containig chloramphenicol and incubated for 48 h at 37 ℃ . The presence of a plasmid in viable colonies was confirmed by PCR, using specific validation primers (Table 3.10). Additionally, the transformants were grown in BHI medium containing chloramphenicol

Table 3.8: *B. succiniciproducens* strains used in this thesis. All deletion strains and the wild type strain DD1 were supplied by the BASF SE. Strains carrying episomal plasmids were transformed during this study.

Strain	Abbreviation	Modifications	Source
DD1	DD1	Wild type	(Becker *et al.*, 2013)
DD1 Δ*pflD*	DD2	Deletion of pyruvate formate lyase *pflD*	(Becker *et al.*, 2013)
DD1 Δ*ldhA* Δ*pflD*	DD3	Deletion of lactate dehydrogenase *ldhA* and pyruvate formate lyase *pflD*	(Becker *et al.*, 2013)
DD1 Δ*ldhA*	DD1 Δ*ldhA*	Deletion of lactate dehydrogenase *ldhA*	BASF SE
DD1 Δ*ldhA* Δ*mgsA*	DD1 Δ*ldhA* Δ*mgsA*	Deletion of lactate dehydrogenase *ldhA* and methylglyoxal synthase *mgsA*	BASF SE
DD1 Δ*fruA*	DD1 Δ*fruA*	Deletion of the fructose PTS *fruA*	BASF SE
DD1 pjFF224-XN	DD1 XN	DD1 with empty episomal plasmid	This study
DD1 pJMK055	DD1 p055	DD1 with episomal expression of fructokinase gene *rbsK* under the native promoter	This study

Table 3.9: Plasmids used in this thesis. The vectors used in this study were episomal plasmids carrying a chloramphenical resistance and were provided by the BASF SE. MCS: multiple cloning site; *oriV*: replication origin; *mob* genes: mobility genes; *cmR*: chloramohenicol resistance; *rbsK*: gene encoding fructokinase; *ackA*: gene encoding acetate kinase.

Plasmid	Specifications
pJFF224-XN	Episomal vector with *oriV*, *mob* genes, *cmR* as selection marker and MCS
pJMK055	pJFF224-XN with *rbsK* and *rbsK* native promoter in MCS

Table 3.10: Oligonucelotides for strain and plasmid validation. Successful transformation of *B. succiniciproducens* strains by electroporation with the episomal plasmids was validated by colony PCR using the listed oligonucleotide primers. The sequences are given in the 5' → 3' direction.

Name	Sequence
fJF046	CCGCCATATATAACAGAAGATA
rJF046	TTCTCATGTTTGACAGCTTATC

to re-isolate the plasmids (QIAprep Spin Miniprep Kit, Qiagen, Hilden, Germany) which were subsequently validated by digestion with specific restriction enzymes, as described below.

3.2.3 Strain validation

Transformed cells were validated by colony PCR in order to confirm the presence of the desired genetic modification. Colonies growing onto selection agar plates after electroporation were, partly, streaked on new selection plates and, partly, used for colony PCR after resuspending the remaining cells in sterile demineralized water. The suspension was used as template for polymerase chain reaction (Phusion Flash High-Fidelity PCR Master Mix, Thermo Fisher Scientific, Braunschweig, Germany), conducted in a thermocycler (PEQLAB Biotechnology GmbH, Erlangen, Germany). The primers used for strain validation, kindly provided by Jonathan Fabarius (Institute of Systems Biotechnology, Saarland University), are listed in Table 3.10. The expected size of the PCR product was 2552 bp for plasmid pJMK055 and 1089 bp for plasmid pJFF224-XN. The PCR products were separated electrophoretically on 1 % agarose gels (Owl EasyCast Gel Electrophoresis System, Thermo Fisher Scientific; current source Major Science, Serva GmbH, Heidelberg, Germany) and visualized under UV light after staining in an ethidium bromide bath (E.A.S.Y. Plus System, Herolab, Wiesloch, Germany; λ_{Ex}: 260 − 360 nm, λ_{Em}: 590 nm).

Additionally, plasmids were re-isolated from transformed *B. succiniciproducens* cells (QIAprep Spin Miniprep Kit, Qiagen, Hilden, Germany). The plasmids were digested with the FastDigest restriction enzymes SmaI and PfoI (Thermo Fisher Scientific Germany BV & Co. KG, Braunschweig, Germany) according to the manufacturer's instructions and analyzed electrophoretically, yielding distinct band patterns for pJFF224-XN (5006 bp, 1478 bp, 1305 bp, 265 bp) and pJMK055 (5006 bp, 3206 bp, 1305 bp).

3.3 Cultivation

3.3.1 Anaerobic cultivation in serum bottles

Routine cultivations were conducted in 30 mL serum bottles, equipped with butyl rubber seals for sampling, and filled with 10 mL medium, under a CO_2 atmosphere at 0.8 bar overpressure. After inoculation from cryo-stocks, first precultures were incubated at 37 ℃ and 130 rpm (Certomat BS-1, Sartorius, Göttingen, Germany), or at 180 rpm (Multitron, Infors AG, Bottmingen, Switzerland), on an orbital shaker. Exponentially growing cells were harvested by centrifugation (3 min, 16 000 x g, 16 ℃), washed with 1 mL medium and used to inoculate a second pre-culture to an initial OD_{600} of 0.3. Again, exponentially growing cells were harvested and washed as described above, and were used to inoculate the main culture, usually to an initial OD_{600} of 0.3. The incubation times of the precultures were adjusted between 7 and 24 h, depending on the strain. For labeling experiments, the main culture was inoculated to lower cell densities, as specified in the respective Chapters.

3.3.2 Inoculation of main cultures for tracer experiments

In principle, ^{13}C tracer cultivations were conducted as described above, replacing carbohydrates in the media with equimolar amounts of the respective tracers. An important aspect for such experiments is, however, the exact size of the inoculum. The influence of the naturally labeled inoculum has to be taken into account, as it can bias the labeling results.

In this work, three approaches to tackle this issue were applied. The first method relied on the exact determination of the concentrations of the inoculum and of the biomass sample for GC/MS analysis. When the exact percentage of unlabeled inoculum in the final sample is known, the mass spectra of the labeled biomass compounds can be calculated from the measured mass spectra. This method was applied for ^{13}C metabolic flux analysis on xylose (Chapter 4.3.3) and on a mixture of xylose and glucose (Chapter 4.3.4). The second method involves inoculation at such a low cell concentration that, at the time of biomass sampling for GC/MS, less than 1 % of the biomass is derived from the inoculum. This approach was chosen for cultivation on sucrose (Chapter 4.2.5). In the third approach, a third precultivation is conducted in which the ^{13}C-labeled tracer is already applied. The advantage compared to the second approach is that the cultivation can be inoculated at higher cell concentrations. Again, when cells are sampled during the main cultivation, the amount of naturally labeled cells is below 1 %. This approach

was chosen on fructose, as a low inoculum strongly hampered growth on this substrate (Chapter 4.2.7).

Serum bottles containing ^{13}C-labeled substrates were usually sampled and harvested at specific cell densities, whereas the naturally labeled controls were sampled after specific incubation times. Samples from all serum bottles were taken into account for determination of product and biomass yields. Only serum bottles, from which samples were withdrawn simultaneously, however, were used for depiction of cultivation profiles. The exact number of replicates contributing to the data shown in tables (yields, kinetic parameters) and figures (cultivation profiles) are mentioned in the respective captions.

3.3.3 Batch cultivation in lab-scale bioreactors and serum bottles for enzyme assays

For enzyme assays, cells had to be grown without $MgCO_3$ since initial experiments revealed that the washing steps required for removal of the solid compound, even when mild citric acid was used, negatively affected the quality of the cell-free extract. Therefore, cells were grown in complex medium (Table 3.3) buffered with $9.38 \, g \cdot L^{-1}$ MOPS, $1.25 \, g \cdot L^{-1}$ $Mg(OH)_2$, $5.8 \, g \cdot L^{-1}$ Bis-Tris and $1.8 \, g \cdot L^{-1}$ $NaHCO_3$ instead of $MgCO_3$. Alternatively, cells were grown in lab scale bioreactors (DASGIP AG, Jülich, Germany) with a working volume of 300 mL employing a Rushton impeller at 300 rpm and a sparging rate of $0.1 \, vvm \, CO_2$, i.e., $30 \, mL \cdot min^{-1}$, in minimal medium (Table 3.4). The bioreactors were inoculated to an OD of 0.8 with cells pre-grown in complex medium (Table 3.3) which were harvested by centrifugation (5000 x g, 16 °C, 5 min) and subsequently resuspended in minimal medium. Base-B (Table 3.6) was added automatically to maintain a pH of 6.5 ± 0.1 throughout the whole process.

3.3.4 Fed-batch production in lab-scale bioreactors

Fed-batch fermentation was carried out in 1 L Multifors bioreactors with Rushton impellers (Infors AG, Basel, Switzerland), filled with 600 mL batch medium (Table 3.7). The CO_2 sparging rate was set to $60 \, mL \cdot min^{-1}$, and the stirrer speed was set to $300 \, min^{-1}$. Process control and online data monitoring was conducted by the process control software BaseLab (BASF SE, Ludwigshafen, Germany). The bioreactors were inoculated with 60 mL of cells pre-grown for 6 h at 37 °C and 230 rpm on a rotary shaker in complex medium (Table 3.5). Throughout the process, the pH was maintained at 6.5 ± 0.02 by automatic addition of Base-FB (Table 3.6). The added volume was determined gravimetrically. The

cultivation temperature was maintained at 37 ± 0.05 ℃. At the end of the batch phase, feeding at a limited feed of $2.42\,\mathrm{g\cdot h^{-1}}$ was initiated manually.

3.3.5 Sampling of biomass and culture supernatant

For analytical purposes, culture broth was sampled at regular intervals. Samples from bioreactors were taken with a sterile syringe. Serum bottles were turned upside down and each rubber stopper was pierced with a hollow needle attached to a single-use plastic syringe. After the desired sample volume had been withdrawn, the hollow needle was carefully removed and discarded.

The culture broth was directly used for quantification of the cell concentration as OD_{600}. The cell pellet and the culture supernatant, separated by centrifugation ($16\,000\,\mathrm{x}\,g$, 4 ℃, $5\,\mathrm{min}$), were stored separately at -20 ℃ until further analysis.

3.4 Analytical Methods

3.4.1 Quantification of cell concentration

Cell growth was monitored photometrically as optical density at $600\,\mathrm{nm}$ (OD_{600}). Prior to measurement (conducted as duplicate), samples were diluted at least tenfold with $1\,\mathrm{M}$ HCl to completely remove insoluble $MgCO_3$ particles. The exact dilution factors were determined gravimetrically. The cell dry mass concentration was calculated using a previously determined correlation factor of $0.331\,\mathrm{(g\cdot L^{-1})\cdot OD_{600}}^{-1}$ (Becker *et al.*, 2013).

3.4.2 Quantification of substrates and products by HPLC

Glucose concentration in glycogen hydrolysates was determined enzymatically with a STAT 2300 Plus™ glucose analyzer (YSI Life Sciences, Yellow Springs, OH, USA). Exact dilution factors were determined gravimetrically.

An enantiospecific enzyme assay (R-Biopharm, Darmstadt, Germany) was used to seperately determine concentrations of D- and L-lactate in appropriately diluted culture supernatants.

Sucrose, fructose, glucose and xylose were quantified in tenfold diluted culture supernatant by high performance liquid chromatography (HPLC) (VWR Chromaster, Hitachi,

Ltd., Tokyo, Japan), equipped with a reversed-phase column (MetaCarb 87C, 300 x 7.8 mm, Agilent Technologies, Santa Clara, CA, USA), a guard column (MetaCarb 87C Guard Column, 50 x 4.6 mm, Agilent Technologies) and a desalting column (Micro-Guard Deashing Cartridge, 30 x 4.6 mm, Bio-Rad, Hercules, CA, USA), to remove interfering ionic compounds such as organic acids from the samples. Water served as mobile phase at 85 °C and a flow rate of $0.6\,\mathrm{mL\cdot min^{-1}}$. The sugars were detected by refraction index measurement, using external standards for quantification. Alternatively, carbohydrates were separated with an Aminex HPX-87H column (300 x 7.8; BioRad, Hercules, CA, USA). In this case, different mobile phases, flow rates and temperatures were used to ensure baseline separation of the analytes from the variety of organic acids and other compounds such as phosphate present in *B. succiniciproducens* culture broth. For quantification of sucrose, $7\,\mathrm{mM}\ H_2SO_4$ was used as mobile phase at a flow rate of $0.6\,\mathrm{mL\cdot min^{-1}}$ and 20 °C, to prevent hydrolysis of the analyte. For the analysis of glucose, $7\,\mathrm{mM}\ H_2SO_4$ was used at $0.7\,\mathrm{mL\cdot min^{-1}}$ and 55 °C. Fructose was measured with $20\,\mathrm{mM}$ H_2SO_4 at $0.7\,\mathrm{mL\cdot min^{-1}}$ and 55 °C. Xylose was analyzed with $0.9\,\mathrm{mM}\ H_2SO_4$ at 55 °C and $0.7\,\mathrm{mL\cdot min^{-1}}$.

Succinic acid, acetic acid, lactic acid, formic acid, fumaric acid and ethanol were measured employing an Aminex HPX-87H column (300 x 7.8; BioRad, Hercules, CA, USA) as stationary phase and $12\,\mathrm{mM}\ H_2SO_4$ as mobile phase at $0.5\,\mathrm{mL\cdot min^{-1}}$ and 45 °C (Becker *et al.*, 2013), or using the methods for xylose, fructose, and glucose quantification as described above. External standards were used for quantification. Because of the higher signal-to-noise ratio, a UV detector at 210 nm was used for detection UV-active compounds such as pyruvate and succinate instead of the refraction index detector.

Amino acids in culture supernatants were analyzed by HPLC (Agilent Series 1200 or 1100; Agilent Technology, Waldbronn, Germany) as described previously (Krömer *et al.*, 2005), using either α-amino butyric acid (ABU) as internal standard for quantification, or using an external standard. Analytes were automatically derivatized with *o*-phthaldialdehyde (OPA) immediately before injection and subsequently separated on a reversed-phase column (Gemini 5μC18 110A, 150 x 4.6 mm; Phenomenex, Aschaffenburg, Germany) equipped with a precolumn (Gemini C18, MAX-RP, 4 x 3 mm; Phenomenex, Aschaffenburg, Germany). As mobile phase, initially solvent A ($40\,\mathrm{mM}\ NaH_2PO_4$ at pH 7.8) was used at a flow rate of $1\,\mathrm{mL\cdot min^{-1}}$ and 40 °C. Separation was achieved in gradient mode, by increasing the ratio of solvent B (45 % acetonitrile, 45 % methanol, 10 % MQ-H_2O) to solvent A from 0 to 0.5 over 45 min, and then to 1 over 5 min. The amino acid OPA-derivatives were detected via fluorescence (excitation at 340 nm, emission at 540 nm; Agilent, Waldbronn, Germany).

3.4.3 Determination of mass isotopomer distributions by GC/MS

The GC/MS system used for the determination of mass isotopomer distributions (MIDs) of amino acids from cellular protein, of glucose from cellular glycogen, and of secreted succinate consisted of a 7890B gas chromatograph (Agilent, Waldbronn, Germany) and a 5977A mass selective detector (MSD) operated in electron ionization mode (Agilent, Waldbronn, Germany) equipped with a HP-5-MS column (5%-phenyl-methylpolysiloxane; 30 m x 0.25 mm x 0.25 μm; Agilent, Waldbronn, Germany) using helium as carrier gas (Wittmann *et al.*, 2002). The analytes of interest were first identified in scan mode (50 m/z – 750 m/z) using external standards to compare the mass fingerprints. Subsequently, the labeled samples were measured in SIM mode, in order to record the exact mass isotopomer distributions (MIDs) presented in Figure 3.1 and listed in Table 3.11. All measurements were carried out as technical duplicates. Naturally labeled samples were measured in SCAN and SIM mode as well, in order to check the accuracy of the measurement.

3.4.3.1 Proteinogenic amino acids

For the ^{13}C-labelling analysis of proteinogenic amino acids, previously harvested cells (Chapter 3.3.5) were washed with 1 M HCl to dissolve residual $MgCO_3$, and were then hydrolyzed by incubation in 6 M HCl (100 μL·[mg cell dry mass][-1]) for 24 h at 105 °C (Kiefer *et al.*, 2004). Cell debris was removed by filtration (0.2 μm, Merck Millipore, Darmstadt, Germany). Subsequently, 15 μL of the obtained hydrolysate was dried under a nitrogen flow. The residue was dissolved in 50 μL dimethylformamide (DMF) , containing 0.1 % pyridine, and derivatized with 50 μL *N*-methyl-*N*-*tert*-butyldimethylsilyl-trifluoroacetamide (MBDSTFA) for 30 min at 80 °C. Using the following temperature profile, baseline separation of all silylated amino acids (Figure 3.1A) was achieved. After 2 min at 120 °C, the temperature was increased to 200 °C at a rate of 8 °C·min^{-1}, and then to 325 °C at a rate of 10 °C·min^{-1}. The temperature of inlet, the interface and the quadrupole were set to 280 °C.

Each amino acid was identified by using an external standard, and by relying on both the retention time and the fragmentation pattern, as recorded in scan mode. The radical ions of the derivatized amino acids, generated through loss of a single electron caused by electron ionization, fragment during mass spectrometry according to a specific pattern. This involves reactions such as elimination of a hydrogen radical or of relatively stable *tert*-butyl radical groups. In Figure 3.1B, the most relevant fragments are displayed.

Table 3.11: Fragment ion clusters of the compounds measured by GC/MS in SIM mode for ^{13}C metabolic flux analysis. The mass attributed to each fragment represents the exact mass of the m+0 isotopomer, sometimes referred to as monoisotopic mass, rather than the molecular mass (a weighted average of all isotopomers), and represents the first mass-to-charge ratio (m/z) of the ion cluster detected by GC/MS. Only the first $n + 1$ isotopomers of each fragment were measured. Here, n denotes the number of carbon-core atoms. These data are sufficient to determine the corrected MID of the carbon core of the analyte (see Chapter 3.6.2). TBDMS: *tert*-butyl-dimethylsilyl; (TMS)$_5$-MOA-glucose: 5-trimethylsilyl-*O*-methyloxime glucose; residue: residue of the amino acid

Analyte	Fragment	Monoisotopic mass [g·mol^{-1}]	Carbon atoms
TBDMS-Alanine	[M-57]	260.15	$1 - 3$
	[M-85]	232.16	$2 - 3$
	[M-159]	158.14	$2 - 3$
TBDMS-Glycine	[M-57]	246.13	$1 - 2$
	[M-85]	218.14	2
TBDMS-Valine	[M-57]	288.18	$1 - 5$
	[M-85]	260.19	$2 - 5$
	[M-residue]	302.2	$1 - 2$
TBDMS-Leucine	[M-57]/[M-residue]	302.20	$1 - 6$ / $1 - 2$
	[M-85]	274.20	$2 - 6$
	[M-159]	200.18	$2 - 6$
TBDMS-Isoleucine	[M-57]/[M-residue]	302.20	$1 - 6$ / $1 - 2$
	[M-85]	274.20	$2 - 6$
	[M-159]	200.18	$2 - 6$
TBDMS-Proline	[M-57]	286.17	$1 - 5$
	[M-85]	258.17	$2 - 5$
TBDMS-Serine	[M-57]	390.23	$1 - 3$
	[M-85]	362.24	$2 - 3$
TBDMS-Threonine	[M-57]	404.25	$1 - 4$
	[M-85]	376.25	$2 - 4$
TBDMS-Phenylalanine	[M-57]	336.18	$1 - 9$
	[M-159]	234.17	$2 - 9$
	[M-residue]	302.20	$1 - 2$
TBDMS-Aspartate	[M-57]	418.23	$1 - 4$
	[M-85]	390.23	$2 - 4$
	[M-159]	316.21	$2 - 4$
TBDMS-Glutamate	[M-57]	432.24	$1 - 5$
	[M-159]	330.23	$2 - 5$
TBDMS-Lysine	[M-57]	418.23	$1 - 4$
	[M-85]	390.23	$2 - 4$
	[M-159]	316.21	$2 - 4$
TBDMS-Arginine	[M-57-NH$_3$]	442.27	$1 - 6$
TBDMS-Tyrosine	[M-57]	466.26	$1 - 9$
	[M-residue]	302.20	$1 - 2$
TBDMS-Succinate	[M-57]	289.13	$1 - 4$
(TMS)$_5$-MOA-glucose	[M-15]	554.26	$1 - 6$
	[M-250]	319.16	$3 - 6$

3.4.3.2 Cellular glycogen

For the analysis of glycogen-derived glucose, 1 mg of previously harvested cells (Chapter 3.3.5) was washed with 1 M HCl, to remove insoluble $MgCO_3$, and was subsequently washed with 20 mM Tris-HCl (pH 7.0), to neutralize the pellet. The cells were then resuspended in 500 μL enzyme solution (70 U·mL^{-1} amyloglucosidase (Sigma-Aldrich, St. Louis, Missouri, US), 1.2 kU·mL^{-1} lysozyme (Sigma-Aldrich) in 20 mM Tris-HCl, pH 7.0) and incubated in a heating block at 37 ℃ for 3 h at 400 rpm. Next, cell debris was removed by centrifugation (5 min, 16 000 x *g*, 4 ℃) and subsequent filtration (0.2 μm, Merck Millipore). Glucose, derived from the enzymatic hydrolysis, was then quantified enzymatically (Becker *et al.*, 2009). For the two-step derivatization prior to analysis, 25 μg glucose was dried by lyophilization, and was then incubated with 50 μL methoxylamine (2 % in pyridine) for 25 min at 80 ℃ to methylate the aldehyde. Subsequently, 50 μL of *N,O-Bis*-trimethylsilyl-trifluoroacetamide (BSTFA, Macherey-Nagel, Düren, Germany) was added. Incubation was then continued for 30 min to silylate the glucose OH-groups (Fig 3.1E). The obtained derivative was then analyzed by GC/MS.

For separation, a temperature gradient was used. After 3 min at 150 ℃, the temperature was increased to 230 ℃ at a rate of 8 ℃·min^{-1}, and then to 325 ℃ at a rate of 25 ℃·min^{-1}. The temperature of inlet, the interface and the quadrupole were set to 280 ℃. The trimethylsilyl *O*-methyloxime derivative of glucose was measured using selected ion monitoring (SIM) of the ion cluster at 554 m/z to 560 m/z, corresponding to a fragment containing carbon atoms 1 to 6, and of the ion cluster at 319 m/z to 323 m/z, corresponding to a fragment containing carbon atoms 3 to 6, as shown in Figure 3.1F (Laine and Sweeley, 1971).
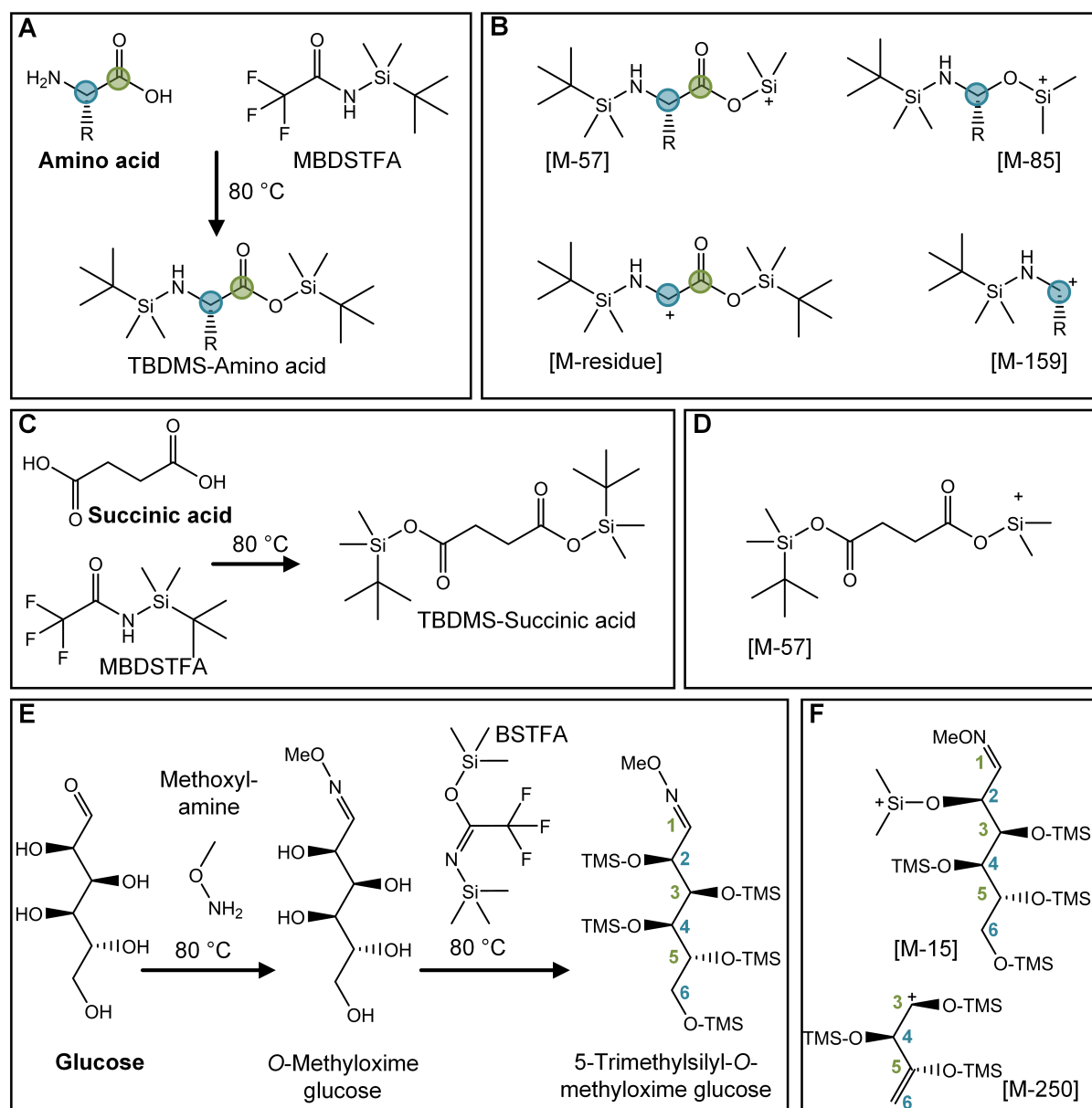
Figure 3.1: Derivatization for and fragmentation during GC/MS analysis of amino acids (A, B), succinic acid (C,D), and glucose (E, F). (A) Amino acids are derivatized with MBDSTFA, yielding the respective TBDMS-derivatives. The carbon atom at position 1 is highlighted in green, and the one at position 2 (α-carbon) is highlighted in blue. (B) Fragmentation yields a number of specific detectable fragments: the [M-57] fragment after loss of a *tert*-butyl group; the [M-85] fragment after additional loss of carbonmonoxide (C1, highlighted in green); the [M-159] fragment after loss of $CO_2Si-TBDMS$; the [M-residue] fragment after loss of the amino acid residue. (C) Succinic acid is derivatized with MBDSTFA (D) and the [M-57] fragment can be detected. (E) Glucose is derivatized first with methoxylamine, then with BSTFA, yielding (F) the [M-15] fragment after loss of a methyl group and the [M-250] fragment, containing carbon atoms 3 − 6.

3.4.3.3 Succinic acid

The labeling pattern of secreted succinic acid in culture supernatant was analyzed as described previously (Becker *et al.*, 2013). Supernatant containing 25 μg succinic acid was dried under a nitrogen flow. The residue was dissolved in 50 μL DMF containing 0.1 % pyridine, and was then derivatized with 50 μL MBDSTFA (Figure 3.1). Using the same temperature profile as for amino acid measurement, the [M-57] fragment of *tert*-butyl-dimethylsilyl (TBDMS) succinic acid was detected.

3.5 Biochemical Methods

3.5.1 Preparation of cell-free extracts for enzyme analysis

For preparation of crude cell-free extracts, cells were harvested by centrifugation (5 min, 5000 x g, 4 ℃), washed with 100 mM Tris-HCl (pH 7.8), and resuspended in the same buffer additionally containing 0.75 mM dithiothreitol to a concentration of 0.33 (g cell wet weight)·mL^{-1}. Up to 1 mL of the cell suspension was then transferred to Lysing Matrix B tubes (MP Biomedicals, Santa Ana, California, US) containing 0.1 mm silica spheres. The cells were then disrupted in a bench-top homogenizer (Precellys 24, Peqlab, VWR International GmbH, Darmstadt, Germany). The cell debris was removed by centrifugation (16 000 x g, 5 min, 4 ℃). The cell-free extract was stored on ice and used immediately for enzyme assays.

3.5.2 Determination protein content

The protein content of cell extracts was determined with a bicinchoninic acid (BCA) protein assay kit (Thermo Scientific, Rockford, IL, USA), using bovine serum albumin as external standard.

3.5.3 Determination of enzymatic activities

All enzymatic activities were determined photometrically at 37 ℃ (Ultrospec 2100 pro UV/Visible Spectrophotometer; GE Healthcare, Little Chalfont, UK). In all assays, either nicotinamide adenine dinucleotide (NADH) or nicotinamide adenine dinucleotide phosphate (NADPH) were oxidized or reduced directly or in a coupled reaction. Both reaction cofactors absorb ultraviolet (UV) light at 340 nm in their reduced, but not

in their oxidized forms, at an extinction coefficient of $\varepsilon = 6.22$ mL·μmol^{-1}·cm^{-1} (Hald *et al.*, 1975). The increase or decrease of absorption at 340 nm was usually recorded for 10 min. Specific enzyme activities (in U = μmol·min^{-1}) were calculated from the initial slope, using the Beer-Lambert law to determine the change in analyte concentration per time.

$$\text{Specific activity [U]} = \frac{\Delta c[\mu mol \cdot mL^{-1}]}{\Delta t[min]} \cdot V_{Cuvette}[mL]$$

$$= \frac{\Delta E}{\Delta t}[min^{-1}] \cdot \frac{V_{Cuvette}[mL]}{d[cm] \cdot \epsilon_{340}[mL \cdot \mu mol^{-1} \cdot cm^{-1}]}$$

(3.1)

All solutions except buffers were freshly prepared and kept on ice throughout the experiments.

Fructokinase

The fructokinase enzyme assay was adapted from Helanto *et al.* (2006). The phosphorylation of fructose into fructose 6-phosphate was measured using two coupling reactions. Fructose 6-phosphate was converted into glucose 6-phosphate which was then oxidized to 6-phosphogluconolactone. The oxidation reaction was coupled to the reduction of NADP$^+$. Fructokinase was assayed in 100 mM Tris-HCl, pH 7.8, containing 10 mM MgCl$_2$, 1 U·mL^{-1} glucose 6-phosphate dehydrogenase, 2 U·mL^{-1} phosphoglucose isomerase, 1 mM NADP$^+$, ATP and fructose. For the kinetic characterization of the enzyme, the concentrations of ATP and fructose were varied in the range of 0.01 mM to 25 mM.

Lactate dehydrogenase

The assay for lactate dehydrogenase, adapted from Bunch *et al.* (1997), was conducted in 100 mM Tris-HCl, pH 7.8, containing 0.25 mM NADH and sodium pyruvate. The enzyme is an oxidoreductase, allowing direct measurement by the decrease of the NADH concentration. For the kinetic characterization of the enzyme, the concentration of sodium pyruvate was varied in the range of 0.1 mM to 25 mM.

Malic enzyme

Malic enzyme has been reported to operate in two directions, e. i., it can both carboxylate and decarboxylate (Gourdon *et al.*, 2000). The reactions require NADP$^+$ or NADPH as cofactor, allowing for direct measurement.

The carboxylation reaction was measured as described by Gourdon *et al.* (2000), with slight adaptations. The reaction mixture contained $5\,\text{mM}$ $MgCl_2$, $0.3\,\text{mM}$ NADPH, and $30\,\text{mM}$ sodium pyruvate, in 100 mM Tris-HCl, pH 7.0, containing $8\,\text{mM}$ NH_4Cl and $50\,\text{mM}$ $NaHCO_3$.

The buffer for the decarboxylation reaction was altered to $100\,\text{mM}$ Tris-HCl, pH 7.8, containing 200 mM KCl, $2\,\text{mM}$ $MgCl_2$, $1\,\text{mM}$ $NADP^+$, and $40\,\text{mM}$ sodium L-malate.

PEP carboxylase and PEP carboxykinase

PEP carboxylase (PEPCX) and PEP carboxykinase (PEPCK) both catalyze the carboxylation of PEP to oxaloacetate. PEP is also a substrate for pyruvate kinase, which catalyzes the ADP-dependent conversion of PEP into pyruvate. When measuring any of these enzymes, it must be ensured that no background activity of the other enzymes leads to false conclusions.

For measurement of PEPCX, activities of both PEPCK and pyruvate kinase have to be prevented. As both competing reactions require ADP as cosubstrate, this can be achieved by omitting ADP from the reaction mixture. To detect the conversion of PEP into oxaloacetate by PEPCX, the reaction was coupled to malate dehydrogenase which catalyzes NADH-dependent reduction of oxaloacetate into malate (Jetten and Sinskey, 1993).

For measurement of PEPCK, background detection of PEPCK and pyruvate kinase has to be prevented. PEPCX was inactivated by adding aspartate, a PEPCX inhibitor, to the reaction mixture. Pyruvate kinase activity could not be excluded in such a way. In cell-free extracts of wild type *B. succiniciproducens*, PEP and ADP are, on the one hand, converted into oxaloacetate and ATP by PEPCK, and, on the other hand, into pyruvate and ATP by pyruvate kinase. Oxaloacetate and NADH are then converted into malate and NAD^+ by malate dehydrogenase. Pyruvate generated by pyruvate kinase, however, also leads to oxidation of NAD^+ when the native lactate dehydrogenase coverts pyruvate into lactate. Therefore, PEPCK was only measured in strain DD1 $\Delta ldhA$, a strain in which this background activity could be excluded due to lack of lactate dehydrogenase activity: although the pyruvate kinase reaction still occurs in parallel to the PEPCK reaction, it does not cause oxidation of NADH so that it does not influence the measurement.

The PEP carboxylase assay was based on the protocol from Jetten and Sinskey (1993). The enzyme was, however, assayed in $80\,\text{mM}$ MOPS, $10\,\text{mM}$ $MnCl_2$, $2\,\text{mM}$ Glutathion,

0.5 mM NADH, and 10 U·mL^{-1} malate dehydrogenase and 10 mM sodium phosphoenolpyruvate as a substrate. PEP carboxykinase was assayed using the same mixture, which additionally contained 30 mM sodium aspartat and 2.5 mM ADP (instead of IDP).

Pyruvate kinase

Pyruvate kinase was measured by coupling conversion of PEP into pyruvate with the NADH-dependent reduction of pyruvate to lactate (Netzer *et al.*, 2004). As buffer, 100 mM Tris-HCl (pH 7.0) was used. The reaction mix contained 15 mM MgCl$_2$, 1 mM ADP, 0.25 mM NADH, and 5.5 U·mL^{-1} lactate dehydrogenase. As substrate, 12 mM sodium pyruvate was used.

Isocitrate dehydrogenase

Isocitrate dehydrogenase, which cataylzes oxidative decarboxylation of isocitrate into 2-oxoglutarate, was directly measured (Becker *et al.*, 2009). The reaction mixture contained 10 mM MgCl$_2$ and 0.5 mM NADP$^+$ in Tris-HCl (pH 7.8). As a substrate, 1 mM isocitrate was used.

Glucose 6-phosphate dehydrogenase

Glucose 6-phosphate dehydrogenase catalyzes NADP$^+$-dependent oxidation of glucose 6-phosphate to 6-phospho-glucono-1,5-lactone and can thus directly be measured. The assay was conducted in a Tris-HCl buffer (pH 7.8) containing 200 mM KCl, 10 mM MgCl$_2$, and 1 mM NADP (Moritz *et al.*, 2000). As substrate, 5 mM glucose 6-phosphate was used.

3.6 Computational Methods

3.6.1 Determination of kinetic parameters for lactate dehydrogenase and for fructokinase

To analyze the kinetic properties of lactate dehydrogenase and fructokinase, the specific activity of the enzymes was determined in crude cell-free extracts for different concentrations of their respective substrates, i. e., pyruvate for lactate dehydrogenase, and ATP and fructose for fructokinase, respectively.

Based on experimental data, the kinetics of fructokinase could be well described by the Michaelis-Menten equation, which describes the dependency of the specific enzyme activity v_0 from the substrate concentration [S] (Michaelis and Menten, 1913):

$$v_0 = \frac{v_{max} \cdot [S]}{K_M + [S]} \tag{3.2}$$

The activity of lactate dehydrogenase, in contrast, showed a sigmoidal substrate dependency, indicating cooperative behavior that could well be described using the Hill equation (Weiss, 1997) which additionally introduces the Hill coefficient n to describe cooperativity:

$$v_0 = \frac{v_{max} \cdot [S]^n}{K_M{}^n + [S]^n} \tag{3.3}$$

The kinetic parameters of fructokinase and lactate dehydrogenase, were determined by a non-linear fit of the data to the respective equation using OriginPro 9.1G.

3.6.2 Correction of mass isotopomer distributions for natural labeling of all atoms except for the carbon backbone

For qualitative inspection of tracer experiments, the mass isotopomer distributions had to be corrected for natural labeling of all atoms except for atoms from the carbon backbone of the respective analyte. This step was, however, not required for ^{13}C metabolic flux analysis, as explained in Section 3.6.3.

To determine the ^{13}C labeling pattern of the carbon backbone of glycogen-derived glucose, succinate, and several amino acids, experimental mass spectra of the derivatized compounds had to be corrected for the natural occurrence of isotopes in all non-carbon atoms and all carbon atoms derived from the derivatization reagent. For this purpose, the method described by Winden *et al.* (2002) was applied, using MATLAB or C++ for calculations.

The corrected mass spectra were used to determine the ^{13}C-incorporation into the compounds summed fractional labeling (SFL), also called molecular enrichment (ME), which is the weighted sum of mass isotopomer fractions (Christensen *et al.*, 2000; Kelleher, 1999). The SFL was calculated according to equation 3.4:

$$SFL = \sum_{i=0}^{n} i \cdot I_{m+i} \tag{3.4}$$

Here, n is the number of backbone carbon atoms in the compound of interest. As there are two stable carbon isotopes, i.e., ^{12}C, also called M0 or m+0, and ^{13}C, called M1 or m+1, the hypothetical molecule – consisiting solely of the backbone carbon atoms – posseses $n + 1$ isotopomers, called $m + 0$, $m + 1$, ..., $m + n$. I_{m+i} is the abundance of the mass isotopomer $m + i$, and i is the number of ^{13}C of this isotopomer.

3.6.3 Determination of intracellular carbon fluxes

Intracellular carbon fluxes were determined using the ^{13}C metabolic flux analysis approach and calculated using the open source software OpenFLUX (Quek *et al.*, 2009). As experimental input, uncorrected GC/MS data were used as the software allows for automatic correction of the simulated MIDs with a correction matrix. In addition, biomass and product yields and the cellular composition of *B. succiniciproducens* representing extracellular and anabolic fluxes were applied to constrain the network.

The complete metabolic models, created, constructed, validated, and used in this study, can be found in the Appendix (Section A.3). The biochemical repertoire deduced from the annotated genome sequences of *M. succiniciproducens* (Hong *et al.*, 2004) and of *B. succiniciproducens* (BASF SE). It comprised the EMP pathway, the PP pathway, a complete TCA cycle, anaplerotic carboxylation and decarboxylation reactions (reversible carboxylation of PEP into oxaloacetate by PEPCX and PEPCK, decarboxylation of oxaloacetate into pyruvate by oxaloacetate decarboxylase, and oxidative decarboxylation of malate into pyruvate by the malic enzyme), fermentation pathways leading to the by-products, including formate, acetate, ethanol, and D-lactate, and anabolic routes into biomass. Qualitative results of this thesis were integrated into the model by adding reversibility to the pyruvate formate lyase reaction. On sucrose and fructose, new by-products were discovered and included into the model, namely isovalerate, acetoin, and L-lactate. Additionally, secretion of pyruvate, fumarate, aspartate, glycine, alanine, valine, isoleucine, leucine, and glutamate was considered.

A number of changes to the metabolic network model were substrate-specific. On fructose, a fructose PTS, catalyzing PEP-dependent fructose conversion into fructose 1-phosphate, followed by ATP-dependent phosphorylation into fructose 1,6-bisphosphate, was added to the network. The phosphofructokinase reaction was replaced by its reverse reaction, catalyzed by fructose 1,6-bisphosphatase. On sucrose, a set of reactions were required to simulate substrate uptake, including (i) a sucrose PTS, (ii) a sucrose 6-phosphate hydrolase, (iii) a fructose PTS, catalyzing PEP-dependent fructose conversion into fructose 1-phosphate, followed by ATP-dependent phosphorylation into fructose 1,6-bisphosphate, and (iv) a fructokinase reaction, leading to ATP-dependent phosphorylation of fructose

into fructose 6-phosphate. On xylose, substrate assimilation included ATP-dependent uptake of the substrate, followed by isomerization into xylulose and phosphorylation into xylulose 5-phosphate. In the network model, the two pentose-phosphates, xylulose 5-phosphate and xylose 5-phosphate, were lumped into a single pentose 5-phosphate pool. On xylose, an additional formate dehydrogenase reaction was included, catalyzing the reversible oxidation of formate into CO_2.

The flux distribution on glucose was previously calculated using a slightly simplified model with a lumped PEP/pyruvate pool and data from a single tracer experiment based on [1-^{13}C] glucose (Becker *et al.*, 2013). In this study, the flux distribution was further refined using the adapted network model and integrating a second labeling data set derived from a 1:1 mixture of [$^{13}C_6$] glucose and naturally labeled glucose. The data had been previously measured but not incorporated into the flux calculation. The data was generated using a slightly different medium that contained small amounts of glutamate and valine. It could be assumed that the potential impact of the two amino acids on the overall fluxes was negligible, as the general physiology of *B. succiniciproducens* was not altered by them significantly.

In order to allow for the integration of up to four separate labeling data sets, the software OpenFLUX was extended as described in the OpenFLUX forum[1]. Multiple parallel labeling experiments proved necessary to resolve all fluxes. For parameter estimation, OpenFLUX combines full isotopomer and metabolite balancing, using the nonlinear programming solver FMINCON from the MATLAB Optimization Toolbox. Energy and redox cofactors, i. e., AMP, ADP, ATP, NAD(H), NADP(H), and menaquinone, were not balanced, but instead later used for validation of the results. The free fluxes defined in the network model were iteratively optimized by minimizing the residual errors between the measured MIDs and the theoretical MIDs, calculated from the current set of free fluxes. Starting from different initial values, this process was repeated up to 100 times to ensure the identification of the global minimum (Wittmann *et al.*, 2002). The set of free fluxes with the smallest deviation between experimental and simulated labeling data was taken as best estimate for the *in vivo* fluxes. Statistical analysis was carried out using a Monte-Carlo approach, as implemented in OpenFLUX, to calculate 90 % confidence intervals for all fluxes (Wittmann *et al.*, 2002).

Reaction reversibilities were calculated from the back flux v_{back} and the net flux v_{net} according to equation 3.5 so that $R = 100\%$ represents infinitely high reversibility and $R = 0\%$ represents an irreversible reaction:

$$R = \frac{v_{back}}{v_{net} + v_{back}} \cdot 100\% \tag{3.5}$$

---

[1]https://sourceforge.net/projects/openflux

3.6.4 Elementary flux mode analysis

While the aim of ^{13}C metabolic flux analysis is to determine the actual experimental flux distribution, elementary flux mode analysis is an approach for determining all independent metabolic pathways that might theoretically occur at steady-state (Melzer *et al.*, 2009). Therefore, elementary flux modes give insight into the potential production capacity of a microbial producer (Zanghellini *et al.*, 2013). Combination of ^{13}C metabolic flux analysis with elementary modes not only allows for an assessment of the current performance of the producer, but can also lead to identification of promising metabolic engineering targets.

Computation of elementary flux modes was carried out as described by Melzer *et al.* (2009), using the software efmtool (Terzer and Stelling, 2008). The stoichiometric network model can be found the Appendix (Section A.3). It contained the same reactions as the model used for ^{13}C metabolic flux analysis, including influx of CO_2 and the respective substrate, and efflux of succinate, biomass, and the main by-products formate, D-lactate, acetate, pyruvate, ethanol. Additionally, the elementary flux mode model considered all redox- and energy cofactors, ammonia, sulfate, and coenzyme A. Influx of the latter three was not limited. During calculation of the elementary modes, the redox co-factors (NAD(H) and NADP(H)) were balanced by the model, whereas an apparent ATP excess was considered possible, due to unknown costs for cellular maintenance.

4

Results and Discussion

4.1 Unraveling Peculiarities of the Central Carbon Metabolism of *Basfia succiniciproducens*

4.1.1 A first look into key reactions by determination of *in vitro* enzymatic activities

Specific enzymatic activities in crude cell-free extracts give interesting insights into microbial metabolism, as they indicate which reactions are present and relevant (Lee *et al.*, 2010a). Knowledge on enzyme capacities can also be crucial for refining an *in silico* metabolic network model, and for interpreting *in vivo* fluxes, e.g., when several reactions cannot directly be distinguished by ^{13}C metabolic flux analysis (Becker *et al.*, 2008). Therefore, initial studies of the rather unexplored fine structures of the *B. succiniciproducens* metabolism focused on the presence and impact of potential key enzymes.

4.1.1.1 Identifying crucial enzymes of the pyruvate node

B. succiniciproducens possesses a large repertoire of enzymes that putatively interconvert C_4 intermediates (oxaloacetate, malate) and C_3 intermediates (PEP, pyruvate) at the interface between the glycolysis and the TCA cycle. Because of their high relevance for succinic acid production, most of these enzymes were studied (Table 4.1). The enzyme exhibiting the highest specific activity ($2.5\,\mathrm{U\cdot mg^{-1}}$) was PEP carboxykinase (PEPCK), underlining its importance for natural succinate production (Lee *et al.*, 2006b; Zeikus *et al.*, 1999).

Similar to other Pasteurellaceae, *B. succiniciproducens* possesses a second enzyme, PEP carboxylase (PEPCX), that catalyzes the carboxylation of PEP. Comprehensive knockout studies in *M. succiniciproducens*, however, indicated a negligible role of PEPCX for

Table 4.1: Specific enzymatic activities in sucrose-grown *B. succiniciproducens*. The activity of PEP carboxykinase (*) was measured in cell-free extracts of a $\Delta ldhA$ deletion strain to avoid background interference, otherwise resulting from PEP conversion into pyruvate and then into lactate via pyruvate kinase and lactate dehydrogenase (Chapter 3.5.3). The data represent mean values and deviation from at least three replicates. PEP: phosphoenolpyruvate; G6P: glucose 6-phosphate

| | Specific enzyme activity [mU·mg^{-1}] | |
	Minimal medium	Complex medium
Lactate dehydrogenase	1658 ± 23	2050 ± 107
Pyruvate kinase	1598 ± 188	2481 ± 150
Malic enzyme, decarboxylating	54 ± 1	10 ± 0
Malic enzyme, carboxylating	39 ± 4	4 ± 0
PEP carboxylase	854 ± 52	690 ± 46
PEP carboxykinase*	n. m.[a]	2528 ± 231
Isocitrate dehydrogenase	5.6 ± 0.3	2.7 ± 0.5
G6P dehydrogenase	82.7 ± 5.9	n. m.[b]

[a] n. m.: not measured (compare Chapter 3.5.3)

[b] n. m.: not measured

growth and succinate production (Kim *et al.*, 2007). In *B. succiniciproducens*, however, PEPCX exhibited a rather high activity of 0.9 U·mg^{-1}, suggesting simultaneous contribution of PEPCK and PEPCX to PEP carboxylation *in vivo*. It should be noted, however, that the actual *in vivo* activities are likely controlled by cell regulatory mechanisms. Nevertheless, the high activity observed for PEPCX was surprising for the following reason: as indicated by the high *in vivo* activity of PEPCK, ADP-dependent PEP carboxylation is a very efficient reaction when HCO_3^- is available. Therefore it should be preferable to the PEPCX reaction, which effectively wastes energy by not phosphorylating ADP.

Pyruvate kinase (1.6 U·mg^{-1}) was highly active as well, whereas malic enzyme showed much lower activity (54 mU·mg^{-1}), but was clearly expressed during growth on sucrose, potentially suggesting its contribution to NADPH formation. Malic enzyme showed both carboxylating and decarboxylating activity, although the carboxylating activity was lower than the decarboxylating activity, and more than 60 times lower than the determined PEPCK activity. Additional measurements showed that all enzymes were also present during growth on complex sucrose medium, whereby their activity varied. The significantly reduced activity of malic enzyme on complex medium might be linked to a reduced demand for redox power, as the medium provides many reduced components for biomass formation.

Enzyme activities at the pyruvate node had previously been studied for the related succinic acid producer *A. succinogenes*, revealing that malic enzyme (up to 0.52 U·mg^{-1}) was indeed more active and more relevant than PEPCK (up to 0.28 U·mg^{-1}) in this organism.

This is clearly distinct from the *B. succiniciproducens* carbon metabolism. The variations in the enzymatic set-up of different Pasteurellaceae might be taken as a piece of evidence that their metabolism indeed differs as well, a picture which was later supported by a number of other findings.

4.1.1.2 Low enzymatic capacity of the PP pathway and of the oxidative TCA cycle

The *in vivo* activity of glucose 6-phosphate dehydrogenase (G6PDH), the entry enzyme into the oxidative PP pathway, and isocitrate dehydrogenase (ICD), the entry enzyme into the oxidative TCA cycle, were rather low (Table 4.1). G6PDH exhibited a clear preference for $NADP^+$ as a cofactor. It showed no activity when NAD^+ was provided but was found active with $NADP^+$ (83 ± 6 mU·mg^{-1}). The activity of isocitrate dehydrogenase, which was also $NADP^+$-specific, was even lower at 5.6 ± 0.3 mU·mg^{-1} and was even further reduced in cells grown on complex medium. The fact that both enzymes were obviously expressed during growth on sucrose, however, potentially suggests their contribution to NADPH formation and to the functional operation of the oxidative PP pathway and to the oxidative branch of the TCA cycle.

4.1.2 Identification of two functional pathways for the production of lactic acid

Two alternative pathways for lactic acid production have been annotated in the *B. succiniciproducens* genome sequence. The first pathway involves the conversion of pyruvate to lactate by lactate dehydrogenase (*ldhA*). The second pathway comprises the synthesis of lactate from dihydroxyacetone phosphate via methylglyoxal synthase (*mgsA*), methylglyoxalase (*gloA*) and hydroxyacyl-glutathione hydrolase (*gloB*). An experimental set-up was designed that allowed to study both pathways and assess their enantiospecificity (Figure 4.1). Lactate dehydrogenase, assessed by enzymatic conversion of pyruvate into lactate by a cell extract of the wild type *B. succiniciproducens*, was found to produce pure D-lactate. When grown on glucose, *B. succiniciproducens* $\Delta ldhA$ still formed small amounts of lactate, which revealed functional operation of the methylglyoxal pathway. The culture broth of the mutant exclusively contained L-lactate. Taken together, *B. succiniciproducens* exhibits two functional pathways for the formation of lactate: lactate dehydrogenase forms D-lactate and the methylglyoxal pathway forms L-lactate (Figure 4.1). The enantioselectivity of the two pathways allowed to precisely differentiate their flux *in vivo* by simple measurement of the amounts of D-lactate and L-lactate in culture

supernatants. The analysis of lactate produced from glucose, sucrose, and fructose, respectively, revealed lactate dehydrogenase as the major lactate-forming enzyme, as on all substrates, more than 95 % of the secreted lactate was D-lactate. As lactate formation on xylose and glucose/xylose mixtures was negligibly low, the lactate enantiomers were not determined for these cultivations.

The kinetic parameters of the major lactate-forming enzyme, D-lactate dehydrogenase, were determined from the specific enzyme activities observed at different substrate concentrations (Figure 4.2). The enzyme exhibited a sigmoidal activity profile, indicating positive cooperativity (Marangoni, 2003). Fitting the data to the Hill equation (Equation 3.3), revealed a Hill coefficient of 2.25 ± 0.05, a K_M of 3.60 ± 0.04 mM, and a high maximal activity of 1.95 ± 0.01 U·mg^{-1}. As the Hill coefficient usually corresponds to the minimum number of substrate binding sites (Marangoni, 2003), *B. succiniciproducens* lactate dehydrogenase possibly acts as a homodimer, as has been described for lactate dehydrogenases from other Gram-negative bacteria (Feldman-Salit *et al.*, 2013; Razeto *et al.*, 2002). Taken together, the cooperativity and the relatively low affinity for the substrate pyruvate might ensure *in vivo* that NADH is only then being recycled through reduction of pyruvate instead of fumarate when pyruvate accumulates intracellularly to undesirably high levels.
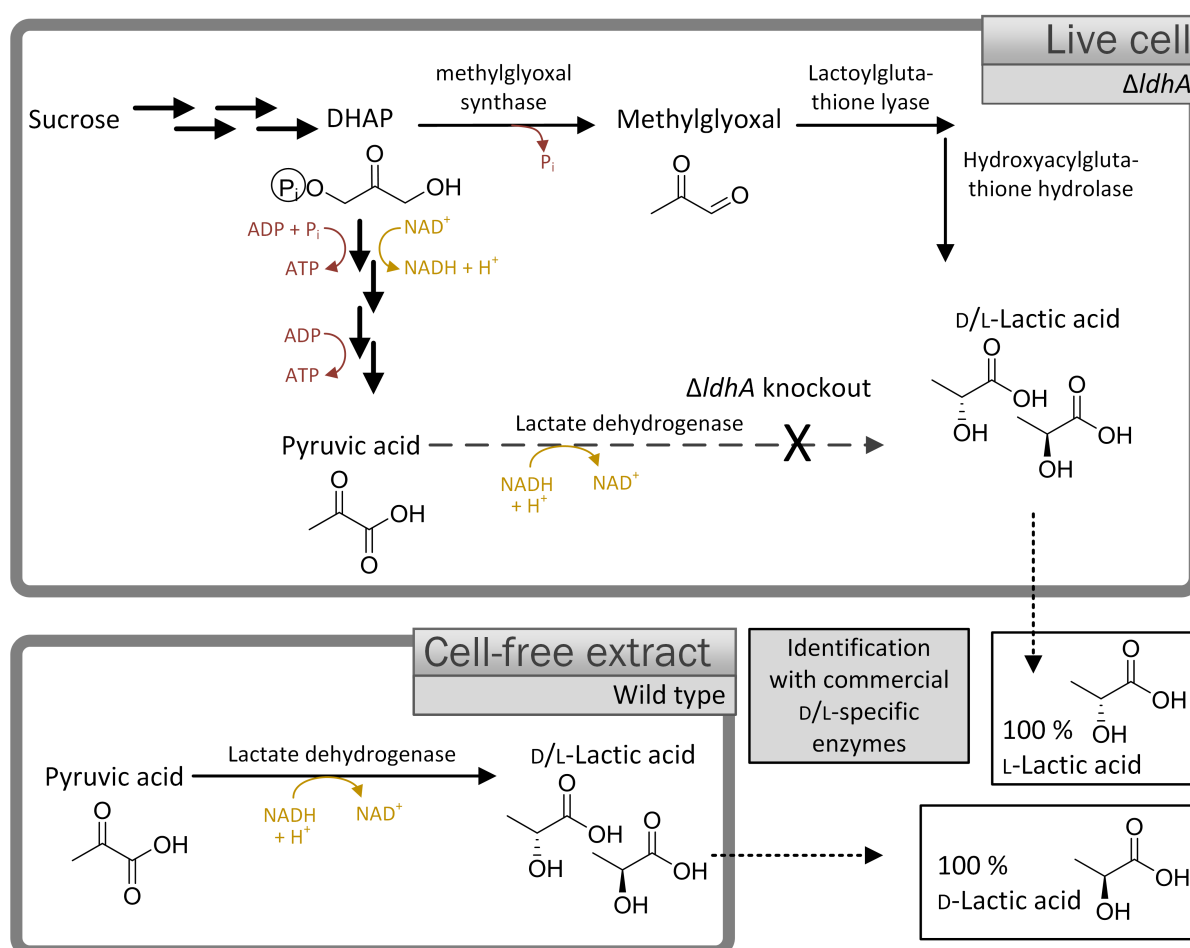
Figure 4.1: Experimental approach to differentiate lactic acid production pathways. Two pathways for production of lactic acid exist in *B. succiniciproducens*. To differentiate these pathways, the configuration of lactic acid produced by either pathway was determined using commercial enantiospecific lactate dehydrogenases: (i) lactic acid produced by *B. succiniciproducens* DD1 Δ*ldhA* Δ*pflD* was used to analyze the methylglyoxal pathway. (ii) For analysis of lactate dehydrogenase, a cell-free extract of *B. succiniciproducens* DD1 was incubated with pyruvate and NADH. The generated lactic acid was then analyzed.
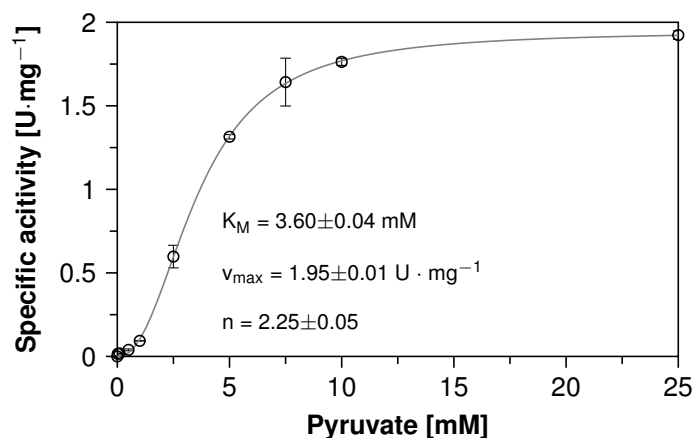
Figure 4.2: Kinetic characterization of *B. succiniciproducens* D-lactate dehydrogenase. The specific activity of D-lactate dehydrogenase was determined in cell-free extracts from sucrose-grown *B. succiniciproducens*. The concentration of the substrate pyruvate was varied. The data, comprising mean values and deviations from at least three replicates, were fit to Equation 3.3 to determine the listed kinetic parameters. K_M: Michaelis constant, v_{max}: maximum reaction rate, n: Hill coefficient.

4.1.3 Pyruvate formate lyase is reversible *in vivo*, whereas pyruvate dehydrogenase is not

The pyruvate node was additionally studied in order to assess enzyme reversibility and to further refine the topology of the metabolic network. As suggested from a previous flux study with *A. succinogenes*, a relative of *B. succiniciproducens*, pyruvate format lyase and pyruvate dehydrogenase are enzymes of high relevance at the node and stable isotopes display a smart and straightforward strategy for reversibility assessment (McKinlay and Vieille, 2008). Here, $[^{13}C_2]$ acetate was added as a co-substrate to glucose-grown cells of the wild type *B. succiniciproducens* DD1 and of the deletion mutant *B. succinicipro-ducens* DD1 $\Delta pflD$, lacking pyruvate formate lyase. By following the distribution of intact $[^{13}C_2]$ units from acetate towards pyruvate, it could be deduced weather any of the two enzymes of interest acted indeed in a reversible manner (Figure 4.3). When $[^{13}C_2]$ acetate was supplied to the culture, the ^{13}C label was quickly identified in intracellular metabolites, although no net-influx was observed, indicating an exchange of acetate with the cell interior. The labeling pattern of glutamate confirmed that the chosen set-up indeed provided intracellular $[^{13}C_2]$ acetyl-CoA. This became obvious from the presence of double labeled [M+2] mass isotopomers of glutamate, which could only originate from $[^{13}C_2]$ acetyl-CoA upon formation of the amino acid through the oxidative TCA cycle (Table 4.2). The *pflD* knockout strain allowed to investigate pyruvate dehydrogenase, as the only remaining reaction potentially forming double labeled [M+2] pyruvate and pyruvate-derived amino acids such as alanine through the reversible nature of the enzyme. The alanine in the cell protein of the *pflD* knockout strain did, however, not contain any ^{13}C enrichment, identifying the reaction catalyzed by pyruvate dehydrogenase as
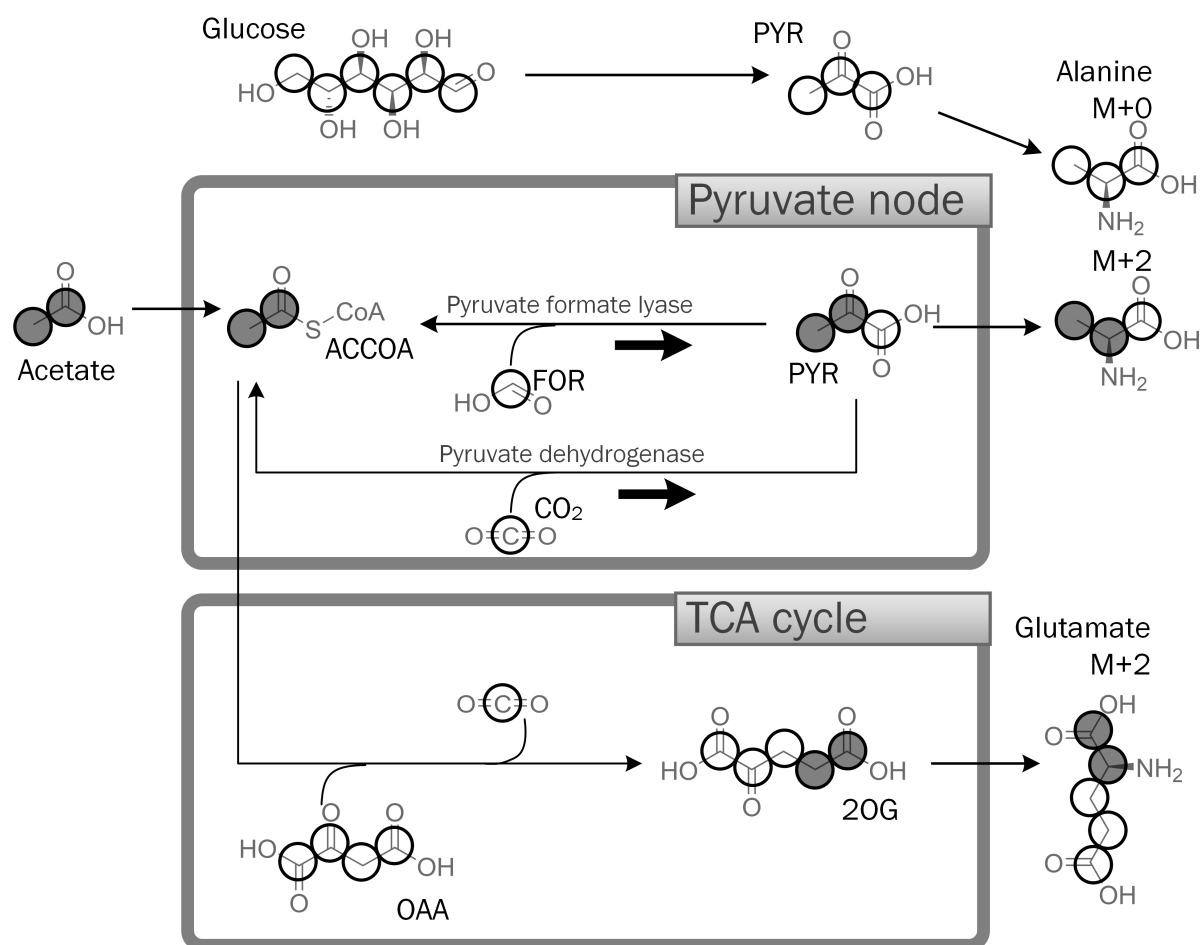
Figure 4.3: Experimental design for analysing the *in vivo* reversibility of pyruvate formate lyase and pyruvate dehydrogenase. To validate *in vivo* reversibility of the pyruvate formate lyase, both *B. succiniciproducens* DD1 and DD1 $\Delta pflD$ were cultivated in on a mixture of naturally labeled glucose and $[^{13}C_2]$ acetate. The labeling could only be incorporated into alanine, a pyruvate-derived amino acid, when the reactions were indeed reversible (indicated by black arrows). Independent of reversibility, the labeling should be incorporated into glutamate, which was used as a control. DHAP: dihydroxyacetone phosphate, P_i: inorganic phosphate, PYR: pyruvate, ACCOA: acetyl coenzyme A, FOR: formate, OAA: oxaloacetate, 2OG: 2-oxoglutarate, TCA cycle: tricarboxylic acid cycle.

irreversible (Table 4.2). In contrast, double labeled alanine was found in the wild type protein hydrolysate. In light of the findings for pyruvate dehydrogenase, it could be concluded that the reaction catalyzed by pyruvate formate lyase is indeed reversible *in vivo*. This was further supported by an increase in the amount of $[^{13}C_2]$ acetate incorporation into alanine when formate was additionally supplied to the medium, which obviously stimulated the back reaction of pyruvate formate lyase. The network model for ^{13}C metabolic flux analysis was revised and adapted accordingly.

Table 4.2: The pyruvate formate lyase reaction is reversible *in vivo*, whereas the pyruvate dehydrogenase reaction is not. The nature of the enzymes was studied by an isotope experiment: [$^{13}C_2$] acetate was supplied as a co-substrate to naturally labeled glucose in cultivations of *B. succiniciproducens* and *B. succiniciproducens* $\Delta pflD$. The mass isotopomer distributions of glutamate and alanine from the cell protein, corrected for interference from natural labeling from all atoms except for the carbon core atoms (Section 3.6.2), give insight into the reactions catalyzed *in vivo*. The data comprise mean values and deviations from two biological replicates. The summed fractional labeling (SFL) was calculated according to Equation 3.4 and is expected to be 1.07 % for naturally labeled carbon.

Analyte	Relative fraction of mass isotopomer			
	Naturally labeled control	DD1 $\Delta pflD$	DD1	DD1+formate
Glutamate				
[M+0]	0.945 ± 0.004	0.751 ± 0.004	0.569 ± 0.003	0.451 ± 0.008
[M+1]	0.052 ± 0.003	0.046 ± 0.001	0.035 ± 0.001	0.031 ± 0.001
[M+2]	**0.003 ± 0.001**	**0.197 ± 0.004**	**0.375 ± 0.004**	**0.462 ± 0.007**
[M+3]	0.000 ± 0.000	0.006 ± 0.001	0.012 ± 0.000	0.015 ± 0.001
[M+4]	0.000 ± 0.000	0.000 ± 0.000	0.009 ± 0.000	0.040 ± 0.001
[M+5]	0.000 ± 0.000	0.000 ± 0.000	0.000 ± 0.000	0.000 ± 0.000
SFL [%]	1.16	9.14	17.19	23.25
Alanine				
[M+0]	0.964 ± 0.001	0.965 ± 0.000	0.891 ± 0.000	0.792 ± 0.000
[M+1]	0.034 ± 0.000	0.034 ± 0.000	0.031 ± 0.000	0.030 ± 0.000
[M+2]	**0.001 ± 0.000**	**0.001 ± 0.000**	**0.076 ± 0.000**	**0.176 ± 0.000**
[M+3]	0.000 ± 0.000	0.000 ± 0.000	0.002 ± 0.000	0.002 ± 0.000
SFL [%]	1.22	1.19	6.27	12.94

4.2 Improving Succinate Production from Fructose and Sucrose

Both sucrose and fructose are major components of molasses, a cheap and abundant raw material for many biotechnological processes. Therefore, both sugars are of particular interest for industrial production of the bulk chemical succinic acid (Liu *et al.*, 2008a). So far, neither sucrose nor fructose metabolism in *B. succiniciproducens* has been analyzed although both substrates have been identified as potential carbon sources for this organism (Scholten and Dägele, 2008).

To date, only two studies describe microbial sucrose catabolism by means of ^{13}C metabolic flux analysis, i.e., aerobic sucrose consumption in Gram positive *C. glutamicum* (Wittmann *et al.*, 2004) and in Gram-negative *E. coli* (Arifin *et al.*, 2014). Likewise, also other nutrients have been only rarely studied at the level of metabolic fluxes. This likely relates to the still high experimental hurdles inherent to such studies as, generally, this technique is one of the most potent strategies to discover metabolic engineering targets (Kohlstedt *et al.*, 2010).

Regarding the succinate-producing rumen bacterium *M. succiniciproducens*, enzymatic assays and gene knockout studies revealed that it orchestrates a number of enzymes for sucrose utilization: (i) a sucrose PTS for uptake (*ptsG*), (ii) a sucrose 6-phosphate hydrolase (*sacC*), (iii) a fructose PTS (*fruA, ptsN*) as well as (iv) a mannose PTS (*manXYZ*), both of which are able to phosphorylate the fructose subunit into fructose 1-phosphate after transient secretion either into the medium or into the periplasm (Lee *et al.*, 2010a), and finally (v) a phosphofructokinase which converts the fructose phosphate into fructose 1,6-bisphosphate, an intermediate of the EMP pathway. A sixth enzyme, a fructokinase, was annotated, but only a negligible activity of 0.03 mU·mg^{-1} was detected. No sucrose-specific repressor was identified, thus explaining the simultaneous consumption of sucrose, glucose and fructose by *M. succiniciproducens* (Lee *et al.*, 2010a).

To completely understand how the disaccharide sucrose, composed of glucose and fructose, is metabolized, it appeared useful to analyze the catabolism of the two subunits as well. Glucose is certainly the most thoroughly characterized carbon source concerning intracellular flux distributions in various microorganisms (Zamboni *et al.*, 2009), including succinate producers (Becker *et al.*, 2013; McKinlay *et al.*, 2007; McKinlay and Vieille, 2008). Fructose has, by comparison, gained far less attention (Kiefer *et al.*, 2004), despite its high industrial relevance. Fructose is not only a major component of molasses but it is also also abundant in high-fructose corn syrup, another raw-material actively used for

industrial succinate production (Mathewson, 2014; Montral Gazette, 2014). In *B. succiniciproducens*, fructose is taken up by the specific fructose PTS (*fruA, ptsN*) which is also relevant during sucrose utilization.

4.2.1 Growth and production behavior on sucrose and fructose

Because of the structural similarity of glucose, fructose, and sucrose, all of which also have similar entry points into the metabolism, one might expect *B. succiniciproducens* to show a similar growth and production behavior on the three substrates. Both growth kinetics and product stoichiometry were, however, clearly distinct (Figure 4.4, Figure 4.5).

During cultivation on minimal sucrose medium, *B. succiniciproducens* DD1 achieved a final succinic acid titer of $18.0\,\text{g·L}^{-1}$, i.e., $153\,\text{mM}$ (Figure 4.4B). In addition, it produced a broad array of by-products. After complete consumption of the substrate, the most abundant by-product was lactate ($8.9 \pm 0.1\,\text{g·L}^{-1}$). Formate ($8.2 \pm 0.2\,\text{g·L}^{-1}$) and acetate ($8.0 \pm 0.3\,\text{g·L}^{-1}$) were nearly as highly concentrated, whereas less ethanol ($1.6 \pm 0.0\,\text{g·L}^{-1}$) accumulated. A high maximum growth rate of $0.44 \pm 0.03\,\text{h}^{-1}$ allowed for complete consumption of $47\,\text{g·L}^{-1}$ ($138\,\text{mM}$) sucrose within $16\,\text{h}$ (Figure 4.4B). As indicated by the relatively low biomass concentration formed ($8\,\text{g·L}^{-1}$), only a minor fraction of carbon was recruited for growth. This became also obvious from the low biomass yield of 76 (g cell dry mass) (mol sucrose)$^{-1}$ (Table 4.4).

When approx. $60\,\%$ of the sucrose had been consumed after $12\,\text{h}$ of cultivation, the cells entered a transition phase. Biomass production was no longer exponential and product yields slightly changed towards increased formation of lactate and succinate (highlighted in gray).

Table 4.3: Growth kinetics of *B. succiniciproducens* DD1 on glucose, sucrose, and fructose. The specific rates, i. e., the substrate uptake rate q_S (as hexose uptake rate in brackets), the succinate production rate q_P, and the specific growth rate μ_{max}, represent mean values and deviations from at least 8 replicates.

Specific rate	Fructose	Sucrose	Glucose[1]
μ_{max} [h^{-1}]	0.26 ± 0.01	0.44 ± 0.03	0.30 ± 0.01
q_S [mmol·g^{-1}·h^{-1}]	10.2 ± 0.4	5.8 ± 0.4 (11.6 ± 0.8)	7.7 ± 0.4
q_P [mmol·g^{-1}·h^{-1}]	3.4 ± 0.1	5.9 ± 0.1	5.8 ± 0.4

[1] data from Becker *et al.* (2013)
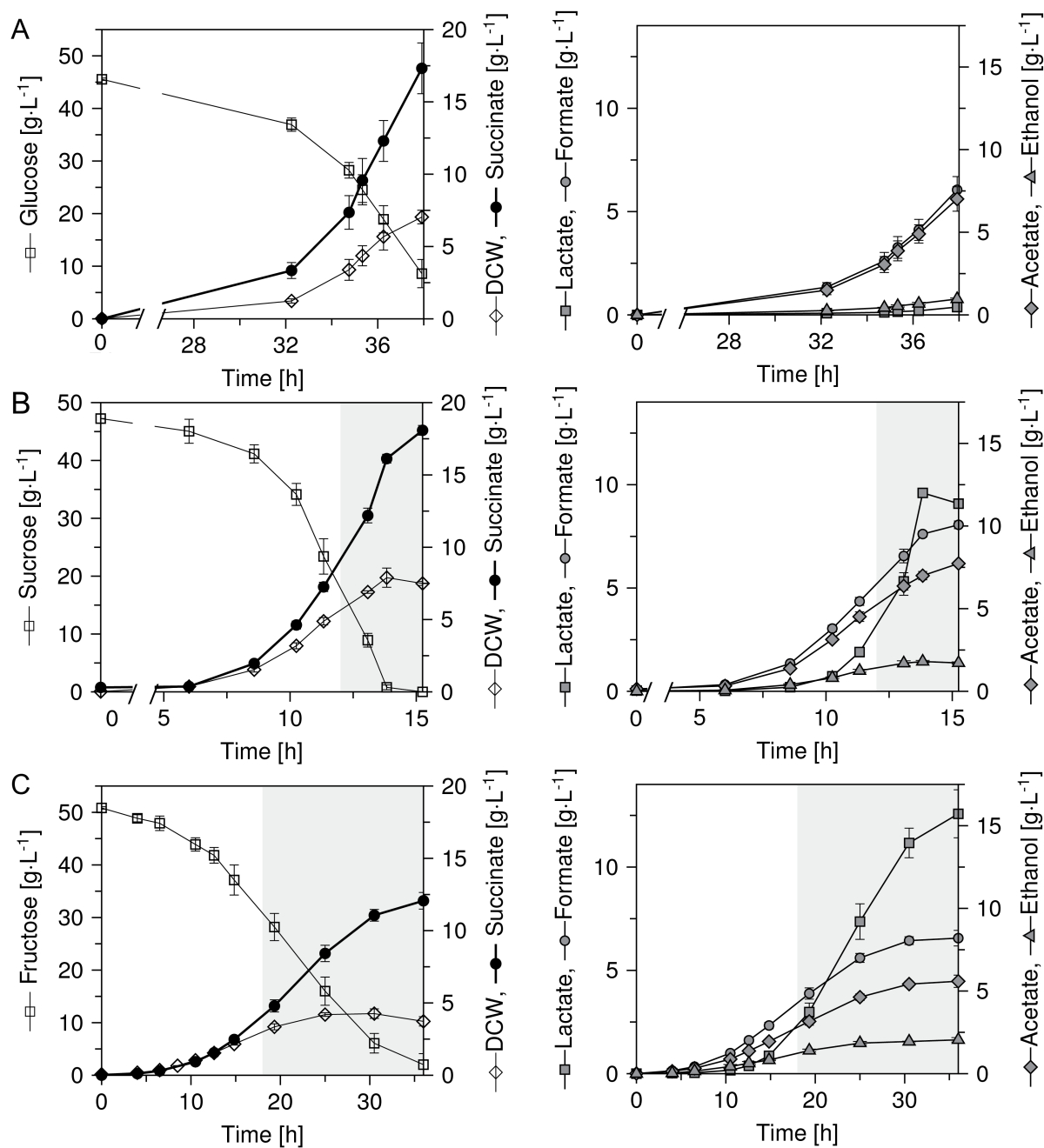
Figure 4.4: Cultivation characteristics of *B. succiniciproducens* DD1 on glucose (A), sucrose (B), and fructose (C). The data comprise biomass growth, substrate consumption, and secretion of succinate and the main by-products acetate, formate, lactate and ethanol for growth on (A) glucose (mean values and deviations from two biological replicates), (B) sucrose, and (C) fructose (each mean values and deviations from three biological replicates). On both sucrose and fructose, the cells exhibited a shift from exponential to non-exponential growth during the final stage of the cultivation that led to changes in product yields. The non-exponential phases are highlighted in gray. Only data from the exponential growth phases were later taken into account for ^{13}C metabolic flux analysis. Units given in axis labels refer to all preceding substances separated by commas. DCW: dry cell weight.

On fructose, 12.8 g·L^{-1} (108 mM) succinic acid, was secreted (Figure 4.4C). After fructose had been completely consumed, lactate had accumulated to 13.1 ± 1.3 g·L^{-1}. Formate (6.7 ± 0.5 g·L^{-1}), acetate (5.7 ± 0.5 g·L^{-1}), and ethanol (2.0 ± 0.1 g·L^{-1}) accumulated as well. Although the maximum growth rate was comparably low at 0.26 ± 0.01 h^{-1}, the specific substrate uptake rate was only slightly reduced as compared to sucrose. The transition phase that had already been observed on sucrose, was entered on fructose even earlier, after approx. 40 % of the substrate had been consumed (Figure 4.4C).

Table 4.4: Product and biomass yields of *B. succiniciproducens* DD1 on glucose, sucrose, and fructose. The data comprise yield coefficients for biomass ($Y_{X/S}$) and secreted products ($Y_{Product/S}$) and represent mean values and deviations from at least 8 replicates. N/A: no data available.

Yield coefficient	Fructose	Sucrose	Glucose[1]
$Y_{X/S}$[a]	25.41 ± 0.35	37.9 ± 0.30	39.2 ± 1.1
$Y_{Succinate/S}$[b]	0.34 ± 0.00	0.50 ± 0.01	0.75 ± 0.02
$Y_{Formate/S}$[b]	0.68 ± 0.01	0.63 ± 0.01	0.69 ± 0.02
$Y_{Acetate/S}$[b]	0.46 ± 0.00	0.50 ± 0.01	0.60 ± 0.02
$Y_{D\text{-}Lactate/S}$[b]	0.44 ± 0.01	0.21 ± 0.01	0.03 ± 0.00
$Y_{Ethanol/S}$[b]	0.24 ± 0.00	0.20 ± 0.00	0.11 ± 0.01
$Y_{D\text{-}Lactate/S}$[c]	4.0 ± 0.1	2.9 ± 0.1	N/A
$Y_{Pyruvate/S}$[c]	8.1 ± 1.2	9.7 ± 0.6	0.00 ± 0.00
$Y_{Fumarate/S}$[c]	4.5 ± 0.2	19.4 ± 1.2	N/A
$Y_{2\text{-}Oxoisovalerate/S}$[c]	6.2 ± 0.5	1.5 ± 0.6	N/A
$Y_{Acetoin/S}$[c]	16.3 ± 1.1	5.1 ± 2.1	N/A
$Y_{Alanine/S}$[c]	20.0 ± 2.0	3.3 ± 0.3	N/A
$Y_{Valine/S}$[c]	18.2 ± 1.4	1.3 ± 0.1	N/A
$Y_{Glycine/S}$[c]	3.5 ± 0.2	1.1 ± 0.1	N/A
$Y_{Leucine/S}$[c]	3.3 ± 0.3	0.3 ± 0.0	N/A
$Y_{Aspartate/S}$[c]	0.4 ± 0.0	1.1 ± 0.0	N/A
$Y_{Glutamate/S}$[c]	0.2 ± 0.0	0.2 ± 0.0	N/A

[1] data from Becker *et al.* (2013)

[a] in g·(mol hexose)$^{-1}$

[b] in mol·(mol hexose)$^{-1}$

[c] in mmol·(mol hexose)$^{-1}$

Culture supernatants were additionally analyzed by a combination of different HPLC methods and ^{1}H-NMR, leading to identification and quantification of various minor by-products, such as fumarate and alanine, which accounted for nearly 3 % of the carbon balance on sucrose and to more than 5 % on fructose. Several other substances were de-

tected in trace amounts (data not shown), including other amino acids such as glutamine, serine and isoleucine. NMR analysis also revealed that by the end of the cultivation, the supplied vitamins were still present, indicating sufficient supply. Product and biomass yields are summarized in Table 4.4.

The growth on sucrose was faster than on glucose, whereas the lowest growth rate was observed on fructose (Table 4.3). Comparison of the substrate uptake rates (as hexose uptake rates) revealed, however, a similar efficiency for sucrose and fructose uptake, which was even better than on glucose. A possible reason for this might be that both fructose and sucrose are taken up by PTS systems, whereas glucose is imported by a so far unidentified, but possibly less efficient, ABC transporter.

Succinate production was highest on glucose, second highest on sucrose and lowest on fructose. The same characteristic resulted for acetate. The opposite trend, i.e. increasing production from glucose, to sucrose to fructose, was observed for lactate and ethanol.

To allow for a systematic comparison of the growth physiology, comprising product portfolio and stoichiometry, on sucrose with corresponding data from glucose and fructose, yields were also calculated on a C-molar basis (Figure 4.5). There is evidently a strong difference between the substrates. Succinate production was highest on glucose, second highest on sucrose and lowest on fructose. The same characteristic resulted for acetate. The opposite trend, i. e., increasing production from glucose, to sucrose to fructose, was observed for lactate and ethanol. Only formate production remained constant. The strong differences were a bit surprising, since all three substrates are structurally similar carbohydrates. Interestingly, the affected by-products all originate from the pyruvate node. This node is specifically linked to the uptake of external substrates. Glucose uptake and phosphorylation in *B. succiniciproducens* is ATP-dependent (Becker *et al.*, 2013) similar to the related rumen bacterium *M. succiniciproducens* (Becker *et al.*, 2013; Lee *et al.*, 2006a; Lee *et al.*, 2005). In contrast, PTS systems have been annotated for fructose and sucrose, which inherently links substrate uptake and phosphorylation to the formation of pyruvate from PEP. This link can indeed explain the enhanced accumulation of pyruvate-derived by-products for the PTS-sugars fructose and sucrose. However, it cannot explain, why the two PTS-sugars differed so much from each other.

In fact, PTS-mediated phosphorylation of both sucrose subunits, as experimentally verified for *M. succiniciproducens* (Lee *et al.*, 2010a), should provide the same amount of pyruvate on sucrose as on fructose. Therefore, the product spectrum of sucrose-grown cells of *B. succiniciproducens* should resemble that on fructose. This was clearly not the case. The production performance on sucrose was significantly better than that on
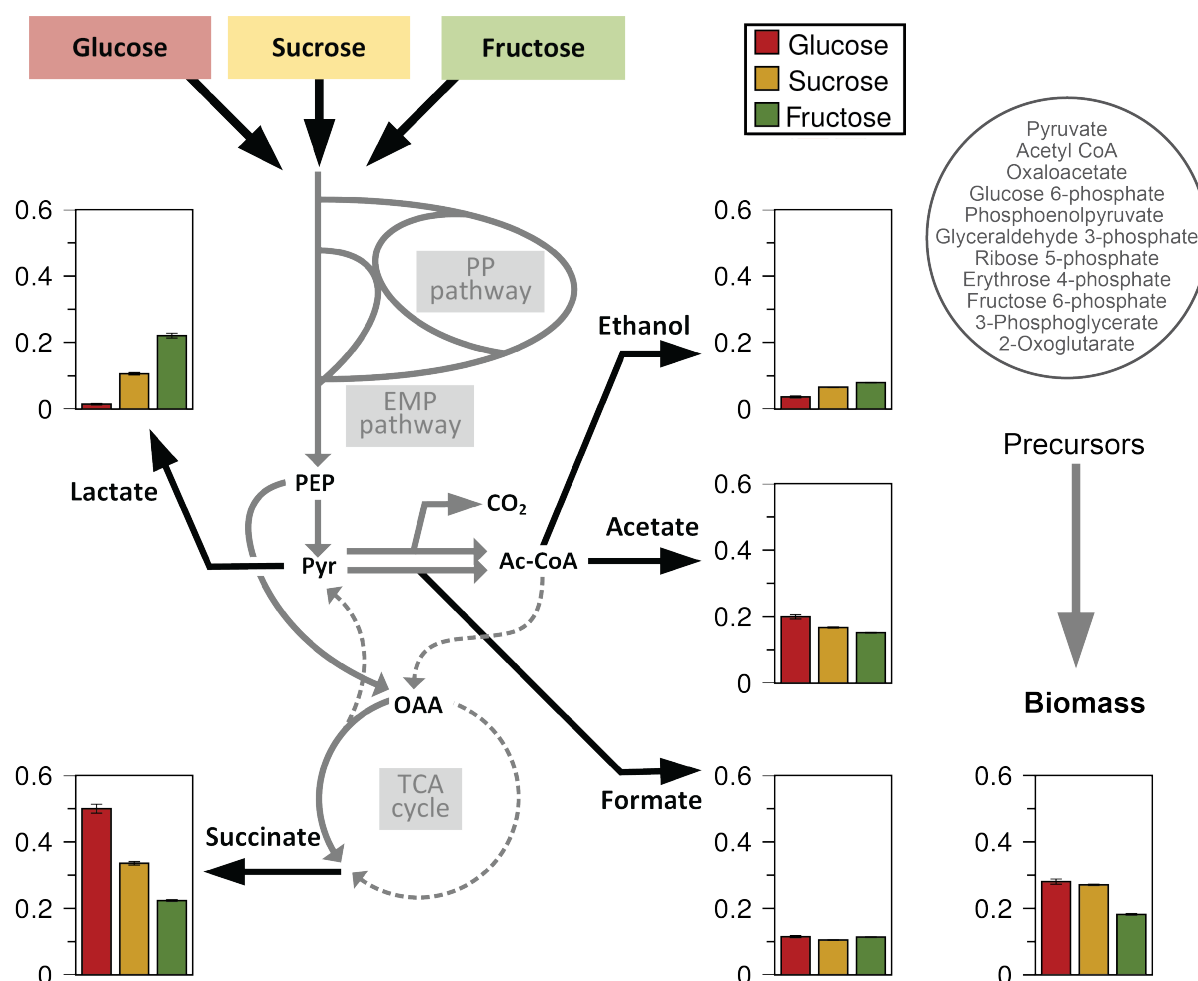
Figure 4.5: Product stoichiometry of *B. succiniciproducens* DD1 on glucose, on sucrose, and on fructose as carbon source. The yield coefficients, given as C-mol$_{product} \cdot$C-mol$_{substrate}^{-1}$, on glucose (red), sucrose (yellow) and fructose (green), showing clear trends for succinate, lactate and ethanol, are displayed as bar charts. The data represent mean values and deviations from at least eight replicates and are placed on a simplified metabolic map of *B. succiniciproducens* to indicate which metabolic precursors the respective products are derived from. PEP: phosphoenolpyruvate; Pyr: pyruvate; Ac-CoA: acetyl-CoA

fructose. The succinate yield was almost 40 % higher on sucrose than on fructose and by-product formation was much weaker. This behavior suggested further studies to shed more light on the obviously unexpected pathways of sucrose catabolism in *B. succiniciproducens*.

4.2.2 Identification of fructokinase in *Basfia succiniciproducens*

Fructokinase is a candidate gene which might cause the improved succinate production on sucrose as compared to fructose in *B. succiniciproducens*. It catalyzes ATP-dependent fructose phosphorylation, so that by using this enzyme instead of the fructose PTS, the overall conversion of PEP into pyruvate might be reduced. The *rbsK* gene, putatively

encoding fructokinase, is annotated for both *B. succiniciproducens* and *M. succinicipro-ducens*, but is evidently inactive in *M. succiniciproducens*. Fructokinase activity was, however, detected in cell-free extracts of *B. succiniciproducens* grown on sucrose (Figure 4.6). In the presence of $5\,mM\ Mg^{2+}$, the maximal specific activity in cell-free extracts was $18.4 \pm 1.1\,mU{\cdot}mg^{-1}$ and $14.6 \pm 0.3\,mU{\cdot}mg^{-1}$ for cells cultivated in complex sucrose and in minimal sucrose medium, respectively. The enzyme showed high substrate affinity for fructose ($K_M = 0.22 \pm 0.03\,mM$) and ATP ($K_M = 0.14 \pm 0.01\,mM$). These results provide evidence that fructokinase is a functional enzyme in *B. succiniciproducens* and might indeed be used during sucrose catabolism. It could be a key enzyme to account for the enhanced production performance on sucrose as compared to fructose.
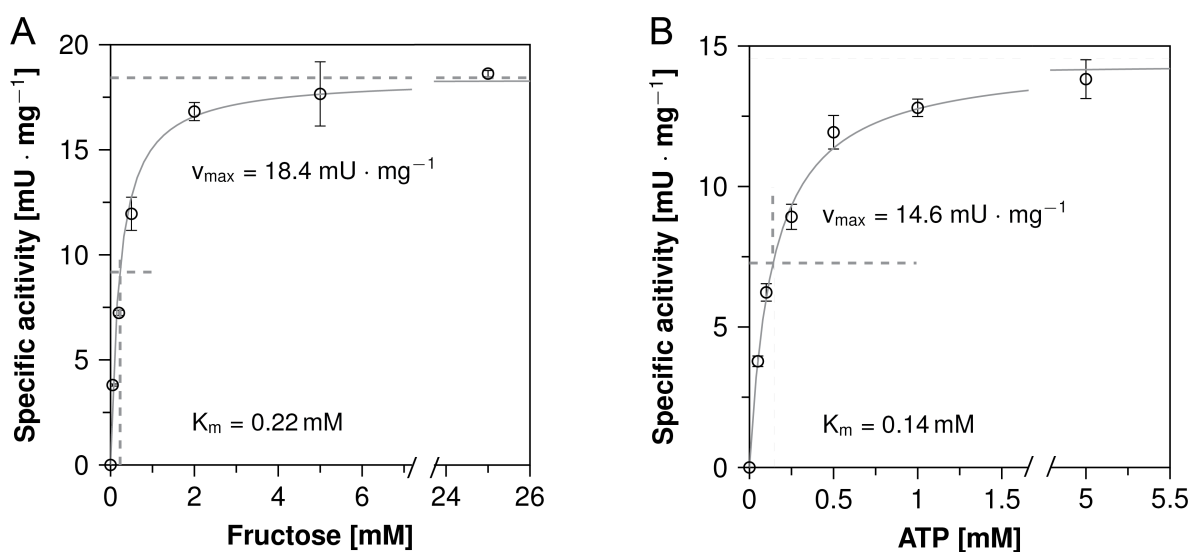
Figure 4.6: *In vitro* **determination of fructokinase enzymatic activity in crude cell extracts of *B. succiniciproducens* DD1.** (A) Determination of the K_M value for the substrate fructose, using 1 mM ATP and crude cell extract from cells grown on complex medium with sucrose as substrate. (B) Determination of the K_M value for the co-substrate ATP, using 25 mM fructose and crude cell extract from cells grown on minimal medium with sucrose as substrate.

To analyze, whether fructokinase was actually encoded by the *rbsK* gene, the candidate gene was cloned into an episomal plasmid under control of its native promoter. The episomal plasmid pJMK055 was successfully transformed into *B. succiniciproducens* DD1, yielding strain DD1 p055. As a control, the empty plasmid pJFF224-XN was also transformed into *B. succiniciproducens* DD1, yielding strain DD1 pXN. Both strains were validated by PCR, plasmid preparation and digestion with specific restriction enzymes (Chapter 3.2.3).

Both strains showed fast growth in complex sucrose medium supplied with $5\,\mu g{\cdot}ml^{-1}$ chloramphenicol. *In vivo* analysis of fructokinase activity revealed a high specific activity of $107\,mU{\cdot}mg$ for DD1 p055, which was more than three times higher than the specific activity of the reference strain (Table 4.5). This result proves that the *rbsK* gene indeed

Table 4.5: Overexpression of the *rbsK* gene in *B. succiniciproducens* DD1. The specific enzymatic activity of fructokinase and the product yields of the reference strain *B. succiniciproducens* pXN and *B. succiniciproducens* p055, overexpression *rbsK*, grown on complex sucrose medium containing chloramphenicol were determined. All data represent mean values and deviations from at least three replicates.

	DD1 pXN	DD1 p55
Fructokinase activity [mU·mg^{-1}]	32.9 ± 1.2	107.4 ± 1.4
Yields after 8 h [mol·mol^{-1}]		
Succinate	1.36 ± 0.02	1.38 ± 0.03
Lactate	0.09 ± 0.02	0.06 ± 0.01
Formate	1.5 ± 0.06	1.46 ± 0.02
Acetate	1.34 ± 0.06	1.31 ± 0.02
Ethanol	0.17 ± 0.01	0.15 ± 0.01
Yields after 24 h [mol·mol^{-1}]		
Succinate	1.37 ± 0.01	1.31 ± 0.04
Lactate	1.08 ± 0.01	0.78 ± 0.01
Formate	0.64 ± 0.02	0.8 ± 0.03
Acetate	0.66 ± 0.02	0.69 ± 0.03
Ethanol	0.08 ± 0.01	0.13 ± 0

encodes an active fructokinase, while inidicating that three to four copies of the episomal plasmid are present in each cell.

Subsequently, both strains were cultivated in triplicates to determine the yield coefficients for succinate and the main by-products during the exponential growth phase after 8 h and after complete consumption of the substrate after 24 h (Table 4.5). Clearly, overexpressing *rbsK* influenced the product yields in *B. succiniciproducens*. As expected, the lactate yield decreased. This did, however, not result in a significantly increased succinate yield. These data are, however, not readily comparable to data from routine cultivations, as a complex medium containing chloramphenicol, instead of a defined minimal medium, was used for strain cultivation (Table 3.3).

4.2.3 Verification of metabolic and isotopic steady state

The curated metabolic network topology and the developed cultivation and analysis set-up were now applied for ^{13}C metabolic flux analysis of *B. succiniciproducens* on sucrose and fructose.

Metabolic flux analysis, as applied here, requires a metabolic and isotopic steady-state of the investigated culture (Becker *et al.*, 2008).

Metabolic steady state was ensured from constant product and biomass yields in all parallel labeling experiments during the exponential growth phase, as shown in Figure 4.7. One should note that only the exponential phases of the cell cultures were taken into account (Figure 4.4).
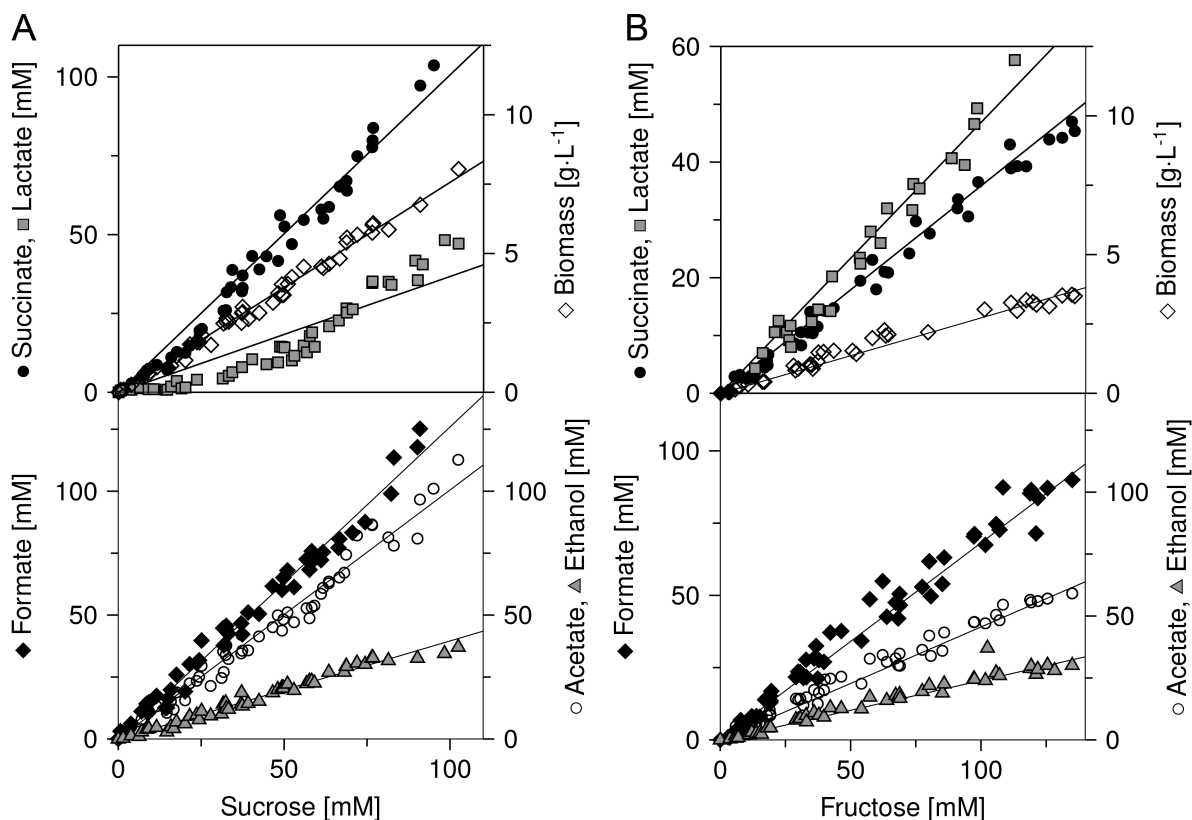
Figure 4.7: Verification of metabolic steady state during the exponential growth phase of *B. succiniciproducens* on sucrose and fructose. The data comprise substrate consumption plotted against product secretion or biomass formation and reflect constant yields of biomass, succinate and the main by-product D-lactate (top) and of additional major by-products (bottom) for utilization of sucrose (A) and fructose (B). The origin reflects the onset of product secretion. Units given in axis labels refer to all preceding substances separated by commas.

Isotopic steady state, i.e., constant isotope distribution throughout the studied phase, was verified by analyzing three samples taken throughout the exponential growth phase by GC/MS. Both on sucrose and on fructose, the MIDs remained constant, as exemplarily shown for glycine, representing the EMP pathway metabolites, phenylalanine, representing the PP pathway metabolites, and succinate, representing the TCA cycle (Figure 4.8).
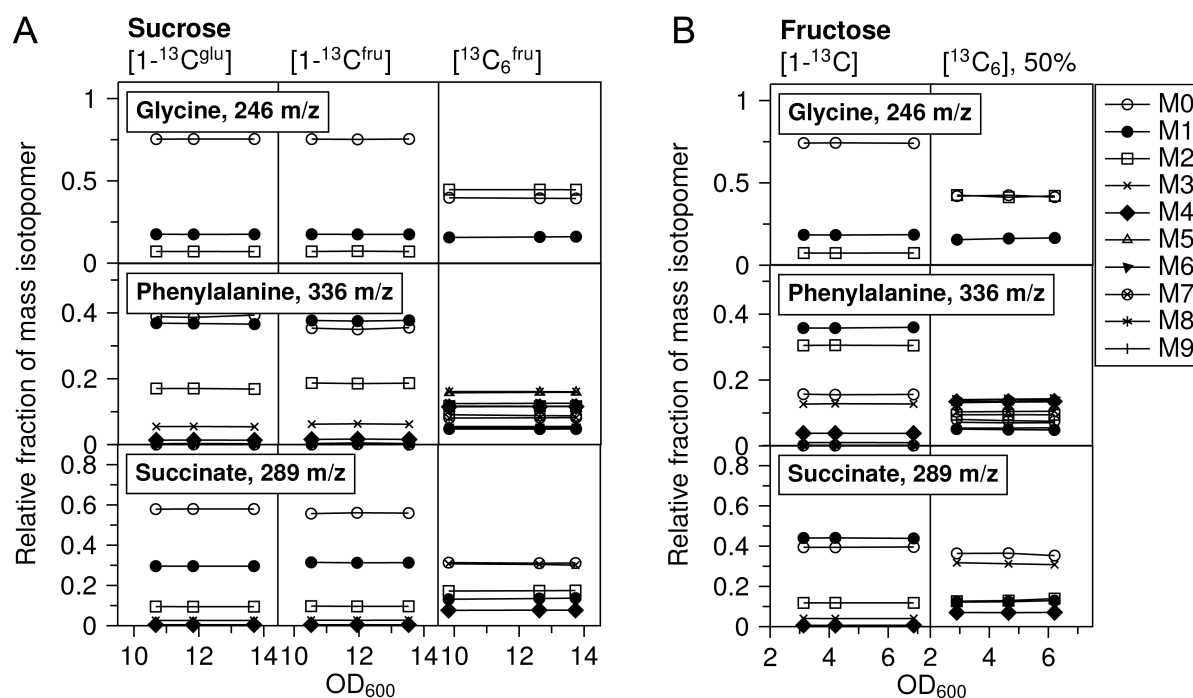
Figure 4.8: Verification of isotopic steady state during the exponential growth phase of *B. succiniciproducens* on sucrose (A) and fructose (B). The isotopic steady state is reflected by the constant labeling pattern of all analytes throughout the cultivation on the various tracer substrates. Exemplarily, mass isotopomer distributions are shown for glycine (representing the EMP pathway), phenylalanine (representing the PP pathway) and succinate (representing the reductive TCA cycle). The legend holds for (A) and (B). Fructose [$^{13}C_6$], 50 % indicates an equimolar mixture of naturally and fully labeled fructose.

4.2.4 Experimental design for ^{13}C metabolic flux analysis and qualitative interpretation of labeling information

Resolving metabolic fluxes with high accuracy requires parallel experiments with different tracers since there is usually not a single ideal tracer to resolve a metabolic network. Different tracers, however, are suited to elucidate certain pathway fluxes (Leighty and Antoniewicz, 2013).

To resolve the fluxes of interest on fructose, the integration of two different labeling sets has previously been successful (Kiefer *et al.*, 2004): the first tracer, [1-^{13}C] fructose, allows differentiation of the EMP pathway flux and the PP pathway flux. A mixture of uniformly labeled [$^{13}C_6$] fructose and naturally labeled fructose was found well suited to resolve the fluxes at the pyruvate node.

The heterodisaccharide sucrose is more complex, so that in a previous study, three parallel labeling experiments were necessary to resolve intracellular fluxes in sucrose-grown *C. glutamicum* (Wittmann *et al.*, 2004). Sucrose tracers in which the C_1 atom of either glucose or fructose was ^{13}C-labeled were required to resolve fluxes in the same fashion

as [1-^{13}C] fructose in the case of fructose-based ^{13}C metabolic flux analysis. Additionally, these two tracers could be used to distinguish the routes of the two hexose moieties through the metabolic network. As a third tracer, [^{13}C$_6$^{Frc}] sucrose, containing a uniformly labeled fructose subunit, was used. In addition to providing useful information about the pyruvate node, this compound is a key tracer for analyzing the sucrose catabolism in *B. succiniciproducens*. In this organism, two putative ways of phosphorylating the fructose moiety exist: on the one hand, via fructose PTS, as described for *M. succiniciproducens*, and on the other hand via the newly discovered fructokinase. As shown in Figure 4.9, the two alternative pathways can be clearly distinguished by analyzing the labeling pattern of glycogen formed during cultivation. When the fructose PTS catalyzes fructose phosphorylation, fructose 1-phosphate (F1P) is generated, which in turn enters the glycolytic chain as fructose 1,6-bisphosphate (F16BP). Since the enzyme phosphofructokinase, catalyzing conversion of fructose 6-phosphate (F6P) into F16BP, is irreversible and fructose 1,6-bisphosphatase can be assumed to be inactive during non-gluconeogenic conditions (Becker *et al.*, 2005), F16BP can only be converted to glucose 6-phosphate (G6P), the glycogen precursor, through the non-oxidative PP pathway interconversions. This leads to formation of triple labeled G6P. When the fructose subunit is, however, phosphorylated by fructokinase, the formed fructose 6-phosphate can directly be converted to G6P, then also uniformly labeled. The experimental data clearly show both (m+3) and (m+6) labeled glycogen subunits, indicating that both pathways are active *in vivo* (Figure 4.9).

The SFL calculated from the labeling results for the three sucrose tracers allowed for a qualitative inspection, how much each of the two hexose subunits contributed to glycogen formation (Table 4.6). A surprisingly large amount of $25 - 30\%$ of the glucose 6-phosphate pool stemmed from the fructose subunit of sucrose. Although the major part was directly formed from hydrolysis of sucrose into fructose and glucose 6-phosphate, there was either a significant back-flux of glyceraldehyde 3-phosphate (GAP) through the PP pathway or fructose actually entered the carbon core metabolism as fructose 6-phosphate, again suggesting fructokinase *in vivo* activity. Concerning the contribution of the two moieties to formation of the product succinate, direct interpretation of the labeling data was not as straightforward. The reason for this is that the reversibility of PEPCK combined with the scrambling of the fumarate labeling, as displayed in Figure 4.10, leads to incorporation of naturally labeled CO_2. Overall, the SFL of succinate was 6.5%, when the glucose moiety was labeled at C_1, and 7.1%, when the fructose moiety was labeled at C_1. This indicates a slightly higher contribution of fructose.

In addition, using $^{13}CO_2$ as a tracer allowed for direct differentiation of the two succinic acid production routes available to *B. succiniciproducens*, as shown in Figure 4.10. In case
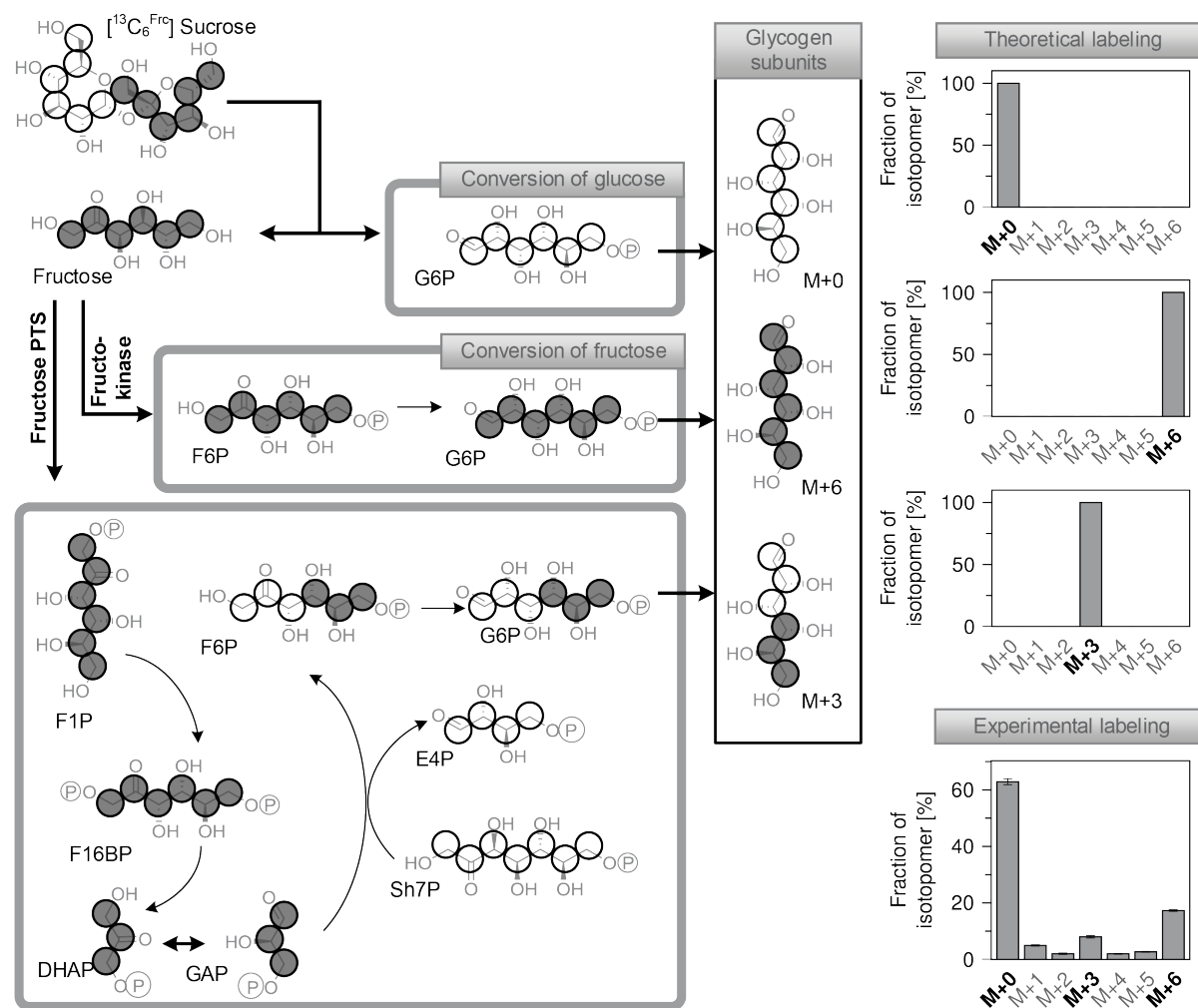
Figure 4.9: Elucidating the fructose phosphorylating pathways in sucrose-grown *B. succiniciproducens* by a ^{13}C labeling experiment. By using [U-^{13}C$^{\mathrm{Frc}}$] sucrose, the two ways of fructose phosphorylation that exist in *B. succiniciproducens*, i. e., ATP-dependent phosphorylation by fructokinase (yielding fructose 6-phosphate) and PEP-dependent phosphorylation by fructose PTS (and possibly mannose PTS, both yielding fructose 1-phosphate) can be differentiated. G6P: glucose 6-phosohate, F6P: fructose 6-phosphate, F16BP: fructose 1,6-bisphosphate, E4P: erythrose 4-phosphate, Sh7P: sedoheptulose 7-phospate, DHAP: dihydroxyacetone phosphate, GAP: glyceraldehyde 3-phosphate, PTS: phosphotransferase system.

succinic acid is produced via the reductive TCA cycle, mostly singly labeled succinic acid is produced whereas usage of the oxidative TCA cycle leads to naturally labeled succinic acid. A mixture of naturally and twice labeled succinic acid can also occur in small amounts if the PEP carboxylating reaction is reversible *in vivo*. Qualitative analysis of the GC/MS data of succinate produced from naturally labeled fructose and sucrose and Mg^{13}CO$_3$ and ^{13}CO$_2$ revealed that most succinic acid was produced via the reductive branch. On both substrates, small amounts of naturally and doubly labeled succinate occurred. At the most, 4 % (sucrose) to 8 % (fructose) of all produced succinate was potentially produced via the oxidative branch of the TCA cycle.

Taken together, the following strategies were used for ^{13}C metabolic flux analysis of *B. suc-*

Table 4.6: Contribution of the sucrose moieties fructose and glucose to glycogen formation. The experimental (Exp.) SFLs were obtained by GC/MS analysis of the trimethylsilyl derivative of glucose at an m/z of 554 to 560 with subsequent correction for natural isotopes. The percentage of contribution of the glucose and fructose subunit is calculated by comparison with theoretical data (Appendix), which was calculated based on several simplifying assumptions. All reversibilities were neglected.

Tracer substrate	Exp. SFL [%]	From glucose [%]	From fructose [%]
$[1\text{-}^{13}C^{Glc}]$-Sucrose	13.2 ± 0.0	74.3 ± 0.2	25.7 ± 0.1
$[1\text{-}^{13}C^{Frc}]$-Sucrose	6.2 ± 0.1	68.7 ± 1.0	31.3 ± 0.5
$[U\text{-}^{13}C^{Frc}]$-Sucrose	26.4 ± 0.8	74.1 ± 2.2	25.9 ± 0.8
Average		72.4 ± 3.2	27.6 ± 3.2

ciniciproducens on sucrose and on fructose: on sucrose, four labeling data sets derived from $[1\text{-}^{13}C^{Glc}]$ sucrose, from $[1\text{-}^{13}C^{Frc}]$ sucrose, from $[^{13}C_6{}^{Frc}]$ sucrose, and from $Mg^{13}CO_3$ and $^{13}CO_2$ were combined. On fructose, three labeling data sets based on $[1\text{-}^{13}C]$ fructose, on $[^{13}C_6]$ fructose, and on $Mg^{13}CO_3$ and $^{13}CO_2$ were required.

Table 4.7: Anabolic demand for precursor metabolites for biomass formation of *B. succiniciproducens*. The data represent the previously determined anabolic demand of *B. succiniciproducens* DD1, derived from the biomass composition (Becker *et al.*, 2013), and were used to calculate fluxes into biomass for growth on different substrates by multiplication with the respective biomass yields determined in this study (Table 4.4, Table 4.9).

Anabolic precursor	Demand [mmol $\cdot$ (g CDW)$^{-1}$]
Glucose 6-phosphate	0.205
Fructose 6-phosphate	0.071
Ribose 5-phosphate	0.853
Erythrose 4-phosphate	0.223
Glyceraldehyde 3-phosphate	0.129
3-Phosphoglycerate	1.221
Phosphoenolpyruvate	0.495
Pyruvate	2.745
Acetyl Coenzyme A	2.887
Oxaloacetate	1.724
2-Oxoglutarate	1.186
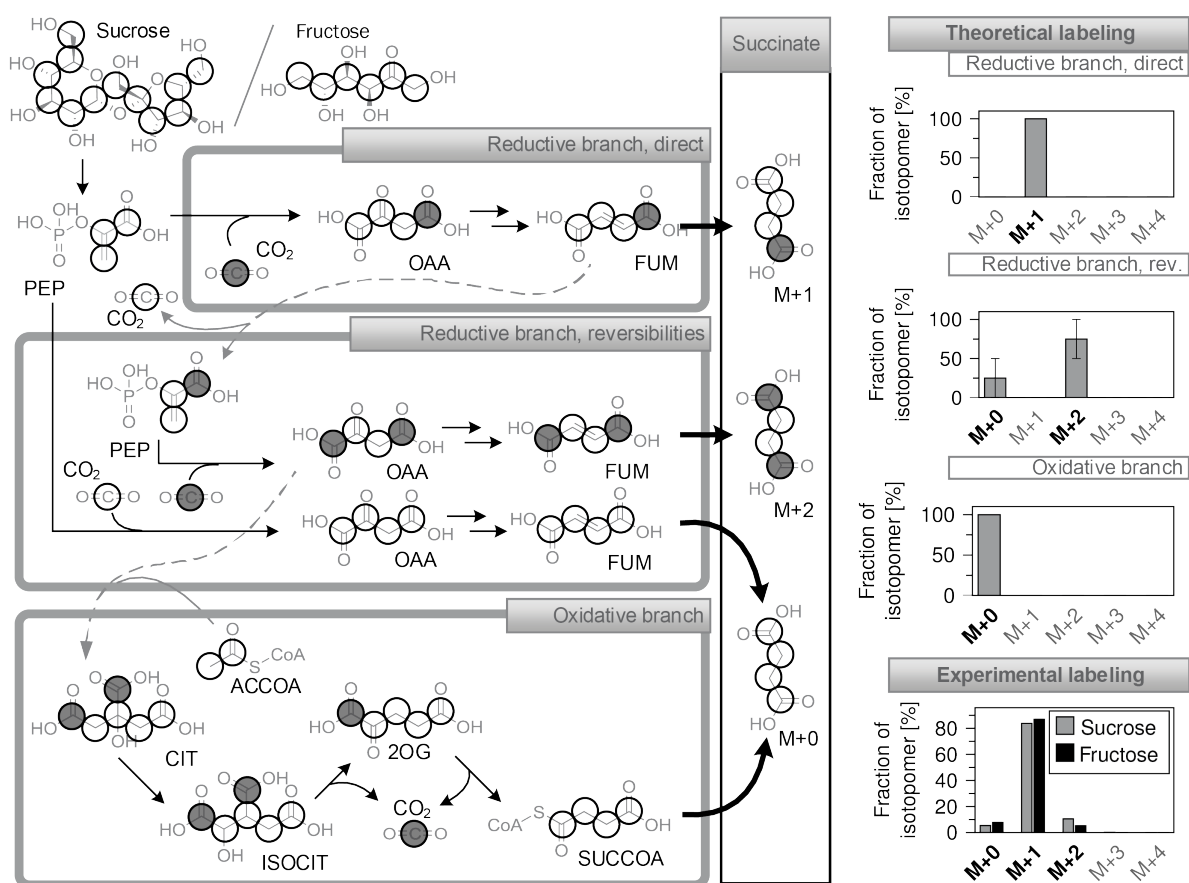
Figure 4.10: Differentiation of the oxidative and the reductive branch of the TCA cycle in sucrose- and fructose-grown *B. succiniciproducens* by $^{13}CO_2$ labeling. Using $^{13}CO_2$ as a tracer allows direct differentiation of oxidative and reductive TCA cycle branches. Only the reductive branch yields singly labeled succinate whereas the oxidative branch can only lead to formation of naturally labeled succinate. Because of reversible carboxylation of PEP, small amounts of naturally labeled and twice labeled succinate can also be formed through the reductive branch. PEP: phosphoenolpyruvate, PYR: pyruvate, ACCOA: acetyl coenzyme A, OAA: oxaloacetate, CIT: citrate, ISOCIT: isocitrate, 2OG: 2-oxoglutarate, SUCCOA: succinate coenzyme A, FUM: fumarate, MAL: malate.

4.2.5 Distribution of central carbon fluxes on sucrose

A highly resolved map of the intracellular carbon flux distribution in sucrose-grown *B. succiniciproducens* was determined by integrating four parallel ^{13}C labeling experiments, comprising a total of 460 individual mass isotopomers.

The calculation of the metabolic fluxes considered growth and product formation (Table 4.4), the anabolic demand for biomass precursors (Table 4.7), and the ^{13}C labeling data from the parallel isotope studies, which were all integrated for the flux calculation. The set of intracellular fluxes that gave minimum deviation between experimental and simulated labeling patterns was taken as best estimate for the intracellular flux distribution (Figure 4.11). An excellent fit of all four parallel labeling data sets to the model was achieved (Figure 4.12). Multiple flux calculations with randomly varied initialization

values for the flux parameters yielded identical results, confirming that the global minimum was identified. Statistical evaluation showed that the fluxes could be determined at rather high precision (Figure 4.11).

4.2.5.1 Both fructose PTS and fructokinase contribute to phosphorylation of the fructose subunit of sucrose

Sucrose was taken up into the cells with a normalized flux of 50 %, equal to 100 % of hexose uptake and the observed mean specific uptake rate of $5.8 \pm 0.4 \, \text{mmol·g}^{-1} \text{·h}^{-1}$. After conversion into glucose 6-phosphate and fructose, 60 % was transiently exported, possibly into the periplasm (no fructose was detected in culture supernatants), and was then reassimilated through the fructose PTS. The remaining fraction of 40 % of the free fructose was directly phosphorylated by fructokinase and entered the central metabolism at the level of fructose 6-phosphate. The reversible nature of phosphoglucose isomerase then resulted in the observed transfer of intact fructose units towards glucose 6-phosphate and then into the glycogen pool.

4.2.5.2 The PP pathway and the oxidative TCA cycle provide precursors for biomass

For further metabolization, the carbon was mainly channeled through the EMP pathway. Only a rather small flux of 7.8 % entered the oxidative PP pathway, where it was almost completely consumed to supply erythrose 4-posphate and ribose 5-posphate as anabolic precursors. As a result, there was almost no back flux of carbon from the PP pathway into the glycolysis. This rather unusual flux distribution seems to be a characteristic property of succinate-producing *Pasteurellaceae*, as it has been observed both in glucose-grown *B. succiniciproducens* and in glucose-grown *Actinobacillus succinogenes* (McKinlay *et al.*, 2007), whereas in other bacteria, e. g., *E. coli* and *C. glutamicum*, the PP pathway flux exceeds the anabolic demand (Kiefer *et al.*, 2004; Leighty and Antoniewicz, 2013; Marx *et al.*, 1996).

Starting from glucose 6-phosphate, the EMP pathway flux increased gradually through co-entry of fructose units at the level of fructose 6-phosphate and fructose-1,6-bisphosphate. At the glyceraldehyde 3-phosphate node, almost the entire carbon was channeled further down the glycolytic chain, except for a low back flux through the reversible reactions of the PP pathway and into the methylglyoxal pathway towards L-lactate.
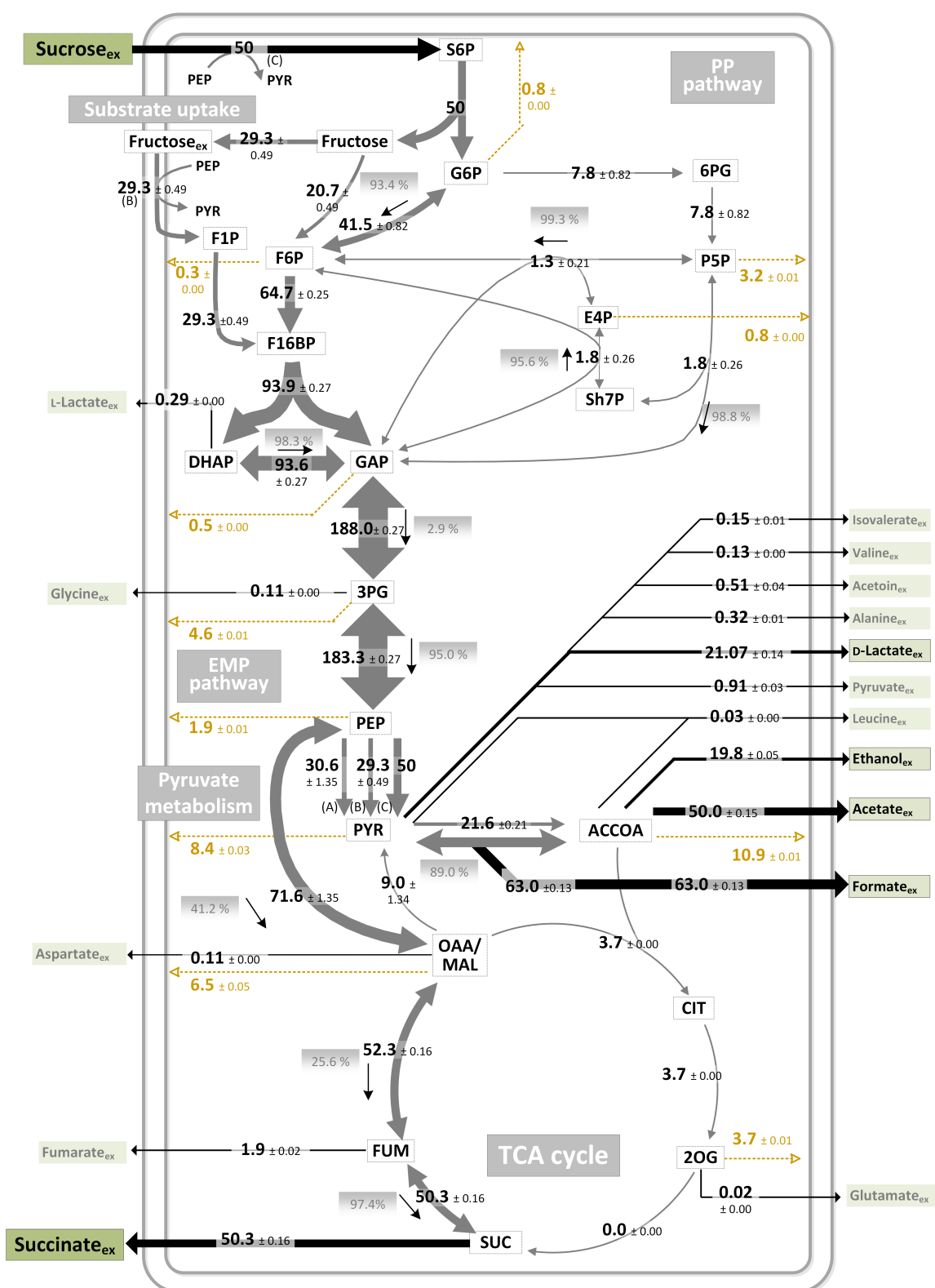
Figure 4.11: Intracellular carbon fluxes of *B. succiniciproducens* DD1 on sucrose as determined by ^{13}C metabolic flux analysis. To allow for better comparison with hexose-based flux maps, all fluxes represent a molar percentage of the mean specific hexose uptake rate of the two sucrose moieties ($11.6 \pm 0.4 \, \text{mmol·g}^{-1} \cdot \text{h}^{-1}$). The arrow thickness is proportional to the corresponding flux. The direction of net fluxes is indicated by small black arrows. Reversibilities, calculated according to Equation 3.5, are displayed gray boxes. Yellow dashed arrows represent fluxes into biomass formation. Black arrows indicate carbon in- and efflux. The three reactions that catalyze conversion of PEP into PYR are: (A) pyruvate kinase, (B) fructose PTS, (C) sucrose PTS. PEP: phosphoenolpyruvate; PYR: pyruvate; S6P: sucrose 6-phosphate; G6P: glucose 6-phosphate; 6PG: 6-phosphogluconate; F1P: fructose 1-phosphate; F6P: fructose 6-phosphate; F16BP: fructose 1,6-bisphosphate; DHAP: dihydroxyacetone phosphate; GAP: glyceraldehyde 3-phosphate; P5P: pentose 5-phosphate; E4P: erythrose 4-phosphate; Sh7P: seduheptulose 7-phosphate; 3PG: 3-phosphoglycerate; ACCOA: acetyl-CoA; OAA/MAL: oxaloacetate/malate; CIT: citrate; FUM: fumarate; SUC: succinate; 2OG: 2-oxoglutarate

4.2.5.3 High conversion of PEP to pyruvate reduces succinate-precursor availability

At the level of PEP, carbon is either converted to oxaloacetate towards the desired product succinate, or to pyruvate, which mainly means effectual carbon loss into the various by-products. Inherently linked to the uptake of sucrose, the sucrose PTS was the major enzyme that formed pyruvate from PEP. In addition, the fructose PTS and to a minor, but significant extent, also pyruvate kinase caused loss of PEP. The flux distribution at this node seemed suboptimal, as the concerted action of three different enzymes resulted in a significant influx into the pyruvate pool, where it triggered the formation of elevated levels of by-products. It is interesting to note that the absolute *in vivo* flux catalyzed by pyruvate kinase, i.e., $3.5\,\text{mmol}\cdot(\text{g protein})^{-1}\cdot\text{h}^{-1}$ on basis of the relative pyruvate kinase flux (Figure 4.11), the specific sucrose uptake rate (Table 4.3) and a protein content of approx. $50\,\%$ (Becker *et al.*, 2013), was dramatically lower than the available capacity of the cell. Inferred from the pyruvate kinase *in vitro* activity (Table 4.1), only $7.4\,\%$ of the capacity of the enzyme ($1.6\,\text{U}\cdot(\text{mg protein})^{-1} = 48\,\text{mmol}\cdot(\text{g cells})^{-1}\cdot\text{h}^{-1}$) were actually utilized.

4.2.5.4 Malic enzyme is active *in vivo* and withdraws carbon from the succinate production pathway

Oxaloacetate was efficiently generated from PEP by carboxylation. However, the valuable precursor was not fully converted into succinate. In fact, malic enzyme was found to recycle carbon back to pyruvate. The contribution of malic enzyme was significant and possibly presents a necessary route to produce NADPH required for biomass formation.

4.2.5.5 Succinate is almost exclusively formed via the reductive branch of the TCA cycle

Similar to the PP pathway, the oxidative branch of the TCA cycle exclusively served as an anabolic route. The observed flux matched with the anabolic demand for 2-oxoglutarate as precursor for amino acids of the glutamate family. A small amount of 2-oxoglutarate even leaked out of the cells at a constant yield. No succinate was formed through this branch. The low flux corresponded to the low *in vitro* activity found for isocitrate dehydrogenase (Table 4.1). Accordingly, succinate was completely provided via the reductive route. The production pathway could apparently not channel the entire flux towards succinate, but exhibited a slight overflow formation of fumarate.

Taken together, *B. succiniciproducens* channeled a remarkable flux of more than 50 % into the desired product, which equaled a yield of more than 1 (mol succinate)·(mol sucrose)$^{-1}$.

4.2.5.6 The redox balance suggests the contribution of a transhydrogenase to supply NAPDH from NADH on sucrose

The complete resolution of metabolic fluxes allows for a detailed quantitative inspection of the redox metabolism of *B. succiniciproducens* (Figure 4.13). The reactions that contribute to NADH supply are glyceraldehyde 3-phosphate dehydrogenase, pyruvate dehydrogenase, and 2-oxoglutarate dehydrogenase. On basis of the flux data and previous analyses of cofactor specificity, glucose-6-phosphate dehydrogenase, 6-phosphogluconate dehydrogenase, malic enzyme and isocitrate dehydrogenase are the NADPH-supplying reactions (Becker *et al.*, 2013, this work). The intracellular reactions involved in NADH consumption comprised alcohol dehydrogenase, lactate dehydrogenase, malate dehydrogenase, and fumarate reductase. It was further assumed that *B. succiniciproducens* possesses an NADH dehydrogenase for electron transfer from NADH to menaquinone (Kim, 2009). Consumption of menaquinol was hence regarded as NADH consumption. The demand for NADPH for biomass formation results from the experimental biomass yield (Table 4.4) and the cellular composition (Table 4.7). The dominating redox equivalent cofactor was NAD(H), which accounts for 70-90 % of the total redox flux. As shown, the total redox balance considering NADP(H) and NAD(H) was mostly closed, which underlines the consistency of the data. NADH consumption did not fully match the corresponding formation, which resulted in an apparent NADH excess. This coincided with an apparent NADPH limitation and points at the presence of additional NADPH sources in *B. succiniciproducens*, most likely, an active transhydrogenase (Becker *et al.*, 2013). Generally, the supply of NADPH was rather low, as compared to other microorganisms. This was mainly due to the fact that the oxidative PP pathway and the oxidative TCA cycle, the major NADPH supplying pathways in other bacteria, have mostly anabolic function. Taken together, the results strongly suggest transhydrogenase activity in *B. succiniciproducens*.

Figure 4.12: Comparison of experimental and simulated mass isotopomer distributions (MIDs) for flux analysis on sucrose. The data represent experimental (exp) MIDs obtained during parallel cultivation of *B. succiniciproducens* DD1 on four different ^{13}C tracers and simulated (sim) MIDs corresponding to the calculated flux distribution for different amino acids (indicated by the respective three letter code abbreviations), succinate (Suc), and glycogen-derived glucose (Glc). The deviation between the experimental and simulated MIDs was exceptionally low for all data sets.
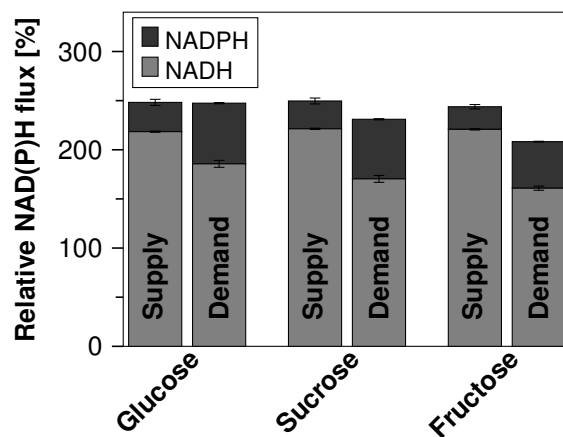
Figure 4.13: Redox balance of *B. succiniciproducens* DD1 on fructose, sucrose, and glucose. The supply and demand of NADH and NADPH was calculated from the metabolic flux distribution, taking into account all participating reactions, as shown in Figure 2.5, and NAD^+ and NADPH requirements for biomass formation. *B. succiniciproducens* was assumed to possess a NADH dehydrogenase for electron transfer from NADH to menaquinone (Kim, 2009). The data reflect mean values and 90% confidence intervals from Monte-Carlo simulations.

4.2.5.7 The *B. succiniciproducens* flux distribution in the context of microbial strategies for sucrose catabolism

So far, microbial sucrose metabolism has been addressed in two previous studies by means of ^{13}C metabolic flux analysis. Each of the studied bacteria, i. e., lysine-producing *C. glutamicum* (Wittmann *et al.*, 2004), *E. coli* W (Arifin *et al.*, 2014), and *B. succinici-producens*, analyzed in this work, has a unique pathway repertoire for sucrose utilization. *E. coli* W assimilates sucrose by means of an H$^+$ symporter. After intracellular hydrolysis into free glucose and fructose, each hexose monomer is phosphorylated by a specific kinase (Bockmann *et al.*, 1992; Jahreis *et al.*, 2002). *C. glutamicum* exhibits a completely different uptake system: sucrose is taken up through a PTS, then hydrolyzed into glucose 6-phosphate and fructose, which is in turn phosphorylated by either a fructose PTS or by a mannose PTS. In a previous report, fructokinase had been shown to be missing in *C. glutamicum* (Dominguez and Lindley, 1996). During growth on sucrose, both PTS systems are active and specifically supply fructose 1-phosphate (90 %) and fructose 6-phosphate (10 %) (Wittmann *et al.*, 2004). As shown here, *B. succiniciproducens* exhibits the most complex sucrose catabolism by orchestrating the concerted action of different PTS systems and a kinase to fully metabolize the disaccharide. It is interesting to note that in the two aerobic cases, sucrose-grown cells reveal a reduced flux into the PP pathway, as compared to glucose, probably linked to the entry points of substrate carbon, which locate downstream of the glucose 6-phosphate node (Arifin *et al.*, 2014; Wittmann *et al.*, 2004, this work). This generally results in a reduced formation of NADPH by the PP pathway enzymes during growth on sucrose. In contrast, the glycolytic flux remains high or is even enhanced. In aerobically growing *C. glutamicum* and *E. coli* this triggers a substantial flux increase into the TCA cycle (Wittmann *et al.*, 2004). The increased flux through NADPH supplying isocitrate dehydrogenase obviously compensates for the reduced NADPH formation by the PP pathway enzymes. In contrast, anaerobic *B. succiniciproducens* does not enhance its oxidative TCA cycle flux, probably due restrictions in redox balancing, but rather channels excess carbon into pyruvate-derived by-products. It seems that malic enzyme is instead activated and transhydrogenase is additionally recruited to compensate for the lower NADPH supply, which is clearly different from *C. glutamicum* and *E. coli*.

4.2.5.8 Metabolic engineering targets for improving succinate-production from sucrose

As discussed in Chapter 2.3.2, different strategies have already been applied to improve succinate production in different production hosts. Analysis of the intracellular carbon

fluxes of *B. succiniciproducens* now allowed for the identification of genetic targets most closely linked to the phenotype and emerging from new discoveries about the biochemistry of *B. succiniciproducens*. In sucrose-grown *B. succiniciproducens*, a high conversion of PEP to pyruvate led to production of increased amounts of lactate and other pyruvate-derived by-products while reducing the available amount of the precursor required for succinate production, i.e., PEP. A straightforward approach to reduce conversion of PEP into pyruvate could be to exploit the already advantageous characteristics of the native sucrose utilization system. In wild type *B. succiniciproducens*, fructokinase already phosphorylated 40 % of the fructose moiety. By deleting the *fruA* gene, encoding the competing fructose PTS, it might be possible to channel all fructose through fructokinase and in turn reduce the conversion of PEP into pyruvate.

Assessment of several other possible metabolic engineering strategies revealed deletion of the *fruA* gene as an especially promising and sucrose-specific target.

4.2.6 Metabolic engineering of *B. succiniciproducens* towards improved sucrose-utilization

4.2.6.1 Deleting the fructose PTS yields an excellent producer: DD1 Δ*fruA*

To channel more fructose through fructokinase and, as a consequence, to reduce conversion of PEP into pyruvate, the *fruA* gene, encoding fructose PTS, was deleted.

B. succiniciproducens DD1 Δ*fruA* was cultivated in sucrose minimal medium in serum bottles. The strain showed reproducible growth and completely consumed the provided substrate within 19 h (Figure A.3). Most strikingly, the succinic acid yield was increased by 44 % to 1.45 ± 0.01 mol·mol^{-1}, while the lactate yield was decreased by 68 % to 0.14 ± 0.02 mol·mol^{-1}, compared to the wild type strain (Figure 4.14).

To evaluate the succinic acid production capacity of *B. succiniciproducens* DD1 and of the mutant strain Δ*fruA*, a comparative fed-batch fermentation in industrial medium (Table 3.7) was carried out (Figure 4.15). A linear feeding strategy was chosen.

In fed-batch fermentation, *B. succiniciproducens* Δ*fruA* achieved a final titer of 71 g·L^{-1} succinic acid, which was 12 % higher than the titer achieved by the wild type (Figure 4.15A, B). Overall, 71.9 g succinic acid were produced from 92.6 g sucrose. Only 7.3 g·L^{-1} lactic acid were produced by the mutant, while the wild type accumulated 9.3 g·L^{-1} lactic acid. The two fed-batch cultivations comprised three distinct phases, respectively: an initial batch phase, a substrate limitation phase, and a substrate accumulation phase before the end of the process. By-product formation and succinic acid
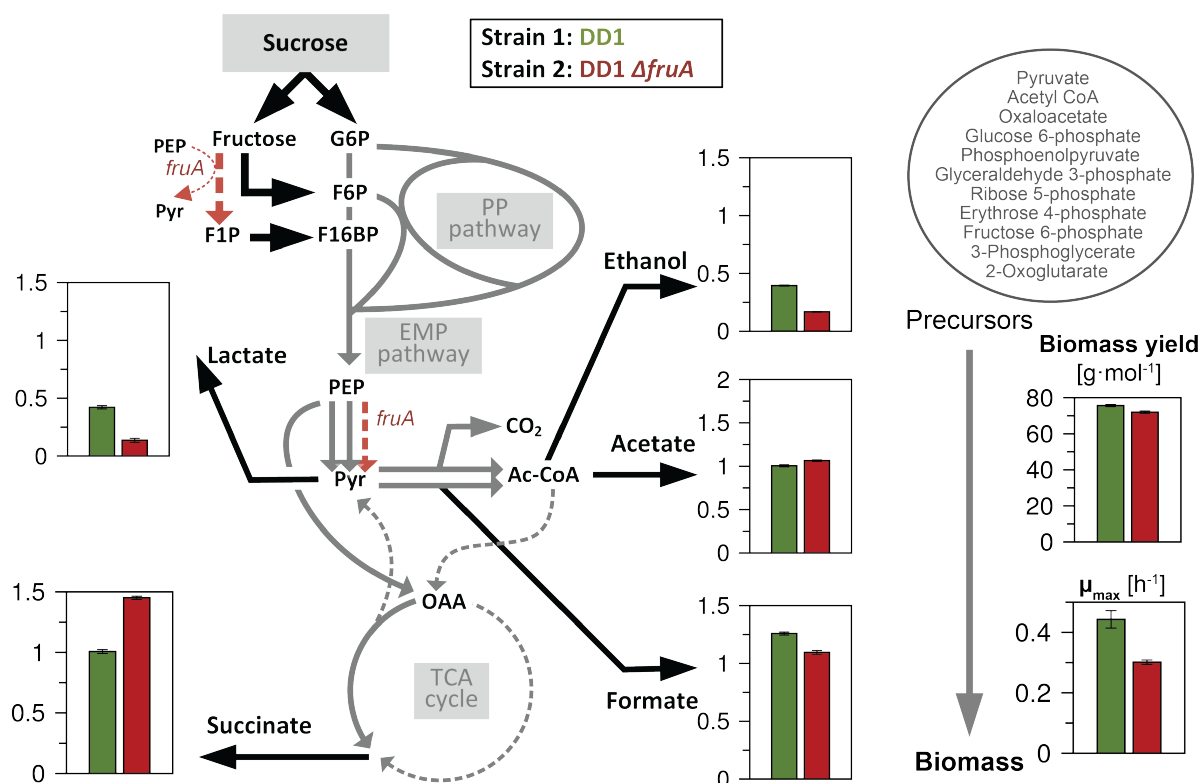
Figure 4.14: Product stoichiometry of sucrose-grown *B. succiniciproducens* DD1 Δ*fruA* reveals improved succinate production. The yield coefficients (in $\text{mol}_{\text{product}} \cdot \text{mol}_{\text{sucrose}}^{-1}$) by the wild type *B. succiniciproducens* DD1 (green) and by the deletion strain *B. succiniciproducens* DD1 Δ*fruA* lacking the fructose PTS (red) are displayed as bar charts, placed on a simplified metabolic map of *B. succiniciproducens* to indicate which metabolic precursors the respective products are derived from. The data represent mean values and deviations from at least three replicates. G6P: glucose 6-phosphate; F6P: fructose 6-phosphate; F1P: fructose 1-phosphate; F16BP: fructose 1,6-bisphosphate; PEP: phosphoenolpyruvate; Pyr: pyruvate; Ac-CoA: acetyl-CoA

yields were clearly distinct in the different phases. During sucrose limitation the two strains produced succinic acid at high, nearly identical yields of $0.85\,\text{g·g}^{-1}$ (wild type) and $0.84\,\text{g·g}^{-1}$ (mutant) (Figure 4.15C, D). The only by-product accumulating during this phase was acetic acid (Figure 4.15A, B). During the batch phase and the substrate accumulation phase, however, the two strains showed clear differences: the succinic acid yield in the mutant was much higher at $0.61\,\text{g·g}^{-1}$ during the batch phase and $0.74\,\text{g·g}^{-1}$ during the accumulation phase, compared to only $0.53\,\text{g·g}^{-1}$ produced by the wild type.

A closer inspection of the effect of substrate limitation on the *B. succiniciproducens* metabolism will certainly shed light on the molecular mechanisms underlying the shift towards higher succinic acid production. So far, it is unclear why during limitation, the presence or absence of the fructose PTS apparently does not affect the process, and why only acetate and succinate accumulate during such process conditions.

Overall, the mutant strain clearly showed a superior performance as compared to the wild type and is a very suitable candidate for large scale production of succinic acid. During large scale fermentations, ensuring a permanently homogenous state of the cultivation broth becomes extremely challenging. Thus, a strain that retains high succinic acid yields even when the local substrate concentration increases, is highly advantageous.

4.2.6.2 Elementary flux mode analysis verifies the excellent performance of DD1 *ΔfruA*

The elementary flux mode space for sucrose-grown *B. succiniciproducens* was calculated using the metabolic network model described in Chapter A.3. As shown in Fig. 4.16A, the overall flux space is strongly influenced by the presence of fructokinase. Without this enzyme, the highest theoretical succinate yield on sucrose is $2\,\text{mol·mol}^{-1}$, whereas it is as high as $3\,\text{mol·mol}^{-1}$ considering elementary modes requiring fructokinase. There is also a clear positive correlation between activity of fructokinase and the corresponding succinic acid yield (Figure 4.16B). Evaluating the experimental yields achieved with the wild type *B. succiniciproducens* and with *B. succiniciproducens ΔfruA* in context of the theoretical flux space shows that there remains a high potential for further improvement. The succinate yield achieved with the substrate limiting feeding strategy applied during fed-batch fermentation, however, reached $82\,\%$ of the theoretical maximum.

Overexpressing the fructokinase encoding *rbsK* gene in *B. succiniciproducens* DD1 *ΔfruA* might further improve sucrose utilization to achieve faster growth and a higher succinate yield especially during batch fermentation.
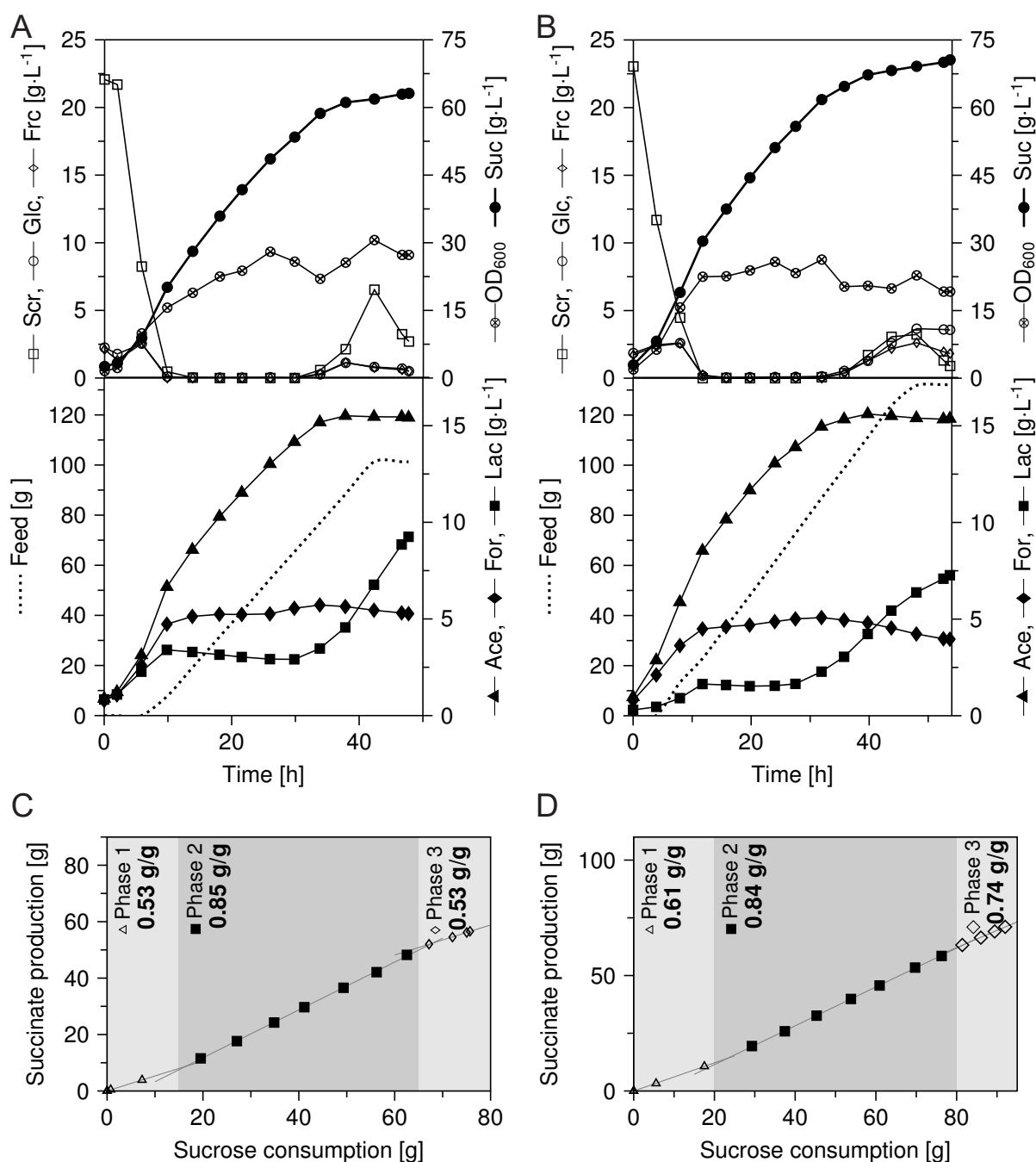
Figure 4.15: Fed-batch production of succinate from sucrose by *B. succiniciproducens* DD1 and the deletion mutant *B. succiniciproducens* DD1 Δ*fruA*. The wild type strain *B. succiniciproducens* DD1 (A, C) and the deletion mutant *B. succiniciproducens* DD1 Δ*fruA* (B, D) were cultivated on sucrose using a linear feeding strategy. The cultivation profiles, including data for feeding, substrate concentrations, and biomass and product concentrations are shown for the wild type strain (A) and the mutant strain (B). The succinate yields for the wild type (C) and the mutant strain (D) were clearly distinct during the three phases of the cultivations: the initial batch phase (Phase 1), the phase of limited feeding (Phase 2), and the final substrate accumulation phase at the end of the process (Phase 3). Units given in axis labels refer to all preceding substances separated by commas. Scr: sucrose; Glc: glucose; Frc: fructose; Suc: succinate; Ace: acetate; For: formate; Lac: lactate
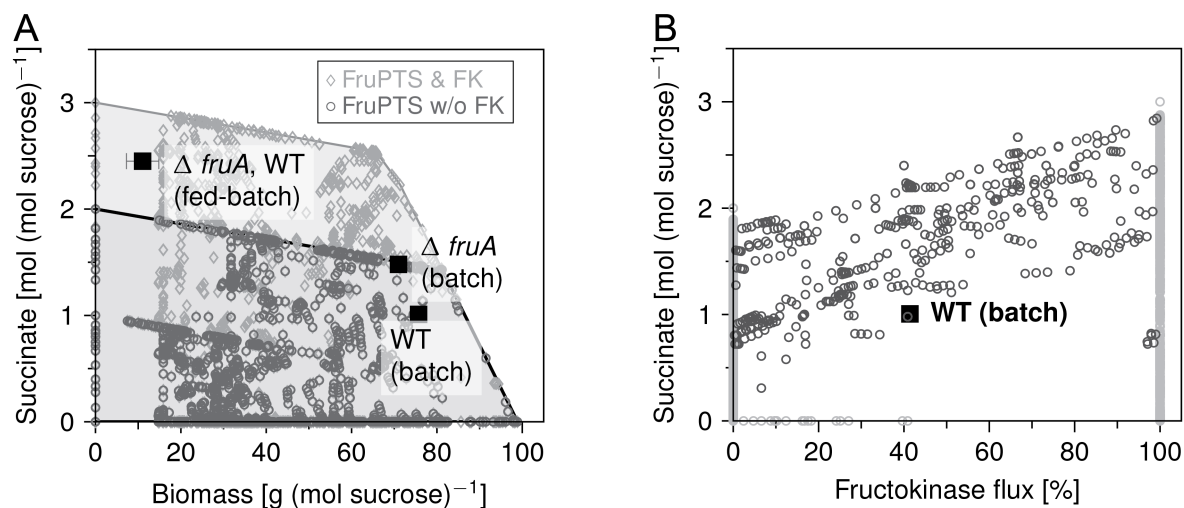
Figure 4.16: Evaluation of the production performance of sucrose-grown *B. succiniciproducens* by elementary flux mode analysis. (A) Light gray diamonds (FruPTS & FK) represent elementary modes leading to biomass formation and/or succinate production, based on the experimentally validated network model including the fructokinase reaction. Dark gray circles (FruPTS w/o FK)represent the elementary modes with zero flux through fructokinase. The data represent theoretical yields for succinate [mol·mol^{-1}] and biomass [g·mol^{-1}] from sucrose, thus spanning a solution space for all feasible production scenarios involving biomass and succinate formation. The experimentally observed yields of the *B. succiniciproducens* wild type and the knockout strain *B. succiniciproducens* DD1 $\Delta fruA$ during batch cultivation in serum flasks (batch) and during the limited feeding phase of the fed-batch fermentation (fed-batch) are displayed as black squares and labeled accordingly. (B) Plotting the theoretical relative fructokinase fluxes, which can vary between 0 % (all fructose is channeled through fructose PTS or secreted) and 100 % (all fructose is phosphorylated through fructokinase), against the corresponding succinate yields shows a clear positive correlation. Extreme elementary modes, with either zero or maximal values for either of the two parameters, are displayed as light gray circles. The black square represents the data from the ^{13}C metabolic flux analysis and is clearly positioned within the feasible solution space.

4.2.7 A detailed flux map of *B. succiniciproducens* DD1 on fructose

To resolve the intracellular carbon fluxes of fructose-grown *B. succiniciproducens*, three parallel ^{13}C labeling data sets, comprising a total of 372 individual mass isotopomers, were simultaneously fit to the network model.

Biomass and product formation (Table 4.4), as well as the experimentally determined *in vivo* enzyme activity of malic enzyme, considered as the upper limit of the corresponding flux, were applied to constrain the model. The small deviation between experimental and simulated labeling pattern (Figure 4.18), indicating an excellent fit, and the small confidence intervals of the calculated fluxes suggest high accuracy (Figure 4.17).

4.2.7.1 Fructose is nearly completely metabolized via the EMP pathway

Before it actively enters the metabolism, fructose is phosphorylated twice: first, to fructose 1-phosphate via the specific fructose PTS, and secondly via phosphofructokinase to form fructose 1,6-bisphosphate. Nearly 97 % of fructose 1,6-bisphosphate continued along the EMP pathway while 3 % were first converted into glucose 6-phosphate and then channeled through the oxidative PP pathway. The PP pathway was strongly downregulated during growth on fructose, only providing sufficient precursors for biomass. The backflux from glyceraldehyde 3-phosphate into the PP pathway was very low (0.5 %).

4.2.7.2 The majority of PEP is converted into pyruvate by the concerted action of fructose PTS and pyruvate kinase

Fructose assimilation was coupled to the conversion of PEP into pyruvate, leading to an inherently high flux of 100 % from PEP to pyruvate. In addition to this, pyruvate kinase converted another 37 % of PEP into pyruvate. On sucrose, the pyruvate kinase flux was similar (31 %), whereas on glucose, it was much higher (84 %). Apparently, the reduced availability of PEP, caused by the respective substrate uptake systems on fructose and sucrose, leads to a reduction of pyruvate kinase *in vivo* activity. Nevertheless, the overall conversion of PEP into pyruvate was very high on fructose (137 %) and sucrose (110 %) as compared to glucose (84 %).

On all substrates, an additional 9 % (sucrose) to 12 % (glucose) of PEP was converted into pyruvate via the concerted action of PEPCK/PEPCK and malic enzyme.
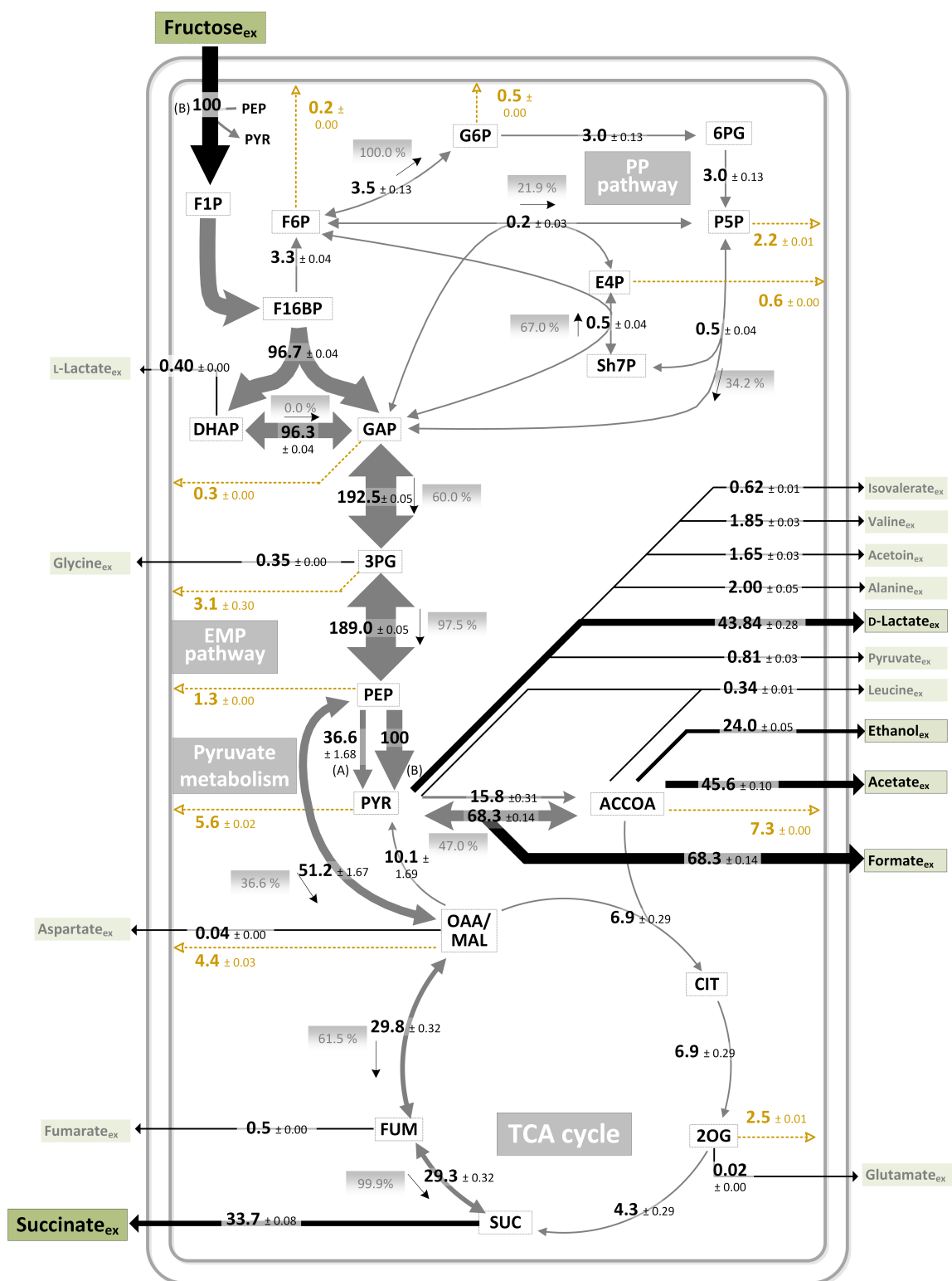
Figure 4.17: Intracellular carbon fluxes of *B. succiniciproducens* DD1 on fructose as determined by ^{13}C metabolic flux analysis. The carbon fluxes were normalized to the fructose influx of $10.2 \pm 0.4\,\mathrm{mmol \cdot g^{-1} \cdot h^{-1}}$, which was set to $100\,\%$. The arrow thickness is proportional to the corresponding flux. The direction of net fluxes is indicated by small black arrows. Reversibilities, calculated according to Equation 3.5, are displayed gray boxes. Yellow dashed arrows represent fluxes into biomass formation. Black arrows indicate carbon in- and efflux. The two reactions that catalyze conversion of PEP into PYR are: (A) pyruvate kinase, (B) fructose PTS. PEP: phosphoenolpyruvate; PYR: pyruvate; G6P: glucose 6-phosphate; 6PG: 6-phosphogluconate; F1P: fructose 1-phosphate; F6P: fructose 6-phosphate; F16BP: fructose 1,6-bisphosphate; DHAP: dihydroxyacetone phosphate; GAP: glyceraldehyde 3-phosphate; P5P: pentose 5-phosphate; E4P: erythrose 4-phosphate; Sh7P: seduheptulose 7-phosphate; 3PG: 3-phosphoglycerate; ACCOA: acetyl-CoA; OAA/MAL: oxaloacetate/malate; CIT: citrate; FUM: fumarate; SUC: succinate; 2OG: 2-oxoglutarate

4.2.7.3 Excess pyruvate is channeled into a range of by-products

On fructose, sucrose, and glucose, pyruvate was converted into acetyl-CoA with a flux of 84 – 86 %. While this flux was sufficient on glucose to handle nearly the entire influx into pyruvate, this was obviously insufficient on sucrose and even more so on fructose. As a consequence, excess pyruvate was converted into D-lactate and a number of other pyruvate-derived by-products, including alanine, valine, acetoin, isovalerate, and leucine. The products were mostly reduced, indicating a need of the cell to regenerate NAD^+ on sucrose and especially on fructose.

4.2.7.4 Succinate is mostly produced via the reductive branch of the TCA cycle

As most of the succinate-precursor PEP was withdrawn towards pyruvate, the flux through PEPCK/PEPCX towards succinic acid was significantly lower on fructose than on other sugars.

Similar to the PP pathway, the oxidative branch of the TCA cycle mostly served as an anabolic route but still accounted for 12.8 % of the total succinate. Despite a reduced flux through the reductive branch, fumarate was secreted at a constant yield. This effect might be traced back to the accumulating lactic acid affecting the outer cell membrane integrity, as was previously observed for other Gram-negative bacteria (Alakomi *et al.*, 2000). Taken together, *B. succiniciproducens* channeled nearly 34 % into the desired product, although the fructose uptake via a specific PTS coupled to a high activity of pyruvate kinase led to withdrawal of significant amounts of the precursor PEP, particularly into lactate.

4.2.7.5 A slight apparent excess of NADH caused by reduced reduction of fumarate points towards an unknown electron acceptor

Considering the flux distributions on glucose, sucrose, and fructose, the substrate-specific redox metabolism of *B. succiniciproducens* could now be analyzed (Figure 4.13). In a living cell, the redox balance has to be closed at any time. Therefore, the total redox balance, considering NADP(H) and NAD(H), calculated from flux data, indicates consistency of the approach. On all three substances, the redox balance was largely closed. On all substrates, the NADPH demand exceeded the NADPH supply, whereas the NADH supply exceeded the NADH demand. This indicates that *in vivo* activity of a transhydrogenase is a general characteristic of sugar-grown *B. succiniciproducens*. On sucrose,

the supply of redox equivalents was slightly higher than the demand, although the redox can still be regarded as closed within the limits of accuracy. Only on fructose, a slight gap in the redox balance indicated an apparent excess of NADH. The excellent fit of the ^{13}C labeling data to the model and the closed carbon balance, however, clearly underline the validity of the determined flux distribution. Furthermore, a similar effect was previously ovserved for other bacteria (Wittmann *et al.*, 2004). The shift in the apparent need for redox equivalent is linked to a shift in product formation: from glucose to sucrose to fructose, the production of succinate decreases, whereas the production of lactate increases. Conversion of PEP via pyruvate into lactate, however, only requires an equimolar amount of NADH. Conversion of PEP via oxaloacetate, malate, and fumarate into succinate requires twice the amount of NADH. As a conclusion, *B. succiniciproducens* seems to possess an unknown way of regenerating NAD$^+$ during growth on fructose and, possibly, to a lesser extent on sucrose.

4.2.7.6 Targets for improving succinate-production from fructose

A close inspection of the *in vivo* fluxes on fructose, including the assessment of different metabolic engineering strategies, revealed deletion of the *ldhA* gene, encoding lactate dehydrogenase, as the most promising target. Lactate production on fructose was extremely prominent because of the high conversion of PEP into pyruvate and the insufficient withdrawal of pyruvate via pyruvate dehydrogenase and pyruvate formate lyase. Furthermore, deletion of *ldhA* in a strain producing high amounts of lactate, namely glucose-grown *B. succiniciproducens* $\Delta pflD$, was previously shown to strongly enhance succinate production while only marginally reducing growth (Becker *et al.*, 2013). As the double deletion mutant *B. succiniciproducens* $\Delta pflD\Delta ldhA$ still produced lactic acid during growth on glucose, we decided to block the second lactate production pathway as well by deleting *mgsA*.
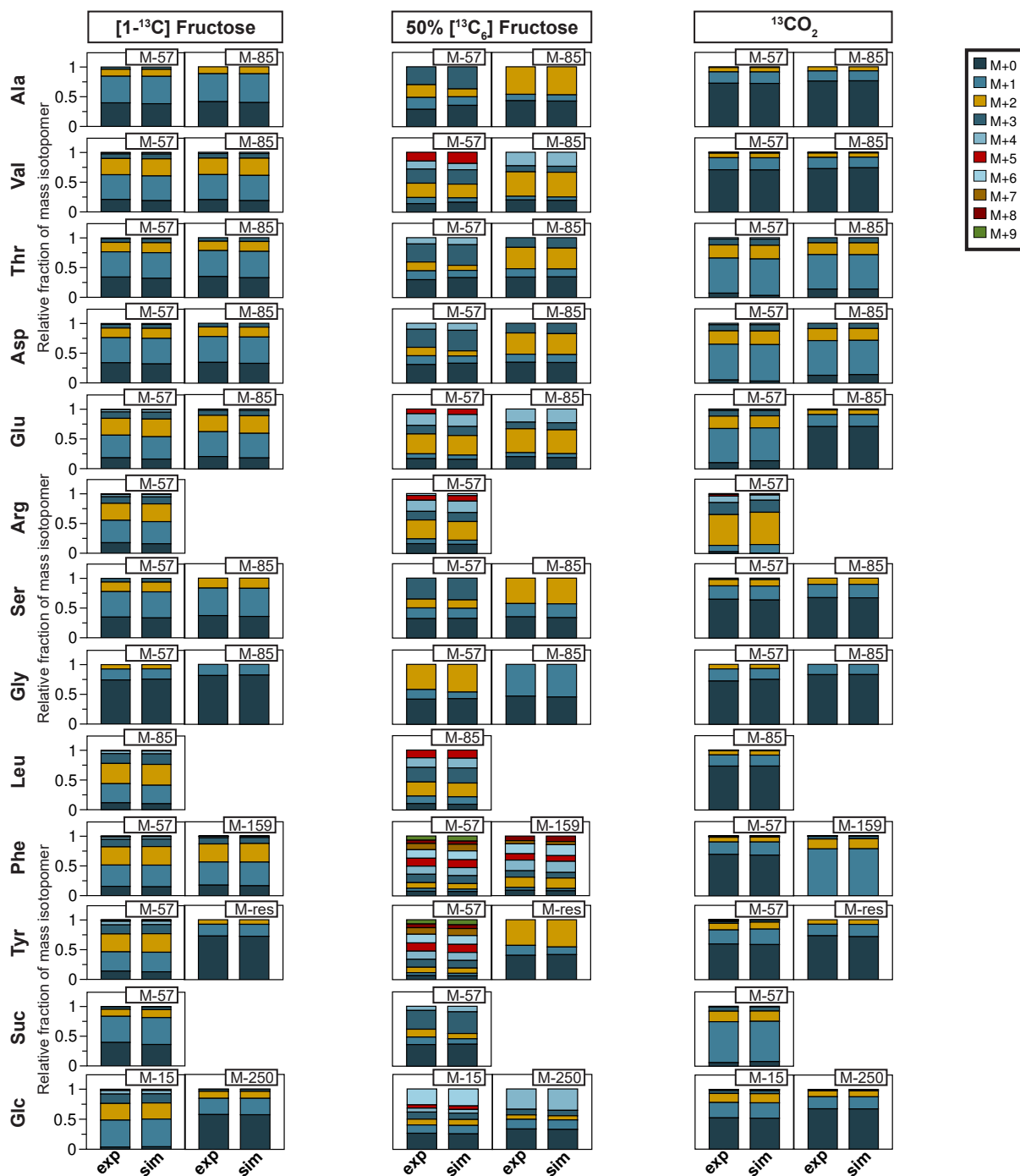
Figure 4.18: Comparison of experimental and simulated mass isotopomer distributions (MIDs) for flux analysis on fructose. The data represent experimental (exp) MIDs obtained during parallel cultivation of *B. succiniciproducens* DD1 on three different ^{13}C tracers and simulated (sim) MIDs corresponding to the calculated flux distribution for different amino acids (indicated by the respective three letter code abbreviations), succinate (Suc), and glycogen-derived glucose (Glc). The deviation between the experimental (exp) and simulated (sim) MIDs was exceptionally low for all data sets. 50 % [^{13}C$_6$] fructose denotes a 1:1 mixture of naturally labeled fructose and fully labeled fructose.

4.2.8 Improved succinate-production on fructose by removal of the competing by-product lactate

Following the proposed metabolic engineering strategy, *ldhA* encoding lactate dehydrogenase was deleted in the wild type *B. succiniciproducens*. To completely prevent production of any lactic acid and thereby facilitating downstream processing in a future production process, *mgsA*, encoding methylglyoxal synthase, was deleted as well, resulting in the double deletion mutant *B. succiniciproducens* $\Delta ldhA \Delta mgsA$. Because of the high loss of carbon into the main by-product lactate, the two lactate-production pathways were knocked out in the wild type *B. succiniciproducens* DD1. By removing lactate dehydrogenase as the main vent for excess pyruvate, pyruvate was expected to accumulate intracellularly, leading to a reduced pyruvate kinase flux from PEP to pyruvate and, in turn, causing a higher rate of PEP carboxylation and succinate production.

B. succiniciproducens DD1 $\Delta ldhA \Delta mgsA$ was cultivated in fructose minimal medium in serum bottles. The strain showed reproducible growth and completely consumed the provided substrate within 42 h (Figure A.3), which was only slightly slower than the wild type strain. The succinic acid yield achieved by the mutant was increased by 40 % to 0.47 ± 0.01 mol·mol^{-1}, while no lactate was secreted (0.44 ± 0.01 mol·mol^{-1}in the wild type cultivation). Besides the succinate yield, the yields of the other main by-products formate, acetate, and ethanol, were also higher during cultivation of the mutant strain (Figure 4.19). This effect was probably driven by the increased intracellular pyruvate concentration, driving the conversion of pyruvate into acetyl-CoA, mostly catalyzed by pyruvate formate lyase.

To evaluate the succinic acid production capacity of *B. succiniciproducens* DD1 and the mutant strain $\Delta ldhA \Delta mgsA$ from fructose, a comparative fed-batch fermentation in industrial medium (Table 3.7) was carried out (Figure 4.20). Similar to the fed-batch fermentation on sucrose, a linear feeding strategy was chosen to ensure substrate limitation throughout most of the process, as this had previously led to higher succinate production.

Overall, *B. succiniciproducens* $\Delta ldhA \Delta mgsA$ reached a maximum titer of 66.1 g·L^{-1} succinic acid in fed-batch fermentation, resulting from the production of 62.9 g succinate from 89.6 g fructose. This was 18.5 % higher than the titer achieved by the wild type (Figure 4.20A, B). No lactic acid was produced by the mutant, while the wild type accumulated 13.2 g·L^{-1} lactic acid. As previously observed for the sucrose fed-batch fermentations, the two fed-batch cultivations on fructose comprised three distinct phases with
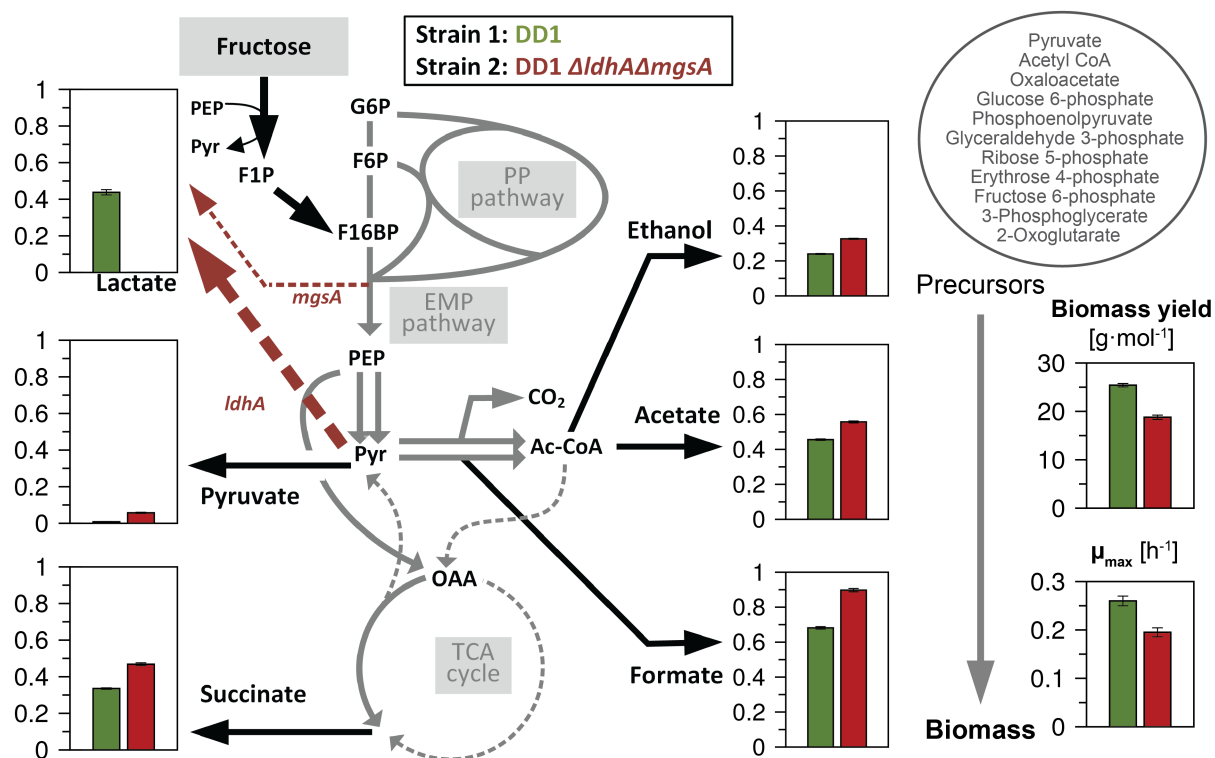
Figure 4.19: Product stoichiometry of fructose-grown *B. succiniciproducens* DD1 $\Delta ldhA$ $\Delta mgsA$ reveals enhanced succinate production. The yield coefficients (in $mol_{product} \cdot mol_{sucrose}^{-1}$) by wild type *B. succiniciproducens* DD1 (green) and by the deletion strain *B. succiniciproducens* DD1 $\Delta ldhA \Delta mgsA$ lacking the two lactate production pathways (red) are displayed as bar charts, placed on a simplified metabolic map of *B. succiniciproducens* to indicate which metabolic precursors the respective products are derived from. The data represent mean values and deviations from at least three replicates. PEP: phosphoenolpyruvate; Pyr: pyruvate; Ac-CoA: acetyl-CoA; G6P: glucose 6-phosphate; F6P: fructose 6-phosphate; F1P: fructose 1-phosphate; F16BP: fructose 1,6-bisphosphate

clearly distinct production characteristics. During fructose limitation, the two strains produced succinic acid at high, similar yields of $0.72\,\mathrm{g\cdot g^{-1}}$ (wild type) and $0.74\,\mathrm{g\cdot g^{-1}}$ (mutant) (Figure 4.20C, D). During this phase, acetic acid and formic acid accumulated as by-products. In the wild type cultivation, the lactic acid concentration remained constant throughout this phase, indicating a slight production to counteract the dilution caused by addition of the feed (Figure 4.20A, B). During the batch phase and the final substrate accumulation phase, the differences between the strains were more profound: the succinic acid yield in the mutant was much higher at $0.57\,\mathrm{g\cdot g^{-1}}$ during the batch phase and increased to $0.86\,\mathrm{g\cdot g^{-1}}$ during the accumulation phase, whereas the wild type produced succinic acid at $0.50\,\mathrm{g\cdot g^{-1}}$ during the initial batch phase and $0.53\,\mathrm{g\cdot g^{-1}}$ during the final accumulation phase.

Apparently, *B. succiniciproducens* manages to dispose of excess pyruvate without the help of lactate dehydrogenase when fructose is fed at a limited rate. The increased formic acid formation, as compared to the sucrose cultivations, indicates that while pyruvate does accumulate at higher amounts, it is converted via pyruvate formate lyase.

Although lactic acid production by the wild type was not very prominent during the feeding phase, the mutant strain overall clearly showed a superior performance. The average succinic acid yield and the final succinic acid titer were significantly higher for the mutant, since the strain retained high succinic acid yields even at non-limiting substrate concentrations. As discussed previously, this behavior is desirable for industrial processes, as high local substrate concentrations are likely to occur during large-scale fermentations. Furthermore, non-limiting conditions allow for a faster progression of the overall process.
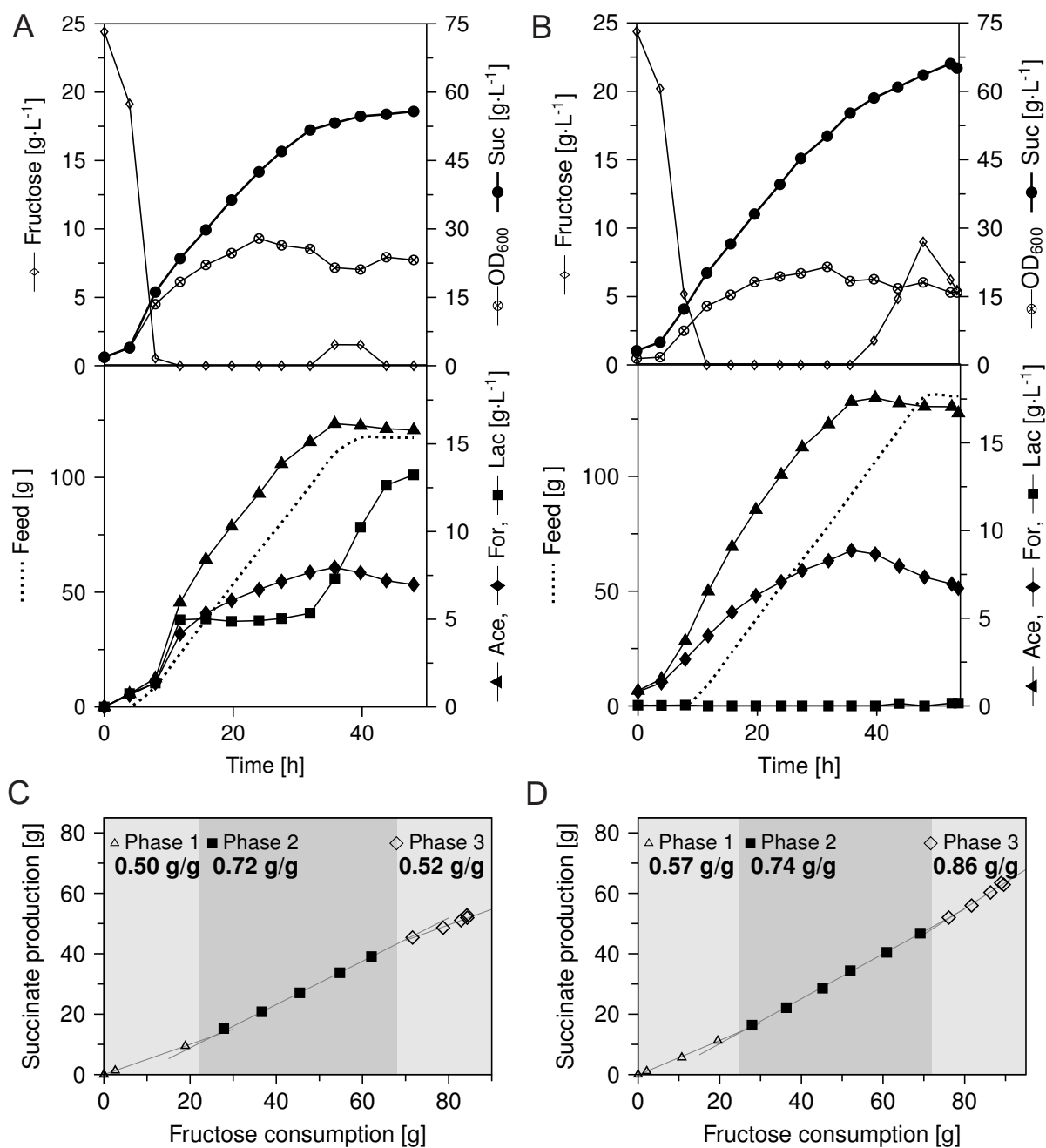
Figure 4.20: Fed-batch production of succinate from fructose by *B. succiniciproducens* DD1 and the deletion mutant *B. succiniciproducens* DD1 Δ*ldhA*Δ*mgsA*. The wild type strain (A, C) and the deletion mutant (B, D) were cultivated on fructose using a linear feeding strategy. The cultivation profiles, including data for feeding, substrate concentrations, and biomass and product concentrations are shown for the wild type strain (A) and the mutant strain (B). The succinate yields for the wild type (C) and the mutant strain (D) were clearly distinct during the three phases of the cultivations: the initial batch phase (Phase 1), the phase of limited feeding (Phase 2), and the final substrate accumulation phase at the end of the process (Phase 3). Units given in axis labels refer to all preceding substances separated by commas. Suc: succinate; Ace: acetate; For: formate; Lac: lactate

4.3 Exploring the Use of Hemicellulose Sugars as Substrates for Succinate Production by ^{13}C Metabolic Flux Analysis

Hemicellulose represents up to 35 % of lignocellulosic biomass, rendering it the second most common polysaccharide in nature, and it can be derived from agricultural or forestry waste (Saha, 2003). Although pretreatment is required to break up the complex lignocellulose polymer (Grimaldi *et al.*, 2015), hemicellulose is a potentially cheap and abundant raw material suitable for biotechnological applications. Hemicellulose-based succinic acid production has not yet been commercialized, but is regarded as particularly promising, independent of the microorganism used for production (Kim *et al.*, 2004; Lee *et al.*, 2003; Li *et al.*, 2010; Salvachúa *et al.*, 2016a,b).

To date, studies on the usability of hemicellulose as a raw material for producing succinic acid focused rather empirically on macroscopic analysis with regard to succinic acid yield and productivity and on the potential impact of toxic compounds in lignocellulose hydrolysates on cultivation (Li *et al.*, 2010; Salvachúa *et al.*, 2016a,b). Our knowledge of the underlying metabolic and molecular details concerning production of succinic acid from this important renewable substrate is by comparison very limited.

In order to establish a commercial process for hemicellulose- or lignocellulose-based succinic acid production, however, it seems crucial to understand in great detail how the differences in sugar composition actually affect succinate production. A straightforward approach that can help to unravel and to understand the observed effects is ^{13}C metabolic flux analysis (Kohlstedt *et al.*, 2010).

Lignocellulose contains 15 − 45 % cellulose, a glucose polymer, and 24 − 50 % hemicellulose, a heteropolymer containing xylose and, to a lesser extent, other sugars and sugar acids (Saha, 2003). Therefore, the actual sugar composition in hydrolysates varies significantly. In two of the above mentioned studies, xylose-enriched hydrolysates containing approx. 10 % (w/w) glucose and 70 % (w/w) xylose were used (Salvachúa *et al.*, 2016a,b). Two other studies used lignocellulose hydrolysates containing approx. 25 − 30 % (w/w) xylose and 70 − 75 % (w/w) glucose, while other carbohydrates were not quantified (Kim *et al.*, 2004; Lee *et al.*, 2003).

We decided to analyze *B. succiniciproducens* metabolism on pure xylose and on a glucose/xylose mixture containing 60 % (w/w) glucose and 40 % (w/w) xylose (equivalent to a molar ratio of 5:4), to cover the possible variations.

4.3.1 Succinate production from xylose and from a glucose/xylose mixture
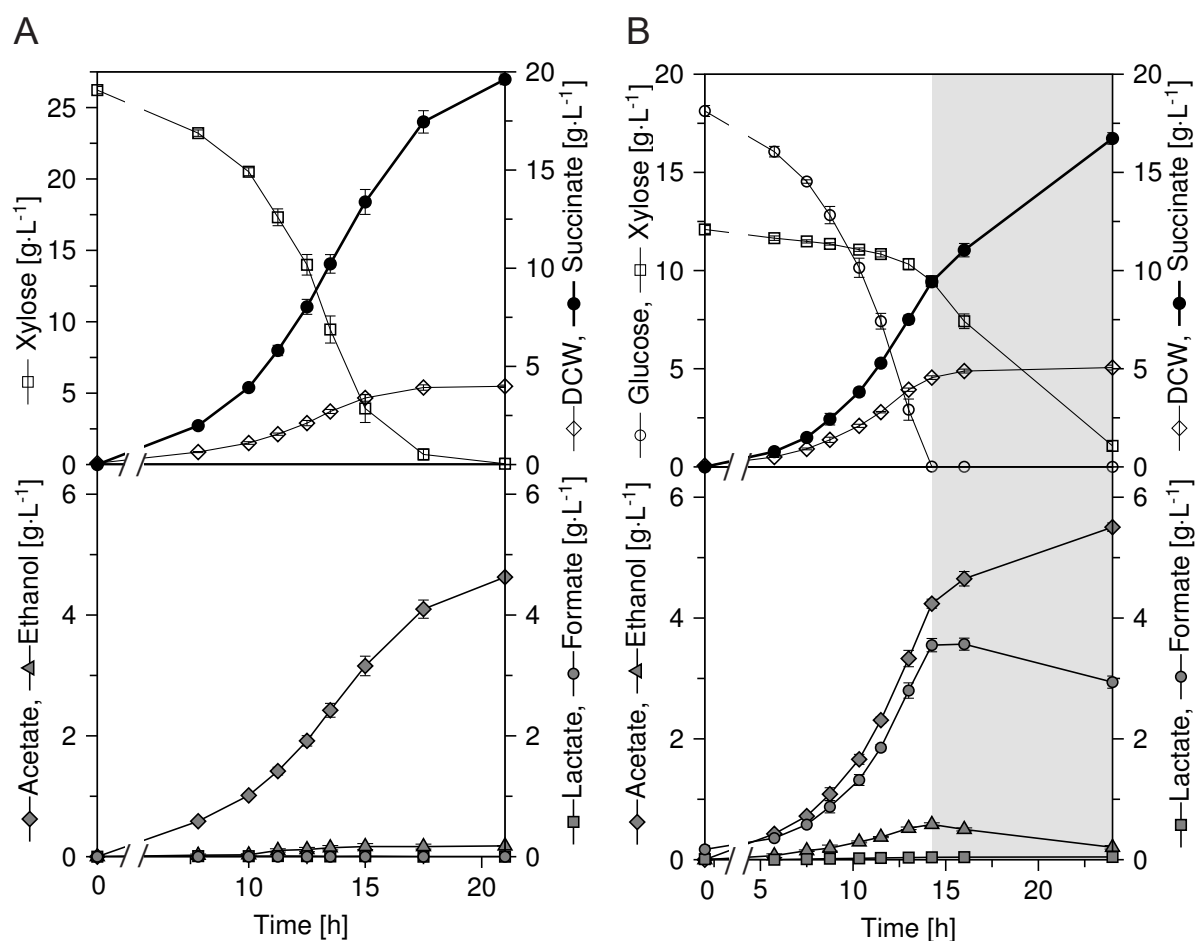
Figure 4.21: Cultivation characteristics of *B. succiniciproducens* DD1 on xylose (A) and on a substrate mixture (18 g·L⁻¹ glucose, 12 g·L⁻¹ xylose) (B). The data comprise mean values and deviations from four biological replicates, respectively, for biomass growth, for substrate consumption, and for secretion of succinate and the by-products acetate, formate, lactate, and ethanol during growth (A) on xylose and (B) on a mixture of 18 g·L⁻¹ glucose and 12 g·L⁻¹ xylose. Here, xylose and glucose were first consumed simultaneously with a higher uptake rate for glucose. After glucose was depleted, the remaining xylose was mostly converted into succinate and acetate with only little biomass formation (highlighted in gray). It should be noted that only data from the exponential growth phases were later taken into account for ^{13}C metabolic flux analysis. Units given in axis labels refer to all preceding substances separated by commas. DCW: dry cell weight.

B. succiniciproducens DD1 was cultivated in minimal medium with xylose as the sole carbon source (Figure 4.21 A). The strain showed exponential growth at a specific growth rate of $0.27 \pm 0.01\,\text{h}^{-1}$, leading to complete consumption of the substrate within 22 h. The specific xylose uptake rate and the specific succinate secretion rate were exceptionally high at $11.5 \pm 0.3\,\text{mmol·g}^{-1}\text{·h}^{-1}$ and $10.2 \pm 0.2\,\text{mmol·g}^{-1}\text{·h}^{-1}$, as compared to uptake rates for sucrose, fructose, and glucose (Table 4.8). Overall, only 4.0 g·L⁻¹ biomass, but 19.6 g·L⁻¹ succinate, 4.6 g·L⁻¹ acetate, and 0.2 g·L⁻¹ ethanol were produced. Surprisingly, no formate was secreted at all, although high formation of formate had previously been observed on

Table 4.8: Growth kinetics of *B. succiniciproducens* DD1 on xylose and on a substrate mixture (18 g·L^{-1} glucose, 12 g·L^{-1} xylose). The specific rates, i.e., the xylose uptake rates q_{Xyl}, the glucose uptake rate q_{Glc}, the succinate production rate q_{SA}, and the specific growth rate μ_{max}, represent mean values and deviations from six replicates, respectively.

Specific rate	Xylose	Glucose/Xylose
μ_{max} [h^{-1}]	0.27 $\pm$ 0.01	0.32 $\pm$ 0.01
q_{Xyl} [mmol·g^{-1}·h^{-1}]	11.5 $\pm$ 0.3	1.1 $\pm$ 0.0
q_{Glc} [mmol·g^{-1}·h^{-1}]	—	7.2 $\pm$ 0.3
q_{SA} [mmol·g^{-1}·h^{-1}]	10.2 $\pm$ 0.2	6.0 $\pm$ 0.3

glucose, sucrose, and fructose (Table 4.4) and therefore seemed to be a typical characteristic of *B. succiniciproducens* metabolism. Lactate and pyruvate were not secreted, either, but trace amounts of fumarate were detected in the supernatant.

Table 4.9: Growth and production stoichiometry of *B. succiniciproducens* DD1 on xylose and on a substrate mixture (18 g·L^{-1} glucose, 12 g·L^{-1} xylose). The data comprise yield coefficients for biomass ($Y_{X/S}$) and secreted products ($Y_{Product/S}$) and represent mean values and deviations from six replicates, respectively. The yields are given on a C-molar basis (as C-mol product per C-mol consumed xylose and glucose), to allow for direct comparison of the two cultivations. To provide values that could be implemented into the OpenFLUX model, in which the uptake of glucose as the main carbon source was set to 100 %, additional pseudo-yields are also given on a molar basis, as mol product per mol consumed main substrate. In this case, the consumption of xylose from the glucose/xylose mixture was consequently ignored for the calculation of the pseudo-yields. The parameter $Y_{Xyl/Glc}$, however, represents the co-consumption ratio, indicating the amount of xylose consumed per mol glucose [mol·mol^{-1}], representing an additional influx of 15 % from xylose in the flux map. Xyl: xylose; glc: glucose

Yield coefficient	Xylose		Glucose/Xylose	
	[C-mol·C-mol^{-1}]	[mol·(mol xyl)$^{-1}$]	[C-mol·C-mol^{-1}]	[mol·(mol glc)$^{-1}$]
$Y_{X/S}$[a]	4.69 $\pm$ 0.05	23.45 $\pm$ 0.25	6.58 $\pm$ 0.04	44.45 $\pm$ 0.30
$Y_{Xyl/Glc}$				0.15 $\pm$ 0.00
$Y_{Succinate/S}$	0.71 $\pm$ 0.00	0.89 $\pm$ 0.01	0.49 $\pm$ 0.00	0.84 $\pm$ 0.00
$Y_{Formate/S}$	n. d.[b]	n. d.	0.11 $\pm$ 0.00	0.75 $\pm$ 0.01
$Y_{Acetate/S}$	0.15 $\pm$ 0.00	0.38 $\pm$ 0.00	0.19 $\pm$ 0.00	0.65 $\pm$ 0.01
$Y_{D-Lactate/S}$	n. d.	n. d.	0.003 $\pm$ 0.000	0.006 $\pm$ 0.000
$Y_{Ethanol/S}$	0.016 $\pm$ 0.001	0.041 $\pm$ 0.002	0.036 $\pm$ 0.000	0.122 $\pm$ 0.002
$Y_{Fumarate/S}$	0.005 $\pm$ 0.001	0.007 $\pm$ 0.001	n. d.	n. d.

[a] in g·(mol)$^{-1}$ or g·(C-mol)$^{-1}$

[b] not detected

On the substrate mixture (18 g·L^{-1} glucose, 12 g·L^{-1} xylose), the specific growth rate even surpassed the rates on either of the single substrates at 0.32 $\pm$ 0.01 h^{-1}. Although both sugars were taken up simultaneously, glucose was the preferred substrate (Table 4.8).

Glucose uptake from the mixture was only slightly reduced when compared to pure glucose (Table 4.8, Table 4.3). Xylose, by contrast, was taken up from the mixture at a significantly reduced rate, indicating a suppressing effect of glucose on xylose uptake (Table 4.8). Overall, the behavior of *B. succiniciproducens* on the glucose/xylose mixture during the co-consumption phase was rather similar to the previous cultivation on glucose alone with regard to by-product formation and yields (Table 4.9). Besides the main product succinate, acetate, formate, and ethanol were produced as by-products. The biomass yield (calculated on a C-molar basis) was similar to that on glucose and thus higher than that on xylose. When glucose was completely depleted after 14 h, the cells entered a second phase (Figure 4.21 B, highlighted in gray). During the next 10 h, growth seized almost completely. The remaining xylose was converted into acetate and succinate, while ethanol and formate were partly re-assimilated.

4.3.1.1 The specific glucose and xylose uptake rates vary with the substrate ratio

To inspect whether a change in the substrate ratio of xylose and glucose would affect the process, another experiment was carried out, this time initially containing $43\,\mathrm{g\cdot L^{-1}}$ xylose and $6.6\,\mathrm{g\cdot L^{-1}}$ glucose, representing a xylose-enriched hydrolysate (Salvachúa *et al.*, 2016a,b). In this cultivation, xylose and glucose were also consumed simultaneously, although at a different ratio: apparently, xylose was the preferred substrate (Figure 4.22 A). The specific uptake rates for xylose and glucose were $2.2 \pm 0.1\,\mathrm{mmol\cdot g^{-1}\cdot h^{-1}}$ and $1.7 \pm 0.0\,\mathrm{mmol\cdot g^{-1}\cdot h^{-1}}$, respectively (Figure 4.22 B), and the specific growth rate was significantly reduced ($0.13\,\mathrm{h^{-1}}$). When glucose was depleted after 30 h, *B. succiniciproducens* entered a second exponential growth phase during which the specific xylose uptake rate and the specific growth rate remained low and did not recover to the values observed in cultivations with xylose as the sole substrate (Figure A.5, Table 4.8).

By plotting xylose consumption against glucose consumption, the molar uptake ratio was determined for both cultivations. This ratio represents the amount of xylose taken up per amount of glucose. Interestingly, in both cultivations, these uptake ratios were six times lower than the substrate ratio at the beginning of each cultivation (Figure 4.22 C). Weather this relation is indeed a specific characteristic of the *B. succiniciproducens* hemicellulose metabolism cannot be conclusively proven on basis of the available data. The fact remains, however, that neither the specific glucose uptake rate nor the specific xylose uptake rates are independent of the actual amount of substrate present in the medium, even at substrate concentrations far above typical substrate affinities of sugar transporters (Jojima *et al.*, 2010; Leandro *et al.*, 2006).
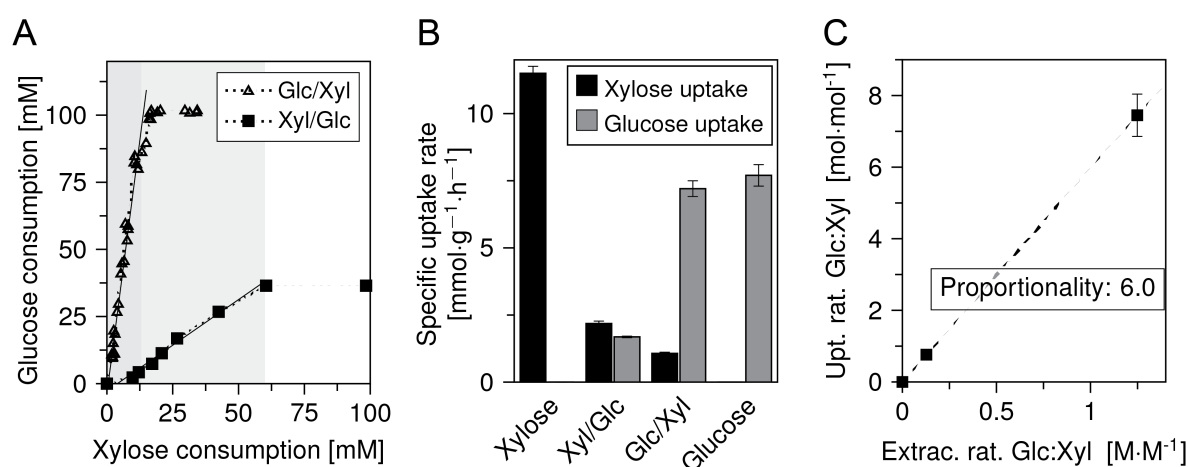
Figure 4.22: Simultaneous consumption of xylose and glucose by *B. succiniciproducens.* Two cultivations with different initial xylose and glucose concentrations were carried out. In the first cultivation (Glc/Xyl), the initial glucose concentration (100 mM) was higher than the initial xylose concentration (80 mM). In the second cultivation (Xyl/Glc), the initial xylose concentration (286 mM) was higher than the initial glucose concentration (36 mM). (A) During both cultivations, the two carbohydrates were consumed simultaneously at a constant ratio. (B) The specific substrate uptake rates, however, differed significantly. Xylose and glucose uptake rates during cultivations with the respective sugar as sole carbon source are shown for comparison. (C) Plotting the uptake ratio (Upt. rat. Glc:Xyl), as shown in (A), against the ratio of the substrate concentrations (Extrac. rat. Glc:Xyl) indicates a possible relationship.

4.3.1.2 Pyruvate formate lyase and formate dehydrogenase are apparently active during growth on xylose

The most surprising feature of the *B. succiniciproducens* xylose metabolism is certainly the absence of formate as a by-product. In *B. succiniciproducens*, formate is produced from pyruvate via pyruvate formate lyase. A second enzyme, pyruvate dehydrogenase, catalyzes the oxidative decarboxylation of pyruvate into acetyl-CoA. At first glance, *B. succiniciproducens* seemed to be relying solely on pyruvate dehydrogenase when growing on xylose, as no formate formation could be observed, suggesting the absence of pyruvate formate lyase. To investigate this, *B. succiniciproducens* $\Delta pflD$ was cultivated on xylose. In case pyruvate formate lyase, encoded by *pflD*, was indeed irrelevant during growth on xylose, the strain should behave as the wild type strain.

The mutant strain did, however, show a completely different behavior, as summarized in Figure 4.23. The specific growth rate was reduced by 60 % and the product yields were influenced by the deletion as well: the succinate yield increased slightly, whereas the acetate and ethanol yields decreased. In addition to these products, pyruvate and lactate accumulated, indicating an insufficient turnover of pyruvate into acetyl-CoA.

Apparently, *B. succiniciproducens* indeed required pyruvate formate lyase for efficient xylose consumption. Nevertheless, no formate was detected in culture supernatants. This leads to the hypothesis that *B. succiniciproducens* might possess a formate dehydrogenase, capable of oxidating formate into CO_2, which is active during growth on xylose, but inactive – or only active to a much lesser extent – during growth on other carbohydrates.

It should be noted that the advantageous properties of formate dehydrogenase for production of succinate and other organic acids have already been discussed in literature. Knocking out the native formate dehydrogenase in recombinant, succinic acid producing *E. coli* led to a reduced succinic acid production, so that the authors concluded that formate generated by pyruvate formate lyase in glucose-grown *E. coli* was indeed used as a source of reducing equivalents (Sánchez *et al.*, 2005). In a more recent study, a recombinant *E. coli* strain overexpressing formate dehydrogenase was constructed that exhibited improved succinic acid productivity and reached higher succinic acid titers in bioreactor cultivations (Balzer *et al.*, 2013). Plasmid-based expression of the native *M. succiniciproducens* formate dehydrogenases in *M. succiniciproducens* and other microorganisms led to improved succinic acid production (Lee *et al.*, 2007), while heterologous expression of a *Candida boidinii* formate dehydrogenase enhanced succinic acid production in *B. succiniciproducens* DD1 (Scholten *et al.*, 2010).
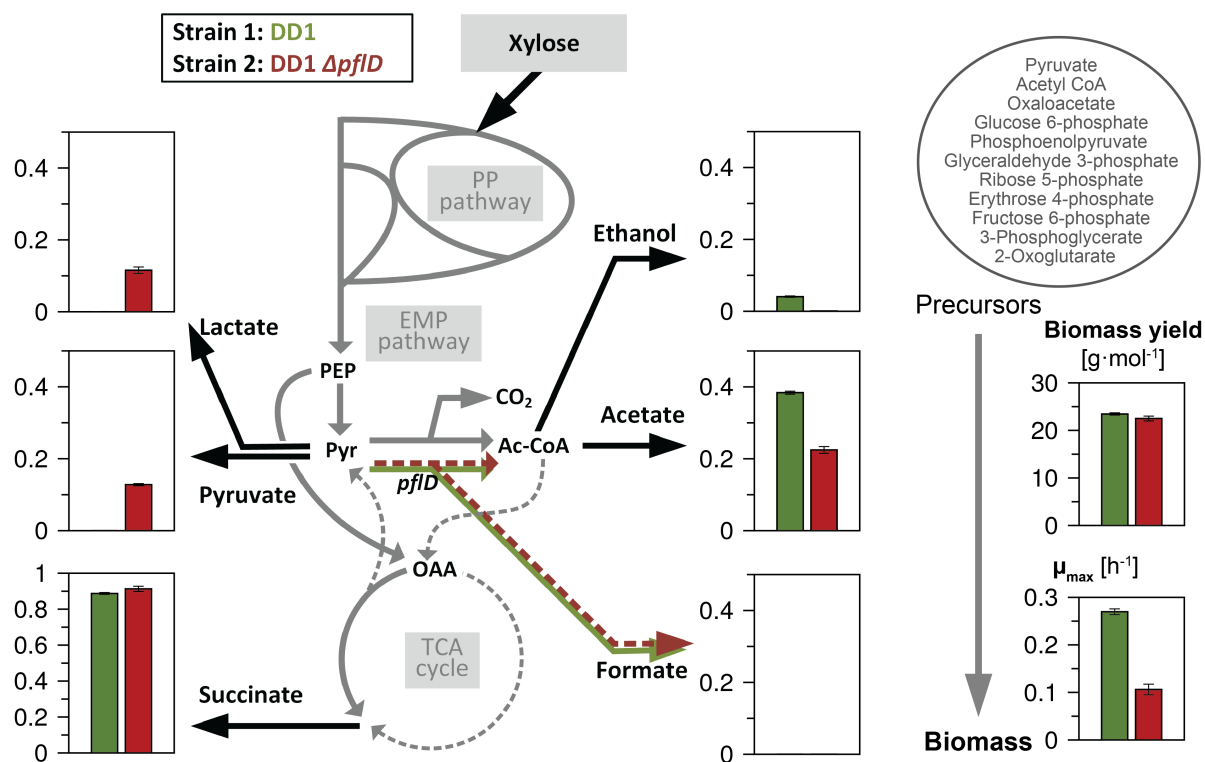
Figure 4.23: Comparison of product portfolio, product yields, and growth of xylose-grown *B. succiniciproducens* DD1 and *B. succiniciproducens* DD1 Δ*pflD*. Yield coefficients (in $\text{mol}_{\text{product}} \cdot \text{mol}_{\text{xylose}}^{-1}$) for succinate, biomass, and the by-products acetate, formate, ethanol, pyruvate, and lactate, as well as the respective growth rates on xylose are displayed for the wild type strain (green) and the Δ*pflD* deletion mutant (red). The data represent mean values and deviations from six (DD1) and three (DD1 Δ*pflD*) replicates and are placed on a simplified metabolic map of *B. succiniciproducens* to indicate which metabolic precursors the respective products are derived from. PEP: phosphoenolpyruvate; Pyr: pyruvate; Ac-CoA: acetyl coenzyme A

The potential of the putative native *B. succiniciproducens* formate dehydrogenase has, however, so far not been recognized or linked to xylose catabolism.

The possible presence of a formate dehydrogenase was indirectly included in the metabolic network model for xylose-grown *B. succiniciproducens* by lumping the two acetyl-CoA forming reactions, catalyzed by pyruvate formate lyase and pyruvate dehydrogenase, into a single, reversible, pyruvate decarboxylating reaction.

4.3.2 Verification of metabolic and isotopic steady state

The adapted metabolic network topology and the developed cultivation and analysis set-up were next applied for ^{13}C metabolic flux analysis of *B. succiniciproducens* on xylose and on a mixture of glucose and xylose.

In a previous study, [1-^{13}C] xylose had been used as the sole tracer to resolve metabolic fluxes in diaminopentane-producing *C. glutamicum* on xylose (Buschke *et al.*, 2013). With this approach, the fluxes at the pyruvate node could, however, not be fully resolved. Therefore, a 1:1 mixture of naturally labeled xylose and [^{13}C$_5$] xylose was additionally used in this study to provide a second labeling data set and to allow for a more complete resolution of the intracellular carbon fluxes of xylose-grown *B. succiniciproducens*.

To fully resolve the fluxes in *B. succiniciproducens* grown on a glucose/xylose mixture, four parallel labeling experiments were conducted, using [1-^{13}C] glucose, [1-^{13}C] xylose, [^{13}C$_6$] glucose, and [^{13}C$_5$] xylose, respectively, as tracers.

Metabolic flux analysis, as applied here, requires a metabolic and isotopic steady-state of the investigated culture (Becker *et al.*, 2008; Buschke *et al.*, 2013).

Metabolic steady state was ensured from constant product and biomass yields in all parallel labeling experiments during the exponential growth phase (Figure 4.24). During cultivation on a xylose/glucose mixture, the two substrates were consumed simultaneously with constant uptake rates. This is visualized by the linear correlation between xylose and glucose uptake during the co-consumption phase (Figure 4.24A). This further indicates that the constant yields shown for the glucose part of the substrate mixture (Figure 4.24A) also hold for the xylose part of the mixture (not explicitly shown).

Isotopic steady state, i. e., constant isotope distribution throughout the studied growth phase, was verified by GC/MS analysis of three samples taken throughout the exponential growth phase. Both on xylose and on the xylose/glucose mixture, the MIDs remained stable, as exemplarily shown for glycine, representing the EMP pathway metabolites,
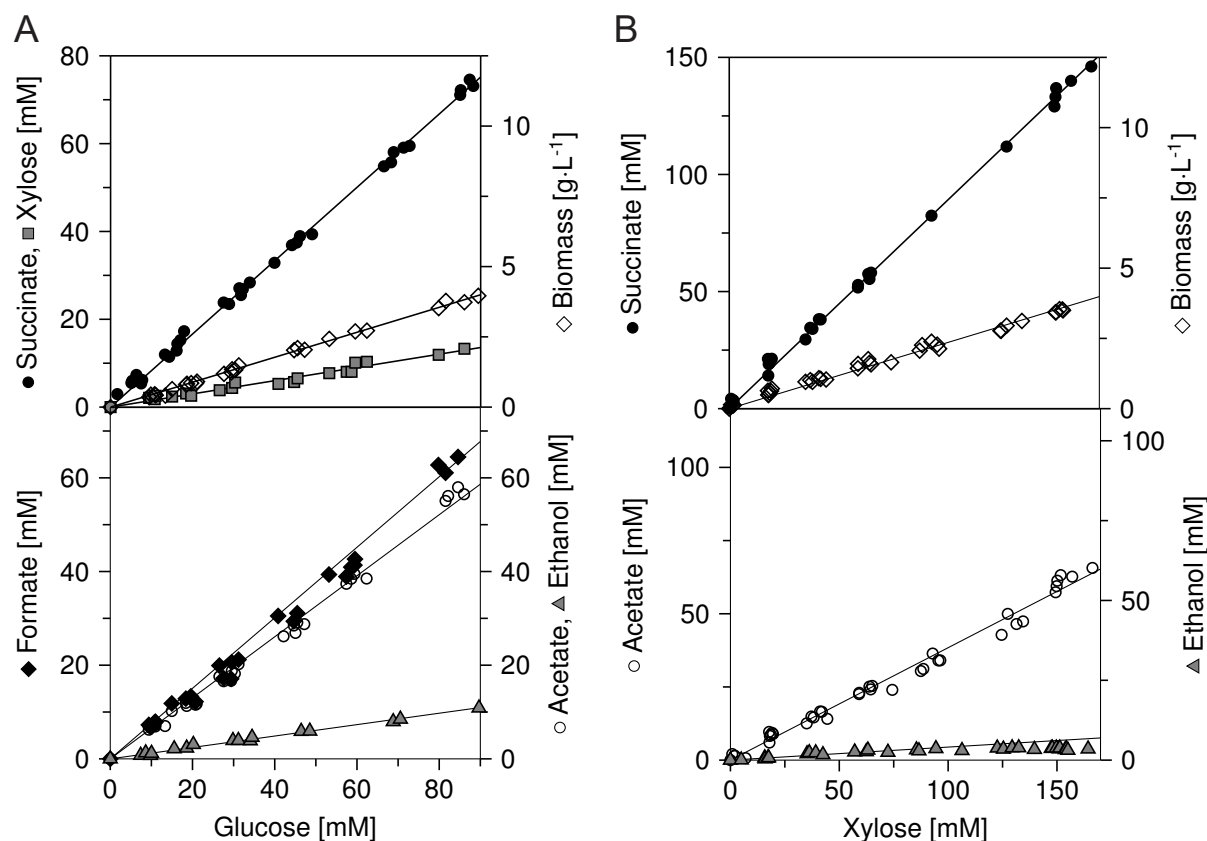
Figure 4.24: Verification of metabolic steady state during the exponential growth phase of *B. succiniciproducens* on a substrate mixture (18 g·L⁻¹ glucose, 12 g·L⁻¹ xylose) and on pure xylose. The data, derived from six biological replicates, respectively, comprise the simultaneous consumption of xylose and glucose during growth on the two substrates (A), as well as constant yields of biomass, succinate and the by-products acetate, formate, and ethanol on xylose (B) and on the substrate mixture (A). Units given in axis labels refer to all preceding substances separated by commas.

phenylalanine, representing the PP pathway metabolites, and succinate, representing the TCA cycle (Figure 4.25). The labeling patterns for the mixture were not as perfectly constant as found for all single substrates (Figures 4.8, 4.25B). This might be due to minor changes in the relative uptake rates of xylose and glucose but can be regarded as negligible given the still prominent steady state. Additional ^{13}C metabolic flux analysis simulations assuming the first and the last data points for the labeling sets, instead of the average, did not reveal any impact on the flux distribution.
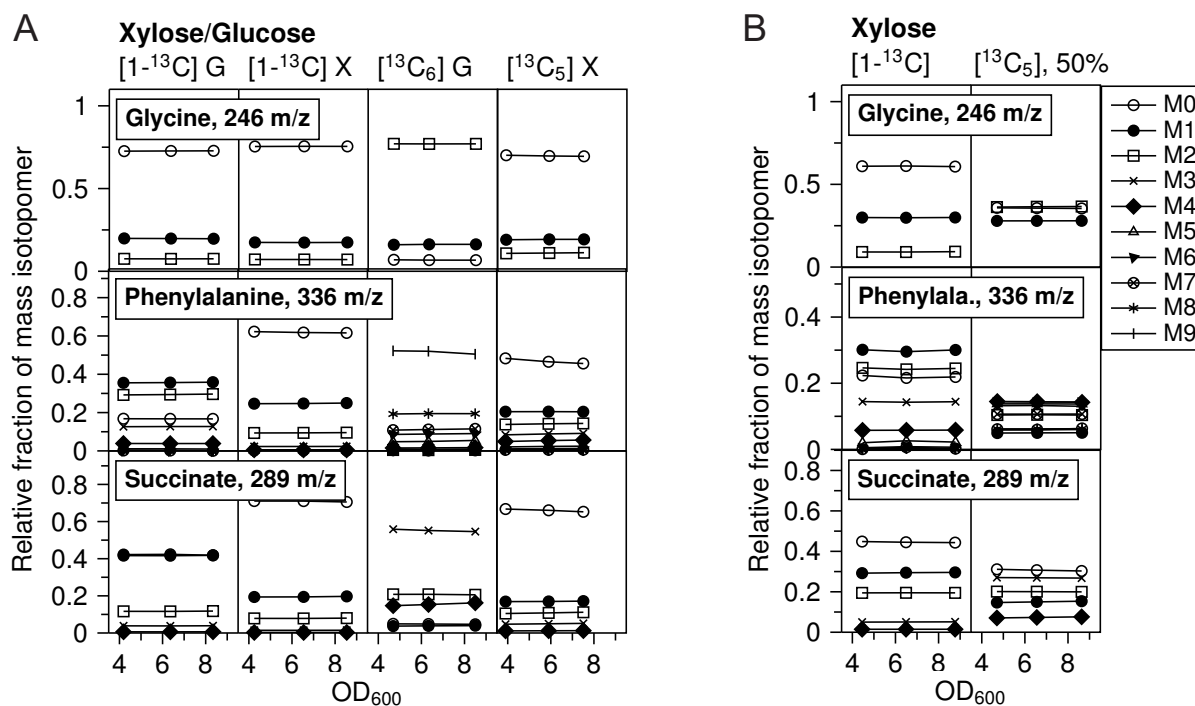
Figure 4.25: Verification of isotopic steady state during the exponential growth phase of *B. succiniciproducens* **on a substrate mixture (18 g·L⁻¹ glucose, 12 g·L⁻¹ xylose) (A) and on pure xylose (B).** The isotopic steady state is reflected by the constant labeling pattern of the analytes throughout the cultivation on the various tracer substrates. Exemplarily, mass isotopomer distributions are shown for glycine (representing the EMP pathway), phenylalanine (representing the PP pathway) and succinate (representing the reductive TCA cycle). The legend holds for (A) and (B). Xylose [$^{13}C_5$], 50 % indicates an equimolar mixture of naturally and fully labeled xylose. Phenylala.: phenylalanine; X: xylose; G: glucose

4.3.3 Central carbon fluxes on xylose reveal highly efficient production

To resolve the intracellular carbon fluxes of xylose-grown *B. succiniciproducens*, a total of 230 individual mass isotopomers, derived from two parallel ^{13}C labeling experiments on [1-^{13}C] xylose and on a 1:1 mixture of naturally labeled xylose and [$^{13}C_5$] xylose, were simultaneously fit to the network model.

Biomass and product formation (Table 4.9), as well as the experimentally determined *in vivo* enzyme activity of malic enzyme, considered as the upper limit of the corresponding flux, were applied to constrain the model. The small deviation between experimental and simulated labeling pattern (Figure 4.26), indicating an excellent fit, and the small confidence intervals of the calculated fluxes underline the consistency of this approach (Figure 4.27).
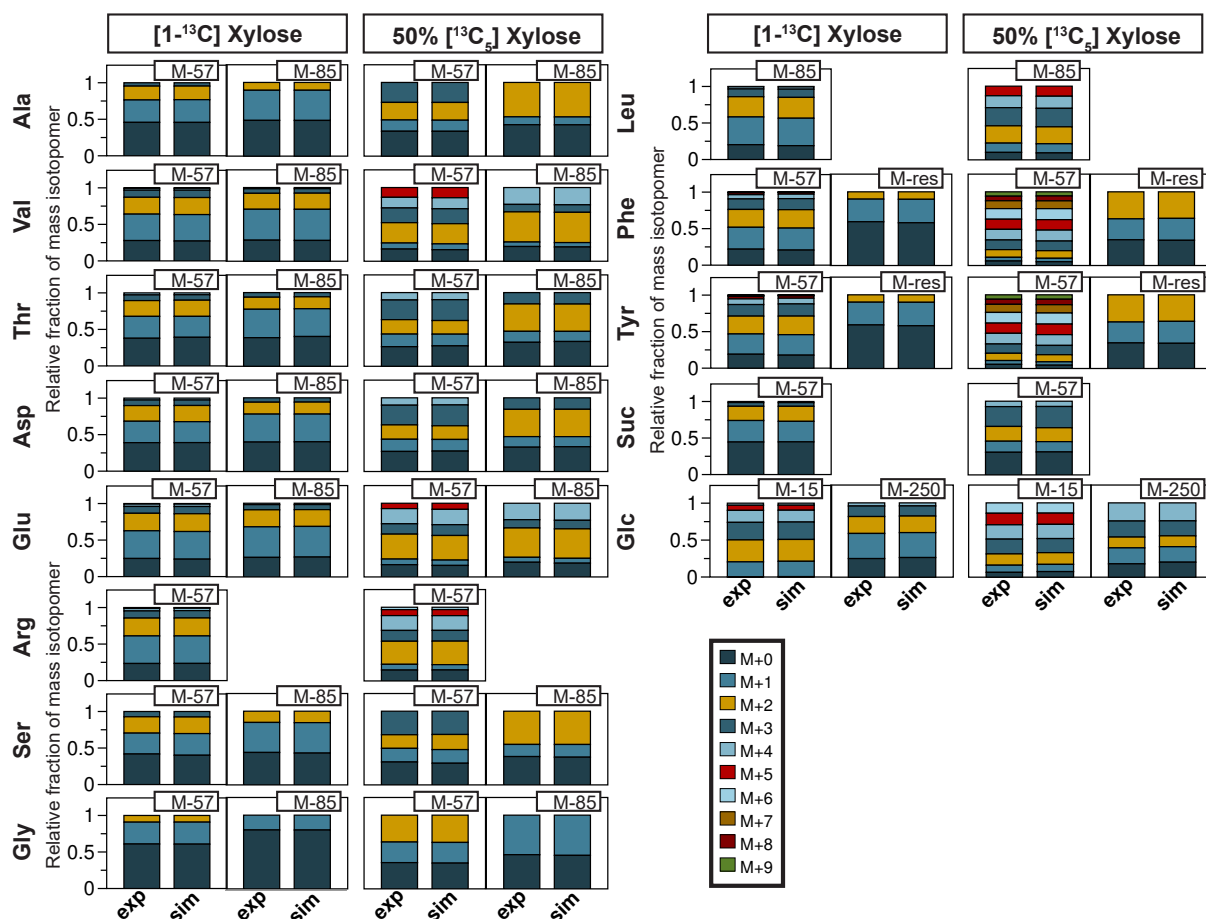
Figure 4.26: Comparison of experimental and simulated mass isotopomer distributions (MIDs) for flux analysis on xylose. The data represent experimental (exp) MIDs obtained during parallel cultivation of *B. succiniciproducens* DD1 on two different ^{13}C tracers and simulated (sim) MIDs corresponding to the calculated flux distribution for different amino acids (indicated by the respective three letter code abbreviations), succinate (Suc), and glycogen-derived glucose (Glc). The deviation between the experimental (exp) and simulated (sim) MIDs was exceptionally low for both data sets. 50 % [^{13}C$_5$] xylose denotes a 1:1 mixture of naturally labeled xylose and fully labeled xylose.
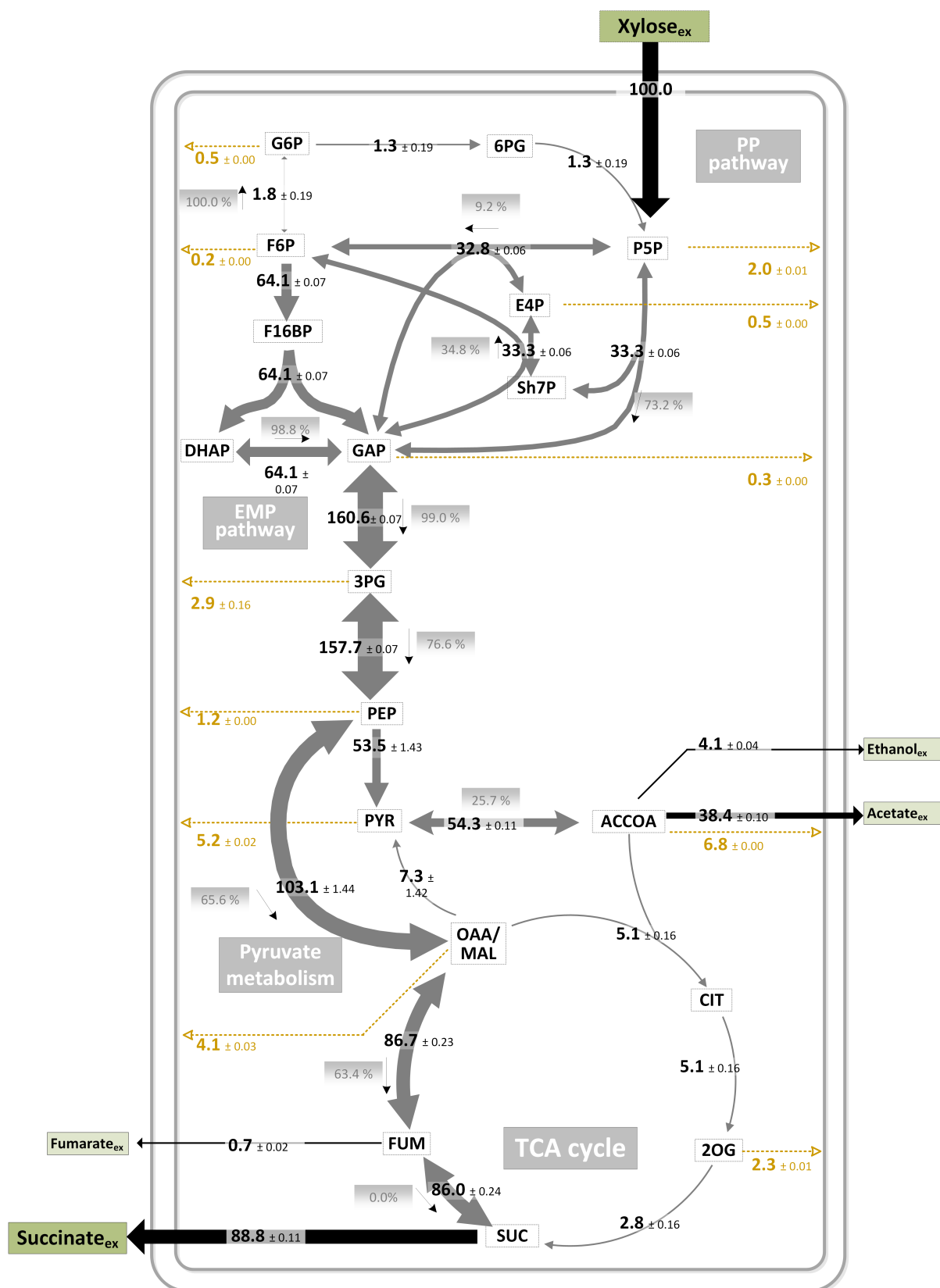
Figure 4.27: Intracellular carbon fluxes of *B. succiniciproducens* DD1 on xylose as determined by ^{13}C metabolic flux analysis. The carbon fluxes were normalized to a xylose uptake of $100\,\%$, equivalent to $11.5 \pm 0.3\,\text{mmol}\cdot\text{g}^{-1}\cdot\text{g}^{-1}$. The arrow thickness is proportional to the corresponding flux. The direction of net fluxes is indicated by small black arrows. Reversibilities, calculated according to Equation 3.5, are displayed gray boxes. Yellow dashed arrows represent fluxes into biomass formation. Black arrows indicate carbon in- and efflux. PEP: phosphoenolpyruvate; PYR: pyruvate; G6P: glucose 6-phosphate; 6PG: 6-phosphogluconate; F6P: fructose 6-phosphate; F16BP: fructose 1,6-bisphosphate; DHAP: dihydroxyacetone phosphate; GAP: glyceraldehyde 3-phosphate; P5P: pentose 5-phosphate; E4P: erythrose 4-phosphate; Sh7P: seduheptulose 7-phosphate; 3PG: 3-phosphoglycerate; ACCOA: acetyl-CoA; OAA/MAL: oxaloacetate/malate; CIT: citrate; FUM: fumarate; SUC: succinate; 2OG: 2-oxoglutarate

4.3.3.1 Fast and efficient xylose uptake reveals a high efficiency of the non-oxidative PP pathway in *B. succiniciproducens*

Xylose, which is taken up by a specific ABC transporter, enters the central carbon metabolism as xylulose 5-phosphate, i.e., as pentose 5-phosphate (P5P) in the *in silico* model. By concerted action of transaldolase and transketolase, approx. one third of the P5P flowed directly into the glyceraldehyde 3-phosphate pool, whereas the remaining two thirds were converted into fructose 6-phosphate.

Remarkably, only a diminutive flux of $1.3 \pm 0.2\,\%$ entered the oxidative PP pathway after conversion of fructose 6-phosphate into glucose 6-phosphate. This was not only much lower than the flux observed on any other substrate analyzed so far for *B. succiniciproducens*, but also lower than in other microorganisms. Intracellular fluxes during xylose catabolism were previously studied in other microorganisms, i.e., in diaminopentane-producing *C. glutamicum* (Buschke *et al.*, 2013), in the anaerobic Gram-negative bacterium *Zymomonas mobilis* (De Graaf *et al.*, 1999), and in the yeast *Saccharomyces cerevisiae* (Wahlbom and Hahn-Hägerdal, 2002), all of which showed much higher backfluxes into the oxidative PP pathway (discussed in more detail in Section 4.3.4.3).

4.3.3.2 The flux from pyruvate to acetyl-CoA is comparably low and bidirectional

Although xylose-grown *B. succiniciproducens* did not secrete any formate, comparison of the cultivation characteristics of the wild type and the $\Delta pflD$ deletion mutant suggested *in vivo* activity of the pyruvate formate lyase, combined with an active formate dehydrogenase that immediately oxidized formate into CO_2. On glucose, fructose, and sucrose, pyruvate formate lyase activity was coupled to formate secretion and could therefore be distinguished from pyruvate dehydrogenase in the flux analysis. On xylose, the two reactions were lumped into a single, reversible flux.

In total, this flux was relatively low at $54.3\,\%$. This corresponds to a hexose-based flux of $65\,\%$. Interestingly, the relative flux through pyruvate formate lyase was this high on glucose ($69\,\%$), sucrose($63\,\%$), and fructose ($68\,\%$), whereas the total flux from pyruvate to acetyl-CoA was $84\,\%$ to $85\,\%$ on all three substrates.

The low conversion of pyruvate to acetyl-CoA can be traced back to the low biomass yield, leading to a reduced demand for acetyl-CoA and 2-oxoglutarate, and to low acetate and ethanol yields.

The pyruvate-acetyl-CoA interconversion showed a significant reversibility of 26 %. As pyruvate dehydrogenase is irreversible *in vivo* (Figure 4.3, Table 4.2), this further proves the *in vivo* activity of pyruvate formate lyase in xylose-grown cells, solely on basis of the ^{13}C labeling data. On the other analyzed carbohydrates, reversibility of pyruvate formate lyase was generally higher at 47 % (on fructose) to 89 % (on sucrose). This indicates that the flux from pyruvate to acetyl-CoA on xylose was partially catalyzed by the pyruvate dehydrogenase enzyme complex, which only allows unidirectional flux from pyruvate into acetyl-CoA.

4.3.3.3 The oxidative TCA cycle contributes to succinate production

The overall flux into succinate was very high at 89 %. This is equivalent to a flux of 107 % on glucose (taking into account the C-molar ratio of xylose to glucose), which was previously achieved by strain *B. succiniciproducens* $\Delta ldhA\Delta pflD$. Similar to the double deletion strain on glucose, xylose-grown *B. succiniciproducens* DD1 leaked a small amount of fumarate (less than 1 %). Approx. 3 % of the accumulated succinic acid was produced via the oxidative TCA cycle branch. This was also similar to strain *B. succiniciproducens* $\Delta ldhA\Delta pflD$ on glucose which produced 2 % of the total succinic acid via the oxidative TCA cycle branch (Becker *et al.*, 2013).

4.3.3.4 The unique characteristics of *B. succiniciproducens* xylose catabolism in the context of other microbial strategies

So far, to our knowledge, four other ^{13}C flux studies have addressed xylose catabolism in addition to this work. Three of them describe ethanol production from xylose, on the one hand, by recombinant *Saccharomyces cerevisiae* (Feng and Zhao, 2013; Wahlbom and Hahn-Hägerdal, 2002), and on the other hand, by recombinant *Zymomonas mobilis* (De Graaf *et al.*, 1999). The fourth describes diaminopentane production from xylose with recombinant *C. glutamicum* (Buschke *et al.*, 2013).

A common issue in the ethanol fermentations is the conversion of the substrate into the by-product xylitol (De Graaf *et al.*, 1999; Wahlbom and Hahn-Hägerdal, 2002) which can be counteracted by addition of electron acceptors such as acetoin to the medium (Wahlbom and Hahn-Hägerdal, 2002). In *S. cerevisiae*, up to 55 % of the substrate were excreted after conversion into xylitol, whereas only 5 % were lost in *Z. mobilis*. In *B. succinicipro-ducens*, xylitol production is not an issue, because xylose assimilation follows a different pathway. Instead of first reducing xylose to xylitol and then oxidizing xylitol to xylulose,
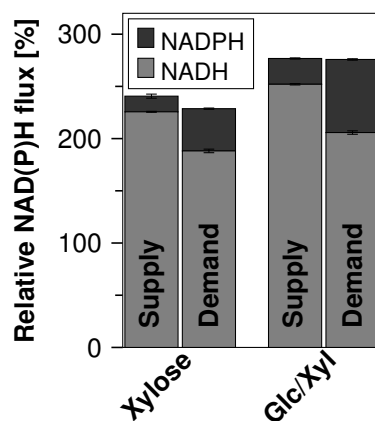
Figure 4.28: Redox balance of *B. succiniciproducens* **DD1 on xylose and on a substrate mixture (18 g·L⁻¹ glucose, 12 g·L⁻¹ xylose).** The supply and demand of NADH and NADPH was calculated from the metabolic flux distribution, taking into account all participating reactions, as shown in Figure 2.5, and NAD⁺- and NADPH-requirements for biomass formation. *B. succiniciproducens* was assumed to possess a NADH dehydrogenase for electron transfer from NADH to menaquinone (Kim, 2009). The data reflect mean values and 90% confidence intervals from Monte-Carlo simulations.

B. succiniciproducens and the recombinant *C. glutamicum* strain (Buschke *et al.*, 2013, 2011) directly convert xylose into xylulose with a specific isomerase.

In *Z. mobilis*, *S. cerevisiae*, and *C. glutamicum*, the oxidative PP pathway plays an important role for NADPH production on xylose, as represented by relative fluxes of 13 % in *Z. mobilis* 17 − 47 % in *S. cerevisiae*, and 44 % in *C. glutamicum*. In *B. succiniciproducens*, the oxidative PP pathway was nearly shut down completely, as indicated by the very small flux of less than 2 %. On all analyzed substrates, including xylose, *B. succiniciproducens* apparently relies on a transhydrogenase and, to a lesser extent, malic enzyme to supply sufficient NADPH for growth (Figures 4.28, 4.13).

Obviously, the metabolism is overall very different in all four microorganisms. *Z. mobilis* has a highly active ED pathway, whereas *B. succiniciproducens* and *S. cerevisiae* use the EMP pathway to channel carbon towards PEP and pyruvate. *B. succiniciproducens* carboxylates PEP into oxaloacetate and mainly relies on the reductive branch of the TCA cycle to produce succinate and regenerate NAD⁺ in the process. *Z. mobilis* converts nearly all pyruvate into ethanol, thereby regenerating NAD⁺. During anaerobic fermentation, *S. cerevisiae* mainly produced ethanol and acetate (Wahlbom and Hahn-Hägerdal, 2002), whereas in microaerobically-grown *S. cerevisiae*, all carbon was either used for biomass production or channeled through the oxidative TCA cycle, while NAD⁺ was regenerated via oxidative phosphorylation (Feng and Zhao, 2013).

4.3.4 Metabolic fluxes during simultaneous consumption of xylose and glucose

To resolve the intracellular carbon fluxes of *B. succiniciproducens* grown on a mixture of xylose and glucose, a total of 460 individual mass isotopomers, derived from four parallel ^{13}C labeling experiments using [1-^{13}C] glucose, [1-^{13}C] xylose, [^{13}C$_6$] glucose, and [^{13}C$_5$] xylose, respectively, as tracers, were simultaneously fit to the network model.

Biomass and product formation (Table 4.9) were applied to constrain the model. The small deviation between experimental and simulated labeling pattern, indicating an excellent fit (Figure 4.29), and the small confidence intervals of the calculated fluxes suggest a highly accurate result (Figure 4.30).
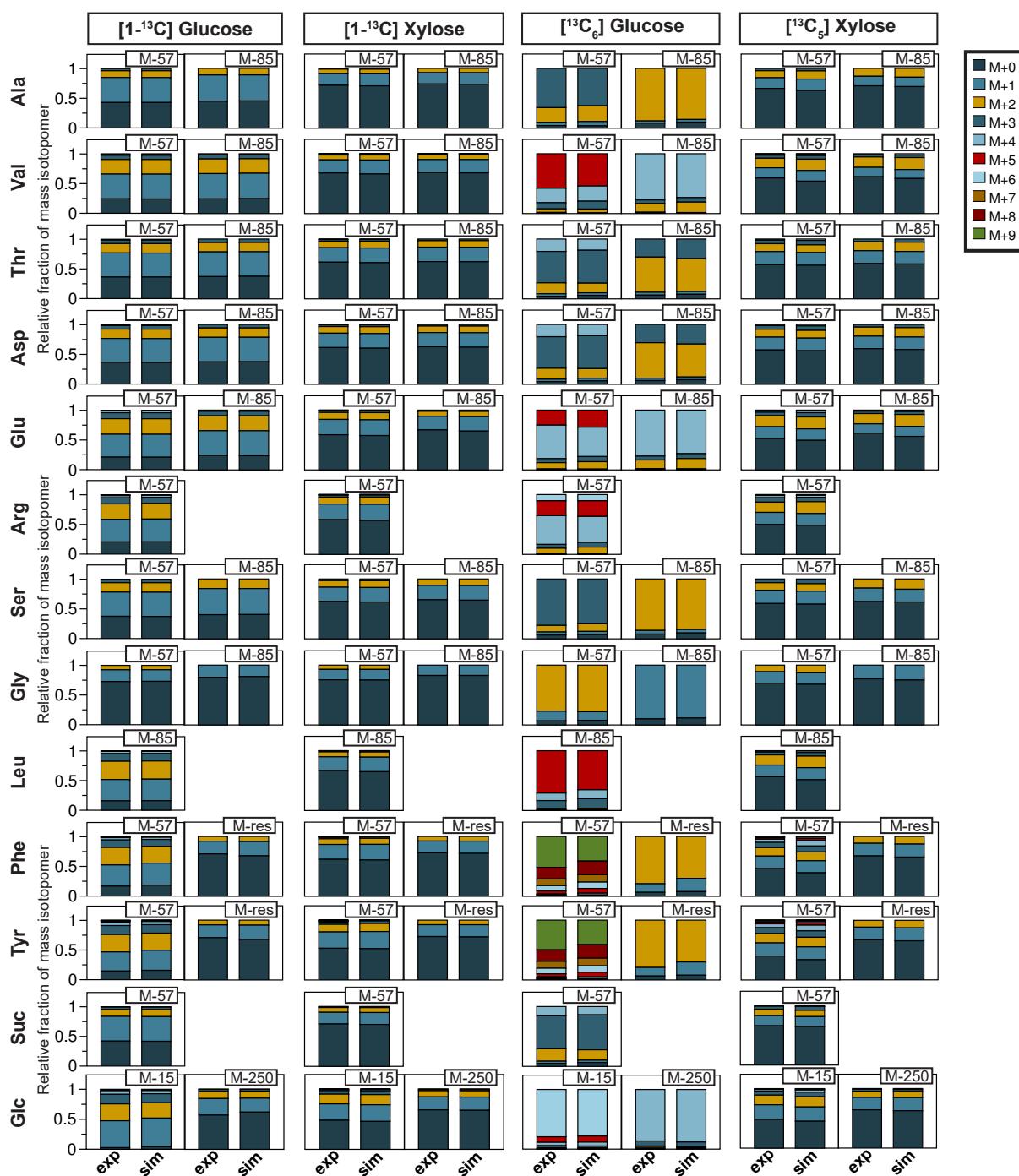
Figure 4.29: Comparison of experimental and simulated mass isotopomer distributions (MIDs) for flux analysis on a mixture of 18 g·L⁻¹ glucose and 12 g·L⁻¹ xylose. The data represent experimental (exp) MIDs obtained during parallel cultivation of *B. succiniciproducens* DD1 on four different ¹³C tracers and simulated (sim) MIDs corresponding to the calculated flux distribution for different amino acids (indicated by the respective three letter code abbreviations), succinate (Suc), and glycogen-derived glucose (Glc). The deviation between the experimental (exp) and simulated (sim) MIDs was exceptionally low for all data sets.
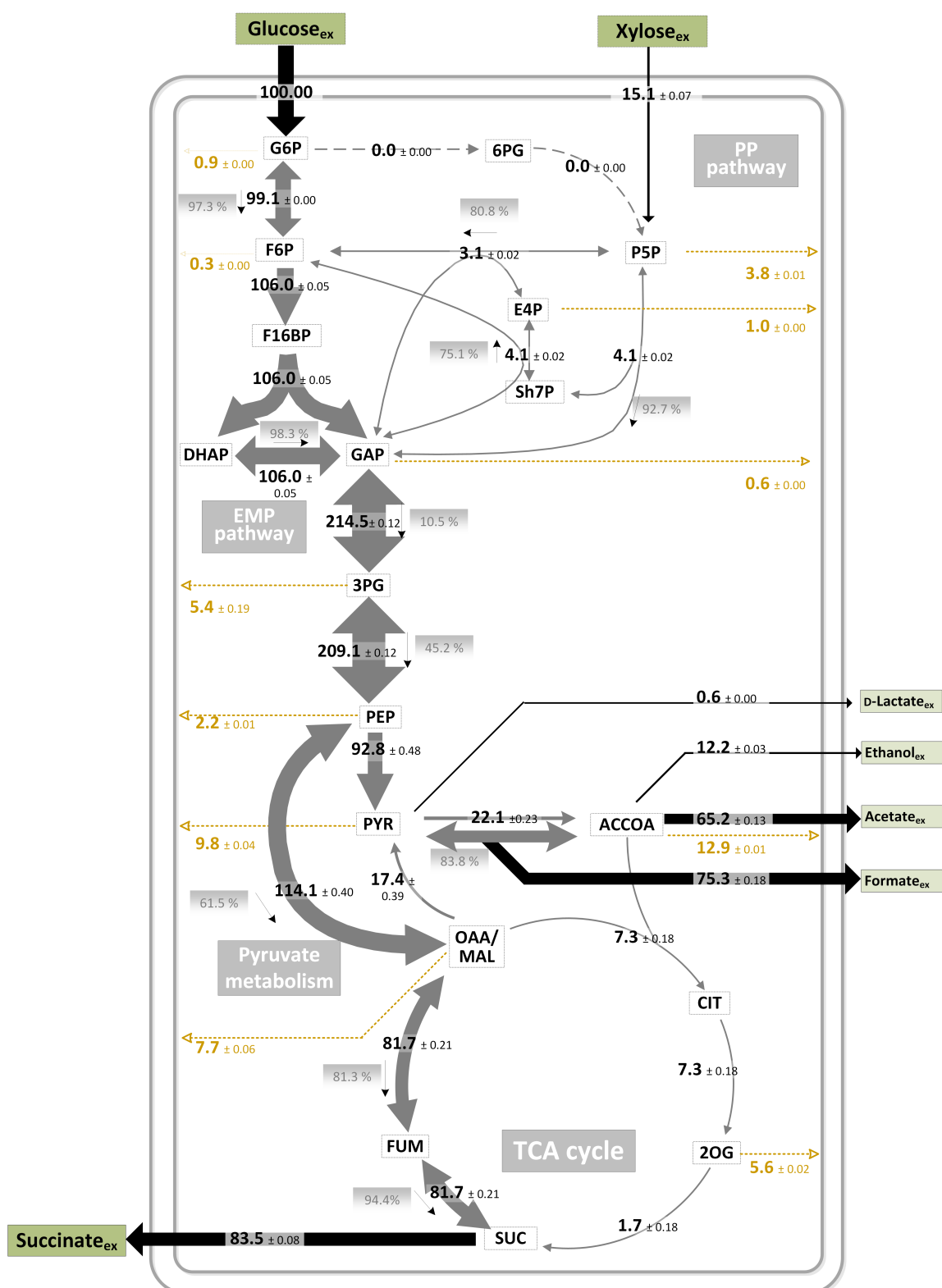
Figure 4.30: Intracellular carbon fluxes of *B. succiniciproducens* DD1 grown on a mixture of 18 g·L⁻¹ glucose and 12 g·L⁻¹ xylose as determined by ¹³C metabolic flux analysis. The carbon fluxes were normalized to the major substrate influx, i. e., the glucose influx, of 7.2 ± 0.2 mmol·g⁻¹·h⁻¹, which was set to 100 %. The arrow thickness is proportional to the corresponding flux. The direction of net fluxes is indicated by small black arrows. Reversibilities, calculated according to Equation 3.5, are displayed gray boxes. Yellow dashed arrows represent fluxes into biomass formation. Black arrows indicate carbon in- and efflux. PEP: phosphoenolpyruvate; PYR: pyruvate; G6P: glucose 6-phosphate; 6PG: 6-phosphogluconate; F1P: fructose 1-phosphate; F6P: fructose 6-phosphate; F16BP: fructose 1,6-bisphosphate; DHAP: dihydroxyacetone phosphate; GAP: glyceraldehyde 3-phosphate; P5P: pentose 5-phosphate; E4P: erythrose 4-phosphate; Sh7P: seduheptulose 7-phosphate; 3PG: 3-phosphoglycerate; ACCOA: acetyl-CoA; OAA/MAL: oxaloacetate/malate; CIT: citrate; FUM: fumarate; SUC: succinate; 2OG: 2-oxoglutarate

4.3.4.1 Glucose and xylose are metabolized separately

During co-cultivation on a glucose/xylose mixture, the two substrates were taken up simultaneously. As revealed by ^{13}C metabolic flux analysis, the two carbohydrates followed completely different routes through the metabolism. While glucose was exclusively metabolized via the EMP pathway, xylose was converted via the non-oxidative PP pathway. Surprisingly, the oxidative PP pathway was completely inactive. Because of the high reversibility of the transaldolase and transketolase reactions, glucose partly contributed to formation of pentose 5-phosphate and erythrose 4-phosphate, the two biomass precursors derived from the PP pathway.

4.3.4.2 The overall flux distribution is closer to that on glucose than xylose

Continuing from glyceraldehyde 3-phosphate, the metabolic fluxes were overall similar to the fluxes observed for the wild type strain on glucose (Figure A.2). In order to allow for a direct comparison of the results, the xylose-glucose fluxes have to be divided by 1.125 to account for the extra influx of xylose. The overall flux from pyruvate to acetyl-CoA was nearly identical under both conditions. The flux through pyruvate formate lyase, however, was slightly reduced on the xylose/glucose mixture, while the flux through pyruvate dehydrogenase was apparently increased by 18 %. This might indicate a slight activity of formate dehydrogenase during co-cultivation on the two substrates, leading to a seemingly decreased flux through pyruvate formate lyase.

The contribution of the oxidative TCA cycle to the overall succinate production was generally low, but slightly higher on the mixture (2 % of the total succinate) than on pure glucose (1 %). Again, this effect might be caused by the co-substrate xylose, as the contribution of the oxidative TCA cycle branch was even slightly higher with xylose as the sole substrate (3 %).

4.3.4.3 Common regulatory mechanisms and unique characteristics of glucose/xylose co-consumption in different microorganisms

The parallel consumption of xylose and glucose has previously been studied in different yeasts, i. e., in *S. cerevisiae* (Pitkänen *et al.*, 2003; Wahlbom *et al.*, 2001) and in *Candida milleri* (Granström *et al.*, 2000), by means of ^{13}C metabolic flux analysis or constraint-based metabolic flux analysis.

As already discussed, recombinant yeasts tend to produce xylitol from xylose, caused by a redox-imbalance during the conversion into xylulose. While this is undesired during

ethanol production, the explicit aim of the *C. milleri* cultivation was to convert xylose into xylitol. It was discovered that *C. milleri* cannot grow on xylose, which is a distinct difference as compared to recombinant *S. cerevisiae* and wild type *B. succiniciproducens*. Growth on xylose and glucose was actually a bioconversion of xylose into xylitol, aided by an adaptation of the central carbon fluxes on glucose to increase the supply of NADPH via aldehyde dehydrogenase, required for xylose conversion. Unexpectedly, the flux through the oxidative PP pathway was decreased, although it was still significant at 10 %. No complete shutdown of the oxidative PP pathway was observed for any of the analyzed organisms, except for *B. succiniciproducens*.

In *S. cerevisiae*, metabolic fluxes were determined for different substrate ratios and different dilution rates in a chemostat (Wahlbom *et al.*, 2001), and during aerobic and anaerobic growth (Pitkänen *et al.*, 2003). Increasing the xylose/glucose ratio towards more xylose led to proportionally higher uptake of xylose and lower uptake of glucose in *S. cerevisiae*, according to the first study (Wahlbom *et al.*, 2001), which is clearly different in *B. succiniciproducens*. In *B. succiniciproducens*, the addition of glucose as a second substrate with a slightly higher concentration led to a decrease of the absolute specific xylose uptake rate by factor 10. In *S. cerevisiae*, increasing the amount of xylose led to a drastic change in glucose catabolization: the flux through the EMP pathway decreased, while the flux through the PP pathway increased. This effect was opposite to *B. succiniciproducens* and might be explained by the increased demand for NADPH caused by the xylose-xylitol-xylulose conversion.

The second study, in which the fluxes were determined by ^{13}C metabolic flux analysis, compares fluxes of glucose-grown cells with fluxes of cells grown on a xylose/glucose mixture, with xylose as the main substrate (Pitkänen *et al.*, 2003). In this study, xylose as a co-substrate was found to induce an increase of the PP pathway flux coupled to a reduction of the EMP pathway flux as well. On the mixture, the oxidative PP pathway flux was increased from 6 % to 49 % during aerobic growth, so that all glucose was metabolized via this pathway. The oxidative PP pathway was additionally supplied from xylose, leading to a net flux from fructose 6-phosphate to glucose 6-phosphate. During anaerobic growth on glucose, the EMP pathway was nearly exclusively used, with only 1 % being metabolized via the oxidative PP pathway. The PP pathway flux increased to 12 % when xylose was the major substrate.

In this study, substrate uptake rates for xylose and glucose were analyzed for different substrate ratios under aerobic conditions. When the medium contained 27 g·L^{-1} xylose and 3 g·L^{-1} glucose, the specific uptake rates (in C-mmol·(g CDW)$^{-1}$·h^{-1}) were 1.95 for glucose and 3.62 for xylose. Under anaerobic conditions, they were 19.1 for glucose and only 15.4 for xylose, although 90 % of the supplied carbohydrate was xylose. When the amount

of glucose supplied to the medium was reduced even further, the specific xylose uptake rate increased, whereas the specific glucose uptake rate decreased. These observations are very similar to the observations made for *B. succiniciproducens* in this work, indicating a regulatory mechanism common among different microorganisms.

4.3.5 Evaluating the *B. succiniciproducens* physiology of succinate-production by means of ^{13}C metabolic flux analysis on xylose

Taken together, the results concerning the performance of *B. succiniciproducens* DD1 on xylose and glucose/xylose mixtures revealed that xylose and hemicellulose hydrolysates are promising substrates for succinate production. In addition, the detailed analyses of the *B. succiniciproducens* metabolism give interesting insights into the hemicellulose-sugar specific physiology of the organism.

The data presented in this work suggest *in vivo* activity of a putative native *B. succiniciproducens* formate dehydrogenase. Under certain conditions, in this case, cultivation on xylose minimal medium, formate dehydrogenase apparently eliminated the by-product formate completely. By concerted action with pyruvate formate lyase, formate dehydrogenase enabled high yield succinate production by providing sufficient NADH without hampering growth. In a previous metabolic engineering approach, formate production had been eliminated by deleting *pflD*, encoding pyruvate formate lyase. This had, however, negative side-effects. Pyruvate dehydrogenase was not able to channel the required flux from pyruvate to acetyl-CoA, leading to accumulation of lactate and strongly decreased growth on glucose (Becker *et al.*, 2013) and xylose (this study). In fact, to retain fast growth and, as a consequence, high succinic acid productivity, it seems reasonable not to inactivate pyruvate formate lyase at all, as previously suggested by Ahn *et al.* (2016) for future engineered *B. succiniciproducens* strains. Indeed, a *M. succiniciproducens* mutant strain was recently constructed that showed fast growth and did not secrete any formate into the medium, despite still harboring its native pyruvate formate lyase (Ahn *et al.*, 2016; Lee *et al.*, 2015).

In the *B. succiniciproducens* genome, two clusters encoding three (equivalent to *M. succiniciproducens* MS1028 – MS1030) and four (equivalent to *M. succiniciproducens* MS0889 – MS0892) formate dehydrogenase subunits, respectively, have been identified. Transcriptomics could be applied to identify the more relevant cluster. Possibly, the gene clusters are under control of a strictly regulated promoter that could be replaced by a

strong, constitutive promoter to ensure expression of the genes independent of the substrate.

Concerning succinate production on xylose, a future goal will be to reduce accumulation of the main by-product acetate. Accumulation of acetate from hemicellulose sugars has been challenging during succinate production with other microorganisms as well, e. g., with *A. succinogenes* (Salvachúa *et al.*, 2016a). In glucose-grown *M. succiniciproducens*, a significant reduction of acetate accumulation was previously achieved by deleting the *ackA* and *pta* genes (Lee *et al.*, 2006b). Although the objective, i. e., reduction of the acetate accumulation, was certainly achieved, this approach might not be ideal when considering the whole metabolism. The overall aim is to increase succinate production to its theoretical maximum. To achieve this, the NADH supply has to be increased. The best way to achieve this and, simultaneously, reduce acetate production, would be to enhance the oxidative TCA cycle. By withdrawing acetyl-CoA towards citrate, less precursor for the production of acetate should be available, and more reducing equivalent should be provided that could be used to reduce fumarate into succinate. Excess carbon would be converted into CO_2 instead of other by-products, which is more advantageous for downstream processing.

5

Conclusions and Outlook

Succinic acid, produced from renewable substrates, has the potential to shape the future of our global bioeconomy (Bozell and Petersen, 2010; Werpy and Petersen, 2004). This work focused on the highly efficient natural succinic acid producer *B. succiniciproducens* which is already actively engaged in a commercial, economical, and bio-based succinate-production process (Becker *et al.*, 2015). The central carbon fluxes of *B. succiniciproducens* during conversion of different carbohydrates into succinic acid were elucidated using state-of-the-art ^{13}C metabolic flux analysis, a very useful tool for systems metabolic engineering (Kohlstedt *et al.*, 2010). Analysis and interpretation of the flux distributions allowed for identification of metabolic engineering targets that led to construction of novel, tailor-made production hosts. Besides providing the basis for future optimization of *B. succiniciproducens* for highly efficient succinate production from various substrates, this work also contributed to our global understanding of the unique characteristics of the central metabolism of capnophilic natural succinic acid producers in general, and in particular of *B. succiniciproducens*.

The mechanisms by which sucrose, fructose, glucose, and xylose were metabolized turned out to be quite distinct, revealing that, to a certain extent, the carbon source dictates the limitations, but also the potential of succinic acid production.

Sucrose-grown *B. succiniciproducens* achieved a lower succinate yield than glucose-grown *B. succiniciproducens*, accompanied by a shift in the by-product spectrum towards lactate as a dominant carbon sink. The overall performance on sucrose was, however, significantly better than on fructose, as fructose-grown *B. succiniciproducens* produced even less succinic acid and even more lactate and ethanol. This effect could be attributed to the different substrate-uptake systems for the three substrates. The PTS systems used for phosphorylation of sucrose and fructose caused a high flux of PEP into pyruvate, leading to reduced availability of the succinate-precursor oxaloacetate. Fructokinase was discovered to play a substantial role in sucrose catabolism by providing an alternative pathway to the fructose PTS for phosphorylation of the fructose moiety. The enzyme was shown

to be functional *in vitro* and also to play a key role *in vivo*, limiting the loss of PEP significantly.

Systems metabolic engineering based on ^{13}C metabolic flux analysis was successfully applied to generate superior production hosts specifically designed for growth on fructose and sucrose. In a previous study, the double deletion mutant *B. succiniciproducens* $\Delta pflD\Delta ldhA$ had been constructed, revealing a highly enhanced succinate-yield from glucose (Becker *et al.*, 2013). The deletion of the pyruvate formate lyase encoding *pflD* gene, however, had caused reduced growth on glucose. As the two deletions restricted the *B. succiniciproducens* metabolism, the wild type was chosen here as basis for optimization towards improved sucrose and fructose utilization. Exploiting the advantageous characteristics of fructokinase, the sucrose uptake system was targeted by deleting *fruA*, encoding the fructose-specific PTS. To improve succinate-production on fructose, the main by-product lactic acid was targeted by deleting the two lactic acid production pathways. The mutant strains were first assessed in serum bottle batch cultivations and showed succinic acid yields increased by more than 40 % on their respective substrate. The strains were then further evaluated in fed-batch cultivations using a linear, limited feeding strategy, as this mode of operation is very similar to actual industrial production (Ahn *et al.*, 2016; Jansen and Gulik, 2014). The high final titers and yields underlined the superior qualities of the two mutant strains.

The fact that xylose is a major component of lignocellulosic biomass makes this substrate especially interesting for biotechnological applications (Saha, 2003). Previous work already showed that *B. succiniciproducens* can efficiently convert xylose-enriched hemicellulose hydrolysates into succinic acid (Salvachúa *et al.*, 2016b). This work therefore focused on elucidating the fluxes during xylose catabolism and during co-consumption of xylose and glucose, as glucose is also abundant in hemicellulose hydrolysates. Succinate production from xylose was extremely efficient compared to the other analyzed carbohydrates. A novel feature of *B. succiniciproducens* was discovered by closer inspection of the results and by comparative studies with a deletion mutant: *B. succiniciproducens* possesses a formate dehydrogenase which apparently completely converts all formate into NADH and CO_2 in xylose-grown *B. succiniciproducens*. This, in turn, led to a high succinate yield and only minor by-product formation. *B. succiniciproducens* was also able to metabolize xylose and glucose in parallel with glucose as the overall preferred substrate. The xylose- and glucose-uptake rates could, however, be influenced by the actual substrate concentrations, providing interesting perspectives for future process design. Activating formate dehydrogenase during growth on substrates other than xylose is certainly the most promising target to increase succinate production with *B. succiniciproducens* while retaining high growth rates and, as a consequence, achieve very high productivities. This

will, however, require intensive genetic engineering and further in-depth analysis for two reasons: formate dehydrogenase consists of multiple subunits, and two spatially separated clusters exist in the *B. succiniciproducens* genome. Also, deregulating an enzyme first requires a detailed understanding of how the regulation occurs, underlining the requirement for further systems-level studies, e. g., transcriptomics.

At the beginning of this thesis, the *B. succiniciproducens* metabolism was analyzed using qualitative ^{13}C-tracer experiments and *in vitro* enzymatic assays, which provided the basis for the highly sophisticated ^{13}C metabolic flux analyses. The results could, on the one hand, be directly applied to refine the metabolic network model, and, on the other hand, revealed a number of features that clearly distinguish *B. succiniciproducens* from other related organisms, proving that succinate-producing rumen bacteria exhibit relevant strain-specific differences.

Among the natural succinic acid producers, *M. succiniciproducens* and *A. succinogenes* are most closely related to *B. succiniciproducens* (Kuhnert and Christensen, 2008; Kuhnert *et al.*, 2010). At a first glance, the three organisms share many common features, including a facultative anaerobic, mesophilic and capnophilic lifestyle. All three are non-toxic, non-pathogenic, and utilize menaquinone to reduce fumarate, the final electron acceptor, into succinate during anaerobic fermentation. *M. succiniciproducens* (Hong *et al.*, 2004) and *B. succiniciproducens* even have a similar genome size, similar 16S rRNA sequences and share more than 2000 homologous open reading frames (Ahn *et al.*, 2016; Kuhnert *et al.*, 2010). One should, however, note that *M. succiniciproducens* and *B. succiniciproducens* harbor more than 300 ORFs without a homologue in the respective other genome. This might explain substantial differences between the two isolates which have a huge impact on industrial production. As shown in this work, *B. succiniciproducens* and *M. succiniciproducens* differ fundamentally in their way to metabolize sucrose. *M. succiniciproducens*, on the one hand, exclusively uses PTS-mediated phosphorylation of the fructose moiety of sucrose, as has been conclusively proven using gene deletion strains and enzymatic analysis (Lee *et al.*, 2010b). *B. succiniciproducens*, on the other hand, additionally uses fructokinase for phosphorylation of the fructose moiety, which in turn results in the beneficial reduction of intracellular pyruvate, enhanced succinate yield and reduced by-product formation. The uptake of xylose relies on different transporters in the three microorganisms as well: *M. succiniciproducens* possesses a xylose-H$^+$ symporter, *B. succiniciproducens* employs a xylose-specific ABC transporter, and *A. succinogenes* harbors both of these xylose transporters, although it has not been analyzed which one is most relevant for xylose utilization. Of the three related microorganisms, only *B. succiniciproducens* does not possess any amino acid auxotrophies. *M. succiniciproducens* requires cysteine and methionine (Song *et al.*, 2008), while *A. succinogenes* is glutamate-

auxotrophic because of an incomplete TCA cycle (Mckinlay *et al.*, 2005). While ethanol is an abundant by-product of *B. succiniciproducens* (Becker *et al.*, 2013, this work) and *A. succinogenes* (Van der Werf *et al.*, 1997), it seems to be only produced by *M. succiniciproducens* when grown on the more reduced substrate mannitol (Lee *et al.*, 2002b). Regarding pathway repertoire, *A. succinogenes* possesses the glyoxylate cycle and the Entner-Doudoroff pathway (McKinlay *et al.*, 2007), which *B. succiniciproducens* lacks, whereas only *B. succiniciproducens* and *M. succiniciproducens* exhibit a fully operational TCA cycle. The most relevant enzymes at the pyruvate node also seem to be different in all three strains. *B. succiniciproducens* exhibited high *in vitro* activities of PEPCX and PEPCK, while malic enzyme only showed reduced activity. In *M. succiniciproducens*, both PEPCX and malic enzyme were discovered to be mostly irrelevant for succinate production (Lee *et al.*, 2006b). Taken together, these findings imply that the simplified view of a fully shared biochemistry and physiology between succinate producing rumen bacteria can be misleading. Each strain deserves its own exploration so that its biosynthetic potential for industrial succinate production can be fully accessed.

Large-scale bio-based production of succinic acid is highly feasible and is clearly on the rise, with a number of companies, including the BASF Corbion Purac joint venture Succinity, already operating commercial produiction plants (Becker *et al.*, 2015). Most processes are currently glucose-based, as they rely on starchy biomass. This work revealed the high potential of utilizing other carbohydrates or even carbohydrate mixtures, including sucrose, fructose, or xylose. The next step is for the chemical industry to acknowledge and support bio-based succinic acid production, despite the currently low oil price, by actually shifting maleic acid based processes towards bio-based succinic acid as a raw material. Only then can the full potential of bio-based succinic acid be exploited, while the chemical industry moves towards a sustainable and economic future.

Bibliography

Abouimrane, A. and Davidson, I. (2007). Solid electrolyte based on succinonitrile and LiBOB interface stability and application in lithium batteries. *J Electrochem Soc* 154, A1031–A1034.

Agren, R., Otero, J. M., and Nielsen, J. (2013). Genome-scale modeling enables metabolic engineering of *Saccharomyces cerevisiae* for succinic acid production. *J Ind Microbiol Biotechnol* 40, pp. 735–747.

Agricola, G. (2004). De Natura Fossilium (Textbook of Mineralogy). Translated from the first Latin edition of 1546 by Mark Chance Bandy and Jean A. Bandy. Dover Publications.

Ahn, J. H., Jang, Y.-S., and Lee, S. Y. (2016). Production of succinic acid by metabolically engineered microorganisms. *Curr Opin Biotechnol* 42, pp. 54–66.

Alakomi, H.-L., Skyttä, E., Saarela, M., Mattila-Sandholm, T., Latva-Kala, K., and Helander, I. (2000). Lactic acid permeabilizes gram-negative bacteria by disrupting the outer membrane. *Appl Environ Microbiol* 66, pp. 2001–2005.

Andersson, C., Hodge, D., Berglund, K. A., and Rova, U. (2007). Effect of different carbon sources on the production of succinic acid using metabolically engineered *Escherichia coli*. *Biotechnol Prog* 23, pp. 381–388.

Anglani, C. (1998). Sorghum carbohydrates – a review. *Plant Foods Hum Nutr* 52, pp. 77–83.

Antoniewicz, M. R. (2015). Methods and advances in metabolic flux analysis: a mini-review. *J Ind Microbiol Biotechnol* 42, pp. 317–325.

Archambault, E., Bertrand, F., Côté, G., Craig-Dupont, O., V. Larivière, É., and Gagné, V. (2004). *Towards a Canadian R&D Strategy for Bioproducts and Bioprocesses*. Tech. rep. National Research Council of Canada.

Arifin, Y., Archer, C., Lim, S., Quek, L.-E., Sugiarto, H., Marcellin, E., Vickers, C. E., Krömer, J. O., and Nielsen, L. K. (2014). *Escherichia coli* W shows fast, highly oxidative sucrose metabolism and low acetate formation. *Appl Microbiol Biotechnol* 98, pp. 9033–44.

Bailey, J. (1991). Toward a science of metabolic engineering. *Science* 252, pp. 1668–1675.

Balzer, G. J., Thakker, C., Bennett, G. N., and San, K.-Y. (2013). Metabolic engineering of *Escherichia coli* to minimize byproduct formate and improving succinate productivity through increasing NADH availability by heterologous expression of NAD^+-dependent formate dehydrogenase. *Metab Eng* 20, pp. 1–8.

Banat, I. M., Satpute, S. K., Cameotra, S. S., Patil, R., and Nyayanit, N. V. (2014). Cost effective technologies and renewable substrates for biosurfactants production. *Front Microbiol* 5, p. 697.

Bartek, T., Blombach, B., Lang, S., Eikmanns, B. J., Wiechert, W., Oldiges, M., Nöh, K., and Noack, S. (2011). Comparative ^{13}C metabolic flux analysis

of pyruvate dehydrogenase complex-deficient, L-valine-producing *Corynebacterium glutamicum. Appl Environ Microbiol* 77, pp. 6644–6652.

BASF and CSM (2012). *BASF and CSM establish 50-50 joint venture for biobased succinic acid.* URL: https://www.basf.com/documents/corp/en/news-and-media/news-releases/2012/10/P444_BASF_Purac_2012_Oct4_e.pdf (visited on 07/07/2016).

Beauprez, J. J., De Mey, M., and Soetaert, W. K. (2010). Microbial succinic acid production: natural versus metabolic engineered producers. *Process Biochem* 45, pp. 1103–1114.

Becker, J., Klopprogge, C., Herold, A., Zelder, O., Bolten, C. J., and Wittmann, C. (2007). Metabolic flux engineering of L-lysine production in *Corynebacterium glutamicum*—over expression and modification of G6P dehydrogenase. *J Biotechnol* 132, pp. 99–109.

Becker, J., Klopprogge, C., Schröder, H., and Wittmann, C. (2009). Metabolic engineering of the tricarboxylic acid cycle for improved lysine production by *Corynebacterium glutamicum. Appl Environ Microbiol* 75, pp. 7866–9.

Becker, J., Klopprogge, C., and Wittmann, C. (2008). Metabolic responses to pyruvate kinase deletion in lysine producing *Corynebacterium glutamicum. Microb Cell Fact* 7, p. 8.

Becker, J., Klopprogge, C., Zelder, O., Heinzle, E., and Wittmann, C. (2005). Amplified expression of fructose 1,6-bisphosphatase in *Corynebacterium glutamicum* increases *in vivo* flux through the pentose phosphate pathway and lysine production on different carbon sources. *Appl Environ Microbiol* 71, pp. 8587–96.

Becker, J., Lange, A., Fabarius, J., and Wittmann, C. (2015). Top value platform chemicals: bio-based production of organic acids. *Curr Opin Biotechnol* 36, pp. 168–175.

Becker, J., Reinefeld, J., Stellmacher, R., Schäfer, R., Lange, A., Meyer, H., Lalk, M., Zelder, O., Abendroth, G. von, Schröder, H., Haefner, S., and Wittmann, C. (2013). Systems-wide analysis and engineering of metabolic pathway fluxes in bio-succinate producing *Basfia succiniciproducens. Biotechnol Bioeng* 110, pp. 3013–23.

Becker, J. and Wittmann, C. (2015). Biotechnologie von Morgen: metabolisch optimierte Zellen für die bio-basierte Produktion von Chemikalien und Treibstoffen, Materialien und Gesundheitsprodukten. *Angew Chem Ger Edit* 127, pp. 3383–3407.

Becker, J., Zelder, O., Häfner, S., Schröder, H., and Wittmann, C. (2011). From zero to hero—design-based systems metabolic engineering of *Corynebacterium glutamicum* for L-lysine production. *Metab Eng* 13, pp. 159–68.

Beckham, G. T., Johnson, C. W., Karp, E. M., Salvachùa, D., and Vardon, D. R. (2016). Opportunities and challenges in biological lignin valorization. *Curr Opin Biotechnol* 42, pp. 40–53.

BioAmber (2008). *Sustainability feedstock development: Feedstock Flexibility.* URL: https://www.bio-amber.com/bioamber/en/productssuccinic_acid (visited on 07/07/2016).

Bockmann, J., Heuel, H., and Lengeler, J. (1992). Characterization of a chromosomally encoded, non-PTS metabolic pathway for sucrose utilization in *Escherichia coli* EC3132. *Mol Gen Genet* 235, pp. 22–32.

Bozell, J. J. and Petersen, G. R. (2010). Technology development for the production of biobased products from biorefinery carbohydrates: the US Department of Energy's 'Top 10' revisited. *Green Chem* 12, p. 539.

Broz, J., Seon, A., and Simoes-Nunes, C. (2010). Use of succinic acid. WO2010031602 A1. Patent.

Bunce, S., Long, E., and Rowan, A. (2006). Nickel electroplating bath designed to replace monovalent copper strike solutions. US20060096868 A1. Patent.

Bunch, P. K., Mat-Jan, F., Lee, N., and Clark, D. P. (1997). The *ldhA* gene encoding the fermentative lactate dehydrogenase of *Escherichia coli*. *Microbiology* 143, pp. 187–195.

Burk, M. J. and Dien, S. V. (2016). Biotechnology for chemical production: challenges and opportunities. *Trends Biotechnol* 34, pp. 187–190.

Buschke, N., Becker, J., Schäfer, R., Kiefer, P., Biedendieck, R., and Wittmann, C. (2013). Systems metabolic engineering of xylose-utilizing *Corynebacterium glutamicum* for production of 1,5-diaminopentane. *Biotechnol J* 8, pp. 557–570.

Buschke, N., Schröder, H., and Wittmann, C. (2011). Metabolic engineering of *Corynebacterium glutamicum* for production of 1,5-diaminopentane from hemicellulose. *Biotechnol J* 6, pp. 306–317.

Chatterjee, R., Millard, C. S., Champion, K., Clark, D. P., and Donnelly, M. I. (2001). Mutation of the *ptsG* gene results in increased production of succinate in fermentation of glucose by *Escherichia coli*. *Appl Environ Microbiol* 67, pp. 148–154.

Chemicals-Technology.com (*2016*). *ARD Bio-Based Succinic Acid Plant, France.* URL: http://www.chemicals-technology.com/projects/agro-industrie-plant/ (visited on 07/07/2016).

Chen, C., Ding, S., Wang, D., Li, Z., and Ye, Q. (2014). Simultaneous saccharification and fermentation of cassava to succinic acid by *Escherichia coli* NZN111. *Bioresour Technol* 163, pp. 100–5.

Chen, Y. and Nielsen, J. (2013). Advances in metabolic pathway and strain engineering paving the way for sustainable production of chemical building blocks. *Curr Opin Biotechnol* 24, pp. 965–972.

Cheng, K. K., Wang, G. Y., Zeng, J., and Zhang, J. A. (2013). Improved succinate production by metabolic engineering. *Biomed Res Int* 2013.

Cheng, K.-K., Zhao, X.-B., Zeng, J., and Zhang, J.-A. (2012). Biotechnological production of succinic acid: current state and perspectives. *Biofuels, Bioprod Biorefin* 6, pp. 302–318.

Choi, S., Song, C. W., Shin, J. H., and Lee, S. Y. (2015). Biorefineries for the production of top building block chemicals and their derivatives. *Metab Eng* 28, pp. 223–239.

Christensen, B., Thykaer, J., and Nielsen, J. (2000). Metabolic characterization of high- and low-yielding strains of *Penicillium chrysogenum*. *Appl Microbiol Biotechnol* 54, pp. 212–7.

Cok, B., Tsiropoulos, I., Roes, A. L., and Patel, M. K. (2014). Succinic acid production derived from carbohydrates: an energy and greenhouse gas assessment of a platform chemical toward a bio-based economy. *Biofuels, Bioprod Biorefin* 8, pp. 16–29.

Collicchio-Zuanaze, R. C., Sakate, M., Schwartz, D. S., Trezza, E., and Crocci, A. J. (2006). Calcium gluconate and sodium succinate for therapy of sodium fluoroacetate experimental intoxication in cats: clinical and electrocardiographic evaluation. *Hum Exp Toxicol* 25, pp. 175–182.

Davis, J. (2000). Nickel, cobalt, and their alloys. ASM specialty handbook. ASM International.

De Graaf, A. A., Striegel, K., Wittig, R. M., Laufer, B., Schmitz, G., Wiechert, W., Sprenger, G. A., and Sahm, H. (1999). Metabolic state of *Zymomonas mobilis* in glucose-, fructose-, and xylose-fed continuous cultures as analysed by ^{13}C- and ^{31}P-NMR spectroscopy. *Arch microbiol* 171, pp. 371–385.

Dewulf, J., Meester, S. D., and Alvarenga, R. A. F., eds. (2016). Sustainability assessment of renewables-based products: methods and case studies, p. 400.

Dominguez, H. and Lindley, N. (1996). Complete sucrose metabolism requires fructose phosphotransferase activity in *Corynebacterium glutamicum* to ensure phosphorylation of liberated fructose. *Appl Environ Microb* 62, pp. 3878–3880.

Economy, G. (1966). Anodizing electrolyte and process. US3280013 A. Patent.

Ernst, T., Oborsh, E., and Oreel, F. (1979). Food preservation. US4158706 A. Patent.

European Commission (2016). *Bio-based products*. Ed. by **Expert Group for Bio-based Products (E02886)**. European Commission. URL: http://ec.europa.eu/growth/sectors/biotechnology/bio-based-products/index_en.htm.

Feldman-Salit, A., Hering, S., Messiha, H. L., Veith, N., Cojocaru, V., Sieg, A., Westerhoff, H. V., Kreikemeyer, B., Wade, R. C., and Fiedler, T. (2013). Regulation of the activity of lactate dehydrogenases from four lactic acid bacteria. *J Biol Chem* 288, pp. 21295–21306.

Feng, X. and Zhao, H. (2013). Investigating xylose metabolism in recombinant *Saccharomyces cerevisiae* via ^{13}C metabolic flux analysis. *Microb Cell Fact* 12, pp. 1–12.

Giaquinta, R. T. (1979). Sucrose translocation and storage in the sugar beet. *Plant Physiol* 63, pp. 828–832.

Goel, M. K. (1994). *Biotechnology: an overview*. URL: https://www.rpi.edu/dept/chem-eng/Biotech-Environ/goel.html (visited on 07/08/2016).

Gourdon, P., Baucher, M.-F., Lindley, N. D., and Guyonvarch, A. (2000). Cloning of the malic enzyme gene from *Corynebacterium glutamicum* and role of the enzyme in lactate metabolism. *Appl Environ Microbiol* 66, pp. 2981–2987.

GrandViewResearch (2014). *Bio-succinic acid market analysis by application (BDO, polyester polyols, PBS/PBST, plasticizers, alkyd Resins) and segment forecasts to 2020*. Grand View Research, Inc.

GrandViewResearch (2016). *Maleic anhydride market analysis by application (unsaturated polyester resins (UPR), 1,4-butanediol (BDO), additives, copolymers) and segment forecasts to 2024*. Grand View Research, Inc.

Granström, T. B., Aristidou, A. A., Jokela, J., and Leisola, M. (2000). Growth characteristics and metabolic flux analysis of *Candida milleri*. *Biotechnol Bioeng* 70, pp. 197–207.

Grimaldi, M. P., Marques, M. P., Laluce, C., Cilli, E. M., and Sponchiado, S. R. P. (2015). Evaluation of lime and hydrothermal pretreatments for efficient enzymatic hydrolysis of raw sugarcane bagasse. *Biotechnol Biofuels* 8, pp. 1–14.

Guettler, M. V., Jain, M. K., and Rumler, D. (1996). Method for making succinic acid, bacterial variants for use in the process, and methods for obtaining variants. US5573931 A. Patent.

Guettler, M. V., Rumler, D., and Jain, M. K. (1999). *Actinobacillus succinogenes* sp. nov., a novel succinic-acid-producing strain from the bovine rumen. *Int J Syst Evol Microbiol* 49, pp. 207–216.

Hald, E., Lehmann, P., and Ziegenhorn, J. (1975). Molar absorptivities of β-NADH and β-NAD at 260 nm. *Clin Chem* 21, pp. 884–887.

Hari, T. K., Yaakob, Z., and Binitha, N. N. (2015). Aviation biofuel from renewable resources: routes, opportunities and challenges. *Renew Sust Energ Rev* 42, pp. 1234–1244.

Hartmann, M. (2015). *BioAmber announces opening of world's largest succinic acid plant in Sarnia. Facility uses biotechnology to produce sustainable chemicals from sugar*. URL: `http : / / investor . bio - amber . com / 2015 - 08 - 06 - BioAmber - announces-opening-of-worlds-largest-succinic-acid-plant-in-Sarnia`.

Harzevili, F. and Chen, H. (2014). Microbial Biotechnology: Progress and Trends. CRC Press.

Helanto, M., Aarnikunnas, J., Palva, A., Leisola, M., and Nyyssölä, A. (2006). Characterization of genes involved in fructose utilization by *Lactobacillus fermentum*. *Arch Microbiol* 186, pp. 51–9.

Hong, S. H. and Lee, S. Y. (2001). Metabolic flux analysis for succinic acid production by recombinant *Escherichia coli* with amplified malic enzyme activity. *Biotechnol Bioeng* 74, pp. 89–95.

Hong, S. H., Kim, J. S., Lee, S. Y., In, Y. H., Choi, S. S., Rih, J.-K., Kim, C. H., Jeong, H., Hur, C. G., and Kim, J. J. (2004). The genome sequence of the capnophilic rumen bacterium *Mannheimia succiniciproducens*. *Nat Biotechnol* 22, pp. 1275–81.

Hui, Y. H. (2006). Bakery Products. Science and Technology.

Hüsing, B., Angerer, G., Gaisser, S., and Marscheider-Weidemann, F. (2003). *Biotechnologische Herstellung von Wertstoffen unter besonderer Berücksichtigung von Energieträgern und Biopolymeren.* Tech. rep. Fraunhofer-Institut für Systemtechnik und Innovationsforschung, Karlsruhe, im Auftrag des Umweltbundesamtes.

Igoe, R. S. (2011). Dictionary of Food Ingredients. Springer Science & Business Media.

Ito, Y., Hirasawa, T., and Shimizu, H. (2014). Metabolic engineering of *Saccharomyces cerevisiae* to improve succinic acid production based on metabolic profiling. *Biosci Biotechnol Biochem* 78, pp. 151–159.

Jacquot, R. and Marion, P. (2009). Method for manufacturing compounds including nitrile functions. US20110288324 A1. Patent.

Jahreis, K., Bentler, L., Bockmann, J., Hans, S., Meyer, A., Siepelmeyer, J., and Lengeler, J. W. (2002). Adaptation of sucrose metabolism in the *Escherichia coli* wild-type strain EC3132. *J Bacteriol* 184, pp. 5307–5316.

Jansen, M. L. A. and Gulik, W. M. van (2014). Towards large scale fermentative production of succinic acid. *Curr Opin Biotechnol* 30, pp. 190–7.

Jantama, K., Zhang, X., Moore, J. C., Shanmugam, K. T., Svoronos, S. a., and Ingram, L. O. (2008). Eliminating side products and increasing succinate yields in engineered strains of *Escherichia coli* C. *Biotechnol Bioeng* 101, pp. 881–93.

Jetten, M. S. and Sinskey, A. J. (1993). Characterization of phosphoenolpyruvate carboxykinase from *Corynebacterium glutamicum*. *FEMS Microbiol Lett* 111, pp. 183–188.

Jiang, M., Wan, Q., Liu, R., Liang, L., Chen, X., Wu, M., Zhang, H., Chen, K., Ma, J., Wei, P., and Ouyang, P. (2014). Succinic acid production from corn stalk hydrolysate in an *E. coli* mutant generated by atmospheric and room-temperature plasmas and metabolic evolution strategies. *J Ind Microbiol Biot* 41, pp. 115–23.

Jojima, T., Omumasaba, C. A., Inui, M., and Yukawa, H. (2010). Sugar transporters in efficient utilization of mixed sugar substrates: current knowledge and outlook. *Appl Microbiol Biotechnol* 85, pp. 471–480.

Jung, W. S., Jung, Y. R., Oh, D.-B., Kang, H. A., Lee, S. Y., Chavez-Canales, M., Georgellis, D., and Kwon, O. (2008). Characterization of the Arc two-component signal transduction system of the capnophilic rumen bacterium Mannheimia succiniciproducens. *FEMS Microbiol Lett* 284, pp. 109–19.

Kamzolova, S. V., Vinokurova, N. G., Shemshura, O. N., Bekmakhanova, N. E., Lunina, J. N., Samoilenko, V. A., and Morgunov, I. G. (2014). The production of succinic acid by yeast Yarrowia lipolytica through a two-step process. *Appl Microbiol Biotechnol* 98, pp. 7959–69.

Kelleher, J. K. (1999). Estimating gluconeogenesis with [U-^{13}C]glucose: molecular condensation requires a molecular approach. *Am J Physiol Endocrinol Metab* 277, E395–E400.

Kiefer, H. (2014). Method for the recovery of succinic acid from fermentation broths. EP2813485 A1. Patent.

Kiefer, P., Heinzle, E., Zelder, O., and Wittmann, C. (2004). Comparative metabolic flux analysis of lysine-producing *Corynebacterium glutamicum* cultured on glucose or fructose. *Appl Environ Microbiol* 70, pp. 229–39.

Kim, D. Y., Yim, S. C., Lee, P. C., Lee, W. G., Lee, S. Y., and Chang, H. N. (2004). Batch and continuous fermentation of succinic acid from wood hydrolysate by *Mannheimia succiniciproducens* MBEL55E. *Enzyme Microb Technol* 35, pp. 648–653.

Kim, M. I. (2009). Continuous production of succinic acid using an external membrane cell recycle system. *J Microbiol Biotechnol* 19, pp. 1369–1373.

Kim, T. Y., Kim, H. U., Park, J. M., Song, H., Kim, J. S., and Lee, S. Y. (2007). Genome-scale analysis of *Mannheimia succiniciproducens* metabolism. *Biotechnol Bioeng* 97, pp. 657–671.

Kohlstedt, M., Becker, J., and Wittmann, C. (2010). Metabolic fluxes and beyond – systems biology understanding and engineering of microbial metabolism. *Appl Microbiol Biotechnol* 88, pp. 1065–75.

Krawczyk, J., Haefner, S., Schröder, H., Dantas, C., Zelder, O., Von, A., Wittmann, C., Stellmacher, R., Becker, J., Lange, A., *et al.* (2015). Improved microorganisms for succinic acid production. WO2015117916 A1. Patent.

Krömer, J. O., Fritz, M., Heinzle, E., and Wittmann, C. (2005). *In vivo* quantification of intracellular amino acids and intermediates of the methionine pathway in *Corynebacterium glutamicum*. *Anal Biochem* 340, pp. 171–173.

Kuhnert, P. and Christensen, H. (2008). Pasteurellaceae: biology, genomics and molecular aspects. Caister Academic Press.

Kuhnert, P., Scholten, E., Haefner, S., Mayor, D., and Frey, J. (2010). *Basfia succiniciproducens* gen. nov., sp. nov., a new member of the family Pasteurellaceae isolated from bovine rumen. *Int J Syst Evol Microbiol* 60, pp. 44–50.

Kwon, Y.-D., Kim, S., Lee, S. Y., and Kim, P. (2011). Long-term continuous adaptation of *Escherichia coli* to high succinate stress and transcriptome analysis of the tolerant strain. *J Biosci Bioeng* 111, pp. 26–30.

Laine, R. A. and Sweeley, C. C. (1971). Analysis of trimethylsilyl O-methyloximes of carbohydrates by combined gas-liquid chromatography-mass spectrometry. *Anal Biochem* 43, pp. 533–538.

Leandro, M., Gonçalves, P., and Spencer-Martins, I. (2006). Two glucose/xylose transporter genes from the yeast *Candida intermedia*: first molecular characterization of a yeast xylose-H$^+$ symporter. *Biochem. J.* 395, pp. 543–549.

Lee, J. W., Choi, S., Kim, J. M., and Lee, S. Y. (2010a). *Mannheimia succiniciproducens* phosphotransferase system for sucrose utilization. *Appl Environ Microbiol* 76, pp. 1699–703.

Lee, J. W. and Lee, S. Y. (2010). Proteome-based physiological analysis of the metabolically engineered succinic acid producer *Mannheimia succiniciproducens* LPK7. *Bioproc Biosyst Eng* 33, pp. 97–107.

Lee, J. W., Lee, S. Y., Song, H., and Yoo, J.-S. (2006a). The proteome of *Mannheimia succiniciproducens*, a capnophilic rumen bacterium. *Proteomics* 6, pp. 3550–66.

Lee, K. Y., Park, J. M., Kim, T. Y., Yun, H., and Lee, S. Y. (2010b). The genome-scale metabolic network analysis of *Zymomonas mobilis* ZM4 explains physiological features and suggests ethanol and succinic acid production strategies. *Microb Cell Fact* 9, p. 94.

Lee, P. C. L. S. Y. and Chang, S. H. H. H. N. (2002). Isolation and characterization of a new succinic acid-producing bacterium, *Mannheimia succiniciproducens* MBEL55E, from bovine rumen. *Appl Microbiol Biot*, pp. 663–668.

Lee, P., Lee, S., Hong, S., Chang, H., and Park, S. (2003). Biological conversion of wood hydrolysate to succinic acid by *Anaerobiospirillum succiniciproducens*. *Biotechnol let* 25, pp. 111–114.

Lee, P. C., Lee, S. Y., Hong, S. H., and Chang, H. N. (2002a). Cloning and characterization of *Mannheimia succiniciproducens* MBEL55E phosphoenolpyruvate carboxykinase (*pckA*) gene. *Biotechnol Bioproc E* 7, pp. 95–99.

Lee, S., Song, H., Jang, Y., and Lim, S. (2007). Novel gene encoding formate dehydrogenases D & E and method for preparing succinic acid using the same. US20070042481 A1. Patent.

Lee, S. J., Song, H., and Lee, S. Y. (2006b). Genome-based metabolic engineering of *Mannheimia succiniciproducens* for succinic acid production. *Appl Environ Microbiol* 72, pp. 1939–1948.

Lee, S. Y., Hong, S. H., and Moon, S. Y. (2002b). *In silico* metabolic pathway analysis and design: succinic acid production by metabolically engineered *Escherichia coli* as an example. *Genome Inform* 13, pp. 214–23.

Lee, S. Y., Lee, D.-Y., and Kim, T. Y. (2005). Systems biotechnology for strain improvement. *Trends Biotechnol* 23, pp. 349–58.

Lee, S. Y., Lee, J. W., Choi, S., and Yi, J. (2014). Mutant microorganism producing succinic acid simultaneously using sucrose and glycerol, and method for preparing succinic acid using same. US8691516 B2. Patent.

Lee, S. Y., Lim, S. W., and Song, H. (2015). Novel engineered microorganism producing homo-succinic acid and method for preparing succinic acid using the same. WO2008013405 A1. Patent.

Lee, S., Mattanovich, D., and Villaverde, A. (2012). Systems metabolic engineering, industrial biotechnology and microbial cell factories. *Microb Cell Fact* 11, pp. 1–3.

Leighty, R. W. and Antoniewicz, M. R. (2013). COMPLETE-MFA: Complementary parallel labeling experiments technique for metabolic flux analysis. *Metab Eng* 20, pp. 49–55.

Li, M. and Borodina, I. (2015). Application of synthetic biology for production of chemicals in yeast *Saccharomyces cerevisiae*. *FEMS Yeast Res* 15, pp. 1–12.

Li, N., Zhang, B., Chen, T., Wang, Z., Tang, Y.-J., and Zhao, X. (2013). Directed pathway evolution of the glyoxylate shunt in *Escherichia coli* for improved aerobic succinate production from glycerol. *J Ind Microbiol Biot* 40, pp. 1461–75.

Li, Q., Siles, J. a., and Thompson, I. P. (2010). Succinic acid production from orange peel and wheat straw by batch fermentations of *Fibrobacter succinogenes S85*. *Appl Microbiol Biot* 88, pp. 671–8.

Liggett, R. W. and Koffler, H. (1948). Corn steep liquor in microbiology. *Bacteriol Rev* 12, p. 297.

Lin, C. S. K., Luque, R., Clark, J. H., Webb, C., and Du, C. (2011). A seawater-based biorefining strategy for fermentative production and chemical transformations of succinic acid. *Energy Environ Sci* 4 (4), pp. 1471–1479.

Lin, C. S. K., Luque, R., Clark, J. H., Webb, C., and Du, C. (2012). Wheat-based biorefining strategy for fermentative production and chemical transformations of succinic acid. *Biofuels, Bioprod Biorefin* 6, pp. 88–104.

Litsanov, B., Brocker, M., and Bott, M. (2012). Toward homosuccinate fermentation: metabolic engineering of *Corynebacterium glutamicum* for anaerobic production of succinate from glucose and formate. *Appl Environ Microbiol* 78, pp. 3325–37.

Liu, Y.-P., Zheng, P., Sun, Z.-H., Ni, Y., Dong, J.-J., and Zhu, L.-L. (2008a). Economical succinic acid production from cane molasses by *Actinobacillus succinogenes*. *Bioresource Technol* 99, pp. 1736–1742.

Liu, Y., Zheng, P., Ni, Y., Dong, J., Wei, P., and Sun, Z. (2008b). Breeding of monofluoroacetate-resistant strains of *Actinobacillus succinogenes* and the mechanism based on metabolic flux analysis. *Sheng wu gong cheng xue bao= Chinese journal of biotechnology* 24, pp. 460–467.

Lohbeck, K., Haferkorn, H., Fuhrmann, W., and Fedtke, N. (2000). Maleic and fumaric acids. *Ullmann's Encyclopedia of Industrial Chemistry*. Wiley-VCH Verlag GmbH & Co. KGaA.

Lynd, L. R., Zyl, W. H. van, McBride, J. E., and Laser, M. (2005). Consolidated bioprocessing of cellulosic biomass: an update. *Curr Opin Biotechnol* 16, pp. 577–583.

Malaisse, W. (1995). The esters of carboxylic nutrients as insulinotropic tools in non-insulin-dependent diabetes mellitus. *Gen Pharmacol-Vasc S* 26, pp. 1133–1141.

Marangoni, A. (2003). Enzyme kinetics: a modern approach. Wiley InterScience electronic collection. Wiley.

MarketsandMarkets (2016). *Succinic Acid Market by Type (Bio-based, Petro-based), Application (Polyurethane, Resins, Coatings & Pigments, Pharmaceuticals, Plasticizers, Food & Beverage, PBS/PBST, Solvents & Lubricants, De-Icer Solutions, Personal Care, and Others), and by Region - Global Forecast to 2021*. MarketsandMarkets.

Marx, A., Graaf, A. A. de, Wiechert, W., Eggeling, L., and Sahm, H. (1996). Determination of the fluxes in the central metabolism of *Corynebacterium glutamicum* by nuclear magnetic resonance spectroscopy combined with metabolite balancing. *Biotechnol Bioeng* 49, pp. 111–129.

Mathewson, G. (2014). *10 things to know about BioAmber.* Ed. by **T. S. Journal**. URL: http://thesarniajournal.ca/10-things-know-bioamber/ (visited on 09/25/2016).

Matson, M. (1990). Preparation of 2-pyrrolidone. US4904804 A. Patent.

Matuszewska, A. (2016). *An outline of the history of research on succinic acid in Baltic amber. AMBERIF 2016: Baltic Amber in the Kaleidoscope of Time.*

Maugard, T. and Legoy, M. D. (2000). Enzymatic synthesis of derivatives of vitamin A in organic media. *J Mol Catal B: Enzym* 8, pp. 275–280.

Maurice, L. (1947). Process for shrinkproofing wool. US2414704 A. Patent.

McKinlay, J. B., Shachar-Hill, Y., Zeikus, J. G., and Vieille, C. (2007). Determining *Actinobacillus succinogenes* metabolic pathways and fluxes by NMR and GC-MS analyses of ^{13}C-labeled metabolic product isotopomers. *Metab Eng* 9, pp. 177–92.

McKinlay, J. B. and Vieille, C. (2008). ^{13}C-metabolic flux analysis of *Actinobacillus succinogenes* fermentative metabolism at different $NaHCO_3$ and H_2 concentrations. *Metab Eng* 10, pp. 55–68.

Mckinlay, J. B., Zeikus, J. G., and Vieille, C. (2005). Insights into *Actinobacillus succinogenes* fermentative metabolism in a chemically defined growth medium. *Appl Environ Microbiol* 71, pp. 6651–6656.

Melzer, G., Esfandabadi, M. E., Franco-Lara, E., and Wittmann, C. (2009). Flux Design: *In silico* design of cell factories based on correlation of pathway fluxes to desired properties. *BMC Syst Biol* 3, pp. 1–16.

Michaelis, L. and Menten, M. L. (1913). Die Kinetik der Invertinwirkung. *Biochemische Zeitschrift* 49, p. 352.

Montral Gazette (2014). *BioAmber to produce "green" base chemical in Sarnia in 2015.* URL: http://montrealgazette.com/business/bioamber-to-produce-green-base-chemical-in-sarnia-in-2015?__lsa=0104-93ba (visited on 09/25/2016).

Moreno, Y., Christensen, D., and Nielsen, O. (2000). A NIR-FT-Raman spectroscopic study of amber. *Asian J Spectro* 4, pp. 49–56.

Moritz, B., Striegel, K., De Graaf, A., and Sahm, H. (2000). Kinetic properties of the glucose-6-phosphate and 6-phosphogluconate dehydrogenases from *Corynebacterium glutamicum* and their application for predicting pentose phosphate pathway flux *in vivo*. *Eur J Biochem* 267, pp. 3442–3452.

Muchow, R., Robertson, M., and Wood, A. (1996). Growth of sugarcane under high input conditions in tropical Australia. II. Sucrose accumulation and commercial yield. *Field Crop Res* 48, pp. 27–36.

Myriant (*2016*). *Integrated Acid: A Commercial Reality.* URL: http://www.myriant.com/platform/operating-plants.cfm (visited on 07/07/2016).

Myriant (2013). *Commercializing Bio-Succinic Acid & Derivatives: Myriant Begins Start-Up Operations at the First Bio-Succinic Acid Plant in North America.* URL: http://www.myriant.com/media/press-kit-files/Myriant-BioSuccinicBrochure-0613.pdf.

Netzer, R., Krause, M., Rittmann, D., Peters-Wendisch, P. G., Eggeling, L., Wendisch, V. F., and Sahm, H. (2004). Roles of pyruvate kinase and malic enzyme in *Corynebacterium glutamicum* for growth on carbon sources requiring gluconeogenesis. *Arch Microbiol* 182, pp. 354–363.

Nicholas J. Russell, G. W. G. (2012). Food Preservatives. Springer US.

Okino, S., Noburyu, R., Suda, M., Jojima, T., Inui, M., and Yukawa, H. (2008). An efficient succinic acid production process in a metabolically engineered *Corynebacterium glutamicum* strain. *Appl Microbiol Biotechnol* 81, pp. 459–64.

Otero, J. M., Cimini, D., Patil, K. R., Poulsen, S. G., Olsson, L., and Nielsen, J. (2013). Industrial systems biology of *Saccharomyces cerevisiae* enables novel succinic acid cell factory. *PLoS One* 8, e54144.

Pandey, A., Höfer, R., Taherzadeh, M., Nampoothiri, M., and Larroche, C. (2015). Industrial biorefineries and white biotechnology. Elsevier Science.

Park, D., Laivenieks, M., Guettler, M., Jain, M., and Zeikus, J. (1999). Microbial utilization of electrically reduced neutral red as the sole electron donor for growth and metabolite production. *Appl Environ Microbiol* 65, pp. 2912–2917.

Park, S. J., Lee, S. Y., Cho, J., Kim, T. Y., Lee, J. W., Park, J. H., and Han, M.-J. (2005). Global physiological understanding and metabolic engineering of microorganisms based on omics studies. *Appl Microbiol Biotechnol* 68, pp. 567–579.

Pérez, J., Muñoz-Dorado, J., Rubia, T. de la, and Martínez, J. (2002). Biodegradation and biological treatments of cellulose, hemicellulose and lignin: an overview. *Int Microbiol* 5, pp. 53–63.

Pinazo, J. M., Domine, M. E., Parvulescu, V., and Petru, F. (2015). Sustainability metrics for succinic acid production: A comparison between biomass-based and petrochemical routes. *Catal Today* 239, pp. 17–24.

Pinto, I. S. S., Neto, I. F. F., and Soares, H. M. V. M. (2014). Biodegradable chelating agents for industrial, domestic, and agricultural applications—a review. *Environ Sci Pollut R* 21, pp. 11893–11906.

Pitkänen, J.-P., Aristidou, A., Salusjärvi, L., Ruohonen, L., and Penttilä, M. (2003). Metabolic flux analysis of xylose metabolism in recombinant *Saccharomyces cerevisiae* using continuous culture. *Metab Eng* 5, pp. 16–31.

Quek, L.-E., Wittmann, C., Nielsen, L. K., and Krömer, J. O. (2009). OpenFLUX: efficient modelling software for ^{13}C-based metabolic flux analysis. *Microb Cell Fact* 8, p. 25.

Raab, A. M., Gebhardt, G., Bolotina, N., Weuster-Botz, D., and Lang, C. (2010). Metabolic engineering of *Saccharomyces cerevisiae* for the biotechnological production of succinic acid. *Metab Eng* 12, pp. 518–25.

Raab, A. M. and Lang, C. (2011). Oxidative versus reductive succinic acid production in the yeast *Saccharomyces cerevisiae*. *Bioeng Bugs* 2, pp. 120–123.

Razeto, A., Kochhar, S., Hottinger, H., Dauter, M., Wilson, K. S., and Lamzin, V. S. (2002). Domain closure, substrate specificity and catalysis of D-lactate dehydrogenase from *Lactobacillus bulgaricus*. *J Mol Biol* 318, pp. 109–119.

Reverdia (*2016*a). *Reverdia Company Overview - Commercializing Biosuccinium Sustainable Succinic Acid.* URL: `http : / / www . reverdia . com / about / company - overview/` (visited on 07/08/2016).

Reverdia (2016b). *Growing Our Leadership Position in the Bio-succinic Market.* URL: `http : / / www . reverdia . com / technology / commercial - plants/` (visited on 07/07/2016).

Rezaei, M. N., Aslankoohi, E., Verstrepen, K. J., and Courtin, C. M. (2015). Contribution of the tricarboxylic acid (TCA) cycle and the glyoxylate shunt in *Saccharomyces cerevisiae* to succinic acid production during dough fermentation. *Int J Food Microbiol* 204, pp. 24–32.

Rottländer, R. C. A. (1970). On the formation of amber from pinus resin. *Archaeometry* 12, pp. 35–52.

Rush, B. J. and Fosmer, A. M. (2013). Methods for succinate production. WO2013112939 A2. Patent.

Saha, B. C. (2003). Hemicellulose bioconversion. *J Ind Microbiol Biot* 30, pp. 279–291.

Salvachúa, D., Mohagheghi, A., Smith, H., Bradfield, M. F. A., Nicol, W., Black, B. A., Biddy, M. J., Dowe, N., and Beckham, G. T. (2016a). Succinic acid production on xylose-enriched biorefinery streams by *Actinobacillus succinogenes* in batch fermentation. *Biotechnol Biofuels* 9, p. 28.

Salvachúa, D., Smith, H., John, P. C. S., Mohagheghi, A., Peterson, D. J., Black, B. A., Dowe, N., and Beckham, G. T. (2016b). Succinic acid production from lignocellulosic hydrolysate by *Basfia succiniciproducens*. *Bioresource technology* 214, pp. 558–566.

Salvador, A. and Chisvert, A. (2011). Analysis of Cosmetic Products. Elsevier Science.

Sánchez, A. M., Bennett, G. N., and San, K.-Y. (2005). Efficient succinic acid production from glucose through overexpression of pyruvate carboxylase in an *Escherichia coli* alcohol dehydrogenase and lactate dehydrogenase mutant. *Biotechnol Progr* 21, pp. 358–365.

Saravanan, R. and Pari, L. (2007). Succinic acid monoethyl ester, a novel insulinotropic agent: effect on lipid composition and lipid peroxidation in streptozotocin–nicotin-amide induced type 2 diabetic rats. *Mol Cell Biochem* 296, pp. 165–176.

Sauer, U. (2006). Metabolic networks in motion: ^{13}C-based flux analysis. *Mol Syst Biol* 2, p. 62.

Scholten, E., Haefner, S., and Schröder, H. (2010). Bacterial cells exhibiting formate dehydrogenase activity for the manufacture of succinic acid. US20100159542 A1. Patent.

Scholten, E. and Dägele, D. (2008). Succinic acid production by a newly isolated bacterium. *Biotechnol Lett* 30, pp. 2143–6.

Scholten, E., Renz, T., and Thomas, J. (2009). Continuous cultivation approach for fermentative succinic acid production from crude glycerol by *Basfia succinicipro-ducens* DD1. *Biotechnol Lett* 31, pp. 1947–51.

Shen, N., Qin, Y., Wang, Q., Liao, S., Zhu, J., Zhu, Q., Mi, H., Adhikari, B., Wei, Y., and Huang, R. (2015). Production of succinic acid from sugarcane molasses supplemented with a mixture of corn steep liquor powder and peanut meal as nitrogen sources by *Actinobacillus succinogenes*. *Lett Appl Microbiol* 60, pp. 544–551.

Silva, G. P. da, Mack, M., and Contiero, J. (2009). Glycerol: a promising and abundant carbon source for industrial microbiology. *Biotechnol Adv* 27, pp. 30–39.

Sims, J. K., Manteiga, S., and Lee, K. (2013). Towards high resolution analysis of metabolic flux in cells and tissues. *Curr Opin Biotechnol* 24, pp. 933–939.

Smolke, C. (2009). The metabolic pathway engineering handbook: tools and applications. The metabolic pathway engineering handbook. CRC Press.

Song, H., Kim, T. Y., Choi, B.-K., Choi, S. J., Nielsen, L. K., Chang, H. N., and Lee, S. Y. (2008). Development of chemically defined medium for *Mannheimia succiniciproducens* based on its genome sequence. *Appl Microbiol Biotechnol* 79, pp. 263–72.

Stellmacher, R., Hangebrauk, J., Wittmann, C., Scholten, E., and Abendroth, G. von (2010). Fermentative Herstellung von Bernsteinsäure mit *Basfia succinicipro-ducens* DD1 in Serumflaschen. *Chem Ing Tech* 82, pp. 1223–1229.

Stephanopoulos, G., Aristidou, A., and Nielsen, J. (1998). Metabolic engineering: principles and methodologies. Elsevier Science.

Strickland, A., Wilson, D., and Brown, E. (1996). Polyamino monoesuccinates for use in photographic processes. US5585226 A. Patent.

Succinity (*2016*a). *Biobased succinic acid - technology*. URL: `http://www.succinity.com/biobased-succinic-acid/technology` (visited on 07/07/2016).

Succinity (*2016*b). *Succinic acid explained easily*. URL: `http://www.succinity.com/biobased-succinic-acid/succinic-acid-explained-easily` (visited on 07/07/2016).

Taylor, P. (2010). *Biosuccinic acid ready for take off*. Ed. by **Royal society of chemistry**. URL: `http://www.rsc.org/chemistryworld/News/2010/January/21011003.asp`.

Terzer, M. and Stelling, J. (2008). Large-scale computation of elementary flux modes with bit pattern trees. *Bioinformatics* 24, pp. 2229–2235.

Thakker, C., Martínez, I., Li, W., San, K.-Y., and Bennett, G. N. (2015). Metabolic engineering of carbon and redox flow in the production of small organic acids. *J Ind Microbiol Biot* 42, pp. 403–22.

Umakoshi, M., Hirasawa, T., Furusawa, C., Takenaka, Y., Kikuchi, Y., and Shimizu, H. (2011). Improving protein secretion of a transglutaminase-secreting

Corynebacterium glutamicum recombinant strain on the basis of ^{13}C metabolic flux analysis. *J Biosci Bioeng* 112, pp. 595–601.

US Department of Agriculture (2016). *11167, Corn, sweet, yellow, raw*. National Nutrient Database for Standard Reference, United States Department of Agriculture.

Van De Graaf, M., Valianpoer, F., Fiey, G., Delattre, L., and Schulten, E. (2015). Process for the crystallization of succinic acid. US20150057425 A1. Patent.

Van der Werf, M. J., Guettler, M. V., Jain, M. K., and Zeikus, J. G. (1997). Environmental and physiological factors affecting the succinate product ratio during carbohydrate fermentation by *Actinobacillus* sp. 130Z. *Arch Microbiol* 167, pp. 332–42.

Vanstone, A. (1976). Erythrodiol derivatives. US4000186 A. Patent.

Vemuri, G. N., Eiteman, M. a., and Altman, E. (2002). Succinate production in dual-phase *Escherichia coli* fermentations depends on the time of transition from aerobic to anaerobic conditions. *J Ind Microbiol Biot* 28, pp. 325–32.

Verwaal, R., Wu, L., Damveld, R. A., and Sagt, C. M. J. (2009). Succinic acid production in a eukaryotic cell. WO2009065778 A1. Patent.

Wahlbom, C. F., Eliasson, A., and Hahn-Hägerdal, B. (2001). Intracellular fluxes in a recombinant xylose-utilizing *Saccharomyces cerevisiae* cultivated anaerobically at different dilution rates and feed concentrations. *Biotechnol Bioeng* 72, pp. 289–296.

Wahlbom, C. F. and Hahn-Hägerdal, B. (2002). Furfural, 5-hydroxymethyl furfural, and acetoin act as external electron acceptors during anaerobic fermentation of xylose in recombinant *Saccharomyces cerevisiae. Biotechnol Bioeng* 78, pp. 172–178.

Wang, W., Li, Z., Xie, J., and Ye, Q. (2009). Production of succinate by a *pflB ldhA* double mutant of *Escherichia coli* overexpressing malate dehydrogenase. *Bioprocess Biosyst Eng* 32, pp. 737–45.

Weingarten, R. A., Taveirne, M. E., and Olson, J. W. (2009). The dual-functioning fumarate reductase is the sole succinate:quinone reductase in *Campylobacter jejuni* and is required for full host colonization. *J Bacteriol* 191, pp. 5293–5300.

Weiss, J. N. (1997). The Hill equation revisited: uses and misuses. *The FASEB Journal* 11, pp. 835–41.

Wendisch, V. (2007). Amino acid biosynthesis – pathways, regulation and metabolic engineering. Microbiology Monographs. Springer Berlin Heidelberg.

Wendisch, V. F., Bott, M., and Eikmanns, B. J. (2006). Metabolic engineering of *Escherichia coli* and *Corynebacterium glutamicum* for biotechnological production of organic acids and amino acids. *Curr Opin Microbiol* 9, pp. 268–274.

Werpy, T. and Petersen, G. R. (2004). *Top Value Added Chemicals From Biomass Volume I: Results of Screening for Potential Candidates*. Tech. rep. U.S. Department of Energy.

Willke, T. and Vorlop, K.-D. (2004). Industrial bioconversion of renewable resources as an alternative to conventional chemistry. *Appl Microbiol Biot* 66, pp. 131–142.

Winden, W. A. van, Wittmann, C., Heinzle, E., and Heijnen, J. J. (2002). Correcting mass isotopomer distributions for naturally occurring isotopes. *Biotechnol Bioeng* 80, pp. 477–9.

Wittmann, C. (2007). Fluxome analysis using GC-MS. *Microb Cell Fact* 6, p. 6.

Wittmann, C. (2010). Analysis and engineering of metabolic pathway fluxes in *Corynebacterium glutamicum. Adv Biochem Eng Biotechnol* 120, pp. 21–49.

Wittmann, C., Hans, M., and Heinzle, E. (2002). *In vivo* analysis of intracellular amino acid labelings by GC/MS. *Anal Biochem* 307, pp. 379–82.

Wittmann, C., Kiefer, P., and Zelder, O. (2004). Metabolic fluxes in *Corynebacterium glutamicum* during lysine production with sucrose as carbon source. *Appl Environ Microbiol* 70, pp. 7277–87.

Yan, D., Wang, C., Zhou, J., Liu, Y., Yang, M., and Xing, J. (2014). Construction of reductive pathway in *Saccharomyces cerevisiae* for effective succinic acid fermentation at low pH value. *Bioresour Technol* 156, pp. 232–9.

Yocum, R. R., Hermann, T., and Hu, X. (2011). Fermentation of glycerol to organic acids. WO2013015770 A1. Patent.

Yuzbashev, T. V., Yuzbasheva, E. Y., Sobolevskaya, T. I., Laptev, I. a., Vybornaya, T. V., Larina, A. S., Matsui, K., Fukui, K., and Sineoky, S. P. (2010). Production of succinic acid at low pH by a recombinant strain of the aerobic yeast *Yarrowia lipolytica. Biotechnol Bioeng* 107, pp. 673–82.

Zamboni, N., Fendt, S.-M., Rühl, M., and Sauer, U. (2009). ^{13}C-based metabolic flux analysis. *Nature protocols* 4, pp. 878–892.

Zanghellini, J., Ruckerbauer, D. E., Hanscho, M., and Jungreuthmayer, C. (2013). Elementary flux modes in a nutshell: properties, calculation and applications. *Biotechnol J* 8, pp. 1009–1016.

Zeikus, J. G., Jain, M. K., and Elankovan, P. (1999). Biotechnology of succinic acid production and markets for derived industrial products. *Appl Microbiol Biotechnol* 51, pp. 545–552.

Zhao, Y., Wang, C.-S., Li, F.-F., Liu, Z.-N., and Zhao, G.-R. (2016). Targeted optimization of central carbon metabolism for engineering succinate production in *Escherichia coli. BMC Biotechnol* 16, p. 1.

Zhu, N., Xia, H., Yang, J., Zhao, X., and Chen, T. (2014). Improved succinate production in *Corynebacterium glutamicum* by engineering glyoxylate pathway and succinate export system. *Biotechnol Lett* 36, pp. 553–560.

Zion Research (2015). *Succinic Acid Market for 1,4-BDO, Resin, Coatings, Dyes & Inks, Pharmaceutical, Polyurethane, Food, Plasticizers, Cosmetics, Solvents & Lubricants and De-Icing Solutions Applications: Global Industry Perspective, Comprehensive Analysis, and Forecast, 2014 - 2020*. Zion Research.

Appendix

A.1 Refined flux map of *B. succiniciproducens* DD1 on glucose

Cultivations and analyses for ^{13}C metabolic flux analysis of *B. succiniciproducens* strains on glucose were carried out by Jasper Schoenian (geb. Hangebrauck) and René Stellmacher. Metabolic flux maps based on the ^{13}C labeling sets derived from the tracer substrate [1-^{13}C] glucose were calculated by Dr. Judith Becker (Becker *et al.*, 2013).

To allow for a better comparison with the results presented in this work, the metabolic fluxes were re-calculated, using the revised metabolic network model described in this work (Section A.3) and integrating a second labeling set, derived from a cultivation of on 50 % [[13]C$_6$] glucose, but originally neglected.

A total of 82 individual mass isotopomers, derived from the two parallel ^{13}C labeling experiments, were simultaneously fit to the network model.

Biomass and product formation (Becker *et al.*, 2013), as well as the experimentally determined *in vivo* enzyme activity of malic enzyme, considered as the upper limit of the corresponding flux, were applied to constrain the model. The small deviation between experimental and simulated labeling pattern (Figure A.1), indicating an excellent fit, and the small confidence intervals of the calculated fluxes suggest a highly accurate result (Figure A.2).
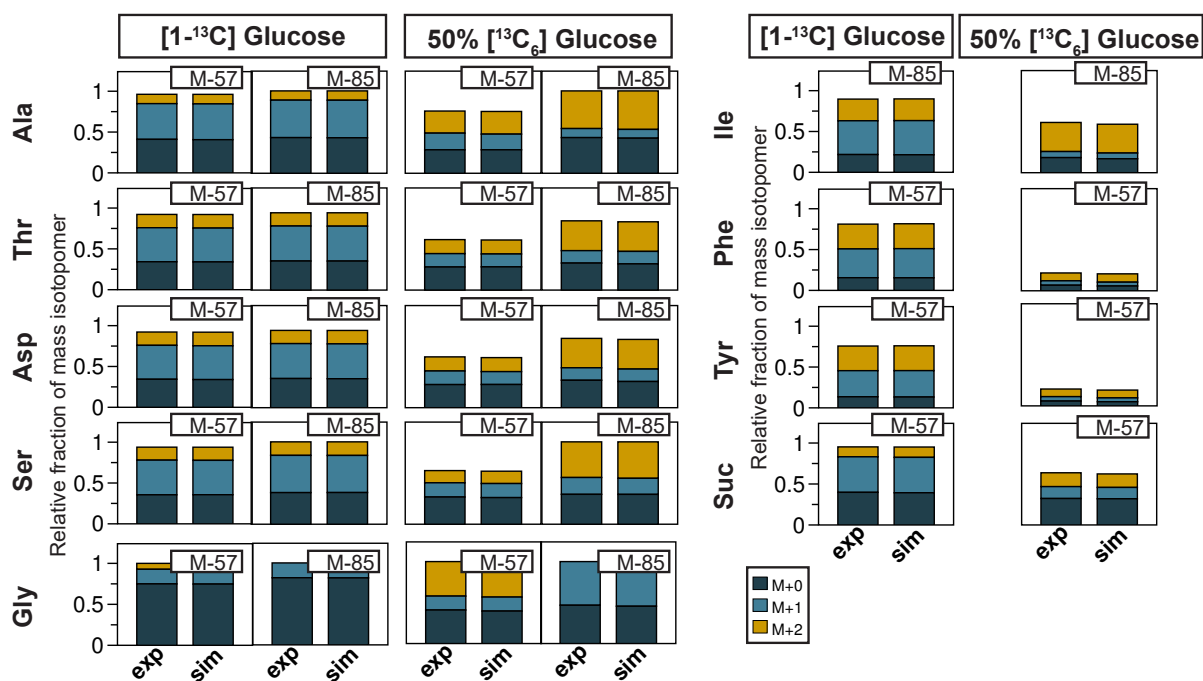
Figure A.1: Comparison of experimental and simulated mass isotopomer distributions (MIDs) for flux analysis on glucose. The data represent experimental (exp) MIDs obtained during parallel cultivation of *B. succiniciproducens* DD1 on two different ^{13}C tracer substrates and simulated (sim) MIDs corresponding to the calculated flux distribution for different amino acids (indicated by the respective three letter code abbreviations), succinate (Suc), and glycogen-derived glucose (Glc). The deviation between the experimental and simulated MIDs was exceptionally low for both data sets. 50 % [^{13}C$_6$] glucose denotes a 1:1 mixture of naturally labeled glucose and fully labeled glucose.
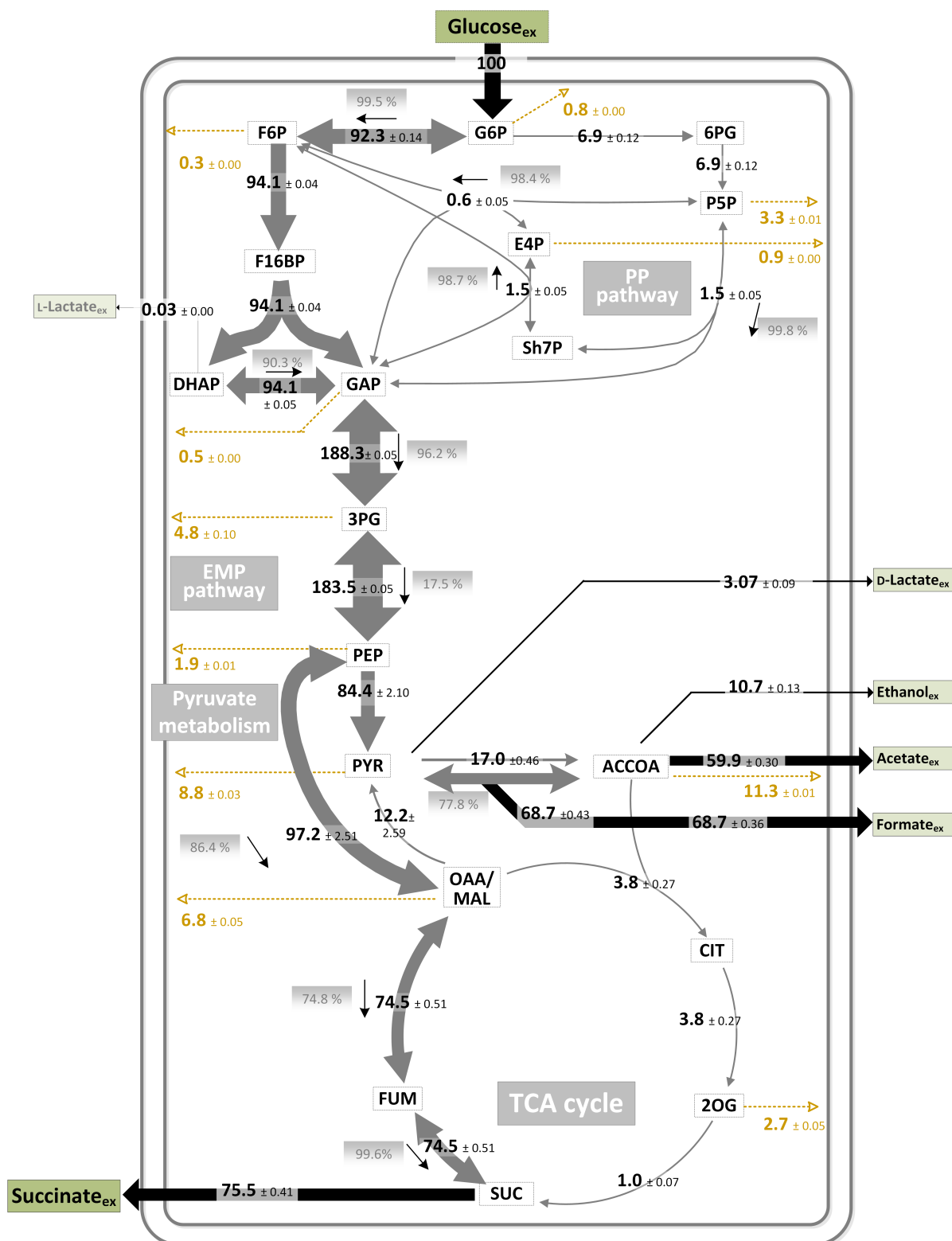
Figure A.2: Intracellular carbon fluxes of glucose-grown *B. succiniciproducens* DD1 as determined by ^{13}C metabolic flux analysis. The carbon fluxes were normalized to the glucose influx of $7.7 \pm 0.4 \, \text{mmol·g}^{-1} \cdot \text{h}^{-1}$, which was set to 100 %. The arrow thickness is proportional to the corresponding flux. The direction of net fluxes is indicated by small black arrows. Reversibilities, calculated according to Equation 3.5, are displayed in gray boxes. Yellow dashed arrows represent fluxes into biomass formation. Black arrows indicate carbon in- and efflux. PEP: phosphoenolpyruvate; PYR: pyruvate; G6P: glucose 6-phosphate; 6PG: 6-phosphogluconate; F6P: fructose 6-phosphate; F16BP: fructose 1,6-bisphosphate; DHAP: dihydroxyacetone phosphate; GAP: glyceraldehyde 3-phosphate; P5P: pentose 5-phosphate; E4P: erythrose 4-phosphate; Sh7P: seduheptulose 7-phosphate; 3PG: 3-phosphoglycerate; ACCOA: acetyl-CoA; OAA/MAL: oxaloacetate/malate; CIT: citrate; FUM: fumarate; SUC: succinate; 2OG: 2-oxoglutarate

A.2 Additional batch cultivation profiles
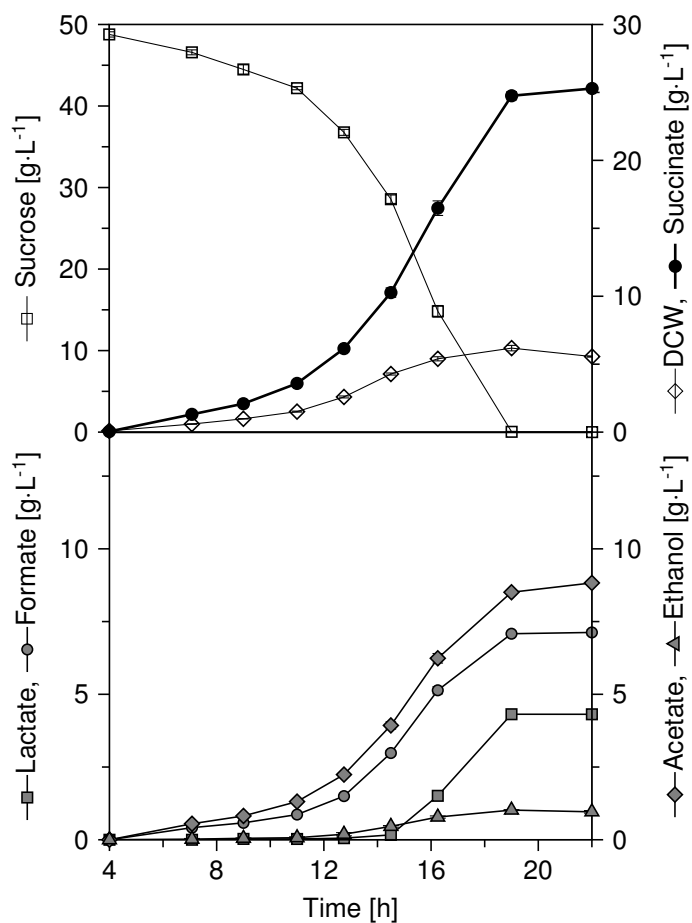
Figure A.3: Batch cultivation profile of *B. succiniciproducens* DD1 Δ*fruA* on sucrose. The data comprise biomass growth, substrate consumption, and secretion of succinate and the main by-products acetate, formate, lactate and ethanol, as mean values and deviations from three biological replicates. Units given in axis labels refer to all preceding substances separated by commas. DCW: dry cell weight
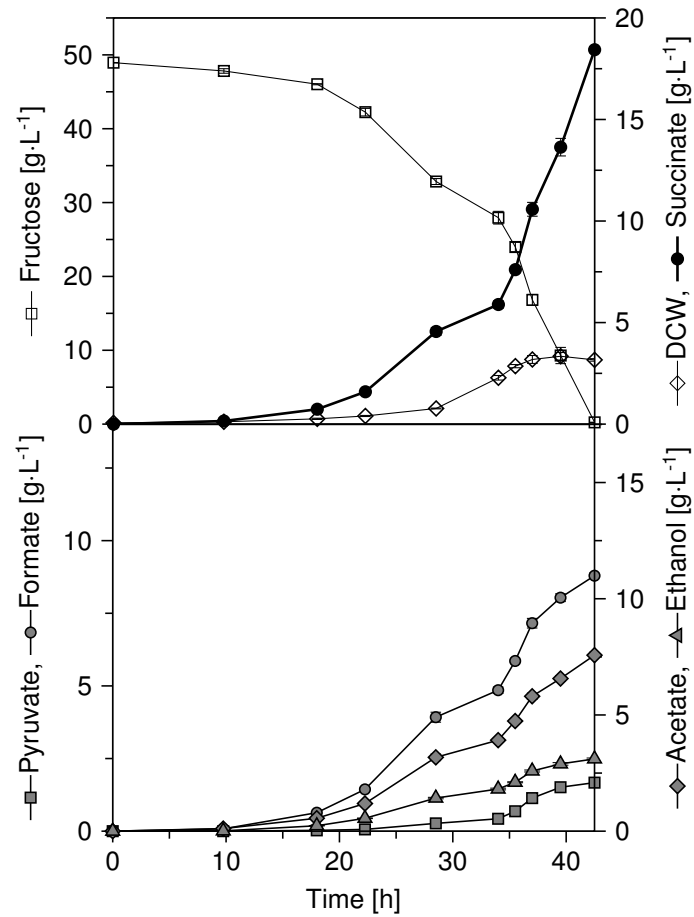
Figure A.4: Batch cultivation profile of *B. succiniciproducens* DD1 Δ*ldhA*Δ*mgsA* on fructose. The data comprise biomass growth, substrate consumption, and secretion of succinate and the main by-products acetate, formate, lactate and ethanol, as mean values and deviations from three biological replicates. Units given in axis labels refer to all preceding substances separated by commas. DCW: dry cell weight
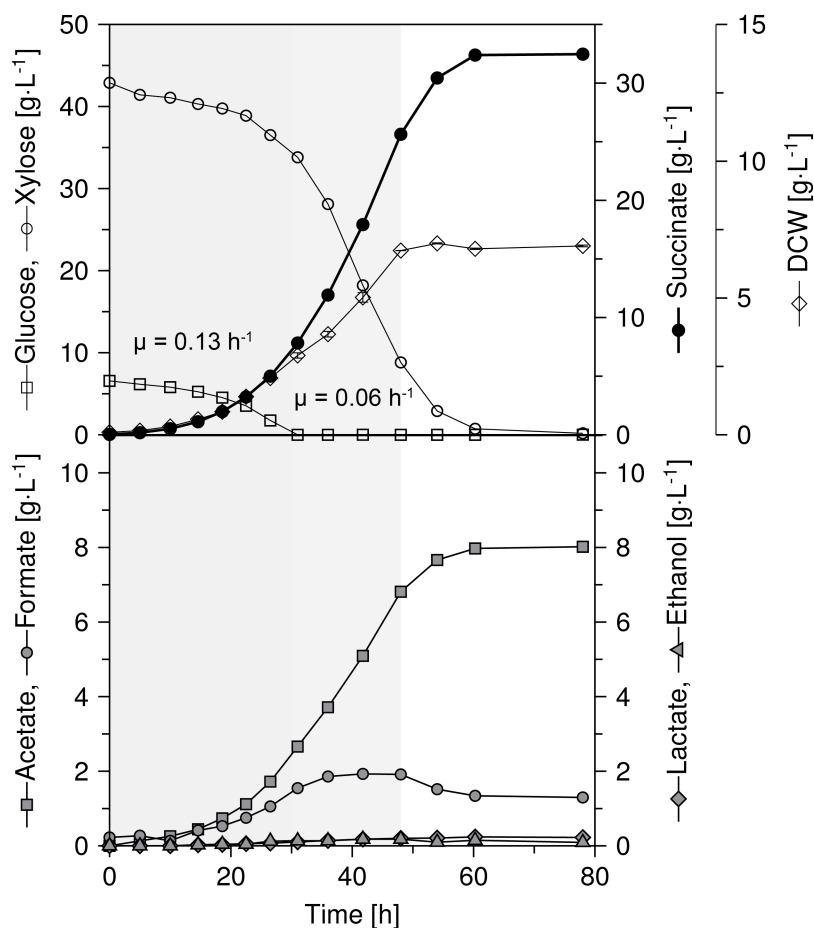
Figure A.5: Batch cultivation profile of *B. succiniciproducens* DD1 on a substrate mixture (43 g·L⁻¹ xylose, 6.6 g·L⁻¹ glucose). The data for biomass growth represent a mean value from three biological replicates, whereas product concentrations were only determined from a single exemplary cultivation. The cultivation comprised three phases: a co-consumption phase, during which xylose and glucose were consumed simultaneously (dark gray) with a specific growth rate of $0.13 \pm 0.01\,\mathrm{h}^{-1}$, a second growth phase on xylose (light gray) with a specific growth rate of $0.06 \pm 0.01\,\mathrm{h}^{-1}$, and a stationary phase, during which the remaining xylose was consumed (white). Units given in axis labels refer to all preceding substances separated by commas. DCW: dry cell weight

A.3 Network models for ^{13}C metabolic flux analysis and elementary flux mode analysis

Table A.1: Metabolic network models for ^{13}C metabolic flux analysis with OpenFLUX. First, the basic network for sucrose catabolism is presented. Then, adaptations for the substrates fructose, glucose, xylose, and glucose/xylose are listed. rxnID: reaction identification number; rxnEQ: reaction equation; cTrans: carbon transitions

rxnID	rxnEQ	cTrans	type
Basic network for sucrose catabolism:			
R001	SUCROSE_EX + PEP = SUCROSE6P + PYR	abcdefghijkl + mno = abcdefghijkl + mno	F
R002	SUCROSE6P = GLC6P + FRC	abcdefghijkl = ghijkl + abcdef	F
R003	FRC = F6P	abcdef = abcdef	F
R004	FRC + PEP = F16BP + PYR	abcdef + ghi = abcdef + ghi	F
R005	GLC6P = F6P	abcdef = abcdef	FR
R006	F6P = GLC6P	abcdef = abcdef	R
R007	F6P = F16BP	abcdef = abcdef	F
R008	F16BP = DHAP + GAP	abcdef = cba + def	F
R009	DHAP = GAP	abc = abc	FR
R010	GAP = DHAP	abc = abc	R
R011	GAP = 3PG	abc = abc	FR
R012	3PG = GAP	abc = abc	R
R013	3PG = PEP	abc = abc	FR
R014	PEP = 3PG	abc = abc	R
R015	PEP = PYR	abc = abc	F
R016	GLC6P = P5P + CO2	abcdef = bcdef + a	F
R017	P5P + P5P = S7P + GAP	abcde + fghij = abfghij + cde	FR
R018	S7P + GAP = P5P + P5P	abcdefg + hij = abhij + cdefg	R
R019	GAP + S7P = E4P + F6P	abc + defghij = ghij + defabc	FR
R020	E4P + F6P = GAP + S7P	abcd + efghij = hij + efgabcd	R
R021	P5P + E4P = GAP + F6P	abcde + fghi = cde + abfghi	FR
R022	GAP + F6P = P5P + E4P	abc + defghi = deabc + fghi	R
R023	PEP + CO2 = OAA_MAL	abc + d = abcd	FR
R024	OAA_MAL = PEP + CO2	abcd = abc + d	R
R025	OAA_MAL = PYR + CO2	abcd = abc + d	F
R026	PYR = ACCOA + CO2	abc = bc + a	F
R027	PYR = FOR + ACCOA	abc = a + bc	FR
R028	FOR + ACCOA = PYR	a + bc = abc	R
R029	PYR = DLAC	abc = abc	F
R030	DHAP = LLAC	abc = abc	F
R031	ACCOA = ACE	ab = ab	F
R032	ACCOA = ETOH	ab = ab	F
R033	OAA_MAL = 0.5 FUM + 0.5 FUM	abcd = 0.5 abcd + 0.5 dcba	FR
R034	FUM = 0.5 OAA_MAL + 0.5 OAA_MAL	abcd = 0.5 abcd + 0.5 dcba	R
R035	FUM = SUC	abcd = abcd	FR
R036	SUC = FUM	abcd = abcd	R
R037	ACCOA + OAA_MAL = CIT	ab + cdef = fedbac	F
R038	CIT = AKG + CO2	abcdef = abcde + f	F
R039	AKG = SUCCOA + CO2	abcde = bcde + a	F
R040	SUCCOA = 0.5 SUC + 0.5 SUC	abcd = 0.5 abcd + 0.5 dcba	FR
R041	SUC = SUCCOA	abcd = abcd	R
R042	GLC6P = GLC6P_B		B
R043	F6P = F6P_B		B

Table A.1: **Metabolic network models for ^{13}C metabolic flux analysis (continued)**

rxnID	rxnEQ	cTrans	type
R044	P5P = P5P_B		B
R045	GAP = GAP_B		B
R046	3PG = 3PG_B		B
R047	PEP = PEP_B		B
R048	PYR = PYR_B		B
R049	ACCOA = ACCOA_B		B
R050	OAA_MAL = OAA_MAL_B		B
R051	AKG = AKG_B		B
R052	AKG = GLU	abcde = abcde	F
R053	E4P + PEP = SHKM3P	abcd + efg = fdcbage	F
R054	SHKM3P + PEP = 0.5 PHE + 0.5 PHE + CO2	abcdefg + hij = 0.5 hijabcdef + 0.5 hijafedcb + g	F
R055	PHE = PHEX	abcdefghi = abcdefghi	F
R056	PHE = TYR	abcdefghi = abcdefghi	F
R057	TYR = TYRX	abcdefghi = abcdefghi	F
R058	SHKM3P + PEP = ANTHR + PYR	abcdefg + hij = gafedcb + hij	F
R059	ANTHR + P5P = IND + GAP + CO2	abcdefg + hijkl = hibgfedc + jkl + a	F
R060	IND + SER = TRP	abcdefgh + ijk = ijkabcdefgh	F
R061	TRP = TRPX	abcdefghijk = abcdefghijk	F
R062	3PG = SER	abc = abc	F
R063	SER = SERX	abc = abc	F
R064	C1 = C1_Z	a = a	F
R065	SER = GLY + C1	abc = ab + c	FR
R066	GLY + C1 = SER	ab + c = abc	R
R067	GLY = GLYX	ab = ab	F
R068	P5P + C1 = HIS	abcde + f = edcbaf	F
R069	HIS = HISX	abcdef = abcdef	F
R070	SER + ACCOA = CYS + ACE	abc + de = abc + de	F
R071	CYS = CYSX	abc = abc	F
R072	PYR = ALA	abc = abc	F
R073	ALA = ALAX	abc = abc	F
R074	PYR + PYR = ACL + CO2	abc + def = abefc + d	F
R075	ACL = ACETOIN + CO2	abefc = febc + a	F
R076	ACL = ISV	abcde = abcde	F
R077	ISV + ACCOA = LEU + CO2	abcde + fg = fgbcde + a	F
R078	LEU = LEUX	abcdef = abcdef	F
R079	THR + PYR = ILE + CO2	abcd + efg = abfcdg + e	F
R080	ILE = ILEX	abcdef = abcdef	F
R081	ISV = VAL	abcde = abcde	F
R082	VAL = VALX	abcde = abcde	F
R083	OAA_MAL = ASP	abcd = abcd	F
R084	ASP = ASPX	abcd = abcd	F
R085	ASP = ASN	abcd = abcd	F
R086	ASN = ASNX	abcd = abcd	F
R087	ASP + PYR = 0.5 LYS + 0.5 LYS + 0.5 CO2 + 0.5 CO2	abcd + efg = 0.5 abcdgf + 0.5 efgdcb + 0.5 e + 0.5 a	F
R088	LYS = LYSX	abcdef = abcdef	F
R089	ASP = THR	abcd = abcd	F
R090	THR = THRX	abcd = abcd	F
R091	ASP + C1 = MET	abcd + e = abcde	F
R092	MET = METX	abcde = abcde	F
R093	GLU = GLUX	abcde = abcde	F
R094	GLU = GLN	abcde = abcde	F
R095	GLN = GLNX	abcde = abcde	F
R096	GLU = PRO	abcde = abcde	F
R097	PRO = PROX	abcde = abcde	F

Table A.1: Metabolic network models for ^{13}C metabolic flux analysis (continued)

rxnID	rxnEQ	cTrans	type
R098	GLU + CO2 = ARG	abcde + f = abcdef	F
R099	ARG = ARGX	abcdef = abcdef	F
R100	FUM = FUM_EX		B
R101	ISV = ISV_EX		B
R102	ACETOIN = ACETOIN_EX		B
R103	ASP = ASP_EX		B
R104	GLY = GLY_EX		B
R105	ALA = ALA_EX		B
R106	VAL = VAL_EX		B
R107	ILE = ILE_EX		B
R108	LEU = LEU_EX		B
R109	GLU = GLU_EX		B
R110	FOR = FOR_EX		B
R111	ACE = ACE_EX		B
R112	ETOH = ETOH_EX		B
R113	PYR = PYR_EX		B
R114	PYR = PYR_UBP		B
R115	DLAC = DLAC_EX		B
R116	LLAC = LLAC_EX		B
R117	SUC = SUC_EX		B
R118	CO2 = CO2_EX	a = a	FR
R119	CO2_EX = CO2	a = a	R
R120	GLC6P = GLC1P	abcdef = abcdef	S

Changes for fructose catabolism:

R001 − R006 were replaced by the following lines:

R001	FRC_EX + PEP = F16BP + PYR	abcdef + ghi = abcdef + ghi	F
R002	F16BP = F6P	abcdef = abcdef	F
R003	F6P = GLC6P	abcdef = abcdef	FR
R004	GLC6P = F6P	abcdef = abcdef	R

All remaining rxnIDs were adapted accordingly.

Changes for glucose catabolism:

R001 − R004 were replaced by the following line:

R001	GLC_EX = GLC6P	abcdef = abcdef	F

All remaining rxnIDs were adapted accordingly.

Changes for xylose catabolism:

R001 − R006 were replaced by the following lines:

R001	XYLOSE_EX = P5P	abcde = abcde	F
R002	F6P = GLC6P	abcdef = abcdef	FR
R003	GLC6P = F6P	abcdef = abcdef	R

R026 − R028 were replaced by the following lines:

R023	PYR = FOR + ACCOA	abc = a + bc	FR
R024	FOR + ACCOA = PYR	a + bc = abc	R
R025	FOR = CO2	a = a	FR
R026	CO2 = FOR	a = a	R

All remaining rxnIDs were adapted accordingly.

Changes for combined glucose and xylose catabolism:

R001 − R004 were replaced by the following lines:

R001	GLC_EX = GLC6P	abcdef = abcdef	F

rxnID	rxnEQ	cTrans	type
R002	XYL_EX = P5P	abcde = abcde	F

All remaining rxnIDs were adapted accordingly.

Table A.2: Metabolic network model for elementary flux mode analysis. The model, used to calculate elementary flux modes for sucrose catabolism with the software efmtool, was adapted from a previous model describing *B. succiniciproducens* glucose catabolism (Becker *et al.*, 2013).

Identifier	Reaction equation
Sucrose	'–> sucrose[e]'
CO2fix	'–> CO2[c]'
NH3_up	'–> NH3[c]'
SO4_up	'–> SO4[c]'
CoA	'–> CoA[c]'
biomass	'biomass[c] –>'
Ace	'acetate[e] –>'
Lac	'lactate[e] –>'
Form	'formate[e] –>'
EtOH	'ethanol[e] –>'
Pyr	'pyruvate[e] –>'
Suc	'succinate[e] –>'
Fruc	'fructose[e] –>'
ATPmain	'ATPmaintenance[c] –>'
CO2 out	'CO2[c] –>'
SucrosePTS	'PEP[c] + sucrose[e] –> PYR[c] + SUC6P[c]'
Suc6PH	'SUC6P[c] –> G6P[c] + FRUC[c]'
Fruc_ex	'FRUC[c] –> fructose[e]'
FructosePTS	'fructose[e] + PEP[c] + ATP[c] –> FBP[c] + PYR[c] + ADP[c]'
FructoseKinase	'FRUC[c] + ATP[c] –> F6P[c] + ADP[c]'
zwf (NADP)	'G6P[c] + NADP[c] –> 6PGluconate[c] + NADPH[c]'
gnd	'6PGluconate[c] + NADP[c] –> RIB5P[c] + CO2[c] + NADPH[c]'
rpe	'RIB5P[c] <–> XYL5P[c]'
rpo	'RIB5P[c] <–> RIBO5P[c]'
tkt1	'S7P[c] + GAP[c] <–> RIBO5P[c] + XYL5P[c]'
ta	'S7P[c] + GAP[c] <–> E4P[c] + F6P[c]'
tkt2	'F6P[c] + GAP[c] <–> E4P[c] + XYL5P[c]'
pgi	'G6P[c] <–> F6P[c]'
pfk	'ATP[c] + F6P[c] –> ADP[c] + FBP[c]'
fbp	'FBP[c] –> F6P[c]'
ald	'FBP[c] <–> GAP[c] + DHAP[c]'
tri	'DHAP[c] <–> GAP[c]'
gapdh	'GAP[c] + NAD[c] <–> 13bPG[c] + NADH[c]'
PG-kin	'ADP[c] + 13bPG[c] <–> ATP[c] + 3PG[c]'
mut	'3PG[c] <–> 2PG[c]'
eno	'2PG[c] <–> PEP[c]'
pyk	'PEP[c] + ADP[c] –> PYR[c] + ATP[c]'
pdh	'PYR[c] + NAD[c] –> AcCoA[c] + NADH[c] + CO2[c]'
cis	'AcCoA[c] + OAA[c] –> CIT[c] + CoA[c]'
aco	'CIT[c] <–> ICI[c]'
icd	'ICI[c] + NADP[c] –> AKG[c] + CO2[c] + NADPH[c]'
akd	'AKG[c] + NAD[c] + CoA[c] –> SUCC-CoA[c] + NADH[c] + CO2[c]'
scs	'SUCC-CoA[c] + ADP[c] <–> SUCC[c] + ATP[c] + CoA[c]'
sdh	'SUCC[c] + MQ[c] <–> FUM[c] + MQH2[c]'

Table A.2: Metabolic network model for elementary flux mode analysis (continued)

Identifier	Reaction equation
fum	'FUM[c] <-> MAL[c]'
mdh	'MAL[c] + NAD[c] <-> OAA[c] + NADH[c]'
pepc_int	'PEP[c] + CO2[c] -> OAA[c]'
pepck_int	'PEP[c] + CO2[c] + ADP[c] -> OAA[c] + ATP[c]'
malE	'MAL[c] + NADP[c] -> PYR[c] + NADPH[c] + CO2[c]'
oadc	'OAA[c] -> PYR[c] + CO2[c]'
ldh	'PYR[c] + NADH[c] <-> LAC[c] + NAD[c]'
pfl	'PYR[c] + CoA[c] <-> FORM[c] + AcCoA[c]'
form-DH	'FORM[c] + NAD[c] <-> CO2[c] + NADH[c]'
pta	'AcCoA[c] <-> AcP[c] + CoA[c]'
ackA	'AcP[c] + ADP[c] <-> ACE[c] + ATP[c]'
acyP	'AcP[c] -> ACE[c]'
eutG	'AcCoA[c] + NADH[c] <-> AcAld[c] + NAD[c] + CoA[c]'
adh	'AcAld[c] + NADH[c] <-> EtOH[c] + NAD[c]'
aldDH	'AcAld[c] + NAD[c] -> ACE[c] + NADH[c]'
LACex	'LAC[c] -> lactate[e]'
ACEex	'ACE[c] -> acetate[e]'
PYRex	'PYR[c] -> pyruvate[e]'
SUCex	'SUCC[c] -> succinate[e]'
FORMex	'FORM[c] -> formate[e]'
EtOHex	'EtOH[c] -> ethanol[e]'
pntAB	'(3) NADH[c] + (3) NADP[c] + ATP[c] -> (3) NAD[c] + (3) NADPH[c] + ADP[c]'
udhA	'NADPH[c] + NAD[c] -> NADP[c] + NADH[c]'
NADH_OR	'NADH[c] + MQ[c] <-> NAD[c] + MQH2[c]'
ATPmain	'ATP[c] -> ADP[c] + ATPmaintenance[c]'
SO4_up	'SO4[c] + (3) NADPH[c] + (4) ATP[c] -> H2S[c] + (3) NADP[c] + (4) ADP[c]'
biomass	'(1.724) OAA[c] + (1.221) 3PG[c] + (0.853) RIBO5P[c] + (36.655) ATP[c] + (15.754) NADPH[c] + (9.284) NH3[c] + (3.094) NAD[c] + (2.887) AcCoA[c] + (2.745) PYR[c] + (1.186) AKG[c] + (0.223) E4P[c] + (0.495) PEP[c] + (0.091) H2S[c] + (0.071) F6P[c] + (0.205) G6P[c] + (0.129) GAP[c] -> biomass[c] + (2.887) CoA[c] + (15.754) NADP[c] + (3.094) NADH[c] + (36.655) ADP[c] + (1.381) CO2[c]'

A.4 Experimental and simulated mass isotopomer distributions

Table A.3: Comparison between experimental and simulated mass isotopomer distributions for ^{13}C metabolic flux analysis on sucrose The experimental data represent mean values of the three samples taken during the exponential phase at isotopic steady state. The simulated data represent mean values from the Monte Carlo simulations during metabolic flux analysis with OpenFLUX. Four labeling data sets derived from parallel cultivations were fit simultaneously to the metabolic network model.

Analyte	Fragment/ C atoms	Mass isotopomer	[1-$^{13}C^{Glc}$] Sucrose		[1-$^{13}C^{Frc}$] Sucrose		[$^{13}C_6^{Frc}$] Sucrose		$^{13}CO_2$	
			exp	calc	exp	calc	exp	calc	exp	calc
Ala	[M-57]	M + 0	0.589	0.591	0.566	0.568	0.269	0.230	0.700	0.735
	1–3	M + 1	0.297	0.294	0.316	0.313	0.196	0.229	0.209	0.182
		M + 2	0.090	0.092	0.093	0.094	0.233	0.245	0.077	0.072
		M + 3	0.023	0.023	0.025	0.025	0.302	0.296	0.015	0.012

Table A.3: Comparison between experimental and simulated mass isotopomer distributions for ^{13}C metabolic flux analysis on sucrose (continued)

Analyte	Fragment/ C atoms	Mass isotopomer	exp	calc	exp	calc	exp	calc	exp	calc
	[M-85]	M + 0	0.610	0.616	0.586	0.591	0.415	0.419	0.762	0.766
	2–3	M + 1	0.301	0.296	0.322	0.317	0.104	0.106	0.169	0.166
		M + 2	0.089	0.088	0.093	0.092	0.480	0.475	0.069	0.068
Val	[M-57]	M + 0	0.754	0.757	0.753	0.760	0.395	0.378	0.715	0.756
	1–5	M + 1	0.175	0.172	0.175	0.170	0.159	0.177	0.208	0.173
		M + 2	0.071	0.071	0.072	0.071	0.446	0.445	0.077	0.071
		M + 3	0.821	0.827	0.820	0.827	0.449	0.448	0.830	0.829
		M + 4	0.179	0.173	0.180	0.173	0.551	0.552	0.170	0.171
		M + 5	0.452	0.457	0.416	0.420	0.128	0.105	0.691	0.717
	[M-85]	M + 0	0.360	0.358	0.376	0.376	0.098	0.111	0.212	0.193
	2–5	M + 1	0.139	0.137	0.153	0.150	0.240	0.227	0.079	0.074
		M + 2	0.039	0.039	0.044	0.043	0.234	0.250	0.015	0.013
		M + 3	0.008	0.008	0.010	0.009	0.148	0.154	0.003	0.002
		M + 4	0.001	0.001	0.002	0.001	0.153	0.153	0.000	0.000
Thr	[M-57]	M + 0	0.458	0.466	0.420	0.428	0.189	0.188	0.728	0.741
	1–4	M + 1	0.360	0.357	0.378	0.376	0.059	0.058	0.186	0.177
		M + 2	0.136	0.132	0.151	0.147	0.405	0.411	0.072	0.070
		M + 3	0.038	0.036	0.042	0.041	0.103	0.103	0.012	0.011
		M + 4	0.008	0.007	0.009	0.009	0.244	0.241	0.002	0.002
	[M-85]	M + 0	0.363	0.368	0.322	0.323	0.093	0.090	0.730	0.732
	2–4	M + 1	0.379	0.380	0.386	0.388	0.122	0.121	0.184	0.183
		M + 2	0.183	0.180	0.204	0.202	0.222	0.226	0.071	0.071
		M + 3	0.058	0.057	0.067	0.067	0.250	0.254	0.012	0.012
Asp	[M-57]	M + 0	0.014	0.014	0.017	0.017	0.168	0.167	0.002	0.002
	1–4	M + 1	0.003	0.002	0.003	0.003	0.145	0.142	0.000	0.000
		M + 2	0.511	0.514	0.491	0.493	0.343	0.336	0.641	0.640
		M + 3	0.318	0.313	0.332	0.330	0.152	0.159	0.227	0.229
		M + 4	0.129	0.131	0.133	0.134	0.119	0.120	0.107	0.106
	[M-85]	M + 0	0.041	0.041	0.044	0.044	0.386	0.385	0.025	0.025
	2–4	M + 1	0.538	0.544	0.519	0.522	0.373	0.387	0.674	0.671
		M + 2	0.330	0.325	0.345	0.342	0.168	0.146	0.222	0.224
		M + 3	0.131	0.131	0.136	0.135	0.458	0.467	0.104	0.104
Glu	[M-57]	M + 0	0.496	0.496	0.478	0.481	0.284	0.283	0.051	0.085
	1–5	M + 1	0.319	0.315	0.331	0.329	0.148	0.153	0.557	0.583
		M + 2	0.132	0.135	0.135	0.135	0.162	0.110	0.254	0.214
		M + 3	0.043	0.043	0.045	0.045	0.297	0.330	0.109	0.095
		M + 4	0.010	0.010	0.011	0.010	0.109	0.125	0.030	0.023
		M + 5	0.508	0.510	0.489	0.493	0.324	0.321	0.137	0.125
	[M-85]	M + 0	0.320	0.318	0.333	0.331	0.141	0.142	0.578	0.585
	2–5	M + 1	0.130	0.131	0.133	0.133	0.377	0.378	0.198	0.201
		M + 2	0.042	0.041	0.044	0.043	0.158	0.158	0.088	0.089
		M + 3	0.389	0.394	0.353	0.360	0.089	0.082	0.691	0.690
		M + 4	0.368	0.366	0.377	0.379	0.047	0.048	0.211	0.213
Arg	[M-57]	M + 0	0.170	0.169	0.186	0.183	0.117	0.119	0.079	0.079
	1–6	M + 1	0.055	0.055	0.062	0.060	0.161	0.164	0.015	0.015
		M + 2	0.014	0.014	0.016	0.015	0.115	0.119	0.003	0.003
		M + 3	0.003	0.003	0.004	0.003	0.158	0.160	0.001	0.000
		M + 4	0.001	0.000	0.001	0.000	0.125	0.122	0.000	0.000
		M + 5	0.000	0.000	0.000	0.000	0.081	0.083	0.000	0.000
		M + 6	0.000	0.000	0.000	0.000	0.055	0.052	0.000	0.000
Ser	[M-57]	M + 0	0.000	0.000	0.000	0.000	0.051	0.051	0.000	0.000

Table A.3: Comparison between experimental and simulated mass isotopomer distributions for ^{13}C metabolic flux analysis on sucrose (continued)

Analyte	Fragment/ C atoms	Mass isotopomer	exp	calc	exp	calc	exp	calc	exp	calc
	1–3	M + 1	0.728	0.726	0.727	0.729	0.388	0.369	0.726	0.724
		M + 2	0.197	0.198	0.197	0.196	0.181	0.190	0.197	0.200
		M + 3	0.075	0.076	0.076	0.076	0.431	0.441	0.076	0.076
	[M-85]	M + 0	0.498	0.495	0.480	0.480	0.289	0.283	0.040	0.085
	2–3	M + 1	0.316	0.315	0.329	0.329	0.149	0.152	0.561	0.582
		M + 2	0.132	0.135	0.135	0.136	0.159	0.111	0.257	0.213
Gly	[M-57]	M + 0	0.043	0.044	0.045	0.045	0.297	0.330	0.112	0.096
	1–2	M + 1	0.010	0.011	0.011	0.011	0.106	0.125	0.031	0.023
		M + 2	0.511	0.509	0.491	0.493	0.328	0.321	0.129	0.125
	[M-85]	M + 0	0.317	0.318	0.332	0.330	0.135	0.142	0.581	0.584
	2	M + 1	0.130	0.132	0.133	0.134	0.377	0.379	0.200	0.201
Leu	[M-85]	M + 0	0.042	0.042	0.044	0.044	0.160	0.158	0.090	0.090
	2–6	M + 1	0.391	0.390	0.362	0.361	0.157	0.147	0.111	0.119
		M + 2	0.354	0.354	0.364	0.366	0.072	0.074	0.563	0.559
		M + 3	0.172	0.172	0.183	0.183	0.332	0.330	0.206	0.204
		M + 4	0.062	0.062	0.067	0.067	0.144	0.150	0.093	0.091
		M + 5	0.017	0.017	0.019	0.019	0.213	0.215	0.022	0.022
Phe	[M-57]	M + 0	0.004	0.004	0.004	0.004	0.082	0.085	0.005	0.005
	1–9	M + 1	0.443	0.446	0.407	0.408	0.191	0.181	0.707	0.707
		M + 2	0.360	0.361	0.376	0.377	0.063	0.064	0.199	0.200
		M + 3	0.145	0.143	0.158	0.157	0.396	0.399	0.077	0.076
		M + 4	0.042	0.041	0.047	0.046	0.114	0.117	0.014	0.014
		M + 5	0.010	0.009	0.011	0.010	0.236	0.238	0.003	0.002
		M + 6	0.383	0.378	0.354	0.354	0.145	0.133	0.013	0.016
		M + 7	0.357	0.357	0.368	0.367	0.072	0.077	0.122	0.177
		M + 8	0.175	0.177	0.185	0.186	0.314	0.303	0.545	0.511
		M + 9	0.063	0.065	0.068	0.068	0.148	0.158	0.200	0.191
	[M-res]	M + 0	0.017	0.018	0.019	0.019	0.204	0.203	0.092	0.081
	1–2	M + 1	0.004	0.004	0.004	0.004	0.085	0.091	0.023	0.019
		M + 2	0.001	0.001	0.001	0.001	0.032	0.035	0.006	0.004
Tyr	[M-57]	M + 0	0.338	0.339	0.306	0.310	0.079	0.071	0.598	0.594
	1–9	M + 1	0.355	0.355	0.360	0.363	0.051	0.050	0.248	0.253
		M + 2	0.196	0.196	0.210	0.209	0.111	0.111	0.112	0.114
		M + 3	0.077	0.078	0.085	0.084	0.154	0.156	0.030	0.030
		M + 4	0.024	0.024	0.027	0.026	0.123	0.124	0.008	0.007
		M + 5	0.006	0.006	0.007	0.007	0.156	0.158	0.002	0.001
		M + 6	0.002	0.001	0.002	0.001	0.129	0.127	0.001	0.000
		M + 7	0.001	0.000	0.001	0.000	0.086	0.091	0.000	0.000
		M + 8	0.001	0.000	0.001	0.000	0.059	0.058	0.000	0.000
		M + 9	0.000	0.000	0.000	0.000	0.052	0.053	0.000	0.000
	[M-res]	M + 0	0.733	0.726	0.733	0.729	0.384	0.369	0.726	0.724
	1–2	M + 1	0.193	0.198	0.193	0.196	0.180	0.190	0.197	0.200
		M + 2	0.074	0.076	0.074	0.076	0.435	0.441	0.076	0.076
Suc	[M-57]	M + 0	0.580	0.575	0.559	0.557	0.312	0.320	0.042	0.098
	1–4	M + 1	0.296	0.296	0.313	0.314	0.134	0.134	0.656	0.662
		M + 2	0.094	0.099	0.096	0.098	0.173	0.096	0.210	0.163
		M + 3	0.026	0.026	0.027	0.027	0.304	0.356	0.077	0.066
		M + 4	0.004	0.005	0.005	0.004	0.077	0.094	0.015	0.011
Glc	[M-15]	M + 0	0.137	0.110	0.363	0.413	0.382	0.363	0.520	0.520
	1–6	M + 1	0.428	0.450	0.311	0.303	0.193	0.197	0.256	0.256
		M + 2	0.227	0.241	0.183	0.178	0.126	0.150	0.153	0.153

Table A.3: Comparison between experimental and simulated mass isotopomer distributions for ^{13}C metabolic flux analysis on sucrose (continued)

Analyte	Fragment/ C atoms	Mass isotopomer	exp	calc	exp	calc	exp	calc	exp	calc
		M + 3	0.127	0.134	0.083	0.073	0.092	0.097	0.050	0.050
		M + 4	0.048	0.046	0.034	0.025	0.049	0.078	0.017	0.016
		M + 5	0.021	0.015	0.015	0.007	0.039	0.049	0.004	0.004
		M + 6	0.011	0.004	0.010	0.002	0.120	0.067	0.001	0.001
	[M-250]	M + 0	0.648	0.636	0.645	0.635	0.511	0.517	0.675	0.675
	3–6	M + 1	0.221	0.227	0.223	0.229	0.175	0.183	0.201	0.201
		M + 2	0.102	0.106	0.102	0.105	0.085	0.093	0.099	0.099
		M + 3	0.023	0.025	0.024	0.025	0.070	0.082	0.020	0.020
		M + 4	0.005	0.006	0.005	0.006	0.159	0.125	0.005	0.005

Table A.4: Comparison between experimental and simulated mass isotopomer distributions for metabolic flux analysis on fructose. The experimental data represent mean values of the three samples taken during the exponential phase at isotopic steady state. The simulated data represent mean values from the Monte Carlo simulations during metabolic flux analysis with OpenFLUX. Three labeling data sets derived from parallel cultivations were fit simultaneously to the metabolic network model.

Analyte	Fragment/ C atoms	Mass isotopomer	[1-^{13}C] Fructose		50 % [^{13}C$_6$] Fructose		^{13}CO$_2$	
			exp	calc	exp	calc	exp	calc
Ala	[M-57]	M + 0	0.397	0.382	0.290	0.357	0.725	0.722
	1–3	M + 1	0.448	0.460	0.198	0.142	0.190	0.192
		M + 2	0.117	0.118	0.213	0.131	0.073	0.074
		M + 3	0.039	0.040	0.299	0.370	0.012	0.013
	[M-85]	M + 0	0.417	0.403	0.434	0.427	0.761	0.766
	2–3	M + 1	0.467	0.480	0.107	0.104	0.169	0.166
		M + 2	0.116	0.117	0.460	0.468	0.070	0.068
Val	[M-57]	M + 0	0.209	0.189	0.142	0.165	0.708	0.705
	1–5	M + 1	0.416	0.416	0.103	0.074	0.200	0.203
		M + 2	0.273	0.288	0.239	0.229	0.075	0.076
		M + 3	0.076	0.080	0.235	0.240	0.014	0.014
		M + 4	0.022	0.023	0.134	0.105	0.002	0.002
		M + 5	0.004	0.004	0.147	0.187	0.000	0.000
	[M-85]	M + 0	0.209	0.192	0.204	0.196	0.726	0.741
	2–5	M + 1	0.418	0.421	0.061	0.057	0.188	0.177
		M + 2	0.275	0.287	0.408	0.413	0.072	0.070
		M + 3	0.077	0.077	0.101	0.100	0.012	0.011
		M + 4	0.021	0.022	0.226	0.234	0.002	0.002
Thr	[M-57]	M + 0	0.341	0.320	0.299	0.332	0.074	0.035
	1–4	M + 1	0.424	0.431	0.148	0.122	0.585	0.610
		M + 2	0.159	0.168	0.147	0.085	0.219	0.228
		M + 3	0.061	0.065	0.301	0.343	0.098	0.103
		M + 4	0.014	0.016	0.105	0.118	0.024	0.025
	[M-85]	M + 0	0.351	0.331	0.342	0.345	0.143	0.143
	2–4	M + 1	0.433	0.440	0.139	0.133	0.574	0.572
		M + 2	0.156	0.165	0.357	0.349	0.196	0.198
		M + 3	0.060	0.064	0.162	0.173	0.086	0.087
Asp	[M-57]	M + 0	0.339	0.319	0.311	0.332	0.053	0.035
	1–4	M + 1	0.422	0.430	0.147	0.122	0.597	0.608
		M + 2	0.161	0.168	0.140	0.085	0.224	0.227
		M + 3	0.063	0.066	0.300	0.343	0.102	0.104

Table A.4: **Comparison between experimental and simulated mass isotopomer distributions for ^{13}C metabolic flux analysis on fructose (continued)**

Analyte	Fragment/ C atoms	Mass isotopomer	exp	calc	exp	calc	exp	calc
		M + 4	0.015	0.016	0.101	0.118	0.025	0.025
	[M-85]	M + 0	0.347	0.330	0.348	0.345	0.132	0.143
	2–4	M + 1	0.431	0.440	0.135	0.133	0.578	0.571
		M + 2	0.160	0.165	0.355	0.349	0.200	0.198
		M + 3	0.062	0.065	0.162	0.173	0.090	0.088
Glu	[M-57]	M + 0	0.183	0.161	0.172	0.161	0.103	0.136
	1–5	M + 1	0.381	0.376	0.080	0.070	0.571	0.548
		M + 2	0.283	0.297	0.331	0.327	0.206	0.201
		M + 3	0.108	0.116	0.143	0.151	0.093	0.089
		M + 4	0.037	0.040	0.194	0.199	0.022	0.021
		M + 5	0.008	0.009	0.079	0.092	0.005	0.005
	[M-85]	M + 0	0.207	0.184	0.204	0.186	0.706	0.707
	2–5	M + 1	0.414	0.410	0.067	0.068	0.201	0.200
		M + 2	0.274	0.293	0.398	0.398	0.076	0.076
		M + 3	0.082	0.088	0.111	0.118	0.014	0.014
		M + 4	0.023	0.025	0.219	0.230	0.002	0.002
Arg	[M-57]	M + 0	0.177	0.159	0.164	0.152	0.029	0.003
	1–6	M + 1	0.377	0.373	0.080	0.070	0.106	0.146
		M + 2	0.286	0.299	0.315	0.311	0.514	0.538
		M + 3	0.111	0.118	0.144	0.150	0.200	0.201
		M + 4	0.037	0.041	0.186	0.191	0.109	0.086
		M + 5	0.010	0.010	0.080	0.091	0.029	0.020
		M + 6	0.003	0.002	0.031	0.034	0.013	0.005
Ser	[M-57]	M + 0	0.348	0.334	0.324	0.328	0.647	0.634
	1–3	M + 1	0.429	0.439	0.179	0.169	0.224	0.233
		M + 2	0.161	0.163	0.147	0.140	0.105	0.107
		M + 3	0.062	0.064	0.350	0.364	0.024	0.026
	[M-85]	M + 0	0.375	0.361	0.354	0.340	0.674	0.671
	2–3	M + 1	0.459	0.469	0.222	0.230	0.222	0.224
		M + 2	0.166	0.170	0.424	0.430	0.104	0.104
Gly	[M-57]	M + 0	0.742	0.756	0.419	0.428	0.722	0.749
	1–2	M + 1	0.184	0.173	0.161	0.111	0.203	0.179
		M + 2	0.074	0.071	0.420	0.462	0.076	0.072
	[M-85]	M + 0	0.814	0.821	0.471	0.455	0.828	0.829
	2	M + 1	0.186	0.179	0.529	0.545	0.172	0.171
Leu	[M-85]	M + 0	0.116	0.100	0.106	0.096	0.732	0.732
	2–6	M + 1	0.322	0.311	0.126	0.124	0.187	0.183
		M + 2	0.341	0.351	0.235	0.230	0.068	0.071
		M + 3	0.165	0.177	0.243	0.251	0.011	0.012
		M + 4	0.045	0.048	0.160	0.163	0.002	0.002
		M + 5	0.011	0.012	0.130	0.136	0.000	0.000
Phe	[M-57]	M + 0	0.156	0.148	0.077	0.073	0.693	0.680
	1–9	M + 1	0.359	0.365	0.050	0.040	0.207	0.220
		M + 2	0.305	0.313	0.095	0.092	0.078	0.081
		M + 3	0.127	0.126	0.140	0.133	0.015	0.016
		M + 4	0.038	0.038	0.135	0.133	0.003	0.003
		M + 5	0.010	0.008	0.133	0.133	0.001	0.000
		M + 6	0.002	0.001	0.142	0.147	0.001	0.000
		M + 7	0.001	0.000	0.104	0.111	0.002	0.000
		M + 8	0.001	0.000	0.054	0.053	0.000	0.000
		M + 9	0.000	0.000	0.071	0.085	0.001	0.000

Table A.4: Comparison between experimental and simulated mass isotopomer distributions for ^{13}C metabolic flux analysis on fructose (continued)

Analyte	Fragment/ C atoms	Mass isotopomer	exp	calc	exp	calc	exp	calc
	[M-159]	M + 0	0.178	0.167	0.090	0.082	0.782	0.785
	2–9	M + 1	0.388	0.397	0.047	0.039	0.165	0.167
		M + 2	0.303	0.312	0.173	0.174	0.045	0.042
		M + 3	0.103	0.099	0.108	0.094	0.006	0.005
		M + 4	0.023	0.021	0.179	0.186	0.001	0.000
		M + 5	0.004	0.003	0.106	0.096	0.000	0.000
		M + 6	0.001	0.000	0.166	0.183	0.000	0.000
		M + 7	0.000	0.000	0.053	0.053	0.000	0.000
		M + 8	0.000	0.000	0.078	0.092	0.000	0.000
Tyr	[M-57]	M + 0	0.139	0.128	0.068	0.064	0.595	0.586
	1–9	M + 1	0.325	0.329	0.049	0.042	0.235	0.258
		M + 2	0.302	0.311	0.091	0.087	0.110	0.116
		M + 3	0.152	0.153	0.134	0.127	0.029	0.031
		M + 4	0.059	0.057	0.135	0.134	0.018	0.007
		M + 5	0.017	0.016	0.137	0.135	0.007	0.001
		M + 6	0.004	0.004	0.145	0.147	0.004	0.000
		M + 7	0.001	0.001	0.109	0.117	0.002	0.000
		M + 8	0.000	0.000	0.062	0.063	0.000	0.000
		M + 9	0.001	0.000	0.071	0.084	0.000	0.000
	[M-res]	M + 0	0.728	0.724	0.406	0.418	0.732	0.717
	1–2	M + 1	0.196	0.200	0.166	0.128	0.192	0.206
		M + 2	0.076	0.076	0.428	0.455	0.075	0.078
Suc	[M-57]	M + 0	0.395	0.361	0.361	0.367	0.059	0.077
	1–4	M + 1	0.440	0.452	0.125	0.091	0.684	0.672
		M + 2	0.118	0.134	0.132	0.088	0.175	0.171
		M + 3	0.040	0.045	0.313	0.362	0.070	0.068
		M + 4	0.007	0.008	0.070	0.093	0.012	0.011
Glc	[M-15]	M + 0	0.035	0.041	0.266	0.256	0.524	0.518
	1–6	M + 1	0.450	0.461	0.138	0.140	0.257	0.257
		M + 2	0.278	0.268	0.096	0.098	0.151	0.153
		M + 3	0.156	0.152	0.117	0.106	0.049	0.050
		M + 4	0.057	0.055	0.065	0.061	0.016	0.017
		M + 5	0.019	0.018	0.054	0.059	0.004	0.004
		M + 6	0.005	0.005	0.263	0.281	0.000	0.001
	[M-250]	M + 0	0.576	0.573	0.337	0.331	0.675	0.673
	3–6	M + 1	0.268	0.271	0.160	0.157	0.202	0.203
		M + 2	0.116	0.116	0.073	0.068	0.098	0.099
		M + 3	0.032	0.032	0.094	0.090	0.020	0.020
		M + 4	0.008	0.007	0.336	0.354	0.005	0.005

Table A.5: Comparison between experimental and simulated mass isotopomer distributions for metabolic flux analysis on glucose. The experimental data were derived from previous work (Becker *et al.*, 2013). The simulated data represent mean values from the Monte Carlo simulations during metabolic flux analysis with OpenFLUX. The two labeling data sets derived from parallel cultivations were fit simultaneously to the metabolic network model.

Analyte	Fragment/ C atoms	Mass isotopomer	[1-^{13}C] Glucose		50 % [^{13}C$_6$] Glucose	
			exp	calc	exp	calc
Ala	[M-57]	M + 0	0.411	0.407	0.285	0.285

Table A.5: **Comparison between experimental and simulated mass isotopomer distributions for ^{13}C metabolic flux analysis on glucose (continued)**

Analyte	Fragment/ C atoms	Mass isotopomer	exp	calc	exp	calc
	1–3	M + 1	0.437	0.438	0.202	0.190
		M + 2	0.114	0.117	0.268	0.275
	[M-85]	M + 0	0.433	0.431	0.433	0.426
	2–3	M + 1	0.455	0.456	0.110	0.106
		M + 2	0.112	0.113	0.457	0.468
Thr	[M-57]	M + 0	0.342	0.340	0.280	0.282
	1–4	M + 1	0.417	0.415	0.162	0.156
		M + 2	0.163	0.166	0.170	0.170
	[M-85]	M + 0	0.353	0.352	0.328	0.318
	2–4	M + 1	0.425	0.424	0.151	0.151
		M + 2	0.161	0.162	0.362	0.360
Asp	[M-57]	M + 0	0.344	0.340	0.281	0.282
	1–4	M + 1	0.415	0.414	0.165	0.156
		M + 2	0.163	0.167	0.171	0.170
	[M-85]	M + 0	0.354	0.352	0.333	0.318
	2–4	M + 1	0.424	0.423	0.151	0.151
		M + 2	0.160	0.163	0.357	0.360
Ser	[M-57]	M + 0	0.355	0.357	0.330	0.323
	1–3	M + 1	0.425	0.421	0.172	0.171
		M + 2	0.159	0.161	0.148	0.150
	[M-85]	M + 0	0.384	0.385	0.363	0.362
	2–3	M + 1	0.452	0.450	0.204	0.195
		M + 2	0.164	0.165	0.433	0.442
Gly	[M-57]	M + 0	0.750	0.747	0.409	0.396
	1–2	M + 1	0.178	0.180	0.170	0.171
		M + 2	0.072	0.072	0.421	0.433
	[M-85]	M + 0	0.819	0.817	0.467	0.455
	2	M + 1	0.181	0.183	0.533	0.545
Leu	[M-85]	M + 0	0.218	0.215	0.183	0.169
	2–6	M + 1	0.414	0.418	0.074	0.070
		M + 2	0.265	0.266	0.353	0.350
Phe	[M-57]	M + 0	0.155	0.154	0.068	0.058
	1–9	M + 1	0.352	0.357	0.053	0.047
		M + 2	0.304	0.305	0.095	0.101
Tyr	[M-57]	M + 0	0.136	0.133	0.059	0.051
	1–9	M + 1	0.320	0.323	0.054	0.047
		M + 2	0.302	0.304	0.092	0.095
Suc	[M-57]	M + 0	0.398	0.393	0.323	0.319
	1–4	M + 1	0.434	0.432	0.145	0.138
		M + 2	0.121	0.126	0.169	0.165

Table A.6: Comparison between experimental and simulated mass isotopomer distributions for metabolic flux analysis on xylose. The experimental data represent mean values of the three samples taken during the exponential phase at isotopic steady state. The simulated data represent mean values from the Monte Carlo simulations during metabolic flux analysis with OpenFLUX. The two labeling data sets derived from parallel cultivations were fit simultaneously to the metabolic network model.

Analyte	Fragment/ C atoms	Mass isotopomer	[1-^{13}C] Xylose exp	[1-^{13}C] Xylose calc	50 % [^{13}C$_5$] Xylose exp	50 % [^{13}C$_5$] Xylose calc
Ala	[M-57]	M + 0	0.457	0.457	0.338	0.337
	1–3	M + 1	0.307	0.311	0.153	0.150
		M + 2	0.190	0.186	0.239	0.241
		M + 3	0.046	0.046	0.271	0.271
	[M-85]	M + 0	0.485	0.485	0.426	0.425
	2–3	M + 1	0.409	0.409	0.107	0.107
		M + 2	0.106	0.106	0.467	0.468
Val	[M-57]	M + 0	0.609	0.607	0.356	0.349
	1–5	M + 1	0.299	0.301	0.279	0.281
		M + 2	0.092	0.091	0.364	0.370
		M + 3	0.799	0.799	0.464	0.454
		M + 4	0.201	0.201	0.536	0.546
		M + 5	0.279	0.272	0.165	0.157
	[M-85]	M + 0	0.362	0.362	0.082	0.079
	2–5	M + 1	0.230	0.233	0.276	0.274
		M + 2	0.097	0.101	0.200	0.203
		M + 3	0.026	0.026	0.144	0.149
		M + 4	0.007	0.006	0.133	0.139
Thr	[M-57]	M + 0	0.286	0.282	0.200	0.194
	1–4	M + 1	0.419	0.422	0.061	0.060
		M + 2	0.217	0.219	0.409	0.411
		M + 3	0.062	0.061	0.102	0.102
		M + 4	0.016	0.016	0.229	0.234
	[M-85]	M + 0	0.203	0.189	0.101	0.094
	2–4	M + 1	0.380	0.376	0.126	0.124
		M + 2	0.277	0.285	0.234	0.230
		M + 3	0.107	0.113	0.247	0.251
Asp	[M-57]	M + 0	0.029	0.030	0.161	0.164
	1–4	M + 1	0.005	0.007	0.130	0.136
		M + 2	0.418	0.401	0.311	0.294
		M + 3	0.286	0.296	0.185	0.185
		M + 4	0.223	0.227	0.185	0.205
	[M-85]	M + 0	0.073	0.075	0.320	0.316
	2–4	M + 1	0.440	0.432	0.385	0.376
		M + 2	0.407	0.413	0.164	0.173
		M + 3	0.153	0.155	0.451	0.451
Glu	[M-57]	M + 0	0.379	0.392	0.266	0.277
	1–5	M + 1	0.299	0.287	0.171	0.158
		M + 2	0.216	0.221	0.196	0.185
		M + 3	0.078	0.074	0.267	0.283
		M + 4	0.028	0.026	0.100	0.096
		M + 5	0.388	0.404	0.325	0.336
	[M-85]	M + 0	0.386	0.377	0.149	0.137
	2–5	M + 1	0.163	0.162	0.372	0.371
		M + 2	0.063	0.058	0.154	0.156
		M + 3	0.219	0.207	0.061	0.052

Table A.6: Comparison between experimental and simulated mass isotopomer distributions for ^{13}C metabolic flux analysis on xylose (continued)

Analyte	Fragment/ C atoms	Mass isotopomer	exp	calc	exp	calc
		M + 4	0.299	0.301	0.050	0.047
Arg	[M-57]	M + 0	0.244	0.252	0.104	0.103
	1–6	M + 1	0.144	0.151	0.132	0.131
		M + 2	0.058	0.062	0.144	0.148
		M + 3	0.023	0.021	0.137	0.142
		M + 4	0.007	0.005	0.144	0.149
		M + 5	0.003	0.001	0.107	0.106
		M + 6	0.002	0.000	0.062	0.067
Ser	[M-57]	M + 0	0.001	0.000	0.059	0.056
	1–3	M + 1	0.594	0.580	0.349	0.342
		M + 2	0.307	0.318	0.284	0.298
		M + 3	0.099	0.102	0.367	0.360
	[M-85]	M + 0	0.390	0.391	0.272	0.277
	2–3	M + 1	0.293	0.286	0.165	0.158
		M + 2	0.214	0.222	0.195	0.185
Gly	[M-57]	M + 0	0.076	0.075	0.268	0.283
	1–2	M + 1	0.026	0.026	0.100	0.097
		M + 2	0.400	0.403	0.330	0.336
	[M-85]	M + 0	0.379	0.376	0.144	0.137
	2	M + 1	0.162	0.163	0.370	0.371
Leu	[M-85]	M + 0	0.059	0.058	0.157	0.156
	2–6	M + 1	0.248	0.239	0.166	0.156
		M + 2	0.379	0.378	0.077	0.073
		M + 3	0.240	0.243	0.338	0.334
		M + 4	0.094	0.100	0.140	0.147
		M + 5	0.032	0.032	0.206	0.208
Phe	[M-57]	M + 0	0.008	0.008	0.073	0.083
	1–9	M + 1	0.265	0.270	0.199	0.187
		M + 2	0.415	0.415	0.067	0.066
		M + 3	0.231	0.228	0.398	0.400
		M + 4	0.070	0.069	0.113	0.116
		M + 5	0.019	0.018	0.223	0.231
		M + 6	0.234	0.235	0.148	0.149
		M + 7	0.377	0.376	0.078	0.072
		M + 8	0.244	0.245	0.313	0.319
		M + 9	0.098	0.101	0.147	0.146
	[M-res]	M + 0	0.034	0.033	0.201	0.200
	1–2	M + 1	0.009	0.008	0.081	0.082
		M + 2	0.004	0.002	0.033	0.032
Tyr	[M-57]	M + 0	0.191	0.178	0.056	0.045
	1–9	M + 1	0.277	0.280	0.052	0.046
		M + 2	0.244	0.255	0.098	0.096
		M + 3	0.158	0.167	0.126	0.127
		M + 4	0.077	0.078	0.145	0.146
		M + 5	0.031	0.031	0.138	0.143
		M + 6	0.014	0.009	0.145	0.150
		M + 7	0.005	0.002	0.110	0.113
		M + 8	0.002	0.001	0.069	0.074
		M + 9	0.001	0.000	0.060	0.060
	[M-res]	M + 0	0.591	0.580	0.347	0.342
	1–2	M + 1	0.308	0.318	0.284	0.298

Table A.6: Comparison between experimental and simulated mass isotopomer distributions for ^{13}C metabolic flux analysis on xylose (continued)

Analyte	Fragment/ C atoms	Mass isotopomer	exp	calc	exp	calc
		M + 2	0.100	0.102	0.369	0.360
Suc	[M-57]	M + 0	0.446	0.447	0.307	0.312
	1–4	M + 1	0.294	0.281	0.150	0.139
		M + 2	0.195	0.206	0.200	0.188
		M + 3	0.051	0.050	0.269	0.288
		M + 4	0.015	0.016	0.073	0.072
Glc	[M-15]	M + 0	0.004	0.006	0.065	0.075
	1–6	M + 1	0.201	0.207	0.096	0.097
		M + 2	0.298	0.296	0.152	0.158
		M + 3	0.237	0.236	0.199	0.190
		M + 4	0.163	0.160	0.192	0.191
		M + 5	0.069	0.068	0.156	0.151
		M + 6	0.028	0.027	0.140	0.138
	[M-250]	M + 0	0.251	0.264	0.180	0.202
	3–6	M + 1	0.338	0.335	0.215	0.208
		M + 2	0.228	0.223	0.146	0.146
		M + 3	0.141	0.136	0.216	0.202
		M + 4	0.042	0.041	0.244	0.242

Table A.7: Comparison between experimental and simulated mass isotopomer distributions for ^{13}C metabolic flux analysis on a mixture of 18 g·L^{-1} glucose and 12 g·L^{-1} xylose. The experimental data represent mean values of the three samples taken during the exponential phase at isotopic steady state. The simulated data represent mean values from the Monte Carlo simulations during metabolic flux analysis with OpenFLUX. Four labeling data sets derived from parallel cultivations were fit simultaneously to the metabolic network model.

Analyte	Fragment/ C atoms	Mass isotopomer	[1-^{13}C] Glucose		[1-^{13}C] Xylose		[^{13}C$_6$] Glucose		[^{13}C$_5$] Xylose	
			exp	calc	exp	calc	exp	calc	exp	calc
Ala	[M-57]	M + 0	0.429	0.429	0.718	0.708	0.044	0.040	0.666	0.631
	1–3	M + 1	0.421	0.420	0.194	0.201	0.054	0.072	0.178	0.190
		M + 2	0.113	0.115	0.075	0.076	0.246	0.264	0.117	0.137
		M + 3	0.036	0.037	0.013	0.014	0.656	0.624	0.039	0.042
	[M-85]	M + 0	0.451	0.456	0.739	0.735	0.086	0.102	0.709	0.696
	2–3	M + 1	0.438	0.434	0.189	0.192	0.036	0.044	0.159	0.157
		M + 2	0.111	0.110	0.072	0.072	0.878	0.854	0.132	0.148
Val	[M-57]	M + 0	0.727	0.731	0.755	0.750	0.068	0.078	0.698	0.681
	1–5	M + 1	0.198	0.195	0.174	0.178	0.162	0.144	0.192	0.191
		M + 2	0.075	0.074	0.071	0.072	0.770	0.778	0.110	0.128
		M + 3	0.796	0.808	0.827	0.827	0.102	0.116	0.770	0.751
		M + 4	0.204	0.192	0.173	0.173	0.898	0.884	0.230	0.249
		M + 5	0.243	0.241	0.679	0.662	0.010	0.004	0.594	0.541
	[M-85]	M + 0	0.418	0.419	0.218	0.232	0.009	0.008	0.171	0.180
	2–5	M + 1	0.245	0.246	0.081	0.084	0.059	0.063	0.160	0.188
		M + 2	0.070	0.072	0.017	0.018	0.104	0.132	0.050	0.060
		M + 3	0.019	0.019	0.004	0.003	0.241	0.253	0.019	0.025
		M + 4	0.004	0.003	0.001	0.000	0.577	0.539	0.006	0.007
Thr	[M-57]	M + 0	0.245	0.248	0.686	0.679	0.015	0.010	0.615	0.586
	1–4	M + 1	0.423	0.425	0.216	0.223	0.008	0.007	0.157	0.150

Table A.7: **Comparison between experimental and simulated mass isotopomer distributions for ^{13}C metabolic flux analysis on a glucose/xylose mixture (continued)**

Analyte	Fragment/ C atoms	Mass isotopomer	exp	calc	exp	calc	exp	calc	exp	calc
		M + 2	0.244	0.242	0.078	0.079	0.144	0.174	0.173	0.199
		M + 3	0.069	0.067	0.016	0.016	0.061	0.075	0.036	0.042
		M + 4	0.019	0.018	0.003	0.003	0.772	0.733	0.019	0.023
	[M-85]	M + 0	0.159	0.161	0.668	0.649	0.007	0.001	0.564	0.515
	2–4	M + 1	0.358	0.363	0.230	0.243	0.009	0.010	0.195	0.200
		M + 2	0.308	0.305	0.082	0.086	0.019	0.026	0.170	0.193
		M + 3	0.131	0.128	0.017	0.019	0.132	0.160	0.048	0.060
Asp	[M-57]	M + 0	0.036	0.035	0.003	0.003	0.124	0.149	0.019	0.025
	1–4	M + 1	0.008	0.008	0.000	0.000	0.709	0.653	0.004	0.006
		M + 2	0.375	0.372	0.625	0.615	0.063	0.071	0.590	0.580
		M + 3	0.409	0.409	0.237	0.242	0.051	0.053	0.222	0.215
		M + 4	0.157	0.159	0.110	0.114	0.110	0.127	0.125	0.125
	[M-85]	M + 0	0.059	0.060	0.027	0.029	0.776	0.749	0.063	0.080
	2–4	M + 1	0.404	0.406	0.654	0.645	0.080	0.098	0.623	0.615
		M + 2	0.436	0.434	0.239	0.245	0.061	0.058	0.225	0.213
		M + 3	0.160	0.160	0.108	0.110	0.860	0.844	0.152	0.172
Glu	[M-57]	M + 0	0.364	0.363	0.613	0.605	0.044	0.059	0.573	0.561
	1–5	M + 1	0.405	0.403	0.241	0.245	0.041	0.042	0.217	0.213
		M + 2	0.158	0.159	0.110	0.114	0.183	0.161	0.132	0.127
		M + 3	0.059	0.060	0.028	0.030	0.525	0.550	0.059	0.075
		M + 4	0.014	0.014	0.007	0.007	0.207	0.187	0.019	0.024
		M + 5	0.372	0.377	0.623	0.621	0.062	0.077	0.591	0.583
	[M-85]	M + 0	0.413	0.410	0.241	0.243	0.048	0.046	0.214	0.209
	2–5	M + 1	0.156	0.155	0.108	0.109	0.588	0.551	0.150	0.155
		M + 2	0.059	0.058	0.028	0.027	0.302	0.327	0.045	0.053
		M + 3	0.167	0.183	0.619	0.608	0.007	0.001	0.468	0.393
		M + 4	0.357	0.371	0.248	0.260	0.003	0.001	0.205	0.202
Arg	[M-57]	M + 0	0.294	0.284	0.094	0.101	0.005	0.008	0.141	0.146
	1–6	M + 1	0.127	0.117	0.023	0.025	0.009	0.014	0.088	0.099
		M + 2	0.038	0.035	0.005	0.005	0.016	0.029	0.053	0.091
		M + 3	0.010	0.008	0.004	0.001	0.051	0.079	0.023	0.033
		M + 4	0.002	0.001	0.002	0.000	0.088	0.106	0.012	0.021
		M + 5	0.002	0.000	0.002	0.000	0.112	0.123	0.006	0.009
		M + 6	0.001	0.000	0.001	0.000	0.194	0.228	0.003	0.003
Ser	[M-57]	M + 0	0.001	0.000	0.001	0.000	0.516	0.411	0.002	0.001
	1–3	M + 1	0.187	0.209	0.701	0.691	0.006	0.001	0.532	0.450
		M + 2	0.386	0.404	0.223	0.235	0.003	0.001	0.183	0.187
		M + 3	0.292	0.275	0.060	0.062	0.009	0.017	0.150	0.161
	[M-85]	M + 0	0.104	0.089	0.011	0.011	0.010	0.013	0.064	0.071
	2–3	M + 1	0.023	0.019	0.002	0.001	0.046	0.081	0.046	0.085
		M + 2	0.005	0.003	0.001	0.000	0.058	0.064	0.014	0.021
Gly	[M-57]	M + 0	0.001	0.000	0.001	0.000	0.133	0.148	0.009	0.020
	1–2	M + 1	0.001	0.000	0.001	0.000	0.152	0.161	0.002	0.003
		M + 2	0.001	0.000	0.001	0.000	0.583	0.514	0.001	0.002
	[M-85]	M + 0	0.709	0.677	0.728	0.719	0.067	0.079	0.675	0.656
	2	M + 1	0.212	0.238	0.197	0.204	0.143	0.222	0.211	0.218
Leu	[M-85]	M + 0	0.079	0.084	0.076	0.077	0.790	0.699	0.113	0.127
	2–6	M + 1	0.366	0.363	0.614	0.603	0.045	0.059	0.574	0.560
		M + 2	0.403	0.403	0.240	0.244	0.040	0.042	0.215	0.212
		M + 3	0.158	0.160	0.111	0.115	0.182	0.161	0.131	0.128
		M + 4	0.060	0.061	0.028	0.030	0.527	0.550	0.061	0.075

Table A.7: Comparison between experimental and simulated mass isotopomer distributions for ^{13}C metabolic flux analysis on a glucose/xylose mixture (continued)

Analyte	Fragment/ C atoms	Mass isotopomer	exp	calc	exp	calc	exp	calc	exp	calc
		M + 5	0.014	0.014	0.007	0.007	0.205	0.188	0.019	0.024
Phe	[M-57]	M + 0	0.374	0.377	0.627	0.619	0.063	0.077	0.596	0.582
	1–9	M + 1	0.411	0.409	0.237	0.242	0.039	0.046	0.210	0.208
		M + 2	0.156	0.156	0.109	0.111	0.593	0.551	0.151	0.156
		M + 3	0.059	0.058	0.027	0.028	0.305	0.327	0.044	0.054
		M + 4	0.211	0.210	0.588	0.575	0.010	0.008	0.525	0.494
		M + 5	0.386	0.387	0.256	0.263	0.006	0.007	0.198	0.192
		M + 6	0.262	0.262	0.116	0.119	0.105	0.123	0.185	0.199
		M + 7	0.100	0.101	0.031	0.033	0.067	0.086	0.057	0.071
		M + 8	0.033	0.033	0.008	0.008	0.560	0.490	0.028	0.033
		M + 9	0.008	0.008	0.001	0.002	0.251	0.286	0.007	0.010
	[M-159]	M + 0	0.243	0.237	0.670	0.649	0.015	0.010	0.613	0.560
	2–9	M + 1	0.413	0.417	0.226	0.242	0.006	0.007	0.157	0.168
		M + 2	0.249	0.250	0.083	0.087	0.145	0.172	0.172	0.199
		M + 3	0.075	0.075	0.017	0.019	0.065	0.082	0.039	0.049
		M + 4	0.021	0.020	0.003	0.003	0.769	0.728	0.019	0.024
		M + 5	0.205	0.206	0.580	0.567	0.008	0.007	0.499	0.486
		M + 6	0.380	0.385	0.260	0.270	0.006	0.006	0.203	0.198
		M + 7	0.261	0.264	0.115	0.120	0.089	0.109	0.171	0.197
		M + 8	0.103	0.103	0.032	0.034	0.063	0.078	0.074	0.073
	[M-res]	M + 0	0.036	0.034	0.009	0.008	0.482	0.435	0.037	0.033
	1–2	M + 1	0.011	0.008	0.002	0.002	0.247	0.261	0.012	0.010
		M + 2	0.004	0.002	0.001	0.000	0.105	0.104	0.004	0.003
Tyr	[M-57]	M + 0	0.146	0.158	0.529	0.523	0.010	0.001	0.399	0.339
	1–9	M + 1	0.322	0.338	0.273	0.286	0.006	0.001	0.220	0.214
		M + 2	0.293	0.288	0.126	0.135	0.006	0.008	0.156	0.160
		M + 3	0.152	0.143	0.039	0.042	0.009	0.014	0.098	0.108
		M + 4	0.059	0.053	0.014	0.011	0.021	0.029	0.064	0.094
		M + 5	0.018	0.015	0.004	0.002	0.050	0.076	0.029	0.042
		M + 6	0.007	0.004	0.007	0.000	0.094	0.108	0.019	0.025
		M + 7	0.002	0.001	0.004	0.000	0.115	0.128	0.008	0.011
		M + 8	0.001	0.000	0.002	0.000	0.193	0.228	0.004	0.004
		M + 9	0.001	0.000	0.001	0.000	0.496	0.408	0.003	0.002
	[M-res]	M + 0	0.707	0.677	0.726	0.719	0.066	0.079	0.673	0.656
	1–2	M + 1	0.213	0.238	0.198	0.204	0.143	0.222	0.212	0.218
		M + 2	0.080	0.084	0.077	0.077	0.791	0.699	0.115	0.127
Suc	[M-57]	M + 0	0.421	0.418	0.709	0.700	0.048	0.065	0.660	0.648
	1–4	M + 1	0.417	0.416	0.195	0.199	0.038	0.039	0.170	0.167
		M + 2	0.117	0.120	0.079	0.082	0.207	0.173	0.108	0.104
		M + 3	0.038	0.039	0.014	0.015	0.552	0.584	0.050	0.066
		M + 4	0.006	0.007	0.003	0.003	0.154	0.139	0.012	0.015
Glc	[M-15]	M + 0	0.026	0.041	0.482	0.463	0.005	0.005	0.483	0.452
	1–6	M + 1	0.449	0.478	0.272	0.276	0.007	0.006	0.245	0.240
		M + 2	0.281	0.256	0.161	0.168	0.011	0.012	0.162	0.172
		M + 3	0.160	0.151	0.058	0.063	0.035	0.029	0.068	0.076
		M + 4	0.060	0.052	0.020	0.022	0.056	0.065	0.028	0.036
		M + 5	0.019	0.018	0.005	0.006	0.093	0.103	0.010	0.015
		M + 6	0.005	0.004	0.002	0.001	0.793	0.780	0.004	0.009
	[M-250]	M + 0	0.568	0.617	0.655	0.647	0.004	0.013	0.643	0.628
	3–6	M + 1	0.274	0.231	0.215	0.219	0.024	0.013	0.208	0.219
		M + 2	0.117	0.115	0.102	0.104	0.024	0.010	0.105	0.104
		M + 3	0.033	0.029	0.022	0.024	0.085	0.083	0.034	0.031

Table A.7: **Comparison between experimental and simulated mass isotopomer distributions for** ^{13}**C metabolic flux analysis on a glucose/xylose mixture (continued)**

Analyte	Fragment/ C atoms	Mass isotopomer	exp	calc	exp	calc	exp	calc	exp	calc
		M + 4	0.008	0.007	0.005	0.006	0.863	0.881	0.011	0.017

A.5 List of Figures

A.6 List of Tables